ELECTRODEPOSITION AND ELECTRODEPOSITED MODIFIERS IN ELECTROTHERMAL ATOMIC ABSORPTION SPECTROMETRY

A thesis submitted in partial fulfilment of the requirements for the degree of

Doctor of Philosophy in Chemistry

At the
University of Canterbury

by

Stephen D. Money

1999

ABSTRACT

The work within this thesis is directed towards optimising and expanding the application of electrodeposition-coupled-electrothermal atomic absorption spectrometry (ED-ETAAS).

The technique involves modifying the surface of the graphite furnace by *in-situ* electro-deposition of a noble metal. The analyte is electrodeposited onto the modifier and the spent sample matrix is aspirated from the furnace, thus separating the analyte from sample matrix components which can interfere with ETAAS analysis. The electrodeposited analyte is then determined by ETAAS.

Parameters for electrodeposition of modifier and analytes were optimised. It was shown that ED-ETAAS could be used to determine lead, cadmium, and copper in 0.5 M NaCl media with sensitivity and detection limits similar to conventional ETAAS. The technique was used to determine copper and cadmium in seawater.

Different noble metal modifiers were compared. Palladium was shown to provide better sensitivity and thermal stabilisation than iridium or rhodium for lead determination.

ED-ETAAS was used for the determination of inorganic mercury. The detection limit for the technique, using a 20 μL sample volume, was *ca.* 18 ppb (corresponding to *ca.* 380 pg), with a characteristic mass of 91 pg. The electrodeposited palladium modifier provided greater analyte stabilisation and sensitivity than gold or ammonium sulphide modifiers. The technique was compared with cold vapour-ETAAS, for which a detection limit of *ca.* 1.7 ppb was determined using an 8.4 mL sample volume. The electrodeposited palladium modifier was shown to provide superior sensitivity to palladium chloride modifier.

ED-ETAAS was examined as a technique for differentiating between free metal ions and those bound in inert and/or stable complexes. This involved selective deposition for fractionation of Bi^{3+}, Pb^{2+}, Ni^{2+} and Cu^{2+} in the presence of varying concentrations of EDTA. Fractionation of bismuth was possible ($Bi\text{-}EDTA^-$ is inert) but in labile systems the quantitative deposition process disturbed the solution equilibria resulting in an over-estimation of the free metal concentration. In an attempted application to natural waters, problems were encountered with adsorption of fulvic acid on the furnace surface. Thus ED-ETAAS is not recommended as a method for fractionating metal-ligand species in natural systems.

The ED-ETAAS technique was successfully used for fractionation of arsenic species. The detection limit for arsenite determination from nitric acid media was 0.58 ppb (corresponding to 22 pg in a 39 μL sample), with a characteristic mass (peak absorbance) of 7.5 pg. Total arsenic was determined from media containing L-cysteine, with a detection limit of 1.3 ppb (51 pg) and a characteristic mass of 6.6 pg. The technique was used to determine As^{III} and total arsenic in two natural waters. The ED-ETAAS technique gave the same results as two comparative techniques (ETAAS and hydride generation ETAAS) provided that peak absorbance measurements were used.

ACKNOWLEDGMENTS

I am extremely grateful to my supervisor Professor Kip Powell for his support throughout the course of this work, for his hours spent reading this manuscript, and for those little thoughts about my work that popped into his head at times when I was thinking of anything but chemistry. Kip's depth of knowledge and breadth of reading has many times offered a spark in the darkness. Kip, thank-you for all your help..

I would also like to thank Professor Jarda Matousek of the University of New South Wales for his valuable input into this work. Also, Doctor Alison Downard of this department for being there at various times when I needed someone to bounce strange electrochemical ideas off while searching for explanations to the often mystifying results obtained in this project. Thank you both for your being willing to share your knowledge.

Thanks very much to the often-overlooked people without whom this research would have ground to a halt—the technical staff of this department; especially Sandy Ferguson, Wayne MacKay, Russell Gillard, John Davis and Bruce Reid. Also thanks to the staff of the Physical Sciences Library for the hundreds of interloan requests and Current Contents updates they have processed for me.

Thanks to all my colleagues and fellow students who have shared ideas, philosophies and coffee with me over the years. In particular, thanks to Vicki Smith, for sharing long hours in the depths of the cleanroom discussing our mutual fascination/phobia with/of ED-ETAAS. Thanks to the coffee-club of recent years—Martin, Kathryn, Azmi, Parveen, and Renu—for offering such a good alternative to working. Sanity amidst madness.

I also appreciate the crazy flatmates I've had—Ema, Hajar, and Justine—who, if I ever wanted to eat, made me cook dinner regardless of how busy I was. Cooking is therapeutic. I'll miss you guys when I'm gone.

I'd also like to thank Khadijah for her love and support during the first part of this project. Thank-you Reneta for being loving and loyal thoughout the final phase of this work.

Finally, I owe a great debt to my parents for allowing me the freedom to choose my path in life without resistance, and for the personal and financial support they have given me up until and during my years as a PhD student. Mum and Dad; thanks, I love you.

Contents

CHAPTER TWO: EXPERIMENTAL

CHAPTER THREE: ELECTRODEPOSITED MODIFIERS

CHAPTER FOUR: REDUCIBLE METALS IN ACID MEDIA

CHAPTER FIVE: REDUCIBLE METALS IN SODIUM CHLORIDE MEDIA

CHAPTER SIX: MERCURY DETERMINATION

CHAPTER SEVEN: METAL SPECIATION

CHAPTER EIGHT: ARSENIC DETERMINATION AND SPECIATION

Figures and Tables

CHAPTER ONE

CHAPTER TWO

CHAPTER THREE

CHAPTER FOUR

CHAPTER FIVE

CHAPTER SIX

CHAPTER SEVEN

CHAPTER EIGHT

Abbreviations used in this thesis

AAS	Atomic absorption spectrometry
AdSV	Adsorptive stripping voltammetry
ASV	Anodic stripping voltammetry
CSV	Cathodic stripping voltammetry
CV-ETAAS	Cold vapour electrothermal atomic absorption spectrometry
DC	Direct-current
DL	Detection limit
DMA	Dimethlyarsenic acid
ED-ETAAS	Electrodeposition-coupled electrothermal atomic absorption spectrometry
EDL	Electrodeless discharge lamp
EDTA	Ethylenediaminetetraacetate
ETAAS	Electrothermal atomic absorption spectrometry
FAAS	Flame atomic absorption spectrometry
FIA	Flow-injection analysis
HCL	Hollow cathode lamp
HG-ETAAS	Hydride-generation-electrothermal absorption spectrometry
HG-ETV	Hydride-generation-electrothermal vaporisation
HMDE	Hanging mercury drop electrode
HPLC	High performance liquid chromatography
ICP-AES	Inductively-coupled plasma-atomic emission spectrometry
ICP-MS	Inductively-coupled plasma-mass spectrometry
MMA	Monomethylarsonic acid
Mo	Characteristic mass
MTFE	Mercury thin film electrode
NAA	Neutron activation analysis
NHE	Normal hydrogen electrode
PDC	Pyrrolidine dithiocarbamate
ppb	Parts-per-billion ($\mu g\ L^{-1}$)
PTFE.	polytetrafluoroethylene
RSD	Relative standard deviation
SCE	Saturated calomel electrode
STP	Stabilised temperature platform
SW-ASV	Square wave-anodic stripping voltammetry
SWV	Square wave stripping voltammetry

Chapter One

Introduction

This chapter describes the development of electrodeposition-coupled electrothermal atomic absorption spectrometry; the technique that is applied throughout the rest of this thesis. Atomic absorption history and theory are outlined, as well as the limitations that led to the development of electrothermal atomic absorption spectrometry. This technique is described in detail, along with the approaches used to deal with the various interferences that can occur. The relative attributes of electrothermal atomic absorption spectrometry compared with other trace metal analysis techniques are discussed. The advantages of coupling electrodeposition to electrothermal atomic absorption spectrometry are evaluated and the literature dealing with this technique reviewed. A final section describes the scope of the present work; to further develop the technique to electrodeposition-coupled electrothermal atomic absorption spectrometry.

1.1 ATOMIC ABSORPTION: HISTORY AND THEORY

1.1.1 Atomic Spectra

In 1900, Max Planck established the quantum law of radiation absorption and emission. The quantum law states that atoms can only absorb radiation of a well-defined wavelength λ; i.e. they can only take up and release definite amounts of energy E. The relationship between the energy transition and the wavelength, where h is Planck's constant, v the frequency, and c the speed of light, is expressed as follows:

$$E = hv = \frac{hc}{\lambda} \tag{1.1}$$

Upon absorbing a quantum of energy, an atom enters an "excited" state. When the atom returns to a lower energy state, it releases the absorbed energy; usually as radiation. Because atoms can exist in many different excited states, many energy transitions are possible. Radiation is emitted at discrete wavelengths, each corresponding to a different energy transition. For atoms that are excited thermally or electrically, absorbed energy can be released as an emission spectrum. If the excitation is by optical radiation, an absorption line-spectrum is observed. Absorption spectra have fewer lines than emission spectra because in an absorption spectrum virtually all lines must come from transitions originating from the ground state.

These absorption lines are referred to as resonance lines since they come into resonance with optical radiation of suitable frequency. For any element, the resonance lines in the absorption spectrum will be common to the emission spectrum. These common lines form the basis of atomic absorption spectrometry (AAS).

Because all elemental absorption spectra are different, it is possible to select resonance lines unique to one element. Hence, from a mixture of gaseous atomic species placed in the path of a radiation source, an element can be selectively determined by measuring the radiation attenuation at this element's resonance line.

1.1.2 Absorbance

The phenomenon of light absorption has been studied for over 200 years. In 1760, Lambert set the theoretical foundations of modern absorption spectrophotometry when he expressed the relationship between incident light intensity I_o, and the transmitted light intensity I_{tr}, for light passing though a layer of thickness l. The absorption coefficient x' measures the layer's light attenuating power.

$$I_{tr} = I_o . e^{-x' l} \tag{1.2}$$

When the absorber is a solution of an absorbing substance in a non-absorbing medium, the absorption coefficient is proportional to the concentration c . The proportionality constant ε is known as the molar absorptivity of the absorbing substance.

$$x' = \varepsilon . c \tag{1.3}$$

Lambert's law was thoroughly examined by Beer in 1852, and re-written to state that absorbance (A) is proportional to the concentration of the absorbing substance, and to the thickness of the absorbing layer. This expression is now known as the Beer-Lambert law. It is usually used in atomic absorption spectrometry in the following form:

$$A = \log \frac{I_o}{I_{tr}} = \varepsilon . N_0 . l \tag{1.4}$$

where N_0 is the number of absorbing (i.e ground state) atoms in the radiation path. If the absorbing atoms are produced from an element in solution, N_0 is proportional to the element's solution concentration.

1.1.3 Atomic Absorption Spectrometry

In 1955, independent publications by Walsh,[1] and Alkemade and Milatz[2] recommended atomic absorption spectrometry as a generally applicable analytical method which combines the selectivity of atomic absorption and the linearity of the concentration-absorbance relationship. In subsequent years, it was principally Walsh and his CSIRO* coworkers who developed atomic absorption into a sensitive and highly selective analytical method. The atomic absorption spectrometers developed by the early AAS researchers contained the same basic features that are now found in modern instruments (Figure 1.1).

1.1.4 Atomic Absorption Instrumentation

The essential parts of an atomic absorption spectrometer are a radiation source, an absorbance cell/atomiser, a monochromator, and a detector which is connected to an amplifier and a recording device.

Radiation Sources: The specificity of AAS is largely due to the narrow width of the resonance lines and the fact that elemental absorption takes place over a very narrow spectral range. The ideal radiation source for AAS would provide high intensity, extremely narrow emission lines.

The most commonly used elemental emission source is the hollow cathode lamp (HCL). This uses an electric discharge between an anode and an elemental cathode to ionise an inert gas. The gas cation then strikes the cathode surface, dislodging atoms of the cathode material. Collisions with inert gas ions then excite the cathode-sourced atoms into radiating their spectral lines. Hollow cathode lamps are available for about seventy different elements, and for most, provide sufficiently intense low-noise radiation.

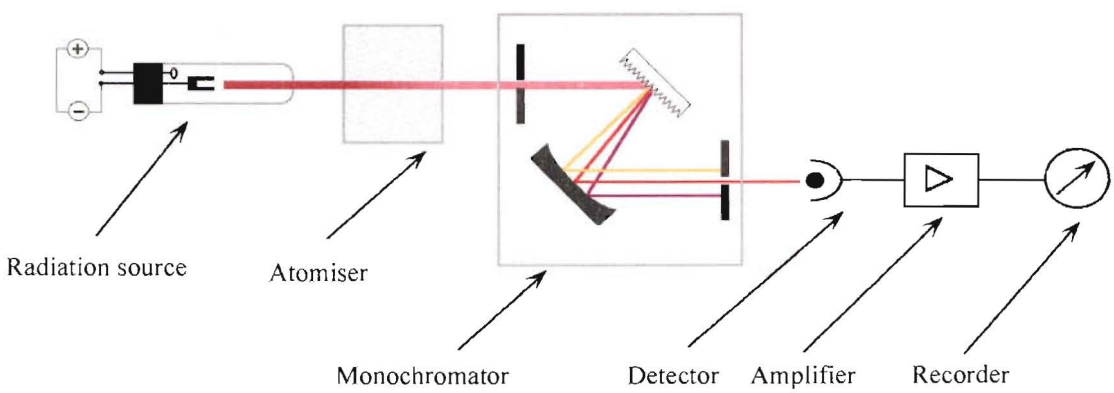

Figure 1.1 Schematic diagram of a modern atomic absorption spectrometer.

*Commonwealth Scientific and Industrial Research Organisation, Australia.

The other most common radiation source used for AAS is the electrodeless discharge lamp (EDL). This consists of a sealed quartz tube which is filled with a few milligrams of the analyte element (as pure metal, halide, or metal with added iodine) under an argon pressure of a few hundred pascal. The tube is mounted within the coil of a high frequency generator (e.g. 2400 MHz) and excited by an output from a few Watts up to 200 Watts. The filler gas forms a plasma, in which collisions with analyte vapour lead to dissociation, excitation and emission. Electrodeless discharge lamps have several advantages over hollow cathode lamps. Firstly, the emission lines are generally narrower than for hollow cathode lamps. They can be produced for all volatile elements, and they emit radiation that is orders of magnitude more intense than that emitted by hollow cathode lamps. The increased radiation intensity leads to better signal to noise ratios, and hence, better precision and lower detection limits. For some elements, especially arsenic where the detection limit is improved by an order of magnitude, electrodeless discharge lamps have almost entirely supplanted hollow cathode lamps.[3]

Atomisers: The analyte emission spectrum from the radiation source is passed through an atomiser which doubles as an absorption cell. Within the cell, the sample is present as atoms which are generated by thermal dissociation. The atomiser's most important function is to produce ground-state (i.e. absorbing) atoms from ionic or molecular analyte in the sample. Sensitivity is directly proportional to the degree of analyte atomisation, so depends strongly on atomisation efficiency. The original atomising technique used by Alkemade and Milatz[2] was to spray the sample solution into a flame using a nebuliser. This technique is still widely used, but has since been joined by others; the hydride, cold vapour and graphite furnace techniques.

It is necessary to eliminate interfering radiation emitted by the hot atomiser (flame etc). This is achieved by pulsing the output of the radiation source. The detector then receives two types of signal; an alternating one from the radiation source, and a constant one from the atomiser. An electronic filter is used to remove the constant signal, passing only the alternating signal from the radiation source to the amplifier.

Monochromators: After passing through the atomised sample, radiation passes through a monochromator before reaching the detector. The monochromator's main purpose is to separate the analytical resonance line from the many emission lines produced by the source. Another is to reject radiation generated by flame emission or by the heated graphite furnace. Light passes into the monochromator through an entrance slit, and is focused onto a diffraction grating by a collimator mirror. Radiation falling onto the grating is reflected and dispersed in a wavelength dependent arc, a portion of which is reflected by a camera mirror and passed through a variable exit slit. Depending on the type of diffraction grating used, and the width of the exit slit, monochromators can resolve a bandpass of 0.05 to 10 nm.[4] For practical purposes, a bandpass of 0.2 to 2.0 nm is sufficient to adequately resolve most elemental resonance lines.

Detectors, Amplifiers and Recorders: Radiation passing through the monochromator exit slit is measured using a photomultiplier tube. The resulting signal is then amplified and fed to a recording device. In early instruments this comprised an analog gauge and/or a chart recorder. Modern instruments generally use a dedicated microcomputer that is also used for controlling instrumental parameters and for data manipulation.

The flame atomiser-AAS used by Walsh,[1] and Alkemade and Milatz[2] is now established as a routine procedure in all branches of inorganic elemental analysis. For most metals, possible interferences are well known, and easily controlled.[5] Analysis in the mg L^{-1} (ppm) range is highly reproducible for many elements, and with quality instruments, precision of 0.2% RSD can be achieved.[6]

1.2 ELECTROTHERMAL ATOMIC ABSORPTION SPECTROMETRY

1.2.1 The Graphite Furnace Atomiser

The search for enhanced detection limits in AAS led L'vov to conceive the graphite furnace.[7] The flame atomiser is inefficient for two main reasons. Firstly, the nebuliser introduces only 1-15% of the sample solution into the flame.[3] Secondly, because of the flame's burning velocity, sample atoms are rapidly swept out of incident radiation beam. These two inefficiencies serve to limit the number of atoms in the light path at any one time, hence lowering sensitivity. L'vov sought to eliminate both of the flame's inefficiencies by using a heated graphite tube as an atomiser. In L'vov's apparatus, the graphite tube was mounted so that the beam from a hollow cathode lamp passed through tube's centre. The sample was dried onto the tip of a carbon electrode which was then inserted through a hole into the graphite tube. The sample was atomised by a dc arc and the transient atomic absorbance recorded. In this system the entire sample volatilises and most is atomised, thus removing nebuliser inefficiencies. In addition, the residence time of the sample atoms in the radiation beam is greatly increased. With an improved version of this atomiser, L'vov obtained absolute detection limits between 10^{-10} g and 10^{-14} g; better by several orders of magnitude than the limits of flame-AAS.[8] Following L'vov's early work, Massmann proposed a much simpler method for graphite furnace atomisation.[9] In Massmann's system, 50 µL of sample was introduced into a 5 cm long graphite tube through a small hole in the tube wall. The tube was then heated resistively by passing a high current (500 A) at low voltage (10 V) through it. This resistance heating permitted fine temperature control, so optimum atomisation conditions could be selected for each element. The Massmann furnace was constantly purged by a stream of argon to prevent atmospheric oxygen from oxidising the tube. This gas purging reduced the residence time of atoms in the tube, and led to detection limits an order of magnitude poorer than those obtained by L'vov. Also, Massman's atomisation time was longer because the resistance heating rate is slower than for L'vov's dc-arc atomisation. However, the simplicity of Massman's system led to it being used as the basis for modern

simplicity of Massmann's system led to it being used as the basis for modern graphite furnace atomisers which have now largely overcome the early system's deficiencies.

Graphite furnace atomic spectrometry is now generally referred to as electrothermal atomic absorption spectrometry (ETAAS). A modern electrothermal atomiser is shown in Figure 1.2.

At the heart of the modern graphite furnace atomiser is the furnace. Of the many different materials that have been used as atomisers, none has been as successful as the pyrolytically-coated graphite tube.[10] In order to ensure good sensitivity and reproducibility, the furnace must exhibit certain properties. Such requirements include: low porosity, chemical inertness, low levels of metal impurities, good thermal and electrical conductivity, high rigidity, high melting point, reasonable cost, good machinability, and low thermal expansion. As a furnace material, graphite satisfies many of these criteria, but does have problems with porosity and chemical inertness. By coating the furnace with a layer (*ca.* 30 μm thick) of pyrolytic graphite, the sample is prevented from penetrating the tube, thus reducing memory effects. The pyrolytic coating also lessens carbide formation; a problem often associated with refractory elements.

1.2.2 Graphite Furnace Operation

In principle, the graphite furnace operating protocol is simple. The furnace is clamped longitudinally between two graphite electrodes as shown in Figure 1.2. The sample is injected (usually by an autosampler) through the hole in the top of the furnace and onto the furnace wall. The furnace is then heated by passing a current between the two supporting electrodes. The furnace temperature is slowly raised to the solvent's boiling point to dry the sample ("drying" step). Then the sample is pyrolysed by raising the temperature to a point where matrix components are decomposed but the analyte is not volatilised ("pyrolysis" step).

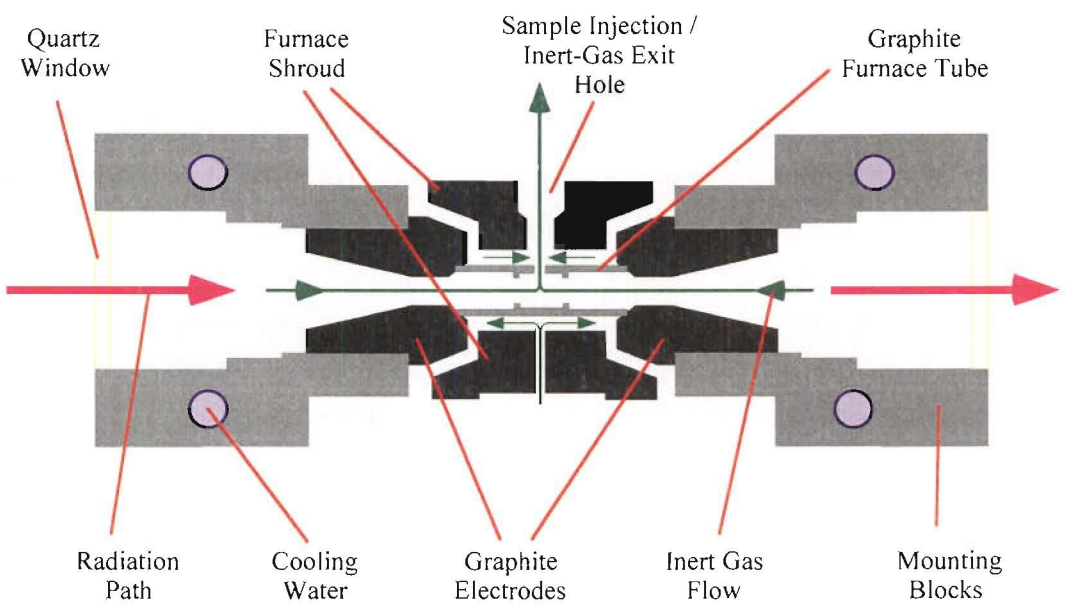

Figure 1.2 Modern electrothermal atomiser (GBC GF3000).

When pyrolysis is complete, the furnace temperature is ramped rapidly (> 1000 °C s^{-1}) to a value where the analyte is atomised ("atomise step"). During the atomise step (three to five second duration), the absorbance is measured, and the sample concentration can be read from a calibration curve. During the drying and pyrolysis steps of the temperature program, the furnace is bathed in an inert gas (usually nitrogen or argon) to prevent atmospheric oxygen from oxidising the graphite; the inert gas flow also serves to accelerate the sample drying. In order to extend the residence time of atoms within the furnace, the inert gas flow is switched off prior to atomisation. The furnace is then allowed to equilibrate for up to ten seconds before atomising.[11] A typical temperature versus time profile for the graphite furnace is shown in Figure 1.4.

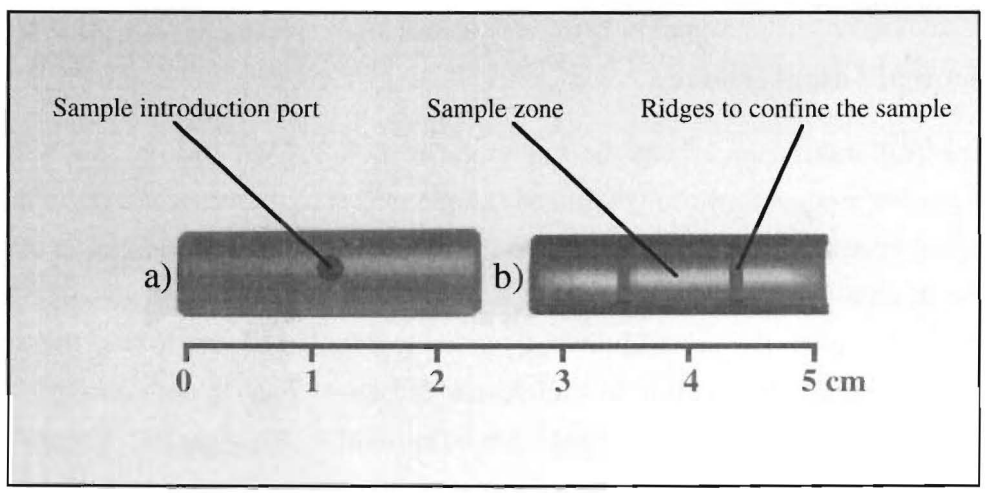

Figure 1.3 A typical pyrolytic graphite-coated furnace tube: a) top view b) longitudinal cross-section.

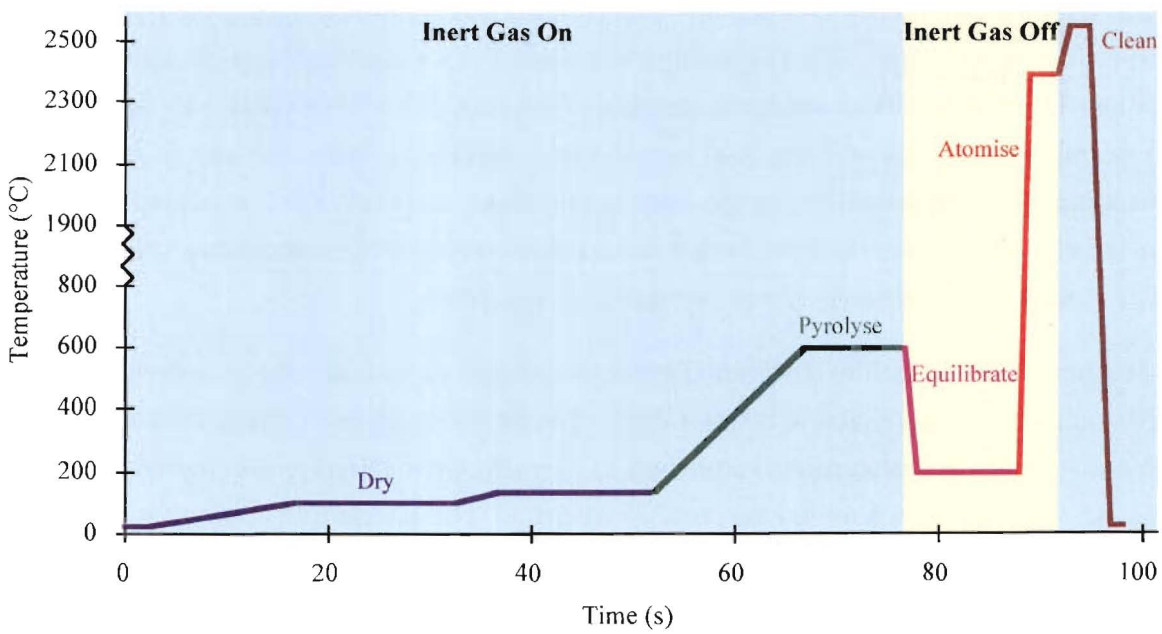

Figure 1.4 Typical temperature versus time profile for graphite furnace atomisation.

Although the operating principles for the graphite furnace atomiser are simple, there are many reasons why measurements may be inaccurate. Such inaccuracies are often associated with sample matrix components (interferents) which enhance or diminish the production of atoms, relative to aqueous standards.

1.3 INTERFERENCES IN ETAAS

Two classes of interference are encountered in ETAAS. Spectral interferences generally arise when absorption by an interfering atomic or molecular species overlaps, or lies so close to the analyte absorption that resolution by the monochromator becomes impossible. Chemical interferences result from various chemical interactions that suppress or enhance analyte volatilisation and atomisation.

1.3.1 Spectral Interferences

Various spectral interferences can be encountered in ETAAS. Most can be traced to molecular species produced by the volatilised sample matrix, however some are a direct result of overlapping spectral lines. In the latter case for example, a vanadium line at 308.211 nm interferes with an aluminium analysis at 308.215 nm. Because it is not possible to resolve such close wavelengths, the aluminium analysis is accomplished employing the 309.27 nm aluminium line instead. In addition to sample-derived interferences, emission lines from the HCL or EDL filler gas (neon or argon) may fall within the spectral bandpass of the monochromator. Such "direct spectral overlaps" are rare, and can be predicted from tables of overlapping elemental resonance lines.[4] More common and more difficult to control are the interferences caused by sample matrix components.

In ETAAS, sample matrix components cannot always be removed during the pyrolysis step. During the atomise step, any remaining components are volatilised along with the analyte. Problems arise when these components persist as molecules or particulates in the gas phase. For example, when determining lead in a sodium chloride medium, the lead is atomised and the sodium chloride volatilised at the same temperature; *ca.* 1100 °C. Radiation scattering by non-volatilised particles, or broad-band molecular absorption by concomitant species such as $NaCl_{(g)}$ gives rise to *non-specific* or *background* absorption.

In practice, it is difficult to differentiate the two causes of background absorbance, however the same measures are taken to counter each. The first strategy is to distinguish between analyte and interferent (background) absorbances by using their differing spectral characteristics. This approach is known as *background correction.* The alternative strategy is to alter the sample matrix in such a way that the analyte and interfering species are no longer volatilised at the same temperature. This technique, known as *chemical modification*, is discussed in section 1.3.2.

1.3.1.1 Background Correction

Several different types of background correction system are used in ETAAS. All are variations on the same concept. The absorbance at the wavelength of the analytical line is the sum of the atomic absorbance and of all other interfering absorbances. If the interferent absorbance can be measured separately (eg. at another wavelength), then the atomic absorbance can be calculated by difference. The two most popular methods used to achieve this are the *Continuum Source*, and *Zeeman* background correction systems.

Continuum Source Background Correction

Light dispersion by particulates and absorption by molecular species is generally across a broad band whereas atomic absorption is restricted to a narrow resonance line. This difference can be exploited by passing radiation from two different light sources alternately through the graphite tube atomiser. One source, a deuterium lamp, provides a continuous source of radiation across the ultraviolet spectrum (190-350 nm). The other source, an EDL or HCL provides the atomic resonance line. Because the monochromator band pass is wide relative to the resonance line, the fraction of the continuous source radiation absorbed by analyte atoms is negligible. Therefore the absorbance measured using the continuous source represents background (molecular) absorbance. The absorbance measured at the resonance line using the atomic source, represents the sum of the background and atomic absorbances. The atomic absorption is calculated by difference.

This system works well within certain limits. Because the deuterium arc lamp used as a continuum radiation source has a low output in the visible region, background correction is limited to the ultraviolet (although this is where molecular absorption is prevalent). Also, if the analyte concentration is high, then the amount of continuum radiation absorbed by analyte atoms becomes significant, and may result in overcorrection. For this reason sample absorbances should be kept below 0.7 absorbance units, diluting when necessary. The continuum source method cannot adequately compensate for highly structured background absorption. Also, it is limited to a maximum background absorbance of around 1.0 absorbance units,[3] a value easily reached, given that matrix components are often present at more than 10^6 times the analyte concentration.

Zeeman Background Correction

When an atomic vapour is exposed to a strong magnetic field (1-10 kG), the electronic energy levels in the atoms are split. This splitting leads to several closely spaced spectral lines arising from each principal electronic transition. The lines differ from one another by about 0.001-0.005 nm with the sum of the lines' intensities being exactly equal to the original line from which they were formed. This phenomenon, known as the *Zeeman effect*, is general for

all atomic spectra. The simplest splitting pattern, which is seen for singlet transitions leads to a central, or π, line at the same wavelength as the original line, flanked by two equally spaced σ lines. This is known as *normal Zeeman splitting*. Spectral lines which arise from non-singlet transitions split into more than three components; *anomalous Zeeman splitting.*

When Zeeman splitting occurs, not only do the spectral lines split, but the radiation is also polarised. The plane of polarisation depends on the direction of the magnetic field relative to the direction of observation (for ETAAS, this is always along the axis of the radiation beam). If the field is applied at right angles to the radiation beam, the π component (of the relevant energy transition) is polarised in a plane parallel to the magnetic field and the σ components are polarised in a plane perpendicular to the magnetic field. Known as the *transverse Zeeman effect*, this is the arrangement usually used for background correction in ETAAS. The alternative situation occurs when the magnetic field is parallel to the radiation beam. In this case, known as the *longitudinal Zeeman effect*, the π component is missing from the spectrum and only the σ components (which are circularly polarised) are observed.

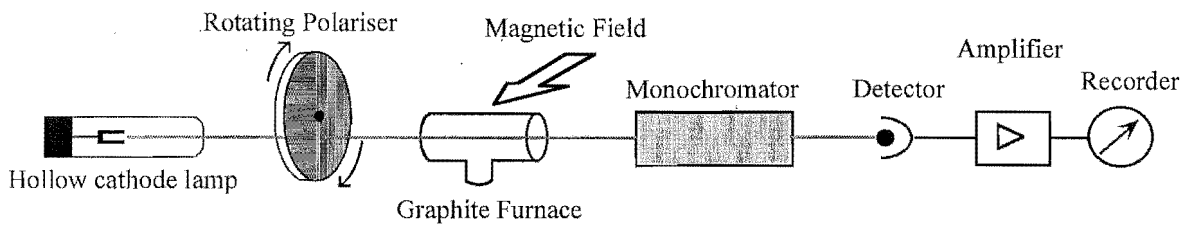

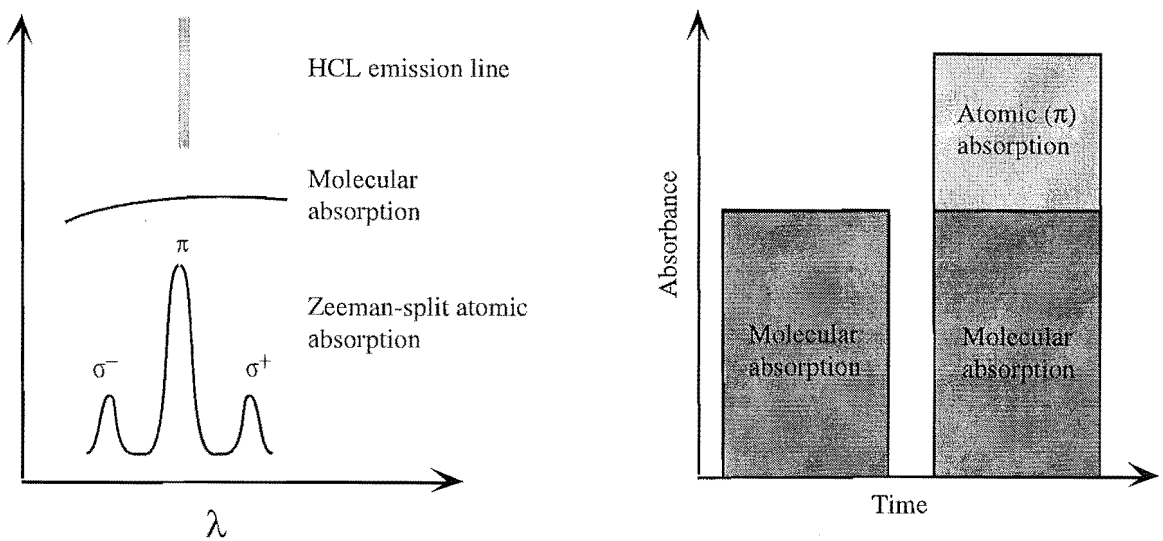

Relative wavelength distributions for atomic emission (HCL), atomic absorption (normal Zeeman splitting) and molecular absorption.

Radiation polarised perpendicular to magnetic field

Radiation polarised parallel to magnetic field

Figure 1.5 Inverse Zeeman-effect background correction— transverse magnetic field configuration.

Because the Zeeman effect is a consequence of splitting energy levels within the atom rather than the actual spectral lines, the magnetic field must be applied directly to a cloud of atoms. There are two possibilities in ETAAS; the magnetic field can be applied to the atom cloud in the radiation source (*direct Zeeman effect*), or to the atom cloud in the atomiser (*inverse Zeeman effect*). Most ETAAS instruments use the inverse background effect because conventional radiation sources perform poorly when placed in strong magnetic fields.

There are several ways of using the Zeeman effect for ETAAS background correction, however practical considerations have made one approach particularly popular. In this system, (shown in Figure 1.5) a rotating polariser is placed between the radiation source and the furnace. The polariser alternately splits the radiation beam into two components, plane polarised at 90 ° to each other. The furnace is placed in a magnetic field, splitting the energy levels of gas-phase analyte atoms. Since the radiation source emits the original (unsplit) resonance line, this radiation cannot be absorbed at the wavelengths of the σ components. The π component for the analyte can only absorb when the radiation is polarised in a direction parallel to the magnetic field. Thus when the radiation is polarised parallel to the magnetic field, both atomic (π) and background absorption are measured. When the radiation is polarised in a direction perpendicular to the magnetic field, the π component for the analyte no longer absorbs and only the background absorbance is measured. As for the continuum source method, the atomic absorption is calculated by difference.

Zeeman-effect background correction can correct for very high background absorbances (up to 2.0 absorbance units[3]) and for very closely overlapping spectral features. Further, the correction is made at or very close to the atomic absorption line, allowing correction for highly structured backgrounds. Although clearly superior to the continuum source method, Zeeman background correction still has limitations. A variety of "Zeeman-specific" effects and interferences can arise. Such anomalies include: spurious signals indirectly caused by thermal gradients around the atomiser,[12] spectral interferences induced by splitting of molecular absorption bands,[13] and rolled-over calibration curves which can occur if σ and π components are insufficiently separated.[3] The complexities of the Zeeman system require an operator who has a thorough understanding of Zeeman background correction and its possible effects. Furthermore, a Zeeman-effect ETAAS system is more expensive than other ETAAS systems because of the additional equipment required.

1.3.2 Chemical Interferences

Chemical interferences are a major problem in ETAAS. These interferences are caused by interactions between the analyte, and the sample matrix components, furnace, or sheath gas. However, all lead directly or indirectly to a lower atomic population on atomisation and hence to decreased sensitivity.

Chemical interferences can be divided into those that originate in the condensed phase and those that originate in the vapour phase. Condensed phase interferences include:

i) Analyte losses during pyrolysis, and early volatilisation during the atomise step due to volatile compound formation.

ii) Incomplete volatilisation during the atomise step due to occlusion, or formation of refractory compounds.

iii) Processes that change the rate at which the analyte is volatilised.

Vapour phase interferences include changes in the rate at which the analyte is removed from the furnace, and formation of analyte molecular species in the gas phase. For example, reactions of analytes with oxygen, nitrogen and carbon to form oxides, nitrides and cyanides. Vapour phase interferences commonly relate to dissociation equilibria of element related components. For example, when chlorides are present during lead atomisation, $PbCl_{2(g)}$ occurs at temperatures below 900 °C, however $Pb_{(g)}$ is the preferred species at temperatures above 1200 °C.[3] The rate at which the chloride is converted to the metal affects analytical sensitivity.

Many types of chemical interferences have been documented and reviewed,[3,14,15] but there is one that deserves special mention. Of all the interferences encountered in ETAAS, the most significant are those arising from chloride. The chloride ion is a common species in many media, especially in marine samples and in biological extracts and fluids. Not only is the chloride ion ubiquitous, but it directly or indirectly suppresses the analytical absorbances for many elements.[3] The mechanisms by which it does so have been the target of several recent studies.[16-18] There is a general consensus that chloride interferes through a variety of independent mechanisms. Because these are common to many other interferents, the chloride mechanisms serve to illustrate typical modes of chemical and spectral interference.

The most severe chloride interferences are observed when metals which form chlorides with low melting points (e.g. lead and cadmium) occur in chloride-containing media. During the pyrolysis stages the volatile metal chlorides may be swept from the furnace by the sheath gas; they can also condense on the cooler ends of the furnace.* Low temperature volatilisation can partly be countered by reducing the pyrolysis temperature to retain the analyte chloride. However, this creates further problems when the chloride matrix components and analyte are co-volatilised on atomisation.

On atomisation, the furnace is heated directly by a high current, but the atmosphere inside the furnace is only heated indirectly through convection and radiation from the furnace wall. Because of this indirect heating, there is a temporal lag between the temperature of the

*For longitudinally mounted furnaces, the tube ends are cooler than the centre because they are in contact with the water-cooled electrodes.

furnace wall and the atmosphere inside the furnace. Therefore, when analyte chlorides are volatilised from the furnace wall, they enter a gas phase of a lower temperature. If the temperature is too low, the analyte chloride may be expelled from the furnace before it can be atomised. In some cases, where the analyte is volatilised in atomic form, it may react with chloride species (especially hydrogen chloride) in the cooler gas phase to form molecular species —thus reducing the atomic population and hence absorbance. This has a two-fold effect on analysis. Firstly, molecular chloride formation lowers the apparent atom concentration, decreasing sensitivity; and secondly, the molecular absorbance adds to the background that must be subtracted by the background correction system. Chlorides condensed in the furnace ends during drying and pyrolysis contribute to this, but with one additional problem. Because the furnace-end temperature lags behind that of the middle, species at the furnace ends are volatilised and atomised later than species in the middle. This change of atom supply rate, serves to broaden the analytical absorbance profile and can also decrease sensitivity. In extreme cases, double absorbance peaks, or sample carryover have been observed. Cumulatively, the extensive problems encountered with chloride interference are so severe that in some cases, such as seawater analysis, the sodium chloride content is too high to allow the direct determination of many metals unless remedial measures are taken.

Three different approaches are commonly used to combat chloride and other chemical interferences: the *stabilised temperature platform*, *chemical modification*, and *matrix removal* methods.

1.3.2.1 The Stabilised Temperature Platform

In L'vov's original graphite furnace atomiser,[7] the sample was atomised into a pre-heated (isothermal) furnace; a furnace design that suffered from fewer interference problems than are encountered with the Massmann-type furnace.[19,20] This is largely because in an isothermal furnace, the sample and concomitant interferents are atomised into an atmosphere of sufficient temperature to effect complete dissociation. Several isothermal furnace designs have been proposed. Woodriff and Ramelow[21] introduced the sample into a preheated tube using a small graphite cup, while Manning *et al.*[20] dried the sample onto a tungsten wire which was then introduced to the preheated furnace. An alternative approach was taken by Chakrabarti *et al*,[22] who used rapid furnace heating (up to 100 K ms^{-1}) to reduce the lag time between heating the furnace tube, and the furnace atmosphere. Due to its simplicity, the most commonly adopted means of approximating isothermal furnace conditions is the *L'vov* or *stabilised temperature platform* (STP). First suggested by L'vov,[23] the stabilised temperature platform is a small piece of pyrolytic graphite which is installed in the graphite furnace as shown in Figure 1.6. Graphite is a poor thermal conductor, and because the platform is in minimal contact with the furnace, it is heated indirectly by the furnace gases rather than by the furnace walls. Because of this indirect heating, the temperature of the platform lags behind that of the furnace gases and walls. Sample deposited on the platform is volatilised into a hotter (and approximately isothermal) atmosphere, thus minimising vapour-phase interferences.

Although isothermal furnace designs have greatly reduced the effects of many interferents, they still do not prevent the loss of volatile samples during pyrolysis. To seek a solution to this problem, analysts have turned to chemical modification.

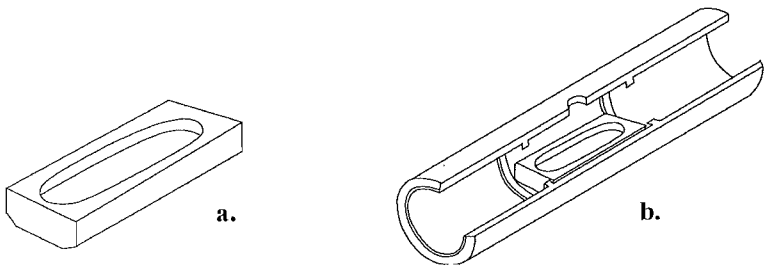

Figure 1.6 (a) The stabilised temperature platform, and (b) cutaway view of the platform installed in the furnace.

1.3.2.2 Principles of Chemical Modification

The objectives of chemical modification are to increase analytical sensitivity, and/or to reduce the effects of interferents. These are achieved by adding an excess of a reagent (modifier) which chemically alters the analyte, the sample matrix, or the furnace surface. There are two principal mechanisms by which chemical modification can improve the properties of an analyte.

Firstly, adding an excess of modifier ensures that the analyte is all present in the same chemical form and is atomised via the same mechanism. Usually, such a modifier includes an anion that forms a thermally stable compound with the analyte. A common example of this type of modification is the addition of nitric acid to samples prior to analysis. Unless high concentrations of other matrix components (e.g. chloride ion) are present, the modification ensures that the analyte is all present as a nitrate. This increases thermal stability for many volatile analytes, and promotes uniform atomisation characteristics.

Secondly, modification can be used to decrease analyte volatility; this "analyte stabilisation" has numerous beneficial effects on sensitivity and on interference reduction.

(i) Reduced analyte volatility prevents analyte losses and transport in the furnace during the pyrolysis stage.

(ii) When the analyte is thermally stable, higher pretreatment temperatures can be used. This permits more efficient interferent removal during the pyrolysis stage.

(iii) For a thermally stabilised analyte, atomisation is delayed until higher temperatures; at this point, furnace conditions are closer to isothermal. The increased temperature gives improved dissociation of volatilised species and hence, reduces vapour phase interferences and improves sensitivity.

(iv) When modification increases analyte stability relative to that of interferents, there is a greater temporal separation between the analyte and background signals on atomisation. This permits more effective background correction and reduces the likelihood of interfering gas phase reactions between the analyte and other matrix components.

There are a variety of mechanisms by which a modifier can thermally stabilise an analyte. The mode of action generally depends on the type of modifier. Tsalev *et al.*[24] have recently proposed classifying inorganic matrix modifiers into three main groups.

Group 1: Includes Mg, Ca, Sr, Sc, Y, La, Ba, Ce and Al. In the graphite furnace, up to temperatures of 1300-2000 °C, these modifiers are present as refractory oxides. At higher temperatures, they form salt-like carbides. These metals probably stabilise analytes by forming mixed oxides between the analyte and the modifier. Thus the analyte is occluded within the refractory bulk matrix of modifier.

Group 2: Includes Ti, Zr, Hf, V, Mn, W, Fe, Co, Nb and Cr. The oxides of these modifiers are transformed to metal-like carbides at lower temperatures than the first group of metals. Analyte stabilisation is probably effected by occlusion within refractory modifier oxides at low temperatures before the modifier begins to form carbides.

Group 3: "Metal" modifiers, include: Ni, Cu, Rh, Pd, Ag, Ir, Pt, Au, and Ru. Salts of these metals are reduced to elemental form at relatively low temperatures, generally below 1000 °C. These modifiers are thought to thermally stabilise analytes by forming solid solutions and/or analyte-modifier compounds that are entrapped within the bulk modifier.

A number of organic modifiers such as ascorbic acid, EDTA and Triton X-100 have also been used successfully. Organic modifiers work in different ways depending on their class. Strong complexing agents such as EDTA displace chloride from the analyte, thus preventing low temperature loss of volatile chlorides.[25] Modifiers such as ascorbic acid are believed to work by assisting analyte reduction (to metallic form). Thermal decomposition of the modifier during pyrolysis, forms carbon monoxide and active carbon which are dispersed with the analyte. Analyte reduction by the active carbon leads to enhanced atomisation kinetics and hence improved sensitivity.[26]

An alternative approach to analyte stabilisation is to promote the atomisation of volatile elements, before matrix vaporisation begins. This method allows temporal separation of the analyte and background signals. For example, Guevremont[27] used a citric acid modifier to directly determine cadmium in seawater. Modification was effected by mixing the seawater sample with 0.1% (w/w) citric acid solution. Upon analysis, sharp cadmium absorption peaks were obtained with maximum absorbances at 600 °C; the background absorbance did not become significant until temperatures above 900 °C. The authors used the same approach to determine zinc in seawater.[28] A citric acid concentration of 0.5% (w/w) produced zinc peaks with maxima at 650 °C; the background absorbance did not become large until temperatures above 1000 °C.

Other reported analyte modifications include decreasing the thermal stability of non-volatile and carbide-forming elements. For such elements, adding suitable modifiers increases sensitivity, and allows reduced atomisation temperatures and durations—resulting in increased furnace lifetimes. Nater *et al.* successfully applied this technique to aluminium determination.[29] Addition of a fluoride modifier promoted aluminium atomisation as fluoride at 1630 °C. The atomisation temperature (using the same experimental setup) of the more usual aluminium oxide was estimated at 1785 °C. A similar technique was used by Scott *et al.* to determine molybdenum.[30] A fluoride modifier decreased the molybdenum appearance temperature, and increased sensitivity by as much as 80%; interference from biological sample matrices was also reduced.

As an alternative to modifying the analyte properties, interferences can be reduced by altering sample matrix properties. The classical approach to matrix modification has been to convert interfering concomitants into volatile species that are more readily eliminated during the pyrolysis stage. An example of this, is the addition of ammonium modifiers to chloride-containing samples to promote ammonium chloride formation; this sublimes at a temperature of only 340 °C, compared to sodium chloride which boils at 1413 °C.[31]

Properties of Chemical Modifiers

In addition to its modifying properties, a useful chemical modifier must have several other attributes.

(i) The modifier must be available in a highly pure form so that it doesn't contribute trace amounts of analyte to the analysis.

(ii) The modifier must not contain an element that may be a future analyte. Some modifiers irreversibly contaminate the graphite parts of the atomiser and cannot be determined at a later stage as analytes. An example of such a modifier is nickel, which is also a routinely determined element.

(iii) The modifier should not contribute any background absorption of its own. For example, phosphate-containing modifiers which were popular in the early development of ETAAS, produce a UV spectrum that often requires Zeeman-effect background correction.[24]

(iv) Some modifiers such as lanthanum have been shown to corrode graphite.[32] The change in surface morphology degrades long-term stability, and shortens furnace life. Such modifiers are less than ideal.

(v) Modifiers should be non-toxic; reagents such as barium, chromium, manganese and thorium, which produce toxic or carcinogenic vapours are undesirable.

(vi) Some modifiers are prone to hydrolysis and are difficult to keep in solution. The ideal modifier is chemically stable.

In addition to the afore-mentioned properties, the ideal modifier would be applicable across a wide range of elements and sample matrices. Since the inception of ETAAS, scores of prospective modifiers have been suggested and trialed, however, most of these modifiers have fallen short in one or more aspects of their performance.* The fact that so many possible modifiers exist, suggests in itself that selecting a chemical modifier for a particular analytical problem is a demanding task. To simplify modifier selection and to reduce the range of modifiers required, a popular goal has been to identify a chemical modifier that is effective across a wide range of applications.

Research over the past ten to fifteen years has determined that a "universal modifier" does indeed exist. Palladium, and combinations of palladium with other metals (or their salts) have been shown to thermally stabilise most volatile analytes (in a variety of matrixes) by hundreds of degrees, thus improving sensitivity and reducing interferences for many elements.[36] Although hailed as a universal, and therefore general purpose modifier, the performance of palladium is not necessarily inferior. For many elements, palladium is demonstrably superior to alternative, more specialised modifiers.[37] Thus, for many applications, palladium has become the modifier of choice. A more detailed discussion of palladium modifiers and their modes of action is given in section 3.1.

1.3.2.3 Matrix Separation

Background correction and chemical modification aim to minimise interferent effects during analysis. The alternative approach is to separate the analyte from the sample matrix before analysis takes place. This can readily be achieved using classical means such as solvent extraction, or ion exchange. Such techniques effectively separate the analyte and sample matrix, and can also be used to preconcentrate the analyte. Unfortunately, these processes are time consuming, prone to contamination, and can also generate hazardous wastes.[38] An alternative is to separate analytes from sample media by electrodeposition. *Ex-situ* electrodeposition techniques can suffer from the same disadvantages as the classical separation methods (cumbersome and prone to contamination) however, recent advances using *in-situ* deposition have overcome these difficulties. A full discussion of electrodeposition-coupled ETAAS is given in section 1.5.

---

*A discussion of the many modifiers that have been proposed, their uses, properties, and their modes of action, is beyond the scope of this introduction. However, for further information the reader is directed to several excellent reviews on chemical modifiers. Modifiers in general have been reviewed by Carnrick *et al*,[33] Ni and Shan,[34] and Tsalev *et al*.[24] Organic modifiers have been recently reviewed by Volynskii.[25] Tsalev has collated a bibliographic index of articles devoted to various aspects of chemical modifiers published between 1973 and 1989.[35]

1.4 ETAAS: RELATIVE ATTRIBUTES

Trace analysis deals with analytes present at the part per million (ppm) level or below. In the past, such concentrations were difficult to quantify because the necessary technology was not available. Nowadays however, there are several ultra-sensitive analytical techniques that can be used to study trace elements in biological systems and the environment. These include neutron activation analysis (NAA), anodic stripping voltammetry (ASV), ETAAS, inductively-coupled-plasma atomic emission spectrometry (ICP-AES) and inductively-coupled-plasma mass spectrometry techniques (ICP-MS).

Neutron activation analysis is a multi-elemental technique that can be used to determine as many as seventy elements with great precision and accuracy.[39] It is one of the most sensitive analytical techniques known, with detection limits as low as 10^{-12} g for some elements.[40] Samples irradiated with neutrons release gamma-radiation which is specific for each irradiated nucleus. Neutron activation analysis involves irradiating samples with neutrons and quantifying the resultant gamma-radiation emissions. There is little need for sample pretreatment and chemical interferences are not a problem. Unfortunately, the technique requires highly trained technicians and a source of high-energy thermal neutrons, usually found in the form of a nuclear reactor; a facility that is not readily available to many analysts. This requirement is probably the main reason why neutron activation analysis has not been adopted as a routine analysis method.

There are two techniques based around the inductively-coupled plasma (ICP). The first, ICP-atomic emission spectroscopy (ICP-AES) compares favourably with flame atomic absorption spectrometry (AAS). ICP-AES is relatively interference-free, and although it is only slightly more sensitive than AAS, it is much faster because many elements can be determined in one analysis. Unfortunately, for many environmental applications, ICP-AES like AAS, is insufficiently sensitive.

The second technique based on the inductively coupled plasma is ICP-mass spectrometry (ICP-MS). This possesses both the multi-element capabilities of ICP-AES and extremely high selectivity and sensitivity. For some elements, the detection limits are similar to those found in neutron activation analysis. ICP-MS is free of spectral interferences, but sample matrix interferences are a problem. The carrier gas, usually argon, forms an array of vapour phase combinations with materials from the matrix, including oxygen, hydrogen, chlorine, nitrogen, phosphorus and more.[41] Any isotopes present that are nearly the same mass as analyte isotopes cause problems. Thus ICP-MS should only be used by experienced analysts. In addition, ICP-MS instrumentation is very expensive, and because of high argon usage, incurs high running costs. For these reasons ICP-MS is restricted to specialist laboratories.

The two remaining techniques, ASV and ETAAS have quite different attributes. However, both use readily available instrumentation and have been widely accepted as routine methods for trace metal analysis. In situations where both techniques are available, the choice of method is dictated by the element to be determined, the sample matrix and whether any other information with respect to analyte speciation is required.

ASV using pulsed stripping methods is an extremely sensitive technique with detection limits below 0.01 ppb for some elements.[42] Other advantages of ASV include:

- an *in-situ* preconcentration step which separates the metallic analyte from its matrix
- ready analysis of samples in high salt matrices such as biological digests and sea-water[43]
- simultaneous analysis for up to four elements
- the possibility of speciation studies as the technique is only sensitive to labile ions.

As with all techniques, ASV has its disadvantages. It requires handling, use, and disposal of metallic mercury. If solid metal electrodes are used in place of mercury, irreproducible electrode surfaces degrade the analytical precision. In samples where a strong electrolyte is not present, one must be added, thereby increasing the risk of sample contamination. The minimum sample volume is around five millilitres, so smaller samples must be diluted to volume.

The biggest drawback of ASV lies in the limited number of analytes that can be determined by the technique. Suitable analytes must be capable of forming an amalgam when reduced, and the analyte must also be oxidised reversibly at a potential lower than that for mercury. Metals such as Ni or Co which don't display reversible electrochemical behaviour at the mercury electrode are also beyond the capabilities of ASV. Such metals can be determined using adsorptive stripping techniques that incorporate electro-active ligands (AdSV). While adsorptive stripping can yield extremely low detection limits (10^{-8}-10^{-10} M),[41] the different analytical conditions required for each element demand specialist knowledge of the analyst. Thus AdSV is used more as a research technique than a routine analysis method.

For ASV analysis, the analyte must be reducible at the mercury electrode surface. Thus the analyte must be present in a labile form such as the simple aqua ion. To obtain a total metal analysis, metals that are strongly complexed, or bound to proteins or colloids must firstly be released by acid digestion and/or UV photolysis. This may also be necessary to prevent macromolecules in the sample from 'poisoning' the electrode surface.[44] Another major disadvantage of ASV is its low resolution, which can result in a high concentration of one analyte masking a lower concentration of another.

ETAAS is able to measure as little as 10^{-10}-10^{-13} g of analyte in samples of between 0.5 and 30 μL.[39] *In-situ* decomposition (pyrolysis) to release metal bound in complexes, proteins and organics dictates that the technique measures only total metal content. Thus, speciation

within a sample is of little relevance; it is neither accessible nor a source of interference. As many as 70 elements can be determined using ETAAS, a far greater range than is possible by ASV (20 elements). The other major advantage of ETAAS over ASV is its ease of automation. Microprocessor controlled ETAAS systems complete with automated sample handling and injection have been available since the mid 1970's whereas similar autosampler instruments for ASV have only recently become available. Although ETAAS has become a standard analytical method over recent years, there are still samples that present problems—even when using Zeeman background correction, furnace modifiers, and the stabilised temperature platform. In high chloride matrices such as seawater or blood, determination of volatile elements* and elements that form volatile chlorides is difficult[45] and requires prior dilution[46] or matrix separation.[47,48] This limitation on an otherwise versatile technique has been the subject of a great deal of research.

One promising approach that has been used to counter analyte volatility problems, is to separate the analyte from its sample matrix by electrodeposition prior to ETAAS analysis. The analyte can be deposited onto an electrode which is then removed from the sample matrix and placed into an electrothermal atomiser for analysis. The electrode can be a wire with a high melting temperature (e.g. tungsten), carbon, or a graphite furnace tube. Alternatively, the electrodeposition can be carried out *in-situ* with the electrode installed in, or used as the atomiser. Full reviews of *ex-situ*, and *in-situ* electrodeposition methods for ETAAS are given in sections 1.5.2 and 1.5.3 respectively.

1.5 ELECTRODEPOSITION-COUPLED ETAAS

1.5.1 Electrodeposition

1.5.1.1 Electrodeposition Theory

Electrodeposition is well established as a preconcentration method and forms the basis of such important analytical techniques as anodic stripping voltammetry and potentiometric stripping analysis. The electrodeposition process is a complex interaction of many variables including the nature of the analyte and its concentration, the material and size of the electrode, and the deposition potential and current density. However, there are several steps that are common to all electrodeposition processes. These processes are summarised overpage and in Figure 1.7.

---

*A number of elements that are volatilised even in the absence of a matrix, at temperatures below 1000°C, are commonly referred to as "volatile elements".[34,37] Elements in this category generally form volatile chlorides. This group includes such elements as antimony, arsenic, bismuth, cadmium, lead, selenium, tin, and thallium.[49] Conversely, metals which have very high melting points, or form refractory compounds (particularly carbides) in the furnace, are referred to as "refractory elements".

(i) Diffusion of ions in solution to the electrode surface.
(ii) Electron transfer at the electrode surface.
(iii) Partial or complete loss of the solvation sheath, resulting in ad-atom formation.
(iv) Surface diffusion of ad-atoms.
(v) Clustering of ad-atoms to form critical nuclei on the electrode surface.
(vi) Development of crystallographic and morphological characteristics of the deposit.

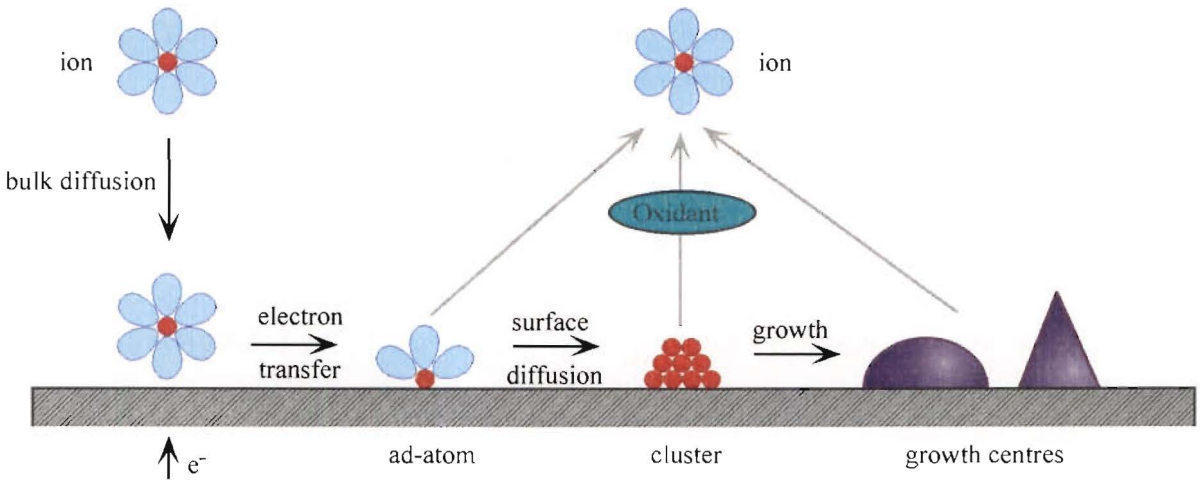

Figure 1.7. Some of the steps involved in metal electrodeposition on a solid electrode

For electrodeposition to occur, the applied potential must be of sufficient magnitude to effect reduction. The equilibrium potential for the metal ion in solution can be calculated according to the Nernst equation:

$$E_{eq} = E^0 + \frac{0.059}{n} \log \frac{a_{Ox}}{a_{Re}} \tag{1.5}$$

where E^0 is the standard electrode potential, n is the number of electrons involved in the half-cell, a_{Ox} is the activity of the metal ion at the electrode, and a_{Re} the activity of the reduced species at the electrode surface[50]. When the reduced species (Re) is a solid, a_{Re} is approximately equal to one. Hence E_{eq} is dependent on a_{Ox}, and therefore to the initial concentration of the metal ion in solution.

Having selected a suitable deposition potential, the rate controlling step for a direct reduction process is generally diffusion of ions from the bulk solution to the electrode surface where reduction takes place. The region next to the electrode surface that has been depleted of metal ions (by reduction) is known as the *Nernstian* or *diffusion layer*. Stirring the solution decreases the thickness of this layer. If the solution is stirred sufficiently quickly, the diffusion layer thickness can be reduced to as little as tens of microns.[51] In this situation, the electrodeposition rate for a simple first-order process can be calculated for the reduction of species *ox* to species *re*.

$$ox + n.e^- \rightarrow re \tag{1.6}$$

Assuming that a linear concentration gradient in *ox* is set up across a diffusion layer of constant thickness, and the potential of the working electrode is sufficiently negative that the concentration of *ox* at the electrode surface is (essentially) zero, then the initial current *i* is given by equation 1.7,

$$i = nFAk_D C^*_{ox} \tag{1.7}$$

where F is the Faraday constant, A the electrode surface area, C^*_{ox} the initial bulk concentration, and k_D the mass transport rate constant.

The number of moles of *ox* reduced is related to the charge transferred by

$$dn_{ox} = -\frac{dQ}{nF} \tag{1.8}$$

Using the two relations $\mathrm{d}Q = i\mathrm{d}t$ and $\mathrm{d}n_{ox} = V\mathrm{d}C_{ox}$ (where V is the solution volume), the change in bulk concentration on passage of current for a time interval $\mathrm{d}t$ is

$$\mathrm{d}C_{ox} = -\frac{i}{nFV}\mathrm{d}t \tag{1.9}$$

By substituting equation 1.7 for i, it can be shown that

$$\mathrm{d}C_{ox} = -\frac{Ak_D C^*_{ox}}{V}\mathrm{d}t \tag{1.10}$$

and hence by integration,

$$C_{ox}(t) = C^*_{ox} e^{-kt} \tag{1.11}$$

where

$$k = k_D \frac{A}{V} \tag{1.12}$$

Thus, the bulk concentration C_{ox} is expected to decrease exponentially at a rate proportional to the rate of mass transport, and to the ratio of the electrode area to the solution volume.[51] Therefore, maximum deposition rates are achieved using efficient stirring, and high area to volume ratios.

1.5.1.2 Limits of Electrolytic Preconcentration

While the first-order kinetic model works well for relatively high metal concentrations ($\geq 10^{-6}$ M), the situation becomes more complicated at lower concentrations. At high metal concentrations, deposition occurs rapidly relative to competing dissolution processes. However, as the initial concentration is lowered, the deposition rate also decreases and the rate of dissolution promoted by chemical oxidants becomes significant. Sioda has modelled

electrodeposition from dilute solutions (<10^{-7} M) and has calculated limits for electrolytic pre-concentration from these solutions.[52-54] He describes the time dependent concentration of the metal ion in solution according to equation 1.13[55]

$$-\frac{dC_{ox}}{dt} = -s(k_1 C_{ox} - xk_2) \tag{1.13}$$

where s is defined as $s=A/V$; the *specific area* of the electrolytic cell, k_1 is the rate constant for deposition, and k_2 the rate constant for dissolution. The time-dependent variable x, is the fraction of the total electrode area (A) that is covered by metal deposit. This is relevant because the rate of dissolution is proportional to the fraction of the electrode surface area that is covered.[56]

At long electrolysis times ($t \rightarrow \infty$), the concentration approaches an equilibrium value C_{eq}, which is the steady state equilibrium concentration of the metal.[52] Equation 1.13 can be integrated for two different limiting cases. The first is where the initial concentration of metal is very low, and there is not enough to cover the electrode surface with a monolayer. In this situation, Sioda calculates an equilibrium concentration that depends on the initial metal concentration (equation 1.14)

$$C_{eq(1)} = \frac{C_{ox} p k_2}{s k_1 + p k_2} \tag{1.14}$$

where p is the *molar monolayer area constant*—characteristic for a metal in question.[55]

The second limiting case is where the initial concentration is moderate or large, and the entire surface of the electrode becomes covered with electrodeposited metal. In this situation, Sioda predicts that the equilibrium concentration is independent of the initial concentration (Equation 1.15).[55]

$$C_{eq(2)} = \frac{k_2}{k_1} \tag{1.15}$$

In a later publication, Ciszewski *et al.*[57] claimed to have verified Sioda's model experimentally. The oxidant responsible for chemical dissolution of the metal deposit was thought to be molecular oxygen. Sioda argued that by electro-reducing potential oxidants so that their concentration was lower than that of the metal, further metal deposition could be achieved.[58] By using a flow-through reactor of sufficient length, he suggested that an iterative process of metal and oxidant reductions would allow high recoveries of metal.

While Sioda's arguments are compelling, a number of publications have claimed higher (close to quantitative) deposition efficiencies from dilute solutions. Volland *et al.*[59] described a flow system using a tubular graphite cathode for metal preconcentration. Using constant current deposition, yields of greater than 98% were achieved from solutions that initially

contained less than 10 ppb of metal. Using a later version of the same system, Hoppstock *et al.*[60] used constant current deposition and applied potentials of 6-9 V to achieve deposition efficiencies of greater than 99% from ppb solutions. In the case of cobalt, an initial concentration of 9.8×10^{-8} M was reduced to $\leq 8.5 \times 10^{-11}$ M. Interestingly, the electrodeposition system of Hoppstock *et al.* was not purged of oxygen, and the bulk recirculated solution was open to the atmosphere throughout the course of the electrolysis.

Matousek and Powell[61] used applied potentials of between 4.0 and 6.0 V to achieve quantitative lead deposition from 20 ppb solutions. The lead was deposited onto a bare pyrolytic-coated graphite platform from 50 µL of 0.02 M acetate buffer (pH 4.7). The electrolysis cell, which comprised a platinum/iridium anode and a pyrolytic graphite cathode, was neither purged of oxygen nor enclosed.

Thus it appears that in certain circumstances, the equilibrium concentration after deposition can be lower than that predicted by the Sioda model. The experiments that have produced the exceptional results have certain features in common. In each case, the electrode area to volume ratio was high and the electrode separation small. In Powell and Matousek's case, this arose from the small sample volume. In the case of the tubular flow electrodes (Volland and Hoppstock), it was because the anode was positioned centrally in the flow cathode creating a very thin sample-layer between the electrodes. The effect of electrode separation was examined by Pretty *et al.*[62] who used a thin-layer flow cell to preconcentrate silver from solutions at parts-per-trillion to parts-per-billion levels prior to ICP-MS determination. The authors found that for a 127 µm electrode separation, the silver deposition efficiency was 42%, but when the electrode spacing was decreased to 16 µm, deposition efficiency increased to 83%. Under optimum conditions with a minimum cell volume of 1.1 µL, deposition efficiency of greater than 90% was achieved. A slight decrease in deposition efficiency was observed over a thousand-fold concentration range (down to 0.025 µg L^{-1}) but not as great as that predicted by Sioda's model.

The second common feature in experiments that produced high deposition efficiencies was the use of high reduction potentials. In conventional voltammetric work, the deposition potential range is restricted because potentials sufficient to reduce water are considered undesirable. This is because hydrogen evolution at the cathode changes the effective electrode area and hence the rate of analyte deposition. This effect is of little consequence in exhaustive deposition processes, provided that the deposition rate remains significantly larger than the dissolution rate.

Beinrohr *et al.*[63] studied the relationship between deposition efficiency and applied potential for manganese deposition. Using part-per-billion concentrations and 0.1 to 1.0 mL sample volumes, quantitative deposition was achieved within five to ten minutes. It was found that quantitative cathodic deposition was only possible where (uncontrolled) potentials negative of -2.5 V were used. Frick and Tallman,[64] used a tubular graphite cathode in a flow system to

preconcentrate mercury from water with a detection limit of 0.08 ppb. This contrasted with the results of other workers, who reported virtually no deposition on glassy carbon below 150 ppb.[65] Frick and Tallman attributed their higher deposition efficiency (lower detection limit) to the use of a deposition potential (-1.0 V) far more negative than that usually considered necessary for mercury deposition.

Beinrohr *et al.*[63] studied the effect of oxidant concentration on electrodeposition. They found that if deposition was effected at sufficiently negative potentials (-3.0 V), manganese could be quantitatively deposited, even in the presence of 0.25% H_2O_2. This is consistent with the results obtained by Powell and Matousek who achieved quantitative deposition, without prior deoxygenation, by using high applied potentials.[61] It may be that high applied potentials can reduce solution oxidants such as molecular oxygen or hydrogen peroxide.

Various authors have reported superior deposition efficiency when a solid electrode is covered with a mercury film.[66,67] The improvement is believed to be due to faster deposition kinetics and slower dissolution kinetics because of amalgam formation. Intermetallic bonds formed in an amalgam stabilise deposited metals and thus lower the rate of dissolution by solution oxidants. This stabilisation can result in a lower equilibrium concentration of metal ion in solution.[68] For example, Pretty *et al.*[62] found that deposition efficiency for vanadium, deposited onto a mercury thin film electrode (MTFE), was not concentration dependent, whereas silver deposition efficiency on bare glassy carbon was. However, Matousek and Powell[61] found no significant change in deposition efficiency on pyrolytic graphite, whether a mercury film was used or not.

Thus, although some theories suggest otherwise, it appears that by using large negative deposition potentials, large surface area to volume ratios, and closely spaced electrodes, highly efficient, perhaps even quantitative deposition can be achieved from very dilute solutions.

1.5.1.3 The Nature of Metal Deposits on Solid Electrodes

The first step of metal growth on an inert substrate such as carbon involves forming a nucleus of the new phase. Nucleation occurs at "active" sites of the electrode surface. In the case of graphite, these active sites are generally defects in the C-C bonded surface structure. As a consequence, the more defects present, the more active the electrode surface will be. For example, in pyrolytic graphite electrodes the edge plane has a higher defect density and is found to be more active than the basal plane.[69] The nucleation centres are disc-like structures one atom thick. These centres expand and coalesce to form the monolayer deposit. Further development requires the nucleation of new centres on the freshly generated surface.

Not all processes proceed by initial deposition of a monolayer.[70] If the rate of nucleation is smaller than the rate of growth, three-dimensional growth centres will form which subsequently overlap to give a continuous deposit. An example of this phenomenon is shown in the recent work of Chen *et al.*[71] who used *in-situ* scanning tunnelling microscopy to study

nickel electrodeposition on highly ordered pyrolytic graphite (HOPG). The resolution of the microscopic technique was sufficient to observe the graphite surface at a molecular level. Bare areas of graphite were gradually covered by multilayer nickel deposits which advanced across the graphite surface over the course of the deposition. This "island growth" mechanism is also seen with mercury which forms micro-droplets on the surface of an electrode.[72,73]

The mode by which deposits grow is related to the metal-substrate (M-S) binding energy.[74] For M-S binding energy values which are lower than the M-M binding energy, nucleation and growth tends to proceed via the island growth mechanism. Conversely, when the M-S binding energy is higher than the M-M binding energy, growth is more likely to proceed by the monolayer mechanism. In this case, one or more monolayers of metal ad-atoms may be formed before bulk metal growth occurs.

There are many other variables which may affect the early growth of metal deposits.[75] These include the deposition potential, the metal ion concentration,[74] the current density,[74,76] the roughness of the electrode surface,[77] and the nature of the electrodeposition medium.[78] The presence of oxidising agents such as chlorine or oxygen has also been shown to affect growth mechanisms.[74,79] Different growth mechanisms in the early stages of deposition lead to vast differences in the morphology of the deposit as deposition proceeds. Various shapes from geometric crystals, to powders to dendrites have been observed.[74,76] Thus small changes in experimental conditions can produce different forms of deposited metals. The morphology of the deposit and the mechanism of growth can affect the relative deposition and dissolution kinetics. This perhaps partially explains the failure of simple models to accurately predict deposition kinetics for all situations.

1.5.2 *Ex-situ* Electrodeposition-coupled ETAAS

There are three possible protocols that can be used in electrodeposition-coupled ETAAS. The first is to isolate part of the analyte from the sample matrix and thus separate it from interferents prior to the ETAAS process. The second possibility is to preconcentrate analytes that are present at concentrations below the ETAAS working range. Neither of these protocols totally depletes the sample solution of analyte. The third protocol quantitatively strips the analyte from the sample matrix and concomitant interferents. Quantitative stripping ensures reproducible deposition efficiency, and requires smaller sample volumes than partial-depletion protocols. Less commonly, workers have used electrodeposition as a way of examining analyte speciation within samples.

Various electrodeposition techniques have been used. Lund and Larsen[80] described a method in which cadmium was deposited onto a tungsten wire using constant potential electrolysis. The sample was atomised by electrically heating the wire in an inert atmosphere within an absorption cell. The detection limit for the technique, using a two minute deposition, was 0.1

ppb cadmium. The method was described as suitable for use with complex sample matrices. The same authors later used a similar technique to determine cadmium in seawater,[81] and by depositing onto a platinum wire, determined cadmium in urine.[82]

Matousek and Czobik[83] used a similar approach when they used electrodeposition to preconcentrate cadmium, silver, lead, and copper onto a tungsten wire. The sample was atomised by placing the wire in a graphite furnace atomiser and heating the furnace in the conventional manner. Using deposition times of between 30 and 300 seconds, sensitivity was improved 1.5 to 15-fold over conventional furnace techniques. The technique's sample-matrix separation was so effective that the authors reported no detectable background absorbance when using the 217.0 nm lead resonance line to determine lead in 0.1 M sodium chloride solution. The procedure was applied to lead analysis in blood and seawater. Zhang *et al.*[84] also used electrodeposition on a tungsten wire, which was then inserted in a graphite furnace, to preconcentrate and determine cadmium in urine. A similar procedure was used by Hoshino *et al.*[85] who determined several elements in the presence of sodium chloride. In both cases, chloride interferences were greatly reduced.

Metal wires have certain disadvantages as electrodeposition substrates. The electrode's effective area varies according to the degree of immersion in the sample. Of the potentially suitable refractory metals such as tungsten, tantalum, molydenum, iridium, rhenium, osmium, niobium, and ruthenium, most show considerably reduced melting temperatures in the furnace's carbon atmosphere. This is due to eutectic melting between the metal and the initial carbide formed. Under graphite furnace conditions, only tantalum and tungsten can withstand temperatures above 2500 °C. Gradual loss of electrode material at high temperatures limits the lifetime and hence the usefulness of the electrode.[83]

Graphite proves to be a good electrode substrate for the same reasons that it is a good furnace material. In addition to its conductive properties, graphite is readily obtained in high purity and can withstand temperatures in excess of 3000 °C. Thomassen *et al.*[86]deposited metals onto graphite electrodes, the ends of which were ground to a powder and transferred to a graphite furnace atomiser. Veber *et al.*[87] used a controlled potential electrodeposition to preconcentrate cadmium onto a graphite rod which was then transferred to a cup atomiser for atomic absorption analysis. Volland *et al.*[59] described a system where constant-current electrolysis was used to deposit nanogram amounts of metals onto a graphite tube housed in a flow cell. The tube was then placed in an atomic absorption spectrometer for analysis. The authors claimed greater than 98% deposition efficiency from solutions containing less than ten parts per billion of analyte. The system was used to determine iron, cobalt, zinc, and bismuth.

Hoppstock *et al.*[60] used a graphite tube to preconcentrate and determine contaminants in high purity ammonium fluoride. The furnace tube was placed in a flow cell and the sample solution pumped through at ≥ 300 mL per minute. The sample was electrolysed for a set time

using a constant current deposition. The tube was then transferred to an atomic absorption spectrometer for trace element determination. The authors reported low levels of furnace contamination (due to handling) for important trace analytes such as copper and zinc.

Other workers have experimented with mercury films on various carbon-based substrates. Batley and Matousek[88] incorporated a tubular pyrolytic-coated graphite furnace in a flow-through cell. Analyte metals were co-deposited with mercury from flowing reagent streams. After deposition, the furnace and deposited sample were transferred to an atomic absorption spectrometer and atomised. The technique was used to determine lead in seawater—a difficult task by conventional ETAAS, because lead and, in particular, its chlorides are volatile. The method was also used to determine cobalt and nickel, elements that are difficult to determine by ASV but are readily measured by atomic absorption. Batley[89] later used mercury-coated furnace tubes for determining lead and cadmium in seawater *in-situ*. The tubes were mercury plated and dried in the laboratory and then carried into the field for analyte deposition. ETAAS determination was carried out on return to the laboratory. The advantage of the technique over ASV analysis, was that deposition could be carried out in the presence of dissolved oxygen and at natural pH, thus measuring the analyte's natural speciation.

Matusiewicz *et al.*[68] used constant potential deposition to preconcentrate analyte metals into a mercury film that was pre-deposited onto a glassy-carbon electrode. The sample was deposited for 180 minutes from 5.0 mL of rapidly stirred solution. After deposition, the electrode was transferred to an electrothermal vaporiser for determination by ICP-AES. The method was used to determine eight trace metals in reference bovine liver extracts and urine samples with detection limits similar to those obtained for conventional ETAAS. The metals analysed included volatile metals such as lead and cadmium, and refractory metals such as chromium.

Mercury film deposition has also been used directly to determine mercury. Frick and Tallman[64] reduced inorganic mercury onto a tubular pyrolytic-coated graphite furnace in a flow-cell and quantified the mercury by ETAAS. The authors found a detection limit of 0.08 ppb — comparable to that obtained using a gold trap/cold vapour method, but with twice the sample throughput.

More recently, Komárek *et al.*[66] deposited labile copper onto a special graphite disk electrode. The electrode formed the end of a probe which could be inserted into a graphite furnace without touching the sides. Thus the sample was atomised into an almost isothermal environment in the manner of platform atomisation. The copper analyte was deposited both onto a bare graphite surface and a mercury film. The atomisation signal was 39% greater when the mercury film was used for deposition. The authors also examined the effects of various complexing agents on the deposition, and compared calculated free metal concentrations with those determined by electrodeposition. Calculated and experimental values agreed within 25%. Vrana and Komárek[90] used the same electrode system to determine labile copper and cadmium in seawater.

The L'vov platform has been used as a substrate for electrodeposition both with, and without mercury films. Vidal *et al.*[91] co-deposited a mercury film and the cadmium analyte onto a pyrolytic-coated graphite platform using a controlled potential. The platform was subsequently placed into a graphite furnace for atomic absorption analysis. Using a ten minute deposition time, the detection limit (0.011 ppb) was an 8-fold improvement over that obtained using conventional ETAAS. The authors used a similar procedure to measure chromium speciation,[92] following the principle applied earlier by Batley and Matousek.[93] By carrying out electrolysis at different applied potentials, hexa- and tri-valent chromium were selectively deposited onto a mercury-coated furnace tube.[92,93] The chromium was then quantified by ETAAS.

Mercury-coated pyrolytic graphite platforms were also used by Shiowatana and Matousek,[67] to determine labile lead in seawater. The platforms were clamped into a special holder and immersed in sample solution that had been spiked with acetate buffer and mercuric nitrate. The sample was stirred and electrolysed for ten minutes using an uncontrolled potential of between two and three volts. A detection limit of 0.15 ppb lead was obtained using a 120 second deposition time. Background correction was not required because interferences were eliminated by the electrodeposition step.

There are several problems associated with using platforms as electrodes for analyte electrodeposition. The analyte deposit on the platform can be fragile, especially if a mercury film has been used. Contact with foreign objects when transferring the platform to the atomiser can cause sample loss, contamination, or altered atomisation kinetics due to changed surface morphology. Also important is the analyte surface coverage on the platform. If the entire surface of the platform is used for deposition, not only is the platform difficult to handle but, when atomised, different heating rates cause atoms on different faces of the platform to be released at different times. In addition to this, atoms from the bottom face of the platform must travel a greater distance to enter the radiation path. The overall effect is peak-broadening for both the analyte and any residual background. This leads to decreased sensitivity and lack of temporal resolution between analytical and background absorbances. Vidal *et al.*[91,92] went to lengths to prevent this by encasing the platform in a watertight PTFE holder prior to electrodeposition. This construction was designed to permit analyte deposition only on the top of the platform.

1.5.3 *In-situ* Electrodeposition-coupled ETAAS

The systems described so far, have all involved sample deposition in some form of electrolysis cell, following which, the electrode and analyte are transferred to an atomic absorption spectrometer for analysis. Handling electroplated platforms and furnaces prior to ETAAS is not only cumbersome, but also prone to contamination; results are frequently irreproducible.

A limited number of publications have described systems where electrodeposition is effected in the graphite furnace while it is in place within the atomiser. This removes the need for electrode handling and opens the door to automated techniques. In one of the earliest publications in this field, Fairless and Bard[94] described an *in-situ* deposition using a carbon rod atomiser. A platinum wire anode and SCE reference electrode were placed in the sample well of the carbon rod which served as a cathode. The sample solution was pipetted into the sample well and electrolysed for between fifteen seconds and two minutes. Prior to atomisation, the anode and reference electrode were lifted away and the test solution was removed with a pipette. Sensitivity was limited by the lack of quantitative deposition, and by the small volume (about ten microlitres) of the sample solution well in the carbon rod.

Torsi *et al.*[95] used an *in-situ* electrodeposition technique to determine lead in seawater. A glassy carbon crucible was used both as a cathode for electrodeposition and as an atomiser. Sample solution was introduced to the crucible through one PTFE tube and sucked away though another. An electrode that served as an anode was placed in the sample solution reservoir so that electrolysis could take place while sample was pumped though the crucible. The seawater sample was passed through the electrolysis cell for a specified time at a rate of 4.0 mL per minute. A rinse solution was then passed through the cell to remove any residual sodium chloride. Using a ten minute electrolysis (40 mL sample), a detection limit of 0.03 ppb was reported for lead in seawater; more than a factor of 10 lower than conventional ETAAS can achieve in non-saline waters.

Matousek and Powell[61] studied the deposition of lead onto a pyrolytic coated graphite platform and determined that by using a sufficiently large uncontrolled potential (six volts applied), quantitative analyte deposition could be effected in less than four minutes. Building on this result, Matousek and Grey[96] described instrumental modifications to allow automated *in-situ* electrodeposition of analytes in a conventional pyrolytic graphite furnace. This system comprised a GBC GF2000 graphite furnace system equipped with a modified PAL2000 autosampler. The autosampler was capable of performing automated sample loading, electrodeposition, electrolyte withdrawal, washing, and chemical pretreatment of the deposited metal.

This same automated *in-situ* deposition system was further developed by Matousek and Powell[97,98] and was used to determine lead and cadmium in 0.5 M sodium chloride solution. In the most elegant example of *in-situ* electrodeposition-coupled ETAAS (ED-ETAAS) seen to date, the method was shown to remove 99.5% of the sodium chloride prior to atomisation. The authors claimed quantitative analyte deposition from 25-40 µL samples within 60 s electrolysis at 3.5-5.0 V. Electrodeposition from sodium chloride solutions using high electrolysis potentials (-6.0 V) led to destructive exfoliation of the pyrolytic-graphite furnace coating within a short time (50-70 atomisation cycles). This was prevented by using an electro-reduced palladium modifier which was deposited prior to each analyte deposition and

renewed for each measurement. A second important function of the palladium modifier was to thermally stabilise the analyte metals. Plots of pyrolysis temperature versus absorbance (pyrolysis loss curves) indicated that the electrodeposited palladium stabilised lead by 500 °C, compared to only 250 °C for thermally reduced palladium.

Use of the electrodeposited palladium modifier, combined with the efficient matrix removal afforded by the analyte electrodeposition and rinsing protocol, enabled Matousek and Powell to determine cadmium with equal sensitivity from sample matrices as diverse as 1% HNO_3 and seawater. The technique appears especially attractive because it is totally automated. This not only makes it less cumbersome to use than other ED-ETAAS methods, but also improves precision and lowers the risk of sample contamination.

1.6 SCOPE OF THIS WORK

Electrothermal atomic absorption spectrometry (ETAAS) is a versatile technique capable of determining a wide range of elements with great sensitivity. ETAAS is one of the most commonly used techniques for trace element analysis because other methods with similar capabilities cost a great deal more; both to purchase and to operate. There are limits to the performance of ETAAS in that it is insensitive to elemental speciation and it is badly affected by certain interferences, most notably the chloride ion. Until recently, protocols proposed to meet these problems were cumbersome and difficult to automate. The method proposed by Matousek and Powell[97,99] is simple and efficient, and promises capacity to deal with the shortcomings of conventional ETAAS. Work within this thesis is aimed at improving the understanding of Matousek and Powell's ED-ETAAS method and expanding its application.

Following this introductory chapter, the second chapter of this thesis describes general experimental protocols and equipment, as well as specifying the reagents used for experimental work.

The third chapter of this work is directed towards understanding the palladium modifier. The relevant properties of palladium as a modifier and a catalyst, as well as its role as an electrode substrate are reviewed. Experimental work was directed towards optimising parameters for palladium modifier electrodeposition. The priorities were to achieve, in the minimum time, a modifier deposit that would give the best sensitivity and thermal stability for an analyte deposited onto it. Preliminary studies of alternative noble metal modifiers are also presented.

The fourth chapter of this thesis deals with electrodeposition of reducible metal analytes in acid media. The experimental aims were to achieve quantitative metal deposition and characterise the thermal stability of the deposit, and the sensitivity of the method. Problems associated with artifacts of the electrodeposition system (i.e. high blanks and sample carryover) were explored, along with possible solutions.

Having developed useful experimental methods for metals in simple sample matrices, the fifth chapter goes on to explore the effects and problems associated with more complex media. A volatile metal halide in seawater was modelled using lead in 0.5 M sodium chloride solution. Experimental work was aimed towards reducing sodium chloride interference so that volatile metals and metals forming volatile halides could be determined in saline matrices. Two such metals, copper and cadmium were determined from seawater.

Mercury, a difficult metal to determine by ETAAS because of its volatility, was determined by ED-ETAAS in the next section of work (Chapter Six). The thermal stability afforded by palladium and other modifiers was examined. The sensitivity was compared to that obtained by more conventional mercury analysis using a cold-vapour technique in which mercury vapour was accumulated on a palladium-coated furnace prior to ETAAS determination.

The advantage of electrodeposition over conventional ETAAS is that, in principle, the speciation of metals can be studied. In the Chapter Seven, the concept and importance of metal speciation are discussed. Experimentally, species fractionation of several metals was examined by ED-ETAAS using EDTA as a model ligand. Comparisons with ASV analyses were used to examine the effect of metal ion lability on ED-ETAAS analyses.

In the final experimental section of this work (Chapter Eight), the determination of arsenic by ED-ETAAS is discussed. The environmental importance of arsenic and its speciation is reviewed along with methods currently used for arsenic analysis. Experimental work initially concentrated on optimising arsenic(III) deposition to achieve quantitative recovery. Subsequent work was directed toward establishing ED-ETAAS conditions that would allow discrimination between the arsenic(III) and arsenic(V) species. A method was developed that demonstrated successful fractionation of arsenic species in synthetic samples. The method was then applied to samples of arsenic-contaminated natural waters, and the results verified by comparison with a second technique: pH-selective arsine generation followed by accumulation in a palladium-coated furnace tube and ETAAS determination.

The concluding section of this work discusses the advantages and disadvantages of the present ED-ETAAS method and suggests directions for future research.

Chapter Two

Experimental

This chapter outlines the equipment, reagents, and general protocols used throughout the experimental work described in this thesis. Specific protocols are described in the relevant chapters.

2.1 CLASS 100 CLEANROOM

2.1.1 Cleanroom Layout and Specification

All sample preparation was carried out within a cleanroom designed to meet or exceed the standards laid down for a Class 100 cleanroom. The requirements for a cleanroom of this standard are as follows:[100]

i) The maximum number of particles ≥ 0.5 μm in size per cubic foot of air must not exceed 100.

ii) There should be zero particles ≥ 5.0 μm in size per cubic foot of air.

Cleanroom conditions are maintained using laminar-flow air changing. Air is pumped through high efficiency particulate air (HEPA) filters in the ceiling of the room, and flows the length of the room with minimum turbulence to exit via a floor level port at the other end of the room. In this way, a constant flow of clean air constantly sweeps away any particulate matter. The air within the cleanroom is changed a minimum of 46 times per hour. The Class 100 cleanroom is separated from the nearest area containing unfiltered air (corridor) by three doors. The pressure increases in graduated 15 Pa steps from ambient in the corridor to 45 Pa above ambient in the Class 100 area. This prevents contaminated corridor air flowing into the clean environment. The room contains a laminar flow hood, an acid hood, a microwave for sample digestion, and vessels for cleaning glassware. To reduce the possibility of contamination from metal items, the only metal fittings used within this room are made of stainless steel, or are sealed by painting or powder coating the surface. No other metal items are permitted in this room. Activity in the Class 100 area is minimised to prevent particulate introduction by workers.

All samples were prepared in the laminar-flow or acid hoods within the Class 100 cleanroom. A glass sheet was used as a work surface because it could be readily cleaned.

Instrumental analysis was carried out in a second cleanroom adjacent to the Class 100 area. This room is only two doors away from the nearest area containing unfiltered air, and has a laminar-flow design with 21 air changes per hour. Because of the closer proximity to the corridor, lower air flow, and greater usage, this cleanroom has a higher particle count than the cleanroom used for sample preparation and is classified as a Class 350 cleanroom. This classification requires particle counts of fewer than 10,000 particles ≥ 0.5 μm per cubic foot, and fewer than 70 per cubic foot for particles ≥ 5.0 μm.

A third cleanroom functions as an anteroom for the Class 350 and Class 100 cleanrooms. The anteroom is designated as a changing room and used for storing and donning cleanroom attire. Because of its proximity to the corridor and because it lacks a dedicated supply of filtered air, the anteroom has not been assigned a clean environment classification.

Disposable sticky mats are placed on the floor inside the entrances to the Class 100 and Class 350 areas. These are designed to remove particulates from the feet of workers passing into and out of the clean areas.

The standard of the cleanroom environment has recently been audited and was found to meet or exceed specifications.[101]

The layout of the cleanroom complex is shown in Figure 2.1.

2.1.2 Cleanroom Practise and Protocols

2.1.2.1 General Cleanroom Use

To prevent contaminants and dust from entering the cleanroom, all articles are wiped with a damp cleanroom wipe in the anteroom prior to their introduction. Once in the cleanroom, equipment is not removed unless absolutely necessary. Any items that inherently produce dust such as paper, are kept to a minimum. Although tissue use is permitted in the Class 350 area, any chemical spills in the Class 100 area are cleaned up using approved cleanroom wipes (Durx™).

So that laminar air-flow is unhindered, sample preparation benches and flow hoods in the cleanrooms are kept clear of equipment. Unused equipment is stored in closed cupboards.

Potential analytes (especially heavy metals) with concentrations greater than 10 ppm are not permitted in either the Class 100 or Class 350 cleanrooms. This prevents residues on glassware or surfaces from contaminating other samples. Experiments requiring analyte concentrations greater than 10 ppm are carried out in the semi-clean environment of the anteroom.

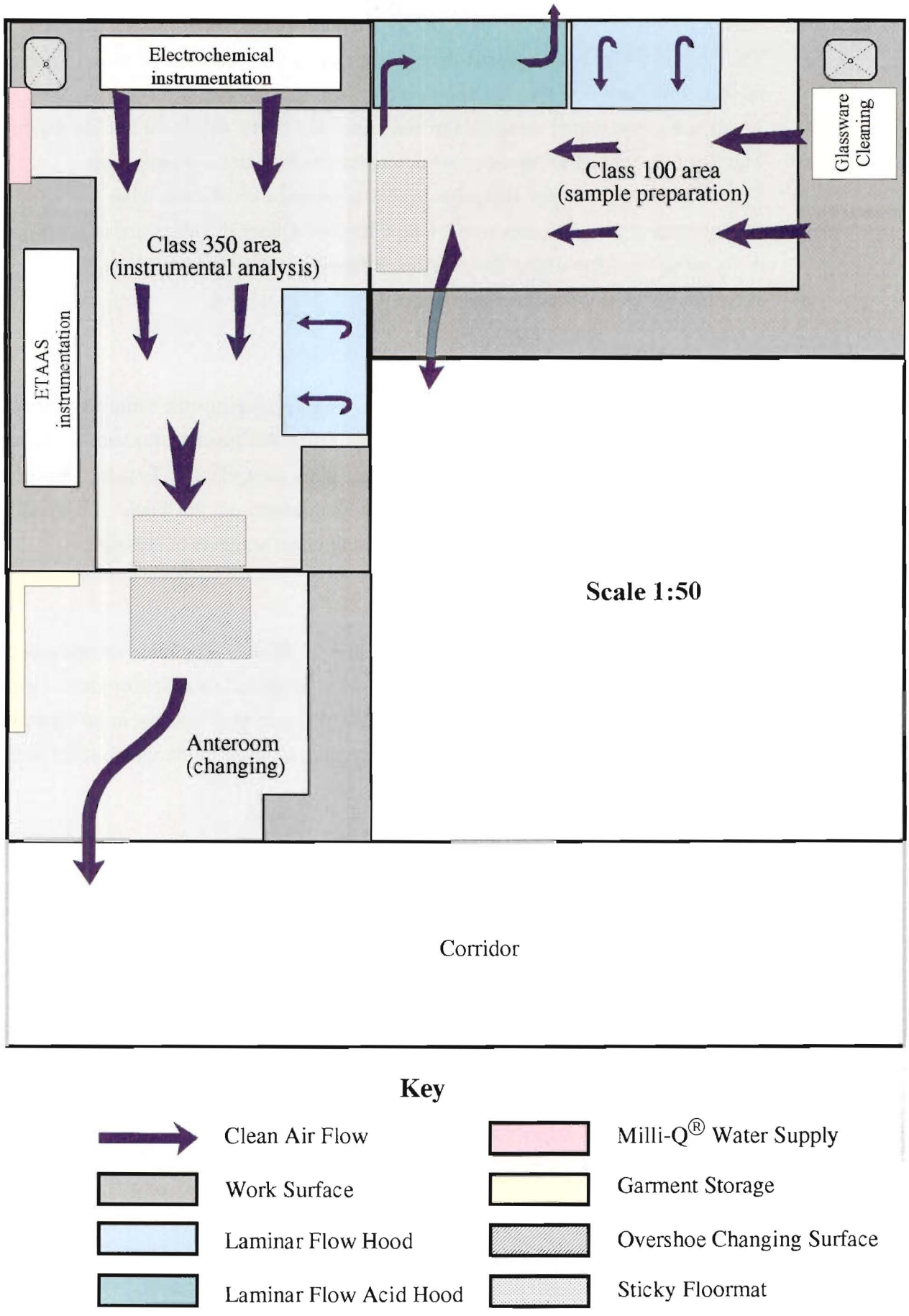

Figure 2.1 Floorplan of the University of Canterbury Chemistry Department cleanroom facility

The cleanrooms are cleaned regularly to remove any dust build-up. The cleaning protocol used is as follows:

i) The floor is swept with a plastic broom, starting in the Class 100 area and moving through the Class 350 area to the anteroom.
ii) The benches are wiped using cleanroom wipes and dilute detergent/hot tap water.
iii) The floor is mopped using the same detergent solution and a sponge mop.
iv) The benches are re-wiped using deionised water and a cleanroom wipe.
v) Sticky mats at the entrances to the Class 100 and Class 350 areas are renewed, as is the paper mat demarking the overshoe changing area in the anteroom.
vi) Any dirty or worn overshoes are replaced.

2.1.2.2 Cleanroom Attire

Cleanroom workers adhere to the following protocol. Before entering the anteroom, shoes must be removed. Once inside, workers don lint-free attire designed to prevent particles dropping from workers into samples. The cleanroom garb comprises a Tyvek™ bonnet, matching overshoes, and a throat-high nylon gown that closes at the back. Disposable polyethylene gloves (Medex) are worn when manipulating clean reagents or samples.

2.1.2.3 Glassware and Cleaning Protocol

All stock solutions were prepared in borosilicate volumetric flasks. The only exceptions to this were stock solutions of $PdCl_2$ and KOH, which were prepared in polypropylene volumetric flasks (Nalgene®). Dilute solutions for analysis were prepared directly in polypropylene autosampler vials. Before initial use, all sample containers used in the cleanrooms were subjected to a rigorous cleaning protocol as follows:

1) In a standard laboratory:
   i) Wash thoroughly using hot tap water and detergent.
   ii) Rinse in doubly distilled water.
   iii) Soak for at least three days in 10% (v/v) Analar HNO_3 / doubly distilled water.
   iv) Rinse in doubly distilled water.
2) In the Class 100 area:
   i) Soak for at least three days in 1% (v/v) Baker Analysed HNO_3/Milli-Q water. This solution was contained in a 5 L polypropylene beaker (Nalgene®) and covered with a glass sheet.
   ii) Soak for at least three days in Milli-Q water.
   iii) Air dry, and store in polythene bags until required.

In subsequent cleanings, only the second part of the cleaning process was used, soaking for at least 24 hours at each stage. Vessels that had been used to contain particularly concentrated solutions (greater than 1 ppm) were re-subjected to the entire cleaning process.

2.2 ETAAS INSTRUMENTATION AND PROTOCOLS

2.2.1 ETAAS Instrumentation

Developmental work was carried out using a GBC 903 atomic absorption spectrometer. This was fitted with a GF2000 graphite furnace system comprising the furnace workhead, control module, and power supply. A PAL 2000 autosampler was used for sample introduction. Results were printed on an Epson LX800 dot matrix printer. This system was used for most ED-ETAAS experiments other than those for determining mercury or arsenic.

Mercury and arsenic systems were investigated using a GBC 908 atomic absorption spectrometer. This was fitted with a GF3000 graphite furnace workhead/power supply, and a PAL 3000 autosampler. The system was controlled by a 486 personal computer running software supplied by GBC. Results were printed using an Epson LX800 dot matrix printer.

The GBC 903 and the GBC 908 spectrometers were both fitted with GBC Ultra-pulse continuum source background correction. All measurements were made with this system switched on.

Both the PAL 2000 and PAL 3000 autosamplers were modified to improve the probe rinsing systems. Forward flush rinsing was used on both autosamplers. This modification required re-plumbing the autosampler so that on receiving the software command to rinse, water flushes directly through the injection tube and capillary to waste. This provides improved rinsing, and removes bubbles from the PTFE capillary. The standard rinse protocol uses the injection syringe to aspirate water from a rinse well and expel it to waste. Under this system, bubbles accumulate in the PTFE tubing, degrading both rinse efficiency and sample volume reproducibility.

2.2.2 ETAAS Accessories

2.2.2.1 Hollow Cathode Lamps

Element	Manufacturer	Operating Current (mA)	Wavelength (nm)	Slit width (nm)
Lead	Photron	4.0	283.3 / 217.0	1.0
Arsenic	Photron	10.0	193.7	1.0
Copper	Photron	4.0	324.8	0.5
Nickel	Varian Techtron	10.0	232.0	0.2
Bismuth	Varian Techtron	8.0	306.8	0.5
Cadmium	SJ	3.0	228.8	0.5
Palladium	GBC	5.0	340.5	0.2
Mercury	Varian Techtron	3.0	253.7	0.5

2.2.2.2 Software Modifications

For ED-ETAAS experiments, specially modified software was supplied by GBC. This was supplied in the form of an electronically programmable read-only memory (EPROM) chip for the GF2000 system, and on floppy disk for the GF3000 system. The modified software changes the autosampler injection mechanism, so that it not only injects a sample into the graphite furnace, but can also remove it after a specified period of time (1-100 s). During this time, a potential can be applied between the graphite furnace and a modified sample injection probe. The sample injection software can be used to switch the applied potential on and off automatically. Temperature and gas flows during the deposition period are controlled by specifying that a given deposition step occurs at a particular stage of the graphite furnace program. Separate steps are available to deposit modifiers, samples, and/or a variety of rinsing protocols. The interfaces for the modified ETAAS software and the available parameters as used with the PAL 2000 and PAL 3000 are shown in Table 2.1. Apart from the electrodeposition modifications, the rest of the software for the two AAS instruments was used as supplied.

(a)

Modifier volume	1-100 µL
Modifier deposition time	1-100 s
Modifier plating	Yes/No
Acid rinse volume	1-100 µL
Acid rinse deposition time	1-100 s
Acid rinse plating	Yes/No
Sample volume	1-100 µL
Sample deposition time	1-100 s
Sample plating	Yes/No
Acid re-deposition volume	1-100 µL
Acid re-deposition time	1-100 s
Acid re-deposition plating	Yes/No
Wash volume	1-100 µL
Wash time	1-100 s
Wash plating	Yes/No
Number of multiple injections	1-255
Number of sample repeats	1-255
Dry steps for multiple injections	1-255
Inject on step number	1-255

(b)

	Solution Options	Inject at Step	Injection Mode	Volume (µL)	Rinse Step	Current On	Current Time (s)
1	Modifier/Blank/Sample/ Automix/Rinse	1-15	Electrodep/ Normal	1-100	Yes/No	Yes/No	1-100
2	Modifier/Blank/Sample/ Automix/Rinse	1-15	Electrodep/ Normal	1-100	Yes/No	Yes/No	1-100
3	Modifier/Blank/Sample/ Automix/Rinse	1-15	Electrodep/ Normal	1-100	Yes/No	Yes/No	1-100
Rinse Step				1-100		Yes/No	1-250

Table 2.1 Modified electrodeposition software interfaces for (a) PAL 2000 and (b) PAL 3000 autosamplers. Adjustable parameters are shown as minimum and maximum allowable values.

2.2.2.3 Electrodeposition Power supply

The power supply used for electrodeposition experiments was custom-built by GBC Scientific Equipment Pty Ltd. Designated the GBC EPS2000, the power supply produces an uncontrolled potential of 0-20 V (DC), or a current of 0-100 mA from a 230 V AC power supply. The EPS2000 can be operated in two modes: automatic, where the potential is switched off and on by the graphite furnace/autosampler software, or manual, where the potential is permanently switched on or off.

2.2.2.4 Platinum / Iridium Autosampler Probe

The standard autosampler injection probe for conventional ETAAS is a length of PTFE tubing. The autosampler was modified by replacing the last section of this tube with a 6 cm length of Pt/Ir capillary (0.7 mm o.d.). The Pt/Ir tube was mounted in the end of the auto-sampler arm using a PTFE bush similar to that used with standard PTFE delivery tube, but with a reduced aperture to hold the smaller Pt/Ir tubing. The Pt/Ir tube and furnace were connected to a DC power supply as shown in Figure 2.2. This allowed sample electrolysis using the Pt/Ir tubing as an anode and the pyrolytic graphite furnace as a cathode. In practice, the probe-furnace distance was set by lowering the probe tip into an empty furnace until a current flowed (touching) and then raising it the minimum amount to prevent current flow (not touching).

2.2.2.5 Combined PTFE Delivery-tube / Electrode

To combat carry-over problems caused by sample adsorption on the inside of the Pt/Ir capillary (discussed in Section 5.2.2.3), a delivery tube combining a continuous PTFE sample delivery path with a platinum electrode was designed and constructed as shown in Figure 2.3. This probe was mounted at the end of the autosampler delivery arm in the same way as the Pt/Ir capillary.

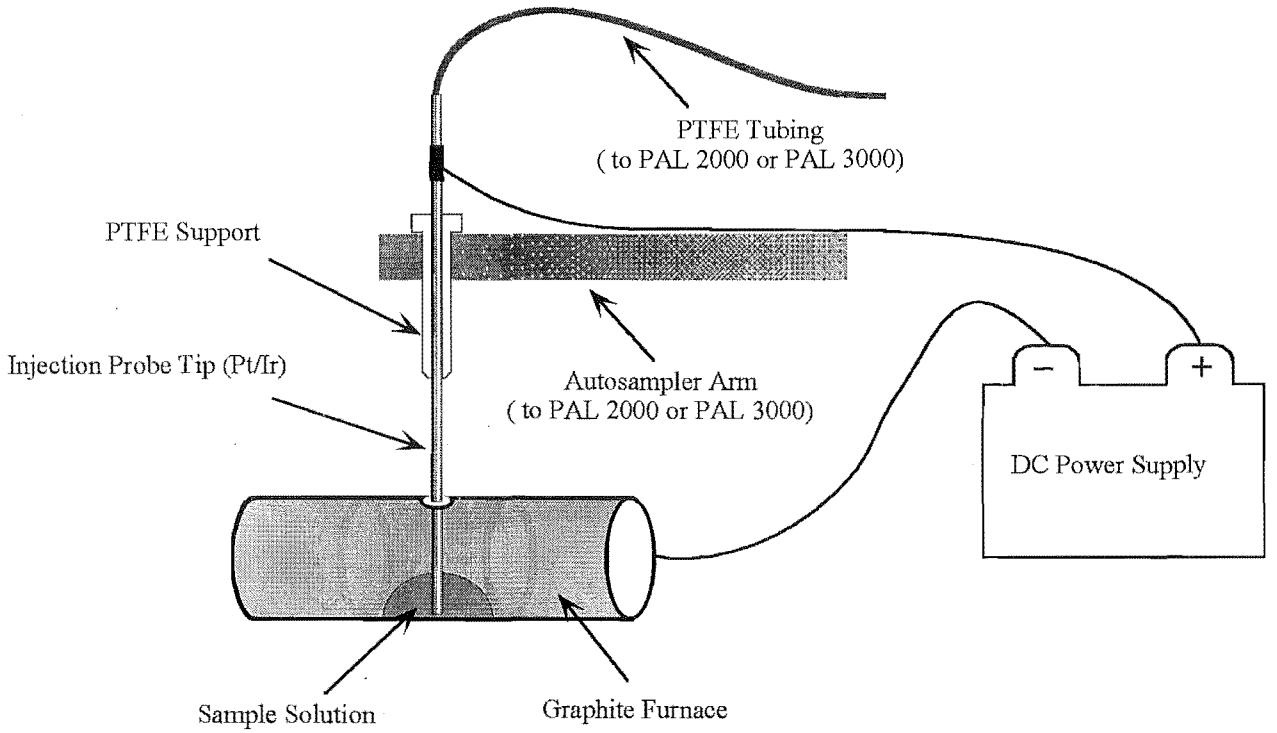

Figure 2.2 Schematic diagram of modified autosampler probe and graphite furnace system for sample electrodeposition.

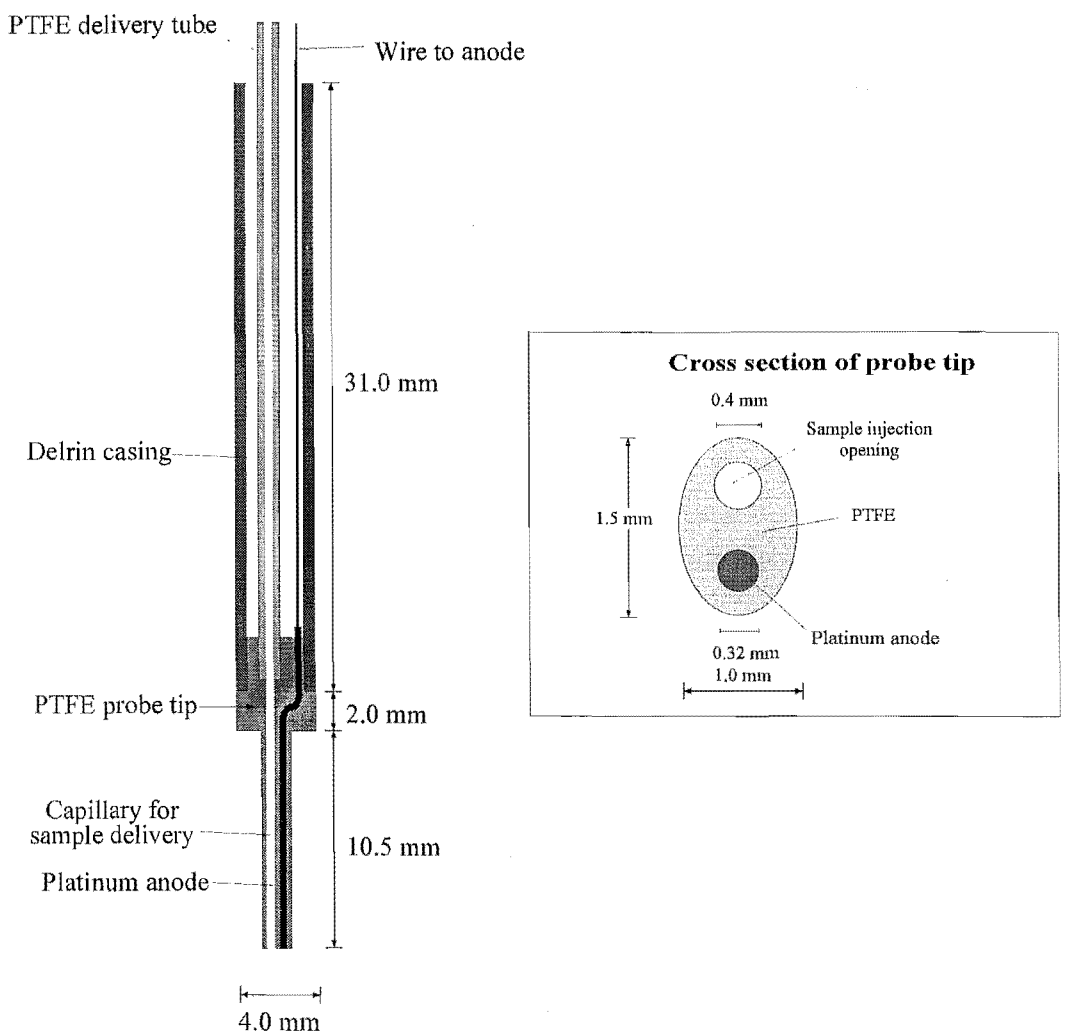

Figure 2.3 Combined PTFE sample delivery tube/Pt anode, for preventing analyte carry-over in ED-ETAAS

2.2.2.6 HG 3000 Hydride Generator

For cold vapour mercury, and arsenic hydride generation experiments, a GBC HG3000 hydride generator was used. The HG3000 incorporates an FIA hydride generation manifold with a gas liquid separator as shown in Figure 2.4. The resulting hydride / mercury vapour is carried to the detector cell by an argon gas stream. Samples were collected by inserting the PTFE tip of the delivery tube into the heated graphite furnace for a specified period and then removing it before firing the furnace. Because there is a lag between the beginning of hydride generation and the hydride reaching the end of the delivery tube, the reactor must be started well before sample collection begins. In this system, the sample reached the end of the delivery tube within 45 seconds of initiating hydride generation; the collection period was timed from this 45 second delay.

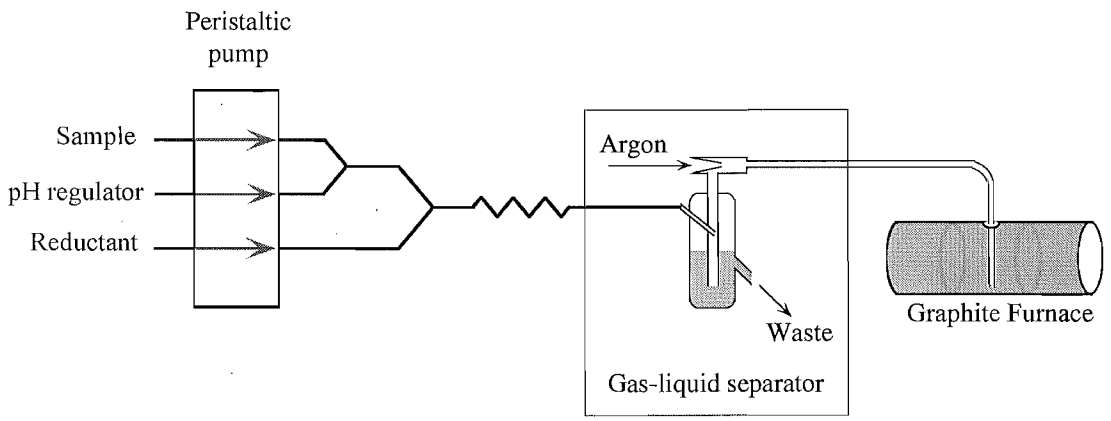

Figure 2.4 Schematic diagram of the HG3000 setup used in this work.

2.2.2.7 Optical Pyrometer and Thermocouple

Graphite furnace temperatures in the range 1000-1500 °C were calibrated using an optical pyrometer; disappearing filament type, Cambridge Instruments. Temperatures from ambient to 1000 °C were measured using a Fluke thermometer (Model 55/KJ) with a Type-K thermocouple.

2.2.3 ETAAS Experimental Protocols

2.2.3.1 Thermal Deposition

For conventional ETAAS analysis, 20 µL of sample was injected into the furnace, and the furnace temperature was heated through steps 4-10 as shown in Table 2.2.

In cases where the furnace was pre-plated with palladium modifier, three extra steps were added to the furnace program (Table 2.2, steps 1-3). These allowed control of temperature and gas flows during modifier deposition, and post-deposition drying. The furnace was held at step one of the furnace control program and 30 µL of modifier solution (10 ppm in 0.1%

v/v HNO_3) was injected into the furnace and deposited for 20 seconds using a potential of E_{app} = 2.0 V. The spent solution was then withdrawn, the deposited modifier dried (step 2), and the furnace returned to a lower temperature for sample injection (step 3). The rest of the protocol was then followed as for conventional thermal deposition.

Step	Final temp (°C)	Ramp time (s)	Hold time (s)	Inert Gas	Read
1. Deposit modifier	*45*	*0.1*	*0.0**	*Yes*	*No*
2. Dry modifier	*150*	*5.0*	*5.0*	*Yes*	*No*
3. Inject sample	variable	1.0	5.0	Yes	No
4. Fast ramp	90	5.0	1.0	Yes	No
5. Drying	120	10.0	15.0	Yes	No
6. Extra drying	150	5.0	5.0	Yes	No
7. Pyrolysis	variable	10.0	10.0	Yes	No
8. Cooling	400	2.0	10.0	No	No
9. Atomisation	variable	minimum	2.0	No	Yes
10. Clean	2500	0.1	2.0	Yes	No

Table 2.2 Furnace control program for ETAAS analysis using thermal sample deposition.

2.2.3.2 Electrodeposition

Furnace control programs used for electrodeposited samples (ED-ETAAS) were similar to those used for thermal deposition with electroplated modifiers (Table 2.2). The main differences were:

- Decreased drying times; due to sample medium withdrawal there are smaller solution volumes to be dried,
- Increased pyrolysis temperatures; possible because electrodeposited metals exhibit greater thermal stability than thermally deposited metals.

A typical autosampler program for sample electrodeposition is shown in Table 2.3. Modifier solution is injected, deposited, removed, and dried as described for thermal analysis. Sample depositions and subsequent rinses / acid re-depositions are carried out at step three of the furnace program. By varying the furnace conditions during the deposition step, it was possible to effect deposition using slightly raised temperatures (*ca.* 45 °C) and with an inert gas flow over the top of the electrolysis solution. This provided convective stirring of the sample, and improved deposition efficiency when deposition potentials were insufficient to produce gas evolution at the electrode surfaces. In this thesis, measurements made using deposition potentials of less than 3.5 V (applied) were generally effected at raised temperature (*ca.* 45 °C) with

*The hold time during modifier or sample electrodeposition is determined by the value entered in the autosampler control program.

an inert gas flow (referred to as "elevated" or "high-temperature deposition"). Measurements made using deposition potentials greater than 3.5 V were generally effected at room temperature with no inert gas flow ("low-temperature deposition"). For metal speciation measurements, regardless of the potential used, deposition was carried out at room temperature with the inert gas flow on.

Deposition potentials varied according to the experiment. The potentials used are given in the relevant section. Unless otherwise stated, the deposition potentials stated, are open circuit (uncontrolled potentials). The actual electrode potentials can be estimated using the plots of applied potential versus measured potential shown in Chapter Seven.

Solution	Inject at Step	Injection Mode	Volume (µL)	Rinse Step	Current On	Current Time (s)
1. Modifier	1	Electrodep	40	No	Yes	20
2. Sample	3	Electrodep	20	No	Yes	60
3. Rinse	3	Electrodep	40	Yes	Yes	40
Rinse Step			30		Yes	10

Table 2.3 Typical autosampler control program for ED-ETAAS.

2.2.3.3 Vapour / Hydride Collection

Pd modifier was electrodeposited as for the previous technique. The furnace was held at an elevated temperature while arsine or mercury vapour was passed into it. The furnace temperature was then ramped to atomisation, and the absorbance measured. A pyrolysis step was not necessary with vapour collection methods as no sample matrix entered the furnace. A typical furnace program for collection of arsine is shown in Table 2.4. The sampler program for vapour collection experiments was only used to control the modifier deposition. The probe introduction and timing were governed manually.

Step	Final temp (°C)	Ramp time (s)	Hold time (s)	Inert Gas	Read
1. Deposit modifier	45	0.1	0.0	Yes	No
2. Dry modifier	150	10.0	10.0	Yes	No
3. Collect sample	400	1.0	5.0	No	No
4. Cool	150	0.2	10.0	No	No
5. Atomise	2400	1.2	2.0	No	Yes
6. Clean	2500	0.1	10.0	Yes	No

Table 2.4. Furnace control program for collecting and atomising arsine gas.

2.3 ELECTROCHEMICAL INSTRUMENTATION

2.3.1 Square Wave Voltammetry

Voltammetric experiments were performed using a Princeton Applied Research (PAR) Model 384B voltammetric analyser coupled to a PAR 303A static mercury drop electrode. The 303A electrode was filled with Suprapur® grade mercury (Merck). Results were printed using a model DMP-40 plotter (Houston Instruments).

Square wave voltammetry was performed using the 303A electrode in hanging-drop mode. Prior to analysis, samples were purged with oxygen-free nitrogen for a minimum of five minutes. Deposition potentials and times varied depending on the type and concentration of the analyte metal. Stripping parameters used were: 2 mV scan increment, 20 mV pulse height, and frequency of 100 Hz. All potentials are expressed relative to the Ag/AgCl reference electrode.

2.3.2 Furnace Simulation Experiments

In order to establish the potentiometric conditions at each electrode in the furnace during ED-ETAAS, a furnace simulation apparatus was constructed. This was a stand designed to hold a Pt/Ir anode at a specified distance from a longitudinally bisected graphite furnace (cathode). The Pt/Ir anode was held above the cathode in a micrometer which was used to precisely control the electrode separation. The power supply used was the same as for ED-ETAAS experiments; the GBC EPS2000. The electrode holder is shown in Figure 2.5.

The furnace was plated with palladium by electrolysing *ca.* 50 µL of 10 ppm palladium/0.1%HNO_3 solution for 60 seconds at 2.0 V. Approximately 30 µL of sample solution was then electrolysed using a range of uncontrolled potentials (0.0-4.0 V). The actual electrode potentials were measured between the relevant cathode/anode and a silver/silver chloride reference electrode. The reference cell was formed by inserting an oxidised silver wire into the 25 µL electrolysis solution which contained ≥ 0.05 M chloride ion. Potentials and currents in the cell were determined using a PHM64 potentiometer (Radiometer Copenhagen) and digital multimeters.

2.4 MISCELLANEOUS EQUIPMENT

2.4.1 Micropipettes

Small solution volumes were measured using Gilson Pipetteman™ micropipettes. The four different pipette sizes used were: The P20 (2-20 µL), P100 (20-100 µL), P200 (50-200 µL), and the P1000 (200-1000 µL). These were gravimetrically calibrated at regular intervals. Appropriate micropipette tips were used as supplied without further cleaning.

2.4.2 Balance

A Mettler AE163 balance was used for all weighings. This balance was regularly calibrated using the internal calibration system.

2.4.3 pH Measurement

Precise pH measurements (± 0.01 pH units) were made using a pH meter (Hanna Instruments HI8424). This pH meter was calibrated using standard buffers obtained from Radiometer Copenhagen: phthalate (pH 4.01 ± 0.01), and phosphate (pH 7.00 ± 0.01). Approximate pH (± 0.4 pH) was measured using pH indicator strips: Merck art.9541 (pH 2.5-4.5), art.9542 (pH 4.0-7.0), and art.9543 (pH 6.5-10.0).

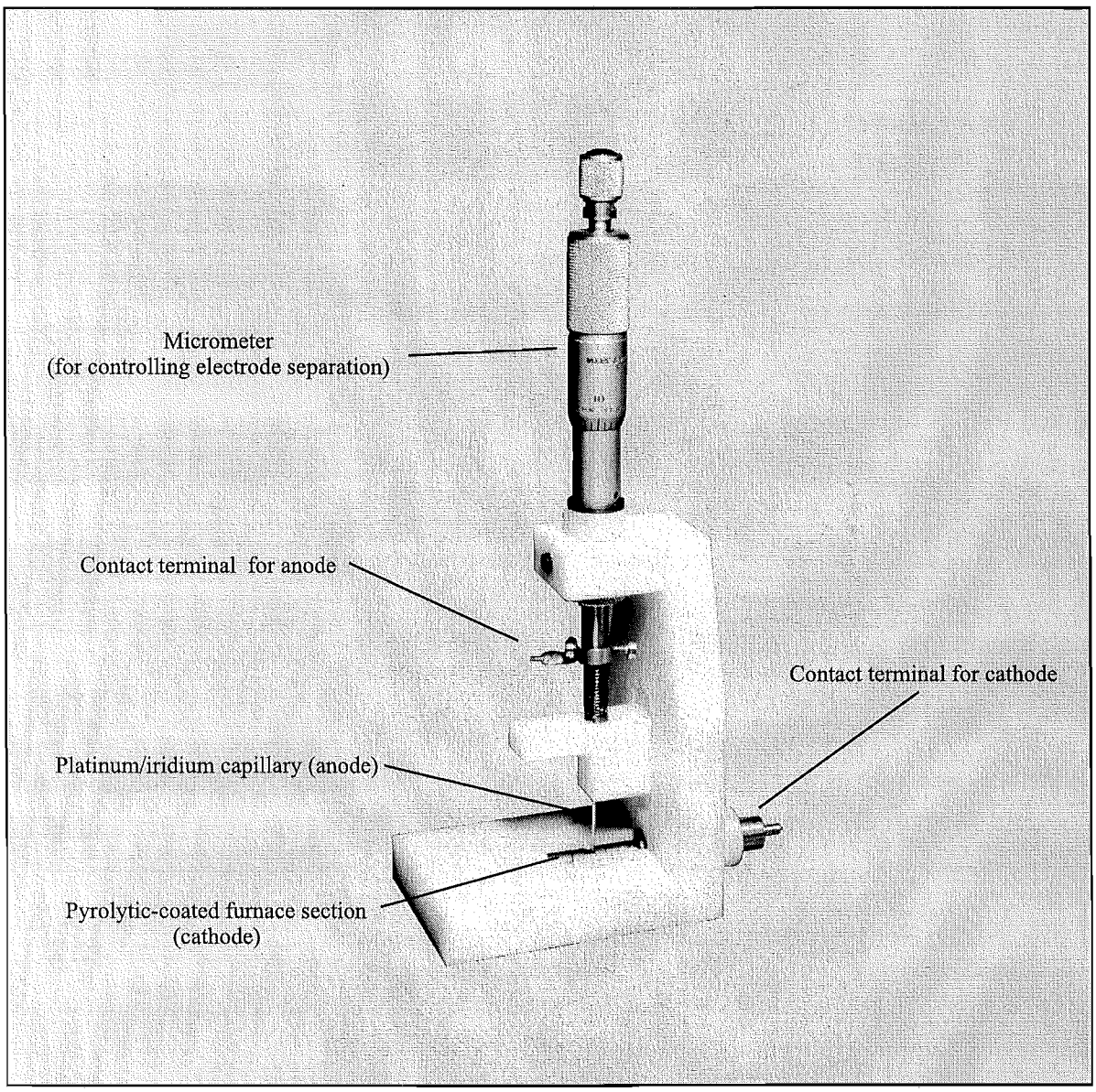

Figure 2.5 Furnace electrochemistry simulation apparatus

2.4.4 Multimeters

Potentials and currents in ED-ETAAS and furnace-simulation systems were measured using digital multimeters (Dick Smith Q-1442).

2.4.5 Microwave Oven

The microwave used for heating samples was a domestic model Sharp R-4A11, with a maximum power rating of 700 W.

2.4.6 Filtration

Cellulose membrane-filters (Millipore® Type HA) were used to filter natural samples. 0.45 μm filters were used to separate so-called soluble and insoluble forms of analytes. Prior to analysis, samples were re-filtered using 0.025 μm filters to remove colloids. Filters were used mounted in an acid-washed plastic vacuum-filtration apparatus (Millipore®).

2.5 ANALYTICAL REAGENTS

2.5.1 Water

Water used for preparing stock standards (100 pm) and for initial washing of glassware was purified by ion exchange, and then doubly distilled in a borosilicate glass still.

Pure water ($\geq$ 15 MΩ cm^{-1}) was used for final cleaning and all other dilutions. This was obtained from a four-bowl Milli-Q® water purification system (Millipore Corp). The Milli-Q system's ion exchange cartridges and carbon filters were changed annually.

2.5.2 Reagents

A list of the acids, bases and buffers and other reagents used, as well as their grades and manufacturers is given in Table 2.5.

2.5.3 Gases

In ETAAS, the furnace is bathed in an inert gas to prevent oxidation of the pyrolytic graphite surface. In all experiments, oxygen-free nitrogen (BOC Gases) was used for this purpose. The same nitrogen was used to purge sample solutions during voltammetric analysis.

2.5.4 Analytical Standards

Lead, copper, nickel, bismuth, and cadmium standards were prepared by diluting 1000 ppm Spectrosol® atomic absorption standards (BDH).

REAGENT	GRADE	MANUFACTURER
Nitric Acid	Instra-analysed Reagent	J.T Baker Inc
Sulphuric Acid	Aristar	BDH
Hydrochloric Acid	Aristar	BDH
Phosphoric Acid	Aristar	BDH
Acetic Acid	Pronalys*AR	May & Baker
Ammonia Solution	Analar	BDH
Potassium Hydroxide	Aristar	BDH
HEPES	> 99.5 %	Sigma
Hexamine	Analar	BDH
Sodium Acetate	Aristar	BDH
Sodium Chloride	Aristar	BDH
Potassium Nitrate	Aristar	BDH
Sodium Nitrate	Suprapur	Merck
L-Cysteine	> 99.5 %	Merck
Hydrazine Sulphate	Analar	BDH
EDTA	Analar	Koch-Light
Sodium Borohydride	GPR	BDH
Ammonium Sulphide	Technical (40% w/v)	Reidel-de Haën

Table 2.5 Reagents used in this work.

Mercury standard was prepared by dissolving metallic mercury (Suprapur®, Merck) in concentrated nitric acid, and diluting to 5% acid.

Arsenic(V) stock solutions (100 ppm) were prepared by dissolving sodium arsenate (BDH Analar) in 1.0% nitric acid. Arsenic(III) stock solutions (100 ppm) were prepared by dissolving arsenic trioxide (BDH Analar) in 2.0 M potassium hydroxide, and then acidifying with sulphuric acid. This solution was prepared daily to prevent oxidation to arsenic(V).

A sample of monomethylarsonic acid (MMA) was provided by Dr. D. Bull of this Department. The MMA was prepared by reacting 20 g of As_2O_3 and 13 mL CH_3I in 60 mL of water containing 24 g NaOH. However, subsequent microanalysis of this compound at Otago University indicated an arsenic content of 20.5% rather than the 40.7% content expected for a pure product. For this work, 0.0123 g of the MMA was dissolved in water to produce a stock solution with a concentration of 0.5 ppm (based on the microanalysis).

Standard gold solution was prepared by dissolving gold metal in *aqua regia.* Palladium standard solution (100 ppm) was prepared by dissolving palladium chloride (> 99.999% Aldrich) in concentrated nitric acid and diluting to 1% acid. Rhodium solution was prepared from a 1000 ppm ICP-MS standard obtained courtesy of Australian Government Analytical Laboratories.

The concentrations of dilute standard acid solutions are given as percentages (v/v) of the stock acid as described in Table 2.5.

2.6 SAMPLE COLLECTION

2.6.1 Seawater

Seawater for copper and cadmium analysis was collected from the log-loading dock at the Port of Lyttelton. Samples were collected in acid-washed polypropylene bottles (Nalgene®), and then 0.45 μm filtered and acidified to 1.0% nitric acid within one hour of collection. Samples were stored at room temperature until required, and then filtered to 0.025 μm prior to analysis. Clean disposable polythene gloves were worn throughout the collection process.

2.6.2 Arsenic-contaminated Waters

Surface water was collected from beside a timber treatment plant at Johns Road. Water was 0.45 μm filtered at the collection site into acid-washed plastic centrifuge tubes (Falcon®). The vials were spiked with nitric acid and hydrazine sulphate preservative solution to give final concentrations of 1.0% nitric acid, and 0.2 mM hydrazine. To further preserve the arsenic speciation, samples were refrigerated until analysis. Clean disposable polythene gloves were worn throughout the collection process.

Water was collected from Devil's Creek in acid-washed polythene bottles. This water was not acidified or preserved, but was refrigerated for a year until analysis.

2.7 SPECIATION CALCULATIONS

Solution speciation was modelled using the computer program SOLGASWATER[102] with appropriate constants selected from the IUPAC Stability Constants Database.[103]

2.8 STATISTICAL CALCULATIONS

Regression lines for calibration plots were calculated using graphing software[104] on an Apple Macintosh computer. Errors for standard addition calibrations were calculated according to the method described by Miller and Miller.[105]

Chapter Three

Electrodeposited Modifiers

This chapter has three sections. The first, Section 3.1, is an introduction to palladium as a chemical modifier for ETAAS. The applications, mechanism of action, and mode of use are reviewed and discussed. In section 3.2, alternative noble metal modifiers, their relative merits and applications are reviewed. Section 3.3 describes experimental work aimed at optimising the deposition parameters and analyte stabilising characteristics for electrodeposited palladium modifier as used by Matousek and Powell.[97,99] A brief investigation of iridium and rhodium as alternative modifiers is also described.

3.1. PALLADIUM MODIFIER

3.1.1 Attributes and Uses

Palladium was first used as a chemical modifier for ETAAS in the late 1970s by Shan and Ni.[106] Since then, hundreds of publications have described analyses using modifiers based on palladium, or combinations of palladium and other metals or reducing agents. Palladium meets the criteria for a successful modifier; its salts can be purchased in high purity, and acidified solutions of these can be stored for long periods without degrading their performance as modifiers. Because palladium is rarely an analyte, it does not contaminate the components of the atomiser. Interferences are only observed in a few specific circumstances,[33] and very little background (molecular) absorbance due to palladium is encountered.[36] Palladium does not corrode pyrolytic coated graphite furnace tubes and has in fact been shown to extend furnace lifetimes.[97,107] The greatest attribute of palladium modifier is the ability to thermally stabilise many elements by several hundred degrees.[26,37] This stabilisation permits higher thermal pretreatment (pyrolysis) temperatures to be used, allowing many interferents to be removed without analyte loss.

Palladium has been used successfully with a variety of analytes, particularly volatile metals such as mercury,[108,109] cadmium,[110-113] and lead.[17,114] Direct determination of volatile semimetals by ETAAS is usually insensitive due to loss of analyte even at low pyrolysis temperatures. However, in the presence of palladium, direct determination with little analyte loss has been reported for arsenic,[46,115,116] germanium,[117,118] and selenium.[119-121] Palladium modifiers have also been used to stabilise and determine a variety of other elements including gold,[122] indium,[123] tin,[124] silicon,[125] and antimony.[49]

A further attribute of palladium is its ability to "trap" gaseous species. Consequently, a palladium-coated graphite furnace can be used to adsorb and pre-concentrate metallic vapours and hydrides prior to ETAAS determination. This approach has been successfully used to pre-concentrate and determine arsenic,[126,127] selenium,[128,129] and other hydride-forming elements.[130-134] Mercury has also been determined by this method.[135]

3.1.2 Mechanism of Action

The precise mechanism by which palladium modifier acts is not known for certain, however the mechanism suggested by Qiao and Jackson[136] adequately explains the observed effects of various palladium modifiers. According to this mechanism, the palladium modifier (added as a salt) is first reduced thermally to palladium metal on the graphite surface; this occurs readily at temperatures below 1000 °C. Next, the analyte is reduced on the surface of the modifier and then "dissolves in the molten modifier", possibly forming intermetallic species. The authors proposed that the rate limiting step for analyte atomisation was diffusion of analyte from droplets of molten palladium.

A considerable amount of evidence has been accumulated to support Qiao and Jackson's palladium modification mechanism. In the first step of the proposed mechanism, the modifier must be reduced to a metal. Therefore, the earlier in the temperature program the modifier is reduced, the lower the temperature at which it becomes effective. This accounts for the improved results often obtained when using a reducing agent, or adding hydrogen to the inert gas.[137]

Scanning electron micrographs have shown that, following its reduction from aqueous solution, palladium metal coalesces into globular clusters when heated on graphite surfaces to temperatures of 1000 °C.[137] These clusters form at temperatures well below the melting point (1554 °C), but sufficiently high that palladium atoms and clusters become mobile, and interatomic attractions can promote droplet formation.[138]

In the second step of a palladium modifier's action, the analyte is reduced to a metal on the surface of the elemental modifier. It is likely that the reduction is catalysed by the palladium. The evidence for palladium mediated catalysis has been reviewed by Volynsky.[139] The reaction scheme shown overpage was used to describe catalytic analyte reduction by platinum-group metal modifiers, where M represents the modifier, A is the analyte, and C^* represents active sites on the graphite surface

The initial form of the analyte shown is an oxide (or a chloride). The oxide arises from decomposition of oxyanions during pyrolysis. For example, in nitric acid matrices, analyte nitrates decompose at low temperatures to form metallic oxides.[140-143] In hydrochloric acid media, chlorides may form oxides by hydrolysis and dehydration.[144]

$$MCl_k + nC^* \rightarrow M + C_nCl_k \quad (3.1)$$

$$A_mO_n + M_{(bulk)} \rightarrow A_mO_{n(ad)}\cdot M_{(bulk)} \quad (3.2)$$

$$ACl_m + M_{(bulk)} \rightarrow ACl_{m(ad)}\cdot M_{(bulk)} \quad (3.3)$$

$$A_mO_{n(ad)} + \tfrac{n}{2}C \xrightarrow{M} mA + \tfrac{n}{2}CO_2 \quad (3.4)$$

$$A_mO_{n(ad)} + nC \xrightarrow{M} mA + nCO \quad (3.5)$$

$$ACl_{m(ad)} \xrightarrow{M} A + \tfrac{m}{2}Cl_2 \quad (3.6)$$

$$kA + nM \rightarrow A_kM_n \quad (3.7)$$

Following its reduction, the analyte interacts with the modifier in such a way as to provide thermal stabilisation. The mode of interaction is not entirely clear, and may vary for different elements. However, it appears that analyte stabilisation is generally a result of compound formation. Several authors have used spectroscopic techniques to identify intermetallic and mixed oxide species formed between palladium modifiers and analytes. Styris and co-workers[145] used palladium modifier to determine selenium by ETAAS. They followed the volatilisation process using mass spectrometry and, from the results obtained, inferred that a mixed selenium-palladium-oxide compound was involved in selenium stabilisation.[145,146] Majidi found evidence for a similar compound by using Rutherford back-scattering spectroscopy.[147]

Xuan used X-ray photoelectron spectroscopy and X-ray diffraction analysis to examine germanium atomisation in the presence of palladium and mixed palladium-magnesium modifiers.[117] The results showed that the intermetallic species Ge_9Pd_{23}, $GePd_2$, and the mixed oxide $MgGeO_3$ were formed. Other studies have found evidence of palladium intermetallic species formed with lead,[148] tin,[149] and indium.[149]

Rettberg and Beach[138] evaluated the effect of palladium on the absorbance signals for several elements, including arsenic. They observed that when the modifier mass was increased, the analyte appearance temperatures shifted to higher values. The peak area also increased with modifier mass. The authors argued that because of the large excess of palladium relative to arsenic, the former effect could not be a result of simple enhancement of the metallic bonding between the two species. Instead, they proposed that "bulk" effects based on the amount of palladium present were influencing the atomisation. This implies that the formation of a "solid solution" may be partly responsible for the effects observed when large quantities of palladium are used.

The "solid solution" theory was also used by Volynsky[150] to explain the differences in selenium stabilisation by various platinum-group metals. It is known from powder metallurgy that the formation of a solid solution from two highly dispersed but mutually soluble substances starts at temperatures of $(0.3\text{-}0.4)t_{melt}$, where t_{melt} is the melting point temperature of the more refractory substance. Volynsky found a correlation between selenium pyrolysis

losses and the $0.3t_{melt}$ values for platinum, palladium, rhodium and iridium. Loss of selenium was greatest with the most refractory modifier, iridium (t_{melt} = 2410 °C), and least with palladium (t_{melt} = 1554 °C). Hence the solid solution theory offers one explanation as to why palladium modifier generally performs better than other platinum group metals for stabilising volatile analytes.

In the presence of palladium, atomisation is thought to proceed by direct release of gaseous analyte atoms from the metallic palladium modifier; the rate limiting step being analyte diffusion out of the globular modifier clusters.[136] This mechanism accounts for the peak broadening observed with increasing masses of palladium.[151] Larger amounts of palladium lead to larger globules and, hence, to slower diffusion of analyte to the surface.

Several researchers have used electron microscopy to examine the effect of palladium cluster size on its efficiency as a modifier. Voth-Beach and Shrader[137] found that when the modifier was evenly dispersed as fine particles, analyte atomic absorption profiles were sharper, and had better-defined Gaussian peak shapes. Fine modifier particles also gave better analyte recoveries from a variety of sample matrices. These results could be attributed to higher surface area to volume ratios for the modifier but, in further research, Klinkenberg *et al.*[152] concluded that the distribution of palladium particle sizes was more important than the absolute size. Uniform particles sizes produced sharp even peaks, while less uniform particles produced broader peaks. This effect was attributed to varying rates of analyte diffusion from the different sizes of palladium particles.

3.1.3 Form of Palladium Modifier

The performance of palladium modifiers may depend on which chemical form of palladium is used. The palladium is usually introduced to the furnace with the sample, prior to drying and pyrolysis, either as a nitrate or a chloride. Which form produces the better results is a matter of debate, with different researchers producing contrary results. In one of the earlier studies published on the subject, Voth-Beach and Shrader[137] found that solutions prepared from palladium chloride behaved differently from solutions prepared by dissolving palladium foil in aqua regia. For a variety of elements, palladium chloride solutions performed better than modifier solutions containing 1-2% nitric acid. More recently however, in a paper comparing various forms of palladium for selenium determination, Volynsky and Krivan[121] cited several references in which researchers preferred palladium nitrate to palladium chloride. For selenium determination, the most effective form of the modifier depended on the sample matrix. In chloride-containing samples, palladium chloride and palladium nitrate performed equally, whereas in pure aqueous solutions, the nitrate-based modifier provided better sensitivity and improved thermal stabilisation.[121]

Schlemmer and Welz[153] proposed a mixed modifier of palladium nitrate and magnesium nitrate, and contended that the mixed modifier could be used in a wider variety of applications than palladium alone. The same authors published a study detailing results obtained for twenty-one elements using the mixed palladium/magnesium modifier.[37] Although these and subsequent authors[117,154,155] achieved an impressive degree of analyte stabilisation using the mixed modifier, other researchers have questioned its superiority.

Shan and Wen[36] examined the performance of various chemical modifiers which were used in determining a number of metals in different sample matrices. They concluded that palladium performed well as a universal modifier, and that adding magnesium nitrate was generally undesirable because it introduced a background absorbance. The need for a reducing agent was matrix-dependent.

Bermejo-Barrera *et al.*[109] compared different modifiers for determining mercury in seawater. They found that a palladium modifier gave better sensitivity than either magnesium nitrate or mixed palladium-magnesium nitrate modifiers. Palladium provided better sensitivity and better stabilisation. Analyte recovery was improved when palladium was used in combination with a reducing agent. This finding concurs with work by other researchers who have used reducing agents such as hydroxylamine,[137] ascorbic acid,[136] and tartaric acid[110] to improve the performance of the palladium modifier.

The temperature at which palladium chloride and palladium nitrate modifiers are reduced to the active (metallic) form depends on the sample matrix. To counter this problem, other less matrix-dependent forms of palladium have been developed. For example, palladium oxalate is readily reduced on graphite at temperatures as low as 100-200 °C and because of the stability of the palladium-oxalate complex, is unaffected by different sample matrices.[121] Colloidal palladium modifiers are similarly unaffected.[156] These have the additional advantage of presenting an active elemental-palladium surface to the analyte even before drying is complete. A disadvantage is that palladium colloid solutions are unstable. Even in the presence of stabilisers, palladium colloids tend to aggregate. This decreases the active surface area, and hence the effectiveness, for a given modifier mass.

Other authors have reduced the palladium thermally before adding the sample solution. Using this protocol, He and Ni[157] reported that lead sensitivity was enhanced by fifty percent compared to the conventional thermal co-reduction of palladium chloride and sample. Qiao *et al.*[158] used a pre-reduced palladium-magnesium modifier to determine thallium in the presence of sodium chloride. The pre-reduced modifier prevented loss of thallium chloride during pyrolysis, whereas up to thirty percent of the thallium was lost when the modifier was pre-mixed with the sample.

3.1.4 Palladium Electrodeposition

Metallic palladium modifier has also been used by workers who reduced the palladium by electrolysis. Bulska and Jedral[107] electrodeposited palladium and rhodium modifiers onto the inside of graphite furnace tubes which were then transferred to an ETAA spectrometer for analyte determination. Electrodeposition was carried out, using a constant current, from modifier solutions of 17 g L^{-1}. The absolute amount of modifier used per tube (17 mg for palladium) was large compared to that used for conventional thermal co-reduction (5-50 μg). Because of the large amounts used, residual palladium modifier was observed on the furnace tube even after 60 atomisation cycles using maximum temperatures of 2700 °C. The effectiveness of electro-reduced palladium modifier was compared with that for thermally pre-reduced modifier. For determination of arsenic and selenium, the electrodeposited modifier increased the maximum pyrolysis temperatures by 150 °C and 200 °C respectively. In the case of silicon, the maximum pyrolysis temperature was unaffected but the characteristic mass was reduced by forty percent. The authors suggested that this sensitivity increase was because a continuous modifier layer over the entire inner furnace surface prevents carbide formation.

An electrodeposited palladium modifier was also used in the *in-situ* electrodeposition-coupled ETAAS technique of Matousek and Powell.[97] In addition to thermally stabilising analytes, the pre-reduced modifier improved the characteristics of the furnace surface. Sample electrodeposition without the modifier quickly led to degradation and exfoliation of the pyrolytic graphite furnace coating. The pre-reduced palladium coating prevented surface degradation, and also improved pyrolysis efficiency. Using the pre-reduced modifier, background absorbances due to sodium chloride were seven times lower than those obtained when the modifier was co-reduced with the sample. It is known that palladium "burrows" into crevices and defects in pyrolytic graphite surfaces.[147] Presumably, this "sealing" effect prevents ingress and thus trapping of sample matrix species in the pyrolytic graphite furnace coating.

Smith[159] used Matousek and Powell's *in-situ* palladium electrodeposition for selenium determination. Palladium modifier was deposited and then used to trap and accumulate hydrogen selenide prior to ETAAS determination. The electrodeposited modifier was compared with thermally pre-reduced palladium, and was shown to be 30% more efficient for hydrogen selenide accumulation. Both palladium reduction protocols provided equal thermal stabilisation for the accumulated selenide; i.e apart from sensitivity differences, the pyrolysis loss curves were identical.

Matousek and Powell later went on to characterise the electrodeposited palladium modifier using scanning electron microscopy.[99] The electron micrographs showed that electrodeposition produced a dense, uniform array of palladium domains on the graphite furnace. These were centred around the area opposite the tip of the anode. This contrasted with the situation

when the modifier was thermally reduced. In this case, the palladium domains were less uniform and were concentrated around the drying edges of the modifier solution. The palladium deposit's morphology also depended on the electrolysis medium. For deposition using an uncontrolled potential of 5.0 V, electron micrographs showed that electrodeposition from 0.5% HCl produced a more uniform, higher density of domains than was achieved from 1.0% HNO_3.

Matousek and Powell's palladium electrodeposition technique requires only a fraction of the palladium mass used for conventional thermal reduction; ca 0.25 μg compared with 50 μg. The advantage of this is that trace contaminants in the modifier solution make a smaller contribution to blank signals. However, such small palladium masses are almost completely removed from the furnace in a single atomisation cycle. Accordingly, fresh modifier must be deposited for every determination. This means that the amount of modifier present is always constant and prevents the gradual loss of analyte signal observed when using a single electrodeposition of a large palladium mass.[107]

3.2 ALTERNATIVE NOBLE METAL MODIFIERS

Of all the noble metals that could be used as a modifier for ETAAS, palladium has been the most studied. However, researchers seeking better analyte stabilisation and/or reusable modifiers have experimented with other noble metals. According to Tsalev,[24] the stabilising mechanism for these metals is similar to that for palladium. Of these, iridium has been particularly popular, having similar characteristics to palladium, but a much higher melting temperature; 2410 °C compared with 1554 °C. The higher melting point means that, provided moderate atomisation temperatures (< 2100 °C) are employed, the iridium modifier remains on the furnace and can be reused.[160]

Rademeyer *et al.* used iridium modifier to determine cadmium, manganese, lead, selenium and vanadium.[161] Iridium was deposited both by sputtering and by conventional thermal reduction. Electron microscopy was used to compare the different iridium deposits, showing that sputtering produced a far more homogenous iridium distribution. Using a tube sputtered a single time with a large iridium mass (9700 μg), stable selenium absorbances were obtained for 750 atomisation cycles. Using a smaller mass of thermally deposited iridium (60 μg), Pozebon *et al.*[162] obtained stable readings for only 100 cycles.

The most common application of iridium modifier in ETAAS has been as a trapping agent for hydride collection. Tsalev *et al.* determined a number of hydride-forming elements after accumulating the hydrides on iridium.[160,163,164] The iridium was thermally deposited onto a platform that had been pre-coated with tungsten or zirconium carbide. Comparison showed that the iridium modifier was more thermally stable than palladium, and thus better suited as a re-usable modifier. Unfortunately, no attempt was made to compare the analyte stabilising properties of the two modifiers.

Combinations of iridium and palladium have also been used for hydride accumulation. Shuttler *et al.* used a 1:1 mixture, aiming to stabilise the palladium with the iridium.[165] This combination gave stable analyte absorbances for up to 300 atomisation cycles. Again, no attempt was made to compare the analyte stabilisation or hydride capture efficiency obtained, with that for the individual modifiers. More recently, this comparison was made by Uggerud and Lund,[166] who used palladium and iridium as trapping agents in hydride generation-electrothermal vaporisation-inductively coupled plasma-mass spectrometry (HG-ETV-ICP-MS). The authors did not attempt to re-use the modifiers, and deposited fresh modifier prior to each determination. Although iridium had better characteristics for the ICP-MS determination, the trapping efficiencies of the two modifiers for the HG-ETV process were similar.

In addition to hydride trapping, noble metal modifiers have also been used to trap mercury vapour. Lee and Jung[167] accumulated mercury vapour on a gold-coated porous graphite disc in a carbon rod atomiser. Because of the low atomising temperature used (600 °C), the modifier could be re-used for up to 1000 determinations. Kumar and Meeravali[168] compared different noble metals as mercury trapping agents using platforms wrapped with metal wire or mesh. The metals used were gold, palladium-gold alloy, and platinum-rhodium alloy. The modified platforms could be re-used for more than 500 determinations with no change in sensitivity. All of the trapping agents provided accurate results for analysis of certified standards, however the sensitivities were not equal. The lowest detection limit was obtained using the gold trap. The sensitivity for the gold trap was 1.5 times that for the palladium-gold, and 1.8 times that for the platinum-rhodium trap.

Direct ETAAS mercury determination by Bulska *et al.*[169] yielded a different order of merit for noble metal modifiers. The gold modifier provided little or no thermal stabilisation, and large amounts of mercury were lost during pyrolysis. However, a mixture of gold and rhodium provided high sensitivity and, provided that temperatures did not exceed 2000 °C, was re-usable for up to 500 determinations; the maximum pyrolysis temperature was 200 °C. The greatest degree of thermal stabilisation was provided by palladium modifier. This allowed a maximum pyrolysis temperature of 400 °C, and provided almost the same sensitivity as the gold-rhodium modifier. The authors reported re-using an electrodeposited palladium modifier for up to 450 determinations, using a maximum temperature of 2200 °C.

Other authors have compared different noble metal modifiers for the direct determinations of gold,[122] arsenic,[170] and lead, cadmium and chromium.[171] Unfortunately, due to the different analytes and different experimental conditions used, it is difficult to draw any conclusions from these publications as to which modifier is best. The most thorough comparison to date has been that of Tsalev and Slaveykova,[172] who compared ruthenium, rhodium and palladium modifiers for the determination of 18 different analytes. The authors found that unless a reducing agent was present, all three modifiers provided similar sensitivity and stabilisation.

When the modifiers were used in conjunction with a reducing agent (ascorbic acid), greater stabilisation was achieved for several analytes. For determination of semi-metallic elements, using the reducing agent, the modifier stabilisation efficiency was ranked: ruthenium > rhodium > palladium. In the presence of chloride ion, absorbances were depressed for several analytes; this was least pronounced when the palladium modifier was used.

3.3 OPTIMISATION AND CHARACTERISATION OF PALLADIUM ELECTRODEPOSITION

Experimental work described in this section was directed towards obtaining a better understanding of the electrodeposited palladium modifier used by Matousek and Powell.[97,99] These authors electrodeposited palladium modifier from 40-50 µL of 10 ppm palladium/0.1-0.5% HNO_3 solution, using an applied potential of 4-5 V for 20 seconds. In the experimental work described in this chapter, the various parameters relating to the deposition were examined individually in order to obtain the optimum deposition protocol; i.e. that which produces the greatest sensitivity and analyte stabilisation, with the minimum mass of palladium and deposition time. The parameters investigated included the deposition medium, time and potential, as well as the mass of modifier used. The modifier's stabilisation efficiency was tested using lead as a model analyte. The pyrolysis curve for the electrodeposited palladium was obtained and compared with that for thermally deposited palladium. A brief investigation of iridium and rhodium as alternative modifiers was also conducted.

3.3.1 Experimental and Results

3.3.1.1 Deposition Time

Palladium deposition as a function of time was studied. The palladium concentration used for this study (200 ppb) was lower than that used by Matousek and Powell, so that absorbances were within analytical working range.

Procedure and Results: 20 µL of 200 ppb palladium solution in 1% (v/v) HNO_3 was deposited at 5.8 V for varying lengths of time using the low temperature deposition protocol described in Chapter Two; i.e. deposition effected at room temperature with no inert gas flow. The deposit was rinsed twice for five seconds with 40 µL of water, dried, pyrolysed at 850 °C for 10 seconds, and atomised at 2300 °C. The resulting absorbance was measured at the 340.5 nm palladium resonance line. The absorbances for several deposition times are plotted in Figure 3.1.

3.3.1.2 Mass of Modifier

To study the effect of the mass of palladium modifier, two different modifier masses were used for lead determination. The two modifier solutions used were 10 ppm and 100 ppm palladium in 0.1% and 1.0% HNO_3 respectively. 30 µL of modifier was deposited for 20

seconds using an applied potential of 3.0 V, and the high-temperature deposition protocol described in Chapter Two (i.e. 45 °C, with inert gas flow on). The deposit was rinsed with acid and dried at 110 °C. A lead sample was then deposited from a 50 ppb solution in 0.5 M NaCl /1% HNO_3 using 60 seconds deposition at 3.0 V. The lead deposit was dried, and atomised at 2300 °C. The absorption profiles for lead atomisation with the two different modifiers are shown in Figure 3.2. The lead absorbances with the 100 ppm palladium modifier solution occurred at higher temperatures than those with the 10 ppm modifier. They were also smaller, both in terms of peak, and integrated absorbances.

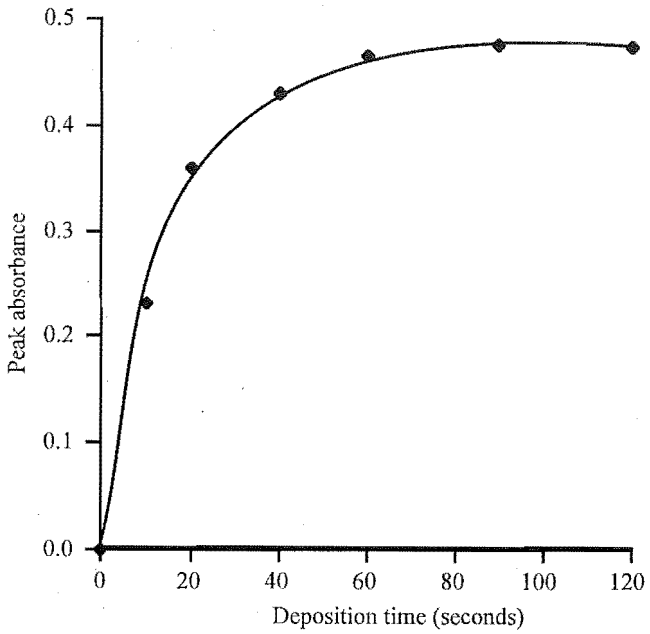

Figure 3.1 Palladium deposition as a function of time. Palladium deposited at 5.8 V from 20 µL of 200 ppb palladium solution in 1% HNO_3. Palladium absorbance measured at 340.5 nm.

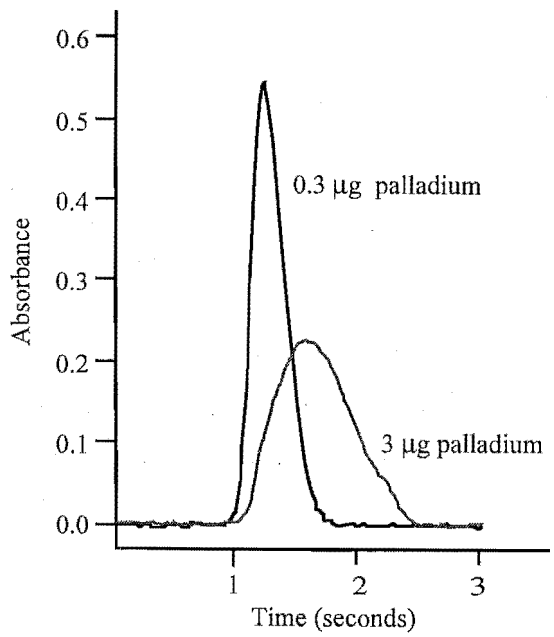

Figure 3.2 Absorbance-time profiles for atomisation of lead deposited for 60 seconds at 2.0 V, from 20 µL of 50 ppb solution in 0.5 M NaCl/1% HNO_3 using two different palladium modifiers: 100 ppm in 1% HNO_3 (3 µg Pd), and 10 ppm in 0.1% HNO_3 (0.3 µg Pd). These were deposited at 3.0 V for 20 seconds. Lead absorbance was measured at 283.3 nm.

3.3.1.3 Deposition Medium

Matousek and Powell[99] observed that palladium deposition from 0.5% HCl produced deposits with a denser and more uniform array of palladium domains than was achieved by deposition from 1% HNO_3. They also found evidence that the HNO_3-deposited palladium did not adhere as well to the furnace surface and was less electrically conductive than the HCl-deposited palladium.

The stabilising effects of palladium modifier deposited from either HCl or HNO_3 were compared. This was done indirectly by studying the atomisation absorbance profiles and sensitivity for a lead sample deposited onto the palladium. The effect of modifier solution acidity was examined using the same protocol.

Procedure and Results: Two 10 ppm palladium solutions were prepared, one in 0.1% HNO_3 and the other in 0.1% HCl. Modifier was deposited at 2.0 V for 20 seconds from 30 µL of solution. The deposit was dried before sample deposition. Lead was deposited at 2.0 V for 60 seconds, from 20 µL of 50 ppb solution in 1% HNO_3, using the high temperature deposition protocol. The deposit was then atomised at 2300 °C and the absorbance measured at the 283.3 nm lead line. Four replicates were measured using the HCl-based modifier solution, followed by four with the HNO_3-based modifier. The mean absorbances for each set of four measurements are shown in Table 3.1. The palladium masses given are approximate, because quantitative deposition is assumed.

Modifier deposition medium	Mean integrated absorbance (n = 4)	Mean peak absorbance (n = 4)
0.1% HCl	0.180 (RSD = 0.71%)	0.781 (RSD = 1.86%)
0.1% HNO_3	0.181 (RSD = 2.09%)	0.814 (RSD = 2.08%)

Table 3.1 Effect of palladium deposition medium on absorbance for lead atomisation (measured at 283.3 nm lead line). 30 µL of 10 ppm palladium solution deposited for 20 seconds at 2.0 V. Lead deposited from 20 µL of 50 ppb solution in 1% HNO_3, at 2.0 V for 60 seconds The high temperature deposition protocol was used throughout. Lead absorbance was measured at 283.3 nm.

Absorbance-time profiles for the lead atomisation are shown in Figure 3.3. The profile for the first measurement using HNO_3-based modifier (following the HCl-based modifier depositions) was shifted to a lower temperature (Reading 2), but subsequent measurements gave absorbance profiles indistinguishable from those obtained using HCl-based modifier solution (Reading 3).

To examine the effect of modifier acidity, the experiment was repeated for modifier solutions containing different HNO_3 concentrations . The results are shown in Figure 3.4.

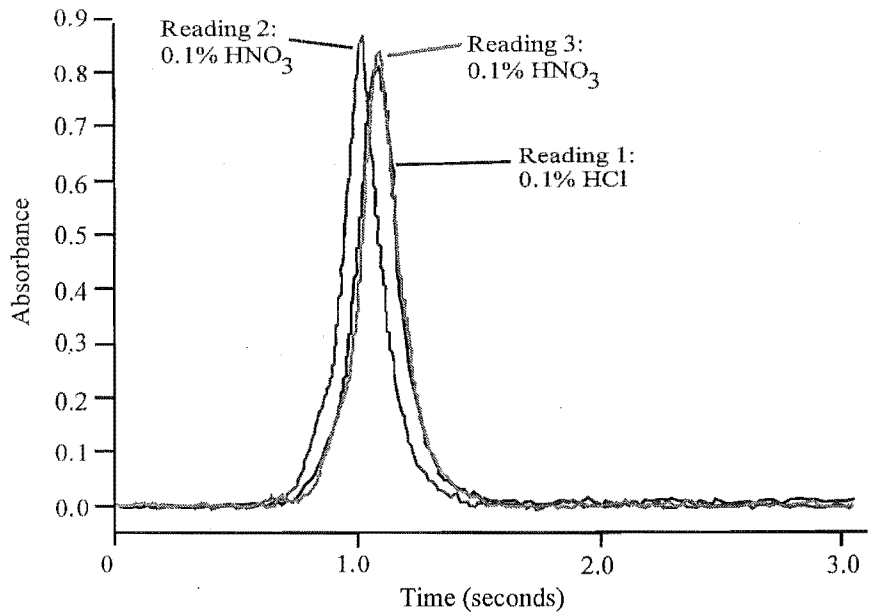

Figure 3.3 Absorbance-time profiles for lead atomisation using two different modifier deposition solutions. 30 µL of 10 ppm palladium solution in either a) 0.1% HCl or b) 0.1% HNO_3, deposited for 20 seconds at 2.0 V. Lead deposited from 20 µL of 50 ppb solution in 1% HNO_3, at 2.0 V for 60 seconds. High-temperature deposition conditions were used. Lead absorbance measured at 283.3 nm.

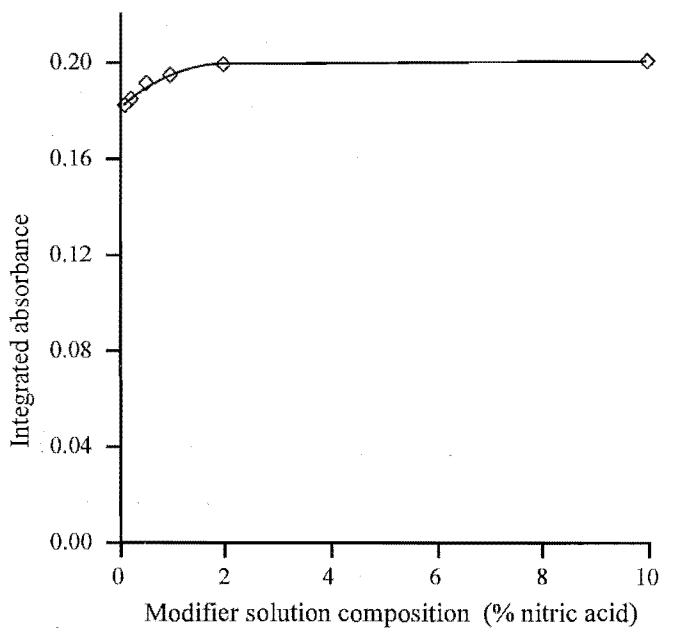

Figure 3.4 Effect of palladium solution acidity on lead atomisation. Palladium was deposited for 20 seconds at 2.0 V, from 30 µL of 10 ppm solutions with varied HNO_3 concentrations. 20 µL of 50 ppb lead in 1% HNO_3 deposited onto the palladium at 2.0 V for 60 seconds. The high-temperature deposition protocol was used throughout. The lead absorbance measured at the 283.3 nm resonance line.

3.3.1.4 Deposition Potential

The amount of palladium deposited under different conditions was examined. Palladium was deposited for 20 seconds from 20 µL of 500 ppb solution, using varying electrolysis potentials. Deposition was effected using the low-temperature protocol. Two different concentrations of acid were employed for the modifier solution; 1.1% and 0.05% HNO_3. The palladium deposit was dried, pyrolysed at 1100 °C, and atomised at 2300 °C. The palladium absorbance was measured at the 340.5 nm resonance line. The results are plotted in Figure 3.5.

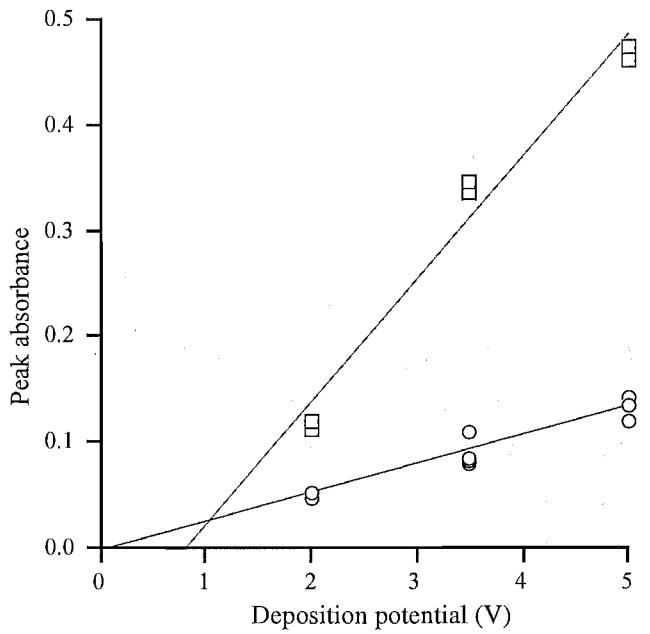

Figure 3.5 Palladium deposition efficiency as a function of deposition potential and deposition medium acidity. Deposition for 20 seconds from 20 µL of 500 ppb palladium solution, in either; (□) 1.1% or (○) 0.05% HNO_3. Low-temperature deposition conditions were used. Palladium absorbance was measured at 340.5 nm.

3.3.1.5 Comparison With Conventional (Thermal) Deposition

The efficiency of palladium electrodeposition was established by comparing peak absorbances for thermally deposited, and electrodeposited (at 2.0 V and 5.0 V) palladium. The absorbance-time profiles for the different deposition methods were used to compare the thermal stability of the palladium deposits. Relatively slow atomisation ramp rates (570 °C s^{-1}) were used to amplify small differences in the atomisation rates.

Electrodeposition: Palladium was electrodeposited for 20 seconds from 30 µL aliquots of solution (200 ppb in 0.1% HNO_3). Deposition was effected using the high-temperature deposition protocol. The deposit was rinsed with 35 µL of water for 10 seconds, dried at 150 °C and then atomised at high temperature (3000 °C) to prevent retention of refractory palladium species on the furnace. The applied potential (2.0 or 5.0 V) remained on for the entire duration of the experiment.

Thermal deposition: 30 µL of the same palladium solution was dried and then pyrolysed at 800 °C for five seconds to effect palladium reduction. The deposit was cooled to 150 °C and then atomised using the same furnace temperature ramp rates as for the electrodeposited sample.

The average integrated absorbances (n=3) for palladium, following electrodeposition at 2.0 and 5.0 V, and for thermal deposition were: 0.477, 0.596, and 0.651 respectively, with relative standard deviations of 0.53%, 1.5% and 1.1%. This corresponds to deposition efficiency of

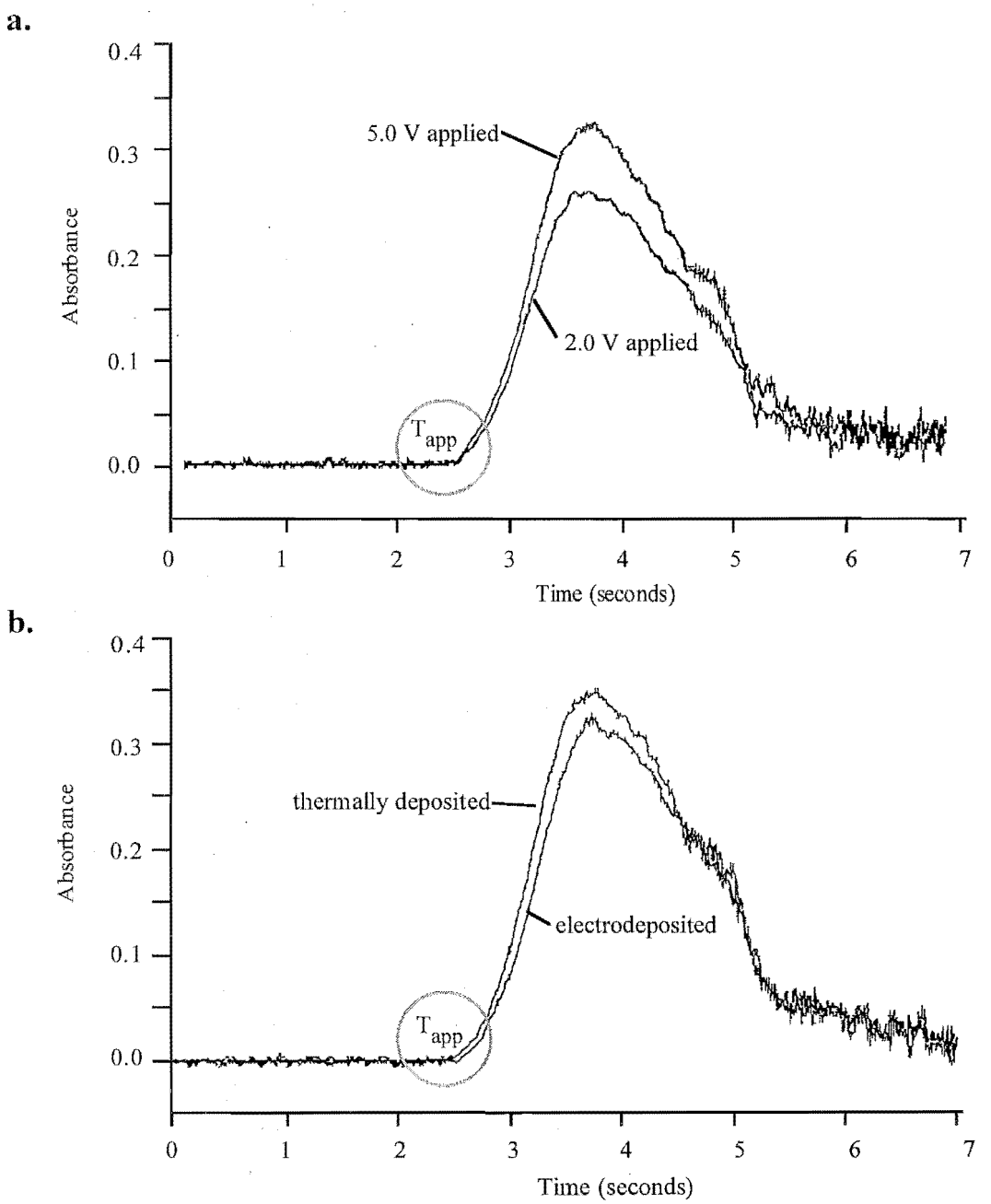

Figure 3.6 Atomisation absorbance profiles for 30 µL of 200 ppb palladium in 1.0% HNO_3 **a)** electrodeposited at 2.0 and 5.0 V. **b)** conventionally (thermally) deposited, and electrodeposited at 5.0 V. Palladium absorbance measured at 340.5 nm.

73% and 92% for the respective 2.0 V and 5.0 V electrolyses relative to the 100% thermal deposition. The atomisation absorption profiles are shown in Figure 3.6. The furnace temperature over the course of the absorption profile increases from 150 °C at time zero, to 3000 °C at five seconds.

3.3.1.6 Effect of Modifier Drying

In this section, the necessity of the modifier rinsing and drying steps was investigated with a view to decreasing analysis times. In previous work using the electrodeposited palladium modifier, the modifier was dried (drying temperature ≥ 110 °C) and rinsed with 3% HNO_3 prior to analyte deposition.[97,159] In subsequent work, Najafi[173] omitted the rinse step but retained the drying step. Further, the previous analysis protocols which required the drying and rinsing steps, used software to control the deposition potential. The potential was applied during the palladium deposition and switched off immediately before the modifier deposition medium was withdrawn. The potential remained off during the course of the acid rinse step. In contrast, most of the electrodeposition experiments described in this thesis were carried out using manual control of the deposition potential. In this situation, the potential remains switched on for the entire duration of the experiment.

The effect of drying or not drying was studied by comparing the lead deposition efficiency for two different modifier deposition protocols. 30 µL of 10 ppm palladium in 1% HNO_3 was electrolysed for 20 seconds using an applied potential of 5.0 V. This was followed by a 110 °C drying step (optional), and a rinse of 30 µL of 3% HNO_3 for five seconds. The potential was switched off during the acid rinse. Lead was deposited onto the modifier from 20 µL of a 20 ppb solution in 1% HNO_3. The average peak absorbance for measurements incorporating the drying step was 0.273 (n=3, RSD 4.6%). For measurements made without the drying step, this dropped by 44% to 0.157 abs (n=2, RSD 0%). These results indicated that with these experimental conditions, modifier drying significantly increases sensitivity.

Several other modifier deposition and drying protocols were compared using manual control of the deposition potential. In contrast to earlier experiments, the deposition potential remained switched on throughout the course of the experiment. Each protocol began by electrolysing 30 µL of 10 ppm palladium solution containing 0.1% HNO_3, for 20 seconds. The deposition was effected using two different applied potentials, 2.0 and 5.0 V, and three different modifier drying protocols: no dry, 150 °C dry, and 1000 °C dry. Deposition was carried out using high-temperature deposition conditions for all experiments except one, in which low-temperature deposition conditions were used in order to replicate the preceding experiment. No acid rinse was included. Following modifier deposition (and drying), 20 µL of lead solution (*ca.* 40 ppb in 1% HNO_3) was deposited for 60 seconds under the same conditions used for deposition of the respective modifier. The absorbances obtained for the lead atomisation are shown in Table 3.2. These results indicate that where no acid rinse is

used, and the deposition potential remains switched on throughout the course of the experiment, drying the modifier has little effect on the sensitivity—regardless of the deposition temperature, potential, or modifier drying temperature.

	Mean lead absorbances (n=4, RSD ≤ 7.6) for the following modifier drying conditions:		
	No dry step	150 °C drying	1000 °C drying
2.0 V, 45 °C, inert gas on	0.506 *(0.129)*	0.513 *(0.126)*	0.520 *(0.128)*
5.0 V, 45 °C, inert gas on	0.498 *(0.146)*	0.511 *(0.150)*	0.535 *(0.156)*
5.0 V, room temperature, inert gas off	0.544 *(0.144)*	0.539 *(0.147)*	0.559 *(0.149)*

Table 3.2 The influence of modifier drying temperature on the deposition efficiency (peak and *(integrated)* absorbances) for lead. Palladium was deposited from 30 µL of 10 ppm solution prepared in 0.1% HNO_3. Lead was deposited from 20 µL of 50 ppb solution in 1% HNO_3. Lead absorbance was measured at the 283.3 nm resonance line

3.3.1.7 Thermal Stability of Palladium

To compare the stability of palladium deposited onto the furnace by thermal and electrodeposition protocols, pyrolysis curves for the two deposition methods were measured. A 200 ppb palladium solution was prepared in 0.1% HNO_3. For electrodeposition, a 30 µL sample was electrolysed for 20 seconds at an applied potential of 2.0 V, using the high-temperature deposition protocol. The deposit was rinsed with 35 µL of water to remove residual solution, and then dried, pyrolysed, and atomised at 2800 °C. For thermal deposition, the same volume of solution was injected into the furnace, dried and pyrolysed at varied temperatures, and then atomised at 2800 °C. The atomisation temperature ramp rate, as described in Chapter Two, was 1900 °C s^{-1}, for both deposition protocols, and for all pyrolysis temperatures.

To aid comparison, the resulting pyrolysis curves (Figure 3.7) have been scaled using the integrated absorbance values for pyrolysis temperatures of 1200 °C. This scaling is necessary because the electrodeposition protocol gives lower sensitivity (due to non-quantitative deposition within the 20 second electrolysis time).

It was observed that when "cleaning" a used furnace tube (by heating to 2800 °C), a significant palladium absorbance was recorded. This was further investigated, by electrodepositing 30 µL of 500 ppb palladium solution in 1% HNO_3 onto a clean furnace, drying, and atomising at low temperature (2300 °C). A peak absorbance of 0.640 was recorded. The furnace was then heated to high temperature (2800 °C) twice, with no further addition of palladium. The absorbance for the first high temperature firing was 0.076, and for the second 0.019

(corresponding to baseline noise). This effect was reproducible for palladium deposited both thermally and by electrodeposition. Atomisation profiles for consecutive low and high temperature atomisations are shown in Figure 3.8. The atomisation temperature ramp began at 850 °C and ended at either 2300 °C or 2800 °C. The relative ramp rates were 1450 °C s^{-1} and 1625 °C s^{-1} respectively. The peak absorbances in both cases appeared at the maximum point of the furnace temperature ramp.

To test whether the amount of the more refractory form of palladium was cumulative, four consecutive depositions and corresponding low-temperature (2300 °C) atomisations were carried out. The furnace was then heated to high temperature (2800 °C) twice. The peak absorbance for the first high temperature firing was 0.235 (corresponding to accumulation from four single depositions) followed by 0.023 for the second firing (corresponding to no remaining palladium).

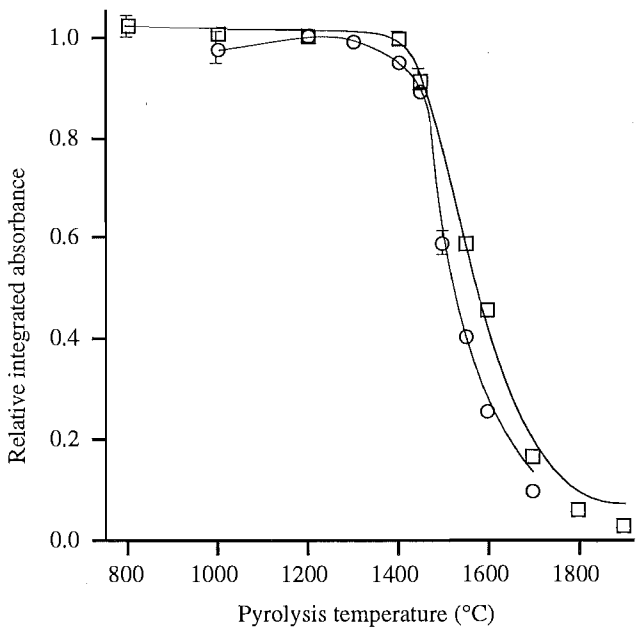

Figure 3.7 Pyrolysis curves for palladium deposited from 30 µL of 200 ppb palladium in 1% HNO_3. By thermal deposition (○) and by electrodeposition for 20 seconds at 2.0 V (□). Electrodeposition was effected under high-temperature conditions. Palladium absorbance was measured at 340.5 nm.

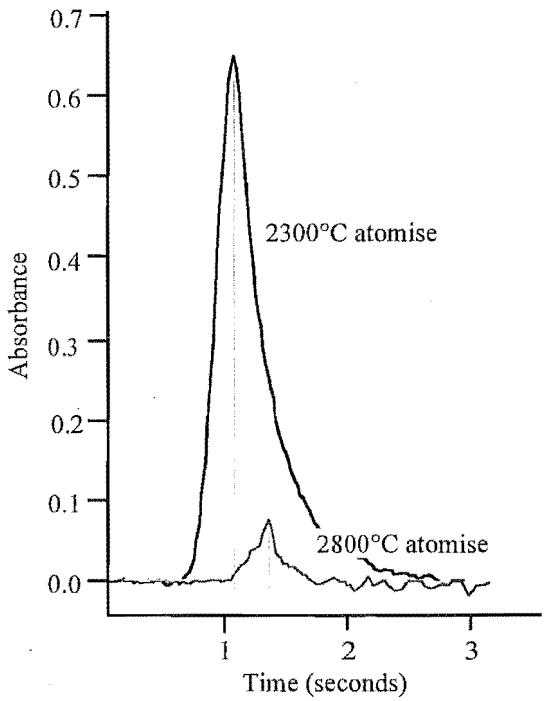

Figure 3.8 Absorption-time profiles for palladium atomised at 2300 °C, and the residual palladium atomised at 2800 °C.

3.3.2 Discussion

3.3.2.1 Deposition Time

The primary aim of this section of work was to optimise the palladium electrodeposition step. That is, to produce in the minimum time, a modifier deposit that gives high sensitivity and thermal stability for the analyte. Figure 3.1 shows that it requires 60 seconds for deposition to be quantitative, however, deposition is more than 80% complete within the first 20 seconds of electrolysis. Provided that sufficient palladium is accumulated to stabilise a subsequently deposited analyte, there is no need to carry out exhaustive electrolysis. As can be seen from Figure 3.2, a twenty second deposition from a 10 ppm solution in 0.1% HNO_3 gives good sensitivity for lead determination (characteristic mass *ca.* 8.0 pg). Figure 3.2 also shows that although larger amounts of palladium further increase the analyte stability, the sensitivity is decreased. This observation agrees well with previously reported findings.[138,173,174]

3.3.2.2 Deposition Medium

Table 3.1 shows that for lead determination, the sensitivity is the same whether using modifier in 0.1% HCl or 0.1% HNO_3. Figure 3.3 shows that palladium deposits produced from the two different media (readings "one" and "three") are equivalent in terms of stabilisation (T_{app}) and the release temperature (T_{max}) for lead. This is contrary to the findings of Najafi,[173] who observed a lower degree of lead stability when using palladium deposited from HNO_3. It is possible that Najafi unwittingly observed the same phenomenon shown in Figure 3.3; i.e. immediately following measurements made using HCl-based modifier, the first lead atomisation

profile using the HNO_3-based modifier was shifted to lower temperature. Subsequent measurements were the same as those for the HCl-based modifier (closely resembling the results presented by Najafi). The reason for this shift is unclear.

An alternative explanation for the different findings is the use of different experimental conditions. These are respectively for this study, and that of Najafi: different acid concentrations for palladium deposition (0.1% acid vs 1%), different media (1% HNO_3 vs 0.5 M NaCl) and different potentials (2.0 V vs 3.0 V) for lead deposition.

Nitric acid was chosen as the palladium deposition medium for use in further studies. For practical purposes, the concentrated nitric acid produces fewer fumes than concentrated hydrochloric acid, and so is easier to handle for preparing dilutions. Also, solutions prepared in nitric acid can be used for both ED-ETAAS and conventional ETAAS analyses, whereas hydrochloric acid is not regarded as a good sample medium for ETAAS.

Figure 3.4 shows that the acid concentration in the palladium modifier solution has a minimal effect on the integrated absorbance for lead analysis. The peak height absorbances (not shown) were unaffected (within error) by the acid concentration. This indicates that under the conditions used, similar amounts of palladium are deposited regardless of the acid concentration.

The nitric acid concentration selected for modifier deposition was 0.1%. This gave good analytical sensitivity, while reducing the size of analyte blanks arising from the nitric acid.

Figure 3.5 shows the effect of deposition potential on the amount of palladium deposited for two different concentrations of nitric acid. For the conditions used, deposition is not quantitative, hence the absorbance reflects the rate of electrodeposition. The results show a strong rate dependence on both the potential and the acid concentration. This is probably related to the current density, and convective stirring arising from hydrogen evolved at the cathode (furnace surface). Within the graphite furnace, hydrogen evolution is first apparent as bubbles on the furnace surface at an applied potential of *ca.* 2.0 V. This is reflected in Figure 3.5, where very little deposition occurs at potentials below 2.0 V. Higher potentials, and higher acid concentrations promote more hydrogen evolution, and hence more efficient sample stirring and electrolysis. The increased current density for the higher acid concentration also contributes to the greater deposition efficiency.

For situations where deposition is effected while using a raised temperature and a constant flow of inert gas above the sample, sample mixing is not dependent on hydrogen evolution. Convection occurs within the sample, as the solution is heated from the bottom by the furnace, and cooled from the top by the inert gas stream. This convectional stirring is readily observed in an experiment to simulate the graphite furnace electrodeposition conditions. When aluminium powder is added to a drop of water on a section of graphite furnace, it slowly settles to the bottom. When the furnace section is placed on a hotplate at 45 °C, and

an inert gas stream is passed over the top of the liquid, the aluminium powder circulates rapidly and does not settle. Under these conditions, sample electrodeposition is efficient at potentials below those where rapid hydrogen evolution occurs, and there is little difference in deposition efficiency at 2.0 V and 5.0 V.

The finding that deposition rate is strongly dependent on deposition potential conflicts with the findings of Najafi,[173] where no such relationship was observed. The difference probably arises from the amount of palladium used in the experiment. For the results presented in Figure 3.5, the amount of palladium present in the deposition solution was 10 ng. The 400 ng used by Najafi produced peak absorbances greater than 2.0—well above the usable linear working range for absorbance measurements. Therefore, few meaningful conclusions can be derived from her results.

3.3.2.3 Thermal Stability of Palladium Deposits

Figure 3.6 compares the thermal stability of palladium deposited thermally with that for palladium deposited by electrolysis at 2.0 and 5.0 V. It can be seen from the relative peak heights and areas, that the electrodeposition is almost quantitative, and that by using convection-controlled deposition (45 °C with inert gas flow), deposition efficiency at 2.0 V is only marginally lower than at 5.0 V. The temperature at which palladium atoms first appear (appearance temperatures) is the same for palladium electrodeposited at both 2.0 V and 5.0 V. There is a slight difference between the appearance temperatures for thermally deposited palladium, and palladium electrodeposited at 5.0 V. Further evidence for a small difference in stability can be seen by comparing the pyrolysis curves (Figure 3.7). These show that thermally deposited palladium begins volatilising at a slightly lower temperature than electrodeposited palladium. Complete volatilisation also occurs at a lower temperature for the thermally deposited modifier. However, the difference is small.

The reason(s) for the improved thermal stability of the electrodeposited palladium could be thermodynamic, kinetic, or a combination of both. For desorption of a metal (e.g. palladium) from a substrate (e.g. graphite), the activation energy and (kinetic) order of release (desorption) depend on such factors as the metal-substrate interaction, the geometry of the particles from which atoms desorb, and the mass of substance desorbing.[175] Given the different morphologies of palladium deposits produced by thermal or electrochemical reduction, all of these factors are likely to influence the deposit stability. Electrodeposited palladium forms very fine particles over the furnace surface[107] while the particles produced by thermal palladium reduction are generally larger and less evenly distributed.[99] Therefore, both the geometry and average mass of the deposits will be different. Because of the smaller particle size, the electrodeposited palladium particles are in more intimate contact with the graphite furnace surface. If the C-Pd interaction is stronger than that for Pd-Pd, then we could expect a smaller palladium particle to be more thermally stable than a larger one.

The other feature of interest in Figure 3.6 is the shoulder that appears on the trailing edge of the absorbance-time profiles. This shoulder implies that atomisation occurs from two forms of palladium; one more thermally stable than the other. Further evidence for this is shown in Figure 3.8 where, following atomisation at 2300 °C, the residual palladium can only be atomised by using temperatures ≥ 2800 °C.

This more refractory form of palladium may correspond to palladium atoms that are in intimate contact with the graphite surface. However, given that the refractory palladium accumulates over several atomisation cycles, it is more likely to correspond to a palladium carbide or palladium that has penetrated into the pyrolytic graphite surface of the furnace. Majidi and Robertson[147] used Rutherford backscattering spectrometry to show that palladium diffused into pyrolytic graphite at elevated temperatures. The diffusion began at temperatures as low as 370 K (97 °C) with palladium diffusing up to 2 nm deep into the surface. At temperatures above 770 K (497 °C), the palladium was shown to penetrate more than 5 nm into the pyrolytic graphite surface. It is likely that the vaporisation and atomisation kinetics of deeply intercalated palladium would be slow compared with those for palladium present on the furnace surface. To explore this hypothesis further would entail performing a series of experiments where different pyrolysis temperatures are held for extended times (*ca.* 60 seconds) prior to atomisation. If intercalated palladium were the refractory species, the amount of refractory palladium formed per atomisation cycle should increase with pyrolysis temperature.

The refractory palladium species showed no capacity to stabilise lead. Furnace tubes that had undergone many atomisation cycles (at 2300 °C) using palladium modifier, and hence would be expected to have accumulated a significant amount of refractory palladium, behaved as unmodified furnaces. Thus for subsequent work, palladium modifier was redeposited for each determination.

3.3.2.4 Modifier Drying and Rinsing

For earlier palladium electrodeposition protocols, as used by Powell and Matousek,[97,99] Smith,[159] and Najafi,[173] it was considered necessary to dry the palladium deposit prior to analyte deposition. Using the original protocol, where the modifier deposition is followed by an acid rinse during which no potential is applied, the drying step seems to be important to the analyte deposition. Sensitivity is greatly decreased if the drying step is omitted. However, Table 3.2, where the deposition protocol does not include the acid rinse step, shows that the drying step has no significant effect on analyte sensitivity, regardless of the deposition conditions. The reasons for the difference are unclear. It is unlikely that palladium deposits can be dissolved by 3% HNO_3, so the difference must lie in the nature of the deposits.

Matousek and Powell[99] reported that palladium deposited from nitric acid appeared to be loosely bound to the furnace surface, and during scanning electron microscopy, exhibited fluorescence (characteristic of non-conducting or semi-conducting materials). Palladium

compounds are readily reduced to palladium metal by hydrogen gas.[176] The modifier deposition protocol employed by Matousek and Powell used a 5.0 V deposition potential. At this voltage, vigorous hydrogen evolution at the cathode (furnace surface) would have saturated the deposition medium with molecular hydrogen. It is likely therefore, that some palladium is chemically reduced by nascent hydrogen rather electro-reduced onto the cathode surface. Such chemically-reduced palladium would be found as free particles rather than the surface-bound deposits formed by electrolysis. Credence is lent to this hypotheses by Matousek and Powell's observation that the spent palladium deposition medium contained palladium metal which could be removed by micro-filtration.[177] This particulate palladium probably corresponds to palladium reduced by nascent hydrogen.

If any hydrogen-reduced palladium adsorbs to the furnace surface, this would account for the loosely-bound, non-conducting palladium deposit that Matousek and Powell observed after deposition from nitric acid. The reason that this was not observed following deposition from hydrochloric acid may lie in the concentration of the acid. The nitric acid deposition medium was 1% nitric acid; approximately 0.16 M. The hydrochloric acid deposition medium was 0.5%; approximately 0.06 M. It may be that the three-fold difference in acidity was sufficient to bring about significant chemical reduction in the nitric acid, but not in the hydrochloric acid.

Loosely-bound or adsorbed palladium particulates on the furnace surface could conceivably be desorbed by a 3% HNO_3 rinse step. The drying step could serve to desolvate the particles, which could then adsorb to the furnace, providing an electrically conductive surface for analyte deposition.* The decrease in analyte sensitivity where the drying step is omitted could have two causes. Particulate palladium that is not secured to the furnace surface by drying could be removed along with deposition or rinse media during subsequent steps. Loss of sufficient modifier could reduce analyte stability and sensitivity. Alternatively, analyte may deposit on, or adsorb to, loosely-bound palladium particles which are then removed from the furnace in subsequent rinse steps. This would have a far more drastic effect on analytical sensitivity, as analyte is actually removed from the furnace prior to atomisation.

The work which showed that modifier drying was unnecessary (where the acid rinse step is omitted), was performed late in the course of this research. Consequently, unless otherwise stated, the palladium deposit was dried at temperatures ≥ 110 °C.

---

* Note: The work of Majidi and Robertson,[147] showing that palladium diffuses into pyrolytic graphite at temperatures as low as 370 K, implies that palladium deposits will be at least partially "mobile" at the 110°C temperature used for drying the deposit.

3.4 ALTERNATIVE NOBLE METAL MODIFIERS

The purpose of this section was to briefly explore other noble metals as modifiers for ED-ETAAS, to see if they offered any significant advantages over the palladium modifier. Such advantages may include: improved analyte stability, improved sensitivity for analyte determination, or the ability to re-use the modifier.

3.4.1 Experimental and Results

3.4.1.1 Pyrolysis Loss Curves

The analyte stabilising properties of three different modifiers (palladium, iridium, and rhodium) were examined by comparing the pyrolysis loss curves for lead deposited onto the modifiers. High-temperature deposition protocols were used to deposit the lead analyte and all three modifiers

Palladium: Palladium was deposited at 5.0 V for 20 seconds from 30 µL of 10 ppm solution in 1% HNO_3. The deposit was rinsed with 3% HNO_3 and dried prior to lead deposition. Lead was deposited from 20 µL of 20 ppb solution in 1% HNO_3.

Iridium: Iridium was deposited from 30 µL of 100 ppm solution using an applied potential of 2.0 V for 20 seconds. The deposit was rinsed with 0.1% HNO_3 and dried at 110 °C prior to lead deposition. Lead was deposited at 2.0 V for 60 seconds from 20 µL of 50 ppb solution in 1% HNO_3.

Rhodium: Rhodium was deposited at 2.0 V for 20 seconds from 20 µL of 10 ppm solution in 0.1% HNO_3. The modifier was dried (no acid rinse) at 110 °C prior to lead deposition. Lead was deposited at 2.0 V for 60 seconds from 20 µL of 50 ppb solution in 1% HNO_3.

In each case, the lead absorbance was measured at the 283.3 nm lead line. The resulting pyrolysis curves, shown in Figure 3.9, have been scaled to compensate for the different amount of lead used in each experiment. The absolute absorbances are shown as a fraction of the absorbance measured at the pyrolysis temperature that gave the highest sensitivity for lead; i.e. 1100 °C for palladium, 900 °C for rhodium, and 800 °C for iridium.

3.4.1.2 Sensitivity For Lead Using Different Modifiers

The analytical sensitivity for lead determination was compared using the three modifiers, palladium, rhodium, and iridium. High-temperature deposition protocols were used to deposit the lead analyte and all three modifiers.

Palladium versus Rhodium: Palladium and rhodium were deposited for 20 seconds at 2.0 V from 10 ppm solutions containing 0.1% HNO_3. The modifier deposits were dried to 110 °C prior to lead deposition. Lead was deposited onto the modifier for 60 seconds at 2.0 V from 50 ppb solution in 1% HNO_3. The lead was pyrolysed at 1100 °C, and atomised at 2300 °C.

The lead absorbance was measured at the 283.3 nm lead line.

The average peak absorbance for the lead signal using palladium modifier was 0.540 (n=2, RSD=0.7%); using the rhodium modifier, the lead absorbance was 0.536 (n=3, RSD=4.5%). Absorbance-time profiles for lead atomisation with the two modifiers are shown in Figure 3.10.

Following the lead determination using the rhodium modifier, lead was determined using no further modifier depositions. The first determination resulted in an absorbance of 0.141, the next was 0.095.

Palladium versus Iridium: Experimental conditions were as for the previous experiment. Iridium was deposited from a 10 ppm solution containing 1% HNO_3.

The average peak absorbance for the lead signal using palladium modifier was 0.562 (n=4, RSD=2.9%); using the iridium modifier, the lead absorbance was 0.565 (n=2, RSD=0.6%). The absorbance-time profile for lead atomised with iridium modifier is shown in Figure 3.10.

Following the lead determination using the iridium modifier, lead was determined without further modifier deposition. The first determination resulted in an absorbance of 0.347, the second determination, 0.359.

3.4.2 Discussion

One of the primary aims of this section of work was to find a modifier which would provide better thermal stabilisation for a lead analyte than achieved with palladium modifier. Figures 3.9 and 3.10 both show that neither rhodium nor iridium offers improved lead stabilisation. Contrary to expectations, the stabilising ability for each of the three modifiers is inversely proportional to its melting point. The melting points for palladium, rhodium and iridium (in order of lead stabilising ability) are 1554 °C, 1966 °C, and 2410 °C respectively.[31]

The inverted order of the modifier's stabilising properties relative to their melting points, implies that diffusion of analyte from clusters of modifier (on atomisation) is influenced more by interactions between analyte and modifier than the melting temperature of the modifier. This lends support to the idea of low temperature intermetallic formation between analyte and modifier metals.

The finding that palladium provides better lead stabilisation than rhodium, concurs with the results of Bulska *et al.*,[169] who found that palladium stabilised mercury to a higher degree than did rhodium. Unfortunately, attempts to find analogous comparisons for palladium and iridium in the literature have proved unsuccessful, most researchers having focussed on the re-usable nature of the iridium modifier rather than its relative stabilising properties.

The finding that all three modifiers produced identical sensitivity for lead determination is not a universally applicable principle. For mercury determination, Bulska *et al.*[169] found that

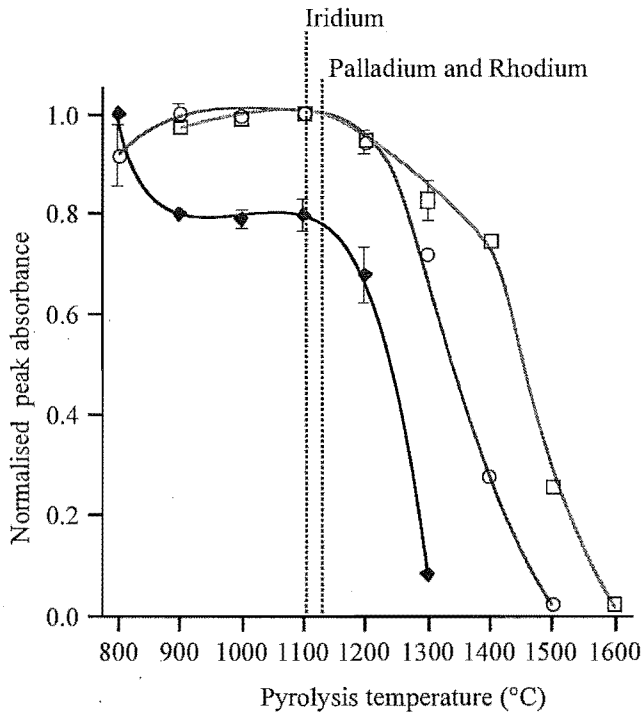

Figure 3.9 Pyrolysis curves for electrodeposited lead using three different electrodeposited modifiers: palladium (□), rhodium (○) and iridium (◆) Lead and palladium deposited from 1% HNO_3, and iridium and rhodium from 0.1% HNO_3. Errors are shown as RSDs. Maximum lead pyrolysis temperatures for each modifier are indicated by the dotted vertical lines.

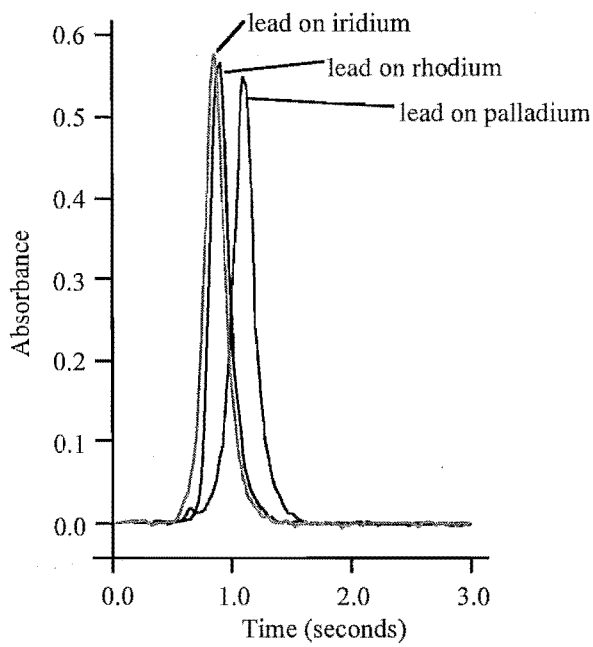

Figure 3.10 Absorbance-time profiles for lead atomisation using three different electrodeposited modifiers. Iridium deposited from 1% HNO_3, rhodium and palladium deposited from 0.1% HNO_3. Lead deposited from 1% HNO_3, and atomised at 2300 °C. Identical furnace temperature ramp rates were used for each experiment.

while rhodium and iridium provided almost the same sensitivity for mercury determination, this was only 60% of the sensitivity achieved using palladium modifier. The difference between the mercury results and those presented within this chapter, may be due to the morphology of the modifier deposit. The modifiers used by Bulska *et al.* were thermally reduced prior to injection of sample into the furnace. The electrodeposition protocol used here, is likely to produce a modifier deposit with a higher surface area and more even particle size distribution, resulting in improved analyte stabilisation and sensitivity.

The attempt to find a modifier that could be re-used proved fruitless. In the case of rhodium, sensitivity for lead determination decreased markedly (>70%) when atomisation took place with no further rhodium addition. The situation for iridium while not quite so marked, still resulted in a considerable sensitivity decrease (*ca.* 40%) for lead determination when no further iridium was used. Although it is likely that some of each modifier (iridium in particular) remains on the furnace after atomising at 2300 °C, either the amount is too little, or the form unsuitable to significantly stabilise the lead analyte—this could not readily be checked. It is possible that whatever modifier remains is deeply intercalated under the pyrolytic graphite surface and hence interacts weakly with the lead analyte. Studies where modifiers have been reused, have generally used large amounts of modifier,[162,165] and/or lower atomisation/ cleaning temperatures[160,163,164,169] than were used in this study. Both of these practices would act to retain a larger amount of modifier in the furnace after each atomisation cycle.

None of the available alternatives to palladium modifier offered any advantage for lead determination. Sensitivity was equal whether using palladium, rhodium, or iridium modifier. None of the modifiers proved to be re-usable without significant sensitivity loss, and palladium modifier provided the best thermal stabilisation for lead determination. Therefore, palladium was selected as the modifier of choice for further work presented in this thesis.

Chapter Four

Reducible Metals in Acid Media

4.1 INTRODUCTION

This chapter describes method development for the ED-ETAAS technique. Initial work used lead in acid media to model a common analyte in a relatively simple sample matrix. The various parameters relating to lead deposition and atomisation, such as the deposition medium, electrolysis time, and washing/rinsing protocols were examined and optimised. The causes of high analyte blanks were investigated, and solutions to these problems tested and evaluated. The method was then characterised by comparing sensitivity and thermal stability for lead determination by ED-ETAAS and conventional ETAAS. The characteristic mass, linear working range, and detection limits for lead determination by ED-ETAAS were determined.

The protocol developed for lead analysis was then adapted for determination of other reducible metals in acid media. These metals were copper, bismuth, cadmium and nickel. The sensitivity, degree of stabilisation achieved by the deposition process, and effect of deposition media were evaluated for each metal.

4.2 LEAD DETERMINATION

4.2.1 Deposition Parameters

The ED-ETAAS protocol used by Matousek and Powell[97] for lead determination (in 1% HNO_3 solution) involved depositing, drying and rinsing the palladium modifier, followed by electrolysis of the lead sample solution (25-30 µL) for 60 seconds at 4.0-5.0 V. The lead deposit was then rinsed with 50-60 µL of water. The purpose of the work described in this section was to optimise the deposition medium and shorten the analysis time, while retaining sensitivity equal to or exceeding that obtained using conventional ETAAS.

4.2.1.1 Deposition Medium

Nitric Acid versus Hydrochloric Acid

Lead deposition efficiency from HCl was compared with that from HNO_3. Following modifier deposition, 20 µL of 50 ppb lead solution was deposited for 60 seconds using an applied potential of 4.5 V. Three different lead sample media were used: 1% HNO_3, 0.5% HNO_3 / 0.73% HCl, and 1.45% HNO_3. Following deposition, the lead deposit was rinsed with 30 µL of HNO_3 for 60 seconds, and then with 30 µL of water for 10 seconds. The potential was

switched on (under automatic control) during each step; deposition was effected using the low-temperature deposition protocol. The samples were pyrolysed at 400 °C, and then equilibrated at 400 °C prior to atomisation at 2300 °C (as described in Chapter Two). The mean lead absorbances (blank corrected), measured at 283.3 nm are shown in Table 4.1.

Lead deposition medium		Mean peak absorbance (n=4)	RSD
1% HNO_3	(*ca.* 0.16 M H^+)	0.435	2.82%
0.5% HNO_3 / 0.73% HCl	(*ca.* 0.16 M H^+)	0.175	6.36%
1.45% HCl	(*ca.* 0.16 M H^+)	0.031	6.46%

Table 4.1 Relative sensitivity for determination of lead by ED-ETAAS, using different sample electrodeposition media. Lead electrodeposited from 20 µL of 50 ppb solution at 4.5 V, onto pre-deposited palladium modifier.

Nitric Acid Concentration

Having established HNO_3 as a suitable electrodeposition medium, the effect of HNO_3 concentration was examined. 20 µL of 50 ppb lead solution (prepared in varying concentrations of HNO_3) was deposited onto palladium, at 2.0 V for 60 seconds. The lead deposit was then rinsed with 30 µL of 1% HNO_3 for 60 seconds, then 30 µL of water for 10 seconds. The deposition potential remained on throughout the entire process. The lead absorbances measured at 283.3 nm are shown in Figure 4.1.

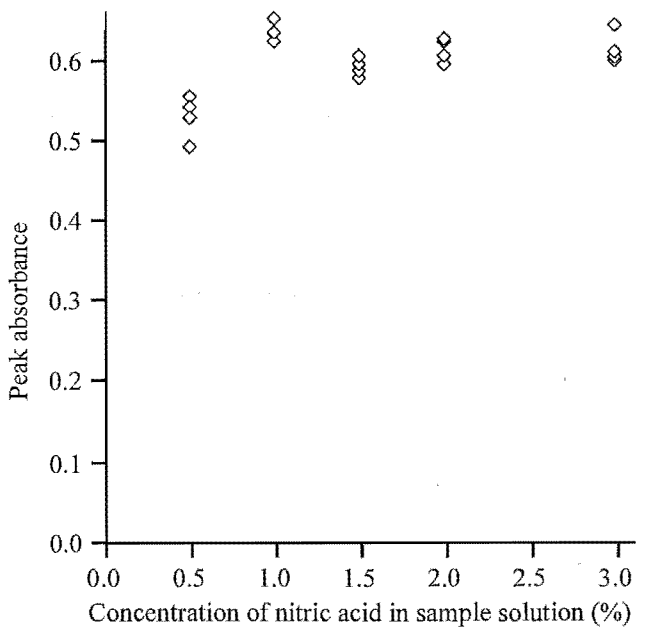

Figure 4.1 Lead deposition as a function of medium acidity. Lead deposited onto palladium, from 20 µL of 50 ppb lead solution, at 2.0 V for 60 seconds, redeposited from 30 µL of 1% HNO_3 for 60 seconds, then rinsed with 30 µL of water for 10 seconds. Lead absorbance measured at 283.3 nm.

4.2.1.2 Deposition Efficiency

Procedure: To determine whether the lead electrodeposition process was quantitative, the spent lead-electrodeposition matrix was analysed using square wave anodic stripping voltammetry (SW-ASV). Palladium was electrodeposited on the furnace for 20 seconds from 30 µL of 10 ppm solution in 0.1% HNO_3. The palladium deposit was rinsed with 30 µL of 1% HNO_3 and dried at 110 °C prior to sample deposition. The lead sample was electrodeposited for 60 seconds from 40 µL of 100 ppb solution prepared in 1% HNO_3. The electrodeposition was carried out using the low-temperature deposition protocol with a deposition potential of *ca.* 4.5 V. After sixty seconds of electrolysis, the lead deposition medium was removed from the furnace using a micropipette tip, and collected in a vial. Once sufficient solution had been collected from replicate depositions, the lead content of the solution was determined using SW-ASV.

SW-ASV analysis was carried out by adding 100 µL of the spent electrodeposition solution to 5.0 mL of water in a borosilicate-glass cell. The solution was acidified with 10 µL of HNO_3 to provide sufficient ionic strength for analysis, and deoxygenated for 10 minutes. A deposition time of 600 seconds and an applied potential of -0.9 V (vs Ag/AgCl) were used to preconcentrate the lead on a hanging mercury drop electrode (HMDE). After a ten second equilibration time, the lead was stripped from the electrode by ramping the cathode potential from -0.9 to -0.2 V. The square wave stripping parameters were: 100 Hz frequency, 2.0 mV scan increment, and 20 mV pulse height.

Measurements were made for the blank stripping medium (0.2% HNO_3), the collected electrodeposition residue, and the original 100 ppb lead solution.

Results:

Sample Composition	SW-ASV stripping current
(1) Blank (0.2% HNO_3)	29.3 nA
(2) (1) + 100 µL of spent electrodeposition medium	47.6 nA
(3) (2) + 100 µL of 100 ppb lead solution	312.7 nA

Hence, the residual lead concentration, calculated as a percentage of the original 100 ppb lead concentration, was 6.9%. This corresponds to a 93% deposition efficiency.

4.2.1.3 Deposition Potential

The effect of the deposition potential for lead was examined. The lead sample was deposited onto a palladium-modified furnace from 20 µL of 50 ppb solution containing 1% HNO_3. The lead deposit was re-deposited from 35 µL of 1% HNO_3 for 60 seconds and rinsed with 35 µL of water for five seconds. The sample was then pyrolysed at 1100 °C, equilibrated at 400 °C, and atomised at 2300 °C. The experiment was repeated using a range of deposition potentials.

Because the deposition rate depends on stirring, deposition was carried out under conditions where stirring was provided by thermal convection (high-temperature deposition protocol). This allowed efficient deposition to occur at potentials below those required for stirring through hydrogen evolution. The thermal convection was effected by depositing at elevated temperature (45 °C) and flowing inert gas across the sample solution. The results are shown in Figure 4.2.

4.2.1.4 Rinses and Acid Re-depositions

Matousek and Powell's electrodeposition protocol employed washing steps which were designed to remove residual sample matrix from the furnace prior to analysis.[97] These steps involved either; "rinsing" the sample deposit with water or dilute nitric acid (no applied potential), or "re-depositing" the sample by using a prolonged acid rinse with the deposition potential switched on. These *rinsing* and *re-deposition* steps were examined to ensure that analyte was not being 'lost' through dissolution and subsequent removal with the rinse/re-deposition solution. Such analyte loss is considered undesirable because of the corresponding decrease in analytical sensitivity.

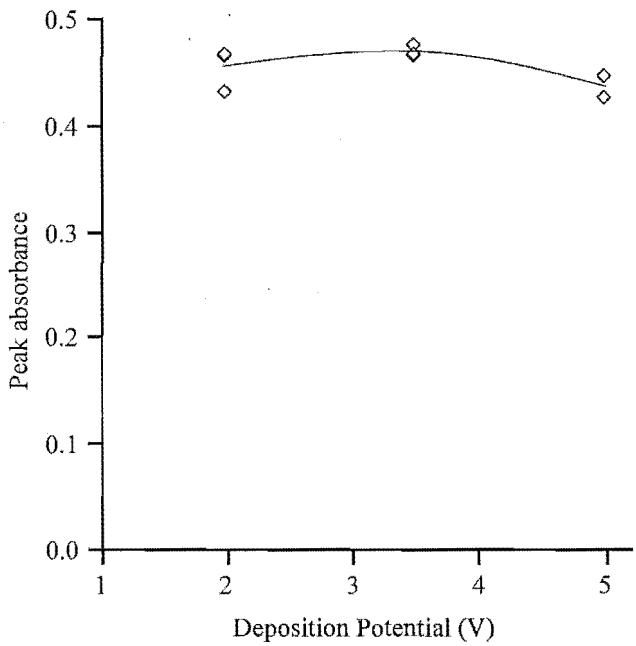

Figure 4.2 Effect of electrolysis potential on lead deposition. Lead deposited onto a palladium-modified furnace from 20 µL of 50 ppb solution containing 1% HNO_3, re-deposited from 35 µL of 1% HNO_3 for 60 seconds, and rinsed with 35 µL of water for five seconds. Lead absorbance was measured at 283.3 nm.

Acid Re-deposition Time

The duration of the re-deposition step was optimised by preparing a plot of re-deposition time versus absorbance for a lead sample. The lead sample was electrodeposited onto a palladium-modified furnace from 20 µL of 20 ppb solution in 1% HNO_3. The solution was electrolysed for 60 seconds using an applied potential of 4.5 V. A 30 µL aliquot of 1% HNO_3 was then injected into the furnace, and the deposition potential applied for varying lengths of time. The lead absorbance was measured at the 283.3 nm lead resonance line. The resulting plot is shown in Figure 4.3.

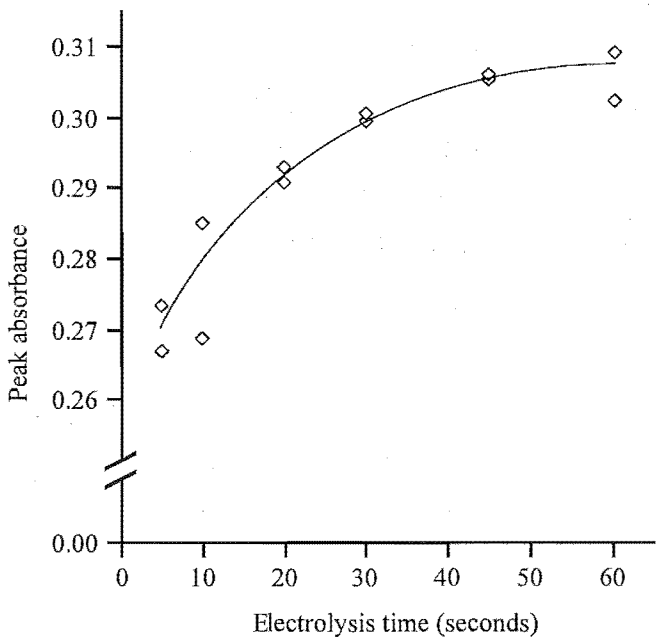

Figure 4.3 The effect of acid re-deposition time on sensitivity for lead determination. Lead deposited onto a palladium-modified furnace from 20 µL of 20 ppb solution in 1% HNO_3. Acid re-deposition effected at room temperature with no inert gas flow, from 1% HNO_3, using an applied potential of 4.5 V.

Analyte Losses Due to Re-deposition and Rinsing

Lead was deposited onto a palladium-modified furnace from 20 µL of 20 ppb solution in 1% HNO_3. Deposition was effected using a potential of 4.5 V. Following lead deposition, three different protocols were evaluated.

a) The lead deposit was dried, pyrolysed, and atomised with no further treatment.

b) Prior to measurement, the lead deposit was re-deposited from 30 µL of 1% HNO_3 for 60 seconds.

c) As for b), except the re-deposition was followed by a 30 µL water rinse for 5.0 seconds.

The results are shown in Table 4.2.

Rinse protocol	Mean peak absorbance (n=6)	RSD
None	0.280	4.5%
60 seconds re-deposition from 1% HNO3	0.278	6.2%
60 seconds re-deposition from 1% HNO3 followed by a five second water rinse	0.272	7.8%

Table 4.2 The effect of different rinse protocols on sensitivity for lead determination. Lead deposited onto a palladium-modified furnace from 20 ppb solution in 1% HNO_3. Electrodeposition at room temperature with no inert gas flow, for 60 seconds at 4.5 V. Lead absorbance measured at the 283.3 nm lead resonance line.

4.2.1.5 Blanks

Detection limits for lead determination were adversely affected by large blank values. The blanks originated from trace contaminants in the deposition media and in the palladium modifier. High blanks originating from contamination in the deposition media (Aristar HNO_3) were countered by using low concentrations of acid where possible, and by using acid that had been freshly diluted; for dilute acid samples that were stored in glass flasks, blank values increased over time. Blanks arising from trace contaminants in the palladium modifier proved more difficult to eliminate. The method used to deal with these impurities, was to selectively electrodeposit the palladium, leaving the contaminants to be removed with the spent deposition medium. This selective electrodeposition was achieved by manipulating the deposition potential.

Procedure and Results: 30 µL of 10 ppm palladium solution containing 1% HNO_3 was deposited for 20 seconds, using two different applied potentials: 0.7 and 2.0 V. The palladium was dried, and a lead sample deposited on top of it. The lead was deposited at 2.0 V from a 50 ppb solution containing 1% HNO_3. The deposit was then rinsed with 40 µL of 1% HNO_3 for 60 seconds and 40 µL of water for 5.0 seconds. All depositions were effected using the high-temperature deposition protocol, and the deposition potential remained on throughout the entire experiment. Following deposition, the sample was pyrolysed at 1100 °C, and atomised at 2300 °C. The lead absorbances measured at the 283.3 nm lead resonance line (not blank-corrected) are shown in Table 4.3.

4.2.2 Method Characterisation

4.2.2.1 Thermal Stability of Lead deposits

The effects of the electrodeposition process and the palladium modifier on the lead deposit's stability were examined. This was done by comparing the pyrolysis curves and atomisation profiles for lead deposited by different methods: electrodeposited, electrodeposited onto palladium modifier, and thermally deposited.

	Mean peak absorbance for 0.7 V modifier deposition	Mean peak absorbance for 2.0 V modifier deposition
1% HNO_3 blank	0.007 (n=2, RSD=10%)	0.040 (n=2, RSD=7.1%)
50 ppb lead in 1% HNO_3	0.580 (n=2, RSD=1.7%)	0.591 (n=2, RSD=1.3%)

Table 4.3 Effect of modifier deposition potential on size of the lead blank. Palladium deposited from 30 µL of 10 ppm solution in 1% HNO_3. Lead deposited at 2.0 V from 20 µL of a 50 ppb solution containing 1% HNO_3. Deposition effected using the high-temperature deposition protocol. Lead absorbances measured at the 283.3 nm lead line.

Pyrolysis Curves

Lead electrodeposited onto graphite: 20 µL of 50 ppb lead solution in 1% HNO_3 was deposited onto the furnace for 60 seconds. The deposit was redeposited from 30 µL of 1% HNO_3 for 60 seconds. Deposition was effected using the low-temperature protocol, and a deposition potential of 4.2 V. The deposit was dried, pyrolysed, and atomised at 2300 °C. The lead absorbance was measured at 283.3 nm.

Lead electrodeposited onto palladium-modified graphite: 30 µL of 10 ppm palladium solution in 1% HNO_3 was deposited onto the furnace for 20 seconds. The deposit was rinsed with 30 µL of 1% HNO_3 for 5.0 seconds (deposition potential switched off). Lead was deposited onto the palladium for 60 seconds from 20 µL of a 20 ppb solution which contained 1% HNO_3. Deposition was effected using the low-temperature protocol, and a deposition potential of 4.5 V. The deposit was dried, pyrolysed, and atomised at 2300 °C. The lead absorbance was measured at 283.3 nm.

The absorbances obtained for different pyrolysis temperatures are shown in Figure 4.4. To aid comparison, the pyrolysis curves have been scaled. This is necessary because the two experiments were carried out using different amounts of lead, hence giving markedly different absorbances. The absorbances for each pyrolysis temperature are shown as a fraction of the highest absorbance obtained for any pyrolysis temperature; i.e. for lead deposited directly onto graphite, absorbances are shown as a fraction of the absorbance obtained for a pyrolysis temperature of 600 °C, for lead on palladium, absorbances are shown as a fraction of the absorbance obtained using a pyrolysis temperature of 800 °C.

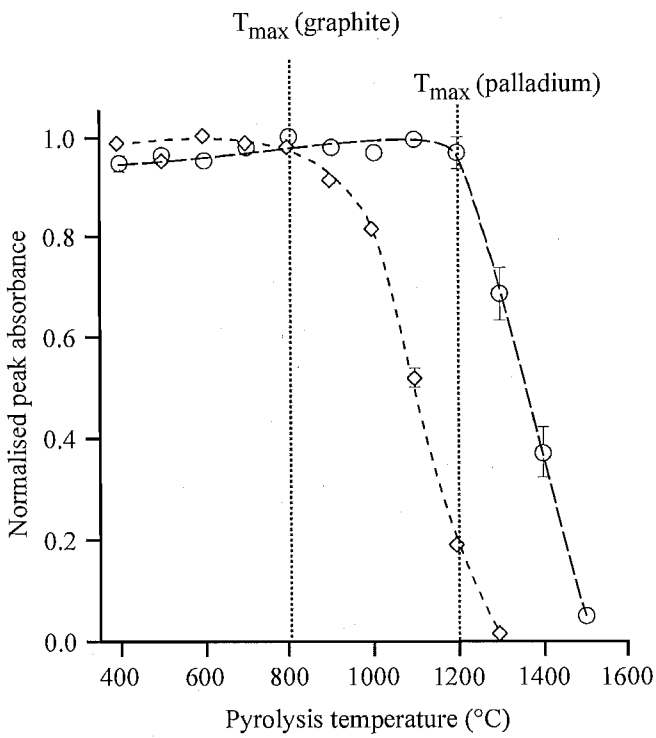

Figure 4.4 Pyrolysis curves for lead electrodeposited onto pyrolytic graphite (◇), and lead deposited onto palladium-modified pyrolytic graphite (○) The lead was deposited from 1% HNO_3 using low-temperature deposition conditions. The absorbance was measured at the 283.3 nm lead resonance line.

Atomisation Profiles

Atomisation profiles were compared for lead deposited by different means, and onto different surfaces. Lead was deposited conventionally (thermally), and by electrodeposition, onto both unmodified pyrolytic graphite, and palladium-modified pyrolytic graphite. In each case, the lead was introduced to the furnace as 20 µL of 50 ppb solution, prepared in 1% HNO_3. The palladium modifier (where used) was electrodeposited for 20 seconds from a 10 ppm solution prepared in 0.1% HNO_3. Pyrolysis temperatures of 600 °C, and atomisation temperatures of 2300 °C were used throughout. In order to achieve better resolution of the absorption profiles, the atomisation temperature-ramp was slowed to 380 °C s^{-1}. Lead absorbance was measured at 283.3 nm. Four different lead deposition protocols were used; the experiments were carried out in the order listed below.

1. The lead sample was analysed by conventional ETAAS (using a new furnace).
2. The lead was electrodeposited onto the unmodified furnace for 60 seconds using the high-temperature deposition protocol and a deposition potential of 2.0 V.
3. The furnace was modified with electrodeposited palladium prior to thermal lead deposition.
4. The furnace was modified with electrodeposited palladium prior to lead electrodeposition.

All electrodepositions, for both modifier and lead, were effected using the high temperature deposition protocol and a deposition potential of 2.0 V. The different absorbance-time profiles obtained for lead atomisation with each different deposition protocol are shown in Figure 4.5.

4.2.2.2 Detection Limit

The detection limit (DL) for lead electrodeposited on palladium was calculated using replicate measurements for a 1% HNO_3 blank, and a 50 ppb lead sample. The furnace was modified with palladium by depositing 30 µL of a 10 ppm solution containing 0.1% HNO_3 for 20 seconds. The palladium deposit was rinsed with 30 µL of 1% HNO_3 for 5.0 seconds and then dried at 110 °C prior to lead deposition. The lead sample was deposited for 60 seconds from a 2.0 ppb solution prepared in 1% HNO_3. All depositions were effected at 4.5 V, using the low-temperature deposition protocol. The lead sample was pyrolysed at 400 °C, and then atomised at 2300 °C. Lead absorption was measured at the 283.3 nm resonance line.

The mean absorbance for the blank (n=14) was 0.0212, σ=0.0016. The mean absorbance for 50 ppb lead in 1% HNO_3 (n=4) was 0.476, RSD=0.76%. The calculated detection limit ($3\sigma_{blank}$) for the sample size used (calibrated volume of 23.8 µL) was 0.53 ppb. This corresponds to 1.3 pg of lead.

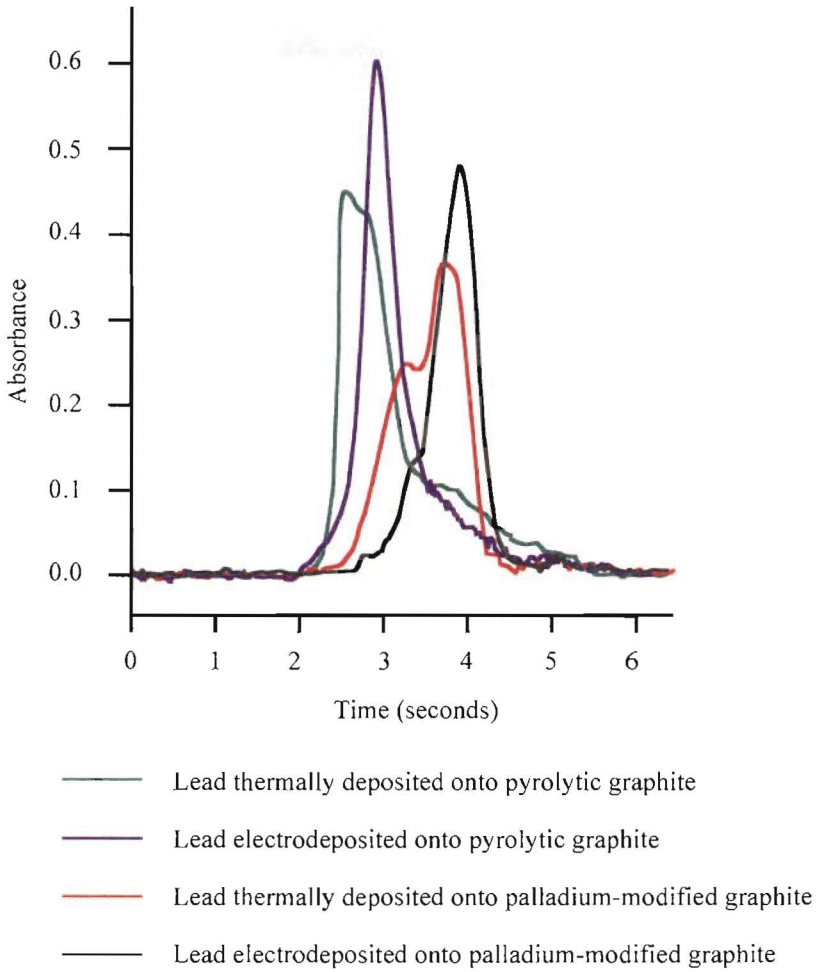

Figure 4.5 Comparison of absorbance-time profiles for atomisation of lead deposited by different methods: The lead was deposited from 20 µL of 50 ppb solution. For electrodeposited lead, a deposition time of 60 seconds was used. Palladium (where used) was electrodeposited for 20 seconds from 30 µL of 10 ppm solution in 0.1% HNO_3. All electrodepositions were carried out at 2.0 V using the high temperature deposition protocol. Lead absorption was measured at 283.3 nm.

4.2.2.3 Calibration Curves

Calibration curves were compared for lead determination by conventional ETAAS and ED-ETAAS. Palladium modifier (where used) was 10 ppm in 0.1% HNO_3. The modifier solution was electrolysed for 20 seconds, rinsed for 5 seconds with 1% HNO_3, and then dried at 110 °C prior to sample deposition. Lead samples (20 µL in 1% HNO_3) were determined using both thermal deposition, and electrodeposition (60 seconds electrolysis). Electrodeposition was accomplished using low-temperature deposition conditions, and an applied potential of *ca.* 4.2 V. Samples were dried, pyrolysed at 400 °C, and atomised at 2300 °C. Lead absorbance was measured at the 283.3 nm resonance line.

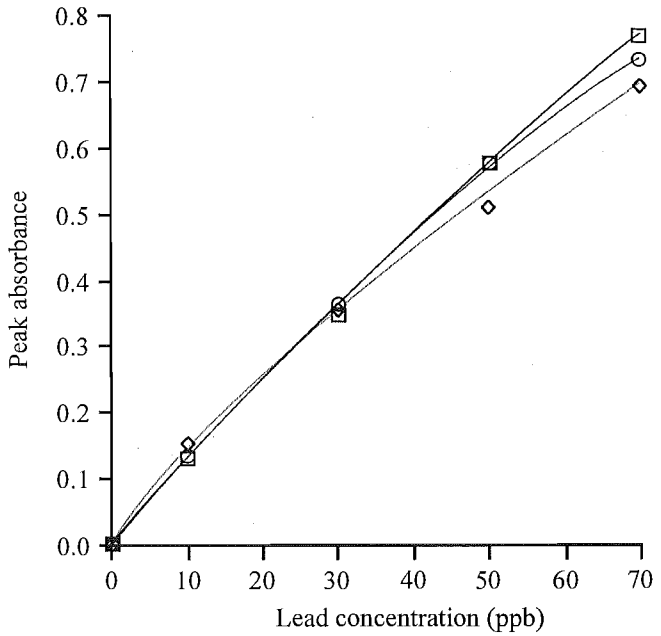

Figure 4.6 Calibration curves for lead: thermally deposited on pyrolytic graphite (◇) , electrodeposited on pyrolytic graphite (○), and electrodeposited on palladium-modified pyrolytic graphite (□). Lead depositions effected from 1% nitric acid media, palladium from 10 ppm solution containing 0.1% HNO_3. Electrodepositions were carried out using the low-temperature deposition protocol, and a deposition potential of 4.2 V. Lead absorbance measured at the 283.3 nm resonance line.

4.2.2.4 Characteristic Mass

The characteristic mass was calculated from the calibration curve for lead electrodeposited onto palladium-modified pyrolytic graphite (shown in Figure 4.6). The lower part of the calibration curve (≤ 50 ppb lead) has a slope of 0.011 (r^2=0.998). Therefore, a peak absorbance of 0.0044 corresponds to a lead concentration of 0.4 ppb, or a mass of 9.5 pg.*

4.2.3 Discussion

4.2.3.1 Sample Deposition Medium

The aim of the experimental work described in this section was to optimise and characterise the electrodeposition protocol developed by Matousek and Powell.[97] The first parameter investigated was the deposition medium. Table 4.1 shows that under the deposition conditions used, nitric acid is a superior deposition medium to hydrochloric acid. The difference could be due either to non-quantitative deposition or to chloride interference during the atomisation process. The former is more likely, because the lead deposit received one nitric acid rinse and one water rinse prior to atomisation. The amount of chloride remaining on the furnace after these rinse steps is relatively low. The amount of residual chloride can be calculated using the volume of analyte solution remaining in the furnace after withdrawal of a sample: *ca.* 5 µL (determined by weight). For a 20 µL lead sample containing 2 x 10^{-4} moles of HCl, the

* Calculated using a calibrated sample volume. For a set volume of 20 µL, the PAL2000 autosampler delivers 23.8 µL (by mass).

residual amount of HCl following two 30 µL rinses would be 1.5×10^{-6} moles—less than 1% of the original amount.

Although this experiment did not elucidate the causes of the poor deposition efficiency from HCl media, it did demonstrate that the ED-ETAAS method (as used) is sample matrix dependent. Therefore, for the remainder of work presented in this chapter, nitric acid was used as the preferred sample deposition medium. Causes and countermeasures for the sample matrix-dependence problem are examined in detail in Chapter Five.

Figure 4.1 shows the effect of the nitric acid concentration in the sample deposition medium. The sensitivity is not markedly affected by the acid concentration, although a slight decrease is apparent at nitric acid concentrations below 1.0%. Therefore, 1% nitric acid was used for future work because it provides adequate sensitivity while minimising analyte blanks (arising from impurities in the acid).

4.2.3.2 Deposition Potential and Efficiency

The effect of deposition potential on sensitivity is shown in Figure 4.2. It appears that sensitivity is slightly higher at low deposition potentials. It is difficult to tell whether this effect is due to more efficient deposition, or to different atomisation processes caused by different analyte deposit morphology. However, the reduced sensitivity at higher potentials concurs with the ASV analyses of the spent deposition medium; these found a deposition efficiency of only 93% when using a potential of 4.5 V. The reason for lower deposition efficiency from nitric acid media at higher deposition potentials is uncertain. A possible explanation is that the increased deposition potential causes the formation of dendritic, rather than smooth, lead deposits.[76] The lead dendrites could then be dislodged from the furnace surface by increased hydrogen evolution. It is also possible that the higher deposition potential could further oxidise oxygen (produced at the anode) to ozone.* The presence of powerful oxidants such as ozone would accelerate the lead oxidation processes that compete with deposition, hence increasing the equilibrium lead concentration in solution. This would have the effect of decreasing the overall deposition efficiency (the limits of electrolytic preconcentration are discussed fully in Section 1.5.1).

4.2.3.3 Rinses and Acid Re-depositions

Figure 4.3 shows the effect of acid re-deposition time on sensitivity. It can be seen that a minimum re-deposition time of 50-60 seconds is required to achieve total re-deposition of the sample. The reduced sensitivity at low re-deposition times is thought to arise from lead re-dissolution by oxidation. When the spent sample deposition medium is withdrawn at the end

---

* The E° for this reaction is -2.07 V vs NHE. The potential at the anode for an applied voltage of 4.2 V is ca +2.5 V vs NHE (see Figure 7.5).

of the analyte deposition step, a small volume of acidic solution remains in the furnace. Because the anode is withdrawn from the furnace, no potential is applied, and the lead deposit begins to oxidise and redissolve. It is proposed that the lead that 'dissolves' first, is that which is either present in a finely divided dendritic form, or deposited onto lead rather than palladium; these forms should be more reactive than the bulk of the lead deposit which is stabilised by the palladium modifier. When the re-deposition medium is added to the furnace, the residual solution is diluted, and lead is re-deposited onto the furnace surface. Sufficient time is required for this re-deposition step to reach completion. The lead re-deposits in a more stable form,[99] and hence resists oxidation by residual re-deposition solution when the probe is withdrawn from the furnace. Thus, when the subsequent water rinse is introduced to the furnace, very little analyte is lost through 're-dissolution'. This is shown in Table 4.2.

Thus, for processes where re-deposition and rinsing were required, the re-deposition step was effected from 1% HNO_3, with a duration of 60 seconds. The water rinse was of only 5.0 seconds duration. For analysis of lead solutions prepared in simple nitric acid matrices however, acid re-deposition and rinsing proved unnecessary (as shown in Table 4.2); analysis speed was considerably enhanced by omitting these steps.

4.2.3.4 Blanks

Problems of high lead blanks due to impurities in the palladium modifier were overcome by using selective modifier deposition (Table 4.3). A modifier deposition potential of 0.7 V proved sufficient to deposit the palladium while leaving concomitant lead in solution. The lead was then removed with the spent deposition medium. The blank absorbances obtained using this protocol were not significantly different from baseline noise levels.

Two other protocols intended to lower blank levels were less successful. The first of these was designed to volatilise lead from the modifier deposit by selective pyrolysis prior to analyte deposition. Unfortunately, a pyrolysis temperature sufficient to completely volatilise lead from the palladium, had a detrimental effect on the sensitivity for subsequent lead determination. Whether this was due to palladium volatilisation, or changes in surface morphology is unknown.

The third approach to eliminating blanks, was to selectively dissolve lead from the palladium deposit using a nitric acid rinse. This approach was also unsuccessful, because low acid concentrations failed to lower blanks, while higher acid concentrations increased them. This was probably due to impurities in the acid adsorbing to the palladium modifier.

The most successful approach was the selective modifier deposition protocol. For most purposes where low detection limits were not critical, this protocol was not used because it requires manual adjustment of the deposition potential. However, this technique would be very practical if the deposition potential was under software control.

4.2.3.5 Thermal Stability of Lead Deposits

The pyrolysis curves for lead (Figure 4.4) show the maximum pyrolysis temperatures that can be used for lead electrodeposited on pyrolytic graphite, and lead electrodeposited on palladium-modified pyrolytic graphite. These maximum pyrolysis temperatures are 800 °C and 1200 °C respectively. The 400 °C shift in the presence of palladium is in accordance with literature reports.[34,97] Although the pyrolysis curves show 1200 °C as the maximum pyrolysis temperature for lead electrodeposited onto a palladium modifier furnace, the pyrolysis temperature chosen for use throughout the remainder of this work was 1100 °C. This was simply to allow a safety margin, so that small changes in the pyrolysis curves caused by different experimental conditions, didn't markedly affect sensitivity.

The absorbance-time profiles for lead atomisation shown in Figure 4.5 reveal further information about the nature of lead deposits that are formed by different deposition methods. The least stable form of lead is that which is obtained through conventional reduction on a graphite surface. The relatively broad shape of this profile indicates that the volatilisation / atomisation kinetics are complex relative to those for lead electrodeposited directly on pyrolytic graphite. This is because the electrodeposited lead is atomised and volatilised from a single state; metallic lead bound to carbon. In contrast, the thermally deposited lead must first be decomposed to an oxide and then reduced to the metal before being volatilised and atomised.[144,141] Volatilisation may occur as Pb or PbO.

The absorbance-time profile for lead thermally deposited on pyrolytic graphite displays a shoulder on the trailing edge of the peak (at t=4 seconds). This "double peak" is characteristic of lead absorbance-time profiles. It was explained by Salmon *et al.*[178] as an effect of adsorbed oxygen on the pyrolytic graphite furnace surface; the presence of adsorbed oxygen provides surface sites of different activity, and hence different release mechanisms for lead analyte. In view of this explanation, the single peak observed for electrodeposited lead, could be due to removal of adsorbed oxygen during the electrolysis process. Alternatively, the deposition-dissolution equilibrium during electrolysis in acid solution allows for preferential deposition exclusively on one type of active site.

The absorbance-time profiles for lead atomised in the presence of palladium, are shifted relative to those for lead on pyrolytic graphite. This higher-temperature atomisation, attributed to the palladium, is consistent with the literature and the pyrolysis curves shown in Figure 4.4. The main feature of interest is that thermally and electrodeposited lead have different appearance temperatures (as shown by the absorbance-time profiles). The apparent difference in appearance temperature is caused by the large shoulder on the leading edge of the absorbance-time profile for thermally deposited lead on palladium. This shoulder is barely evident in the case of electrodeposited lead. The shoulder corresponds to lead that is less stable than the bulk of the deposit (which atomises at a higher temperature). This poorly stabilised

lead could be that which is deposited as a multilayer, and is not in intimate contact with the palladium modifier. Lead atoms deposited onto other lead atoms are less stable than those deposited directly on palladium.[99] For lead that is electrodeposited onto the palladium-modified surface the single peak, which is shifted to a higher temperature, indicates that lead is being atomised only from palladium-modified regions of the furnace surface. This implies either, that during electrodeposition, lead is selectively deposited onto the palladium, or that lead migrates to palladium-modified regions of the furnace after deposition. Some support for the latter idea is provided by the work of Chen and Jackson,[179] who demonstrated that lead, thallium, and selenium can migrate from an unmodified pyrolytic graphite surface to a palladium-modified pyrolytic graphite surface. This was shown by modifying one side of a pyrolytic-coated graphite platform with palladium, and then depositing the analyte metal on the reverse side. After thermal pre-treatment, the analyte was found to have been quantitatively transferred to the palladium-modified face of the platform. This migration occurred at temperatures above 600 °C. It is likely therefore, that a similar migration could occur during pyrolysis in the ED-ETAAS system. Lead that has been deposited onto unmodified regions of the furnace surface migrates onto the palladium deposits, hence the absorbance-time profile shows only a single peak.

4.2.3.6 Analytical Sensitivity

The calibration curves shown in Figure 4.6, are very similar, regardless of the lead deposition method. The working range extends from the limit of determination (5 x DL) of 2.5 ppb lead, to more than 70 ppb. Sensitivity is decreased slightly by the palladium modifier. The decrease is proportional to the amount of palladium used, as shown in Figure 3.2 (discussed in Chapter Three). However, for the mass of palladium used in this case (≤ 0.3 µg), the sensitivity decrease is small, and is considered acceptable given the greatly enhanced thermal stability that the palladium modifier provides.

The characteristic mass of 9.5 pg, for lead determination by ED-ETAAS (using peak absorbances), compares favourably with literature values. Tahvonen and Kumpulainen[114] obtained characteristic masses of 5-8 pg using a Zeeman-effect instrument.. Other workers obtained characteristic masses of 10-11 pg[180] and 15 pg[181] using tungsten coil atomisers. Unfortunately, many authors fail to report the measurement mode (peak, or integrated absorbance) used to calculate the characteristic mass. This makes comparison difficult, as measurements made using peak absorbances generally give smaller characteristic masses than those obtained using integrated absorbances.[182]

There are many factors that can affect analytical sensitivity. These include: the deposition conditions, the pyrolysis temperature, the age of the hollow cathode lamp, and the age of the furnace. With the instrument used to collect the data presented in this section (GBC 903), the wavelength-setting constantly drifted off the analytical line. This has a very marked effect on sensitivity when not quickly corrected. Because the data presented in this chapter were

collected over a long period, any of the above factors could alter the sensitivity for a given day. Further, except where indicated, the measurements were not blank corrected. Consequently, measurements do not take into account any possible contamination of modifier, acid re-deposition, or rinse solutions. Therefore, comparisons can only be made for data collected on the same day and under identical conditions, i.e. as presented in any single Figure.

The protocol developed for determination of lead in acid media is similar to that of Matousek and Powell.[97] However, it has been shown that the deposition potential can be varied outside the range used by these authors, in particular, to low voltages. It has also been demonstrated that the acid re-deposition and rinsing steps are unnecessary in simple nitric acid media. The protocol developed for lead determination in nitric acid serves as a basis for determination of other metals in acid media, and for determination of metals in other media such as sodium chloride (discussed in Chapter Five) and pH-buffered solutions (Chapter Seven).

4.3 DETERMINATION OF OTHER METALS

Once a working protocol for determination of lead from nitric acid media had been developed, the method was extended to determination of other metals. The metals were chosen, either because they were potential analytes for seawater analysis (as described in Chapter Five), or because they were suitable metals for use in the complexation studies described in Chapter Seven. The studies described within the remainder of this chapter are more cursory investigations which were designed to establish whether ED-ETAAS determination of these metals was feasible.

4.3.1 Copper

4.3.1.1 Effect of Deposition Time

Sensitivity for copper determination by ED-ETAAS was examined as a function of deposition time, using two different deposition potentials.

Procedure and Results: The furnace was modified with palladium. The palladium was deposited for 20 seconds from 30 µL of 10 ppm solution containing 1% HNO_3. The deposit was rinsed with 40 µL of 0.1% HNO_3 for 5.0 seconds and then dried at 110 °C prior to copper deposition. The copper analyte was deposited from 20 µL of 20 ppb solution containing 1% HNO_3. Deposition for both the modifier and the analyte was effected using the high-temperature deposition protocol, and a potential of either 2.0 or 4.5 V. The sample was dried, pyrolysed at 1100 °C, and atomised at 2300 °C. The copper absorbances for different deposition times, measured at the 324.7 nm copper line, are shown in Figure 4.7.

4.3.1.2 Thermal Stability of Copper Deposits

The thermal stability of the electrodeposited copper on palladium was compared with that for copper conventionally deposited onto pyrolytic graphite. Both the pyrolysis curves and the absorbance-time profiles for copper atomisation were compared.

Pyrolysis Curves

The experimental conditions for electrodeposition were the same as for the deposition time experiment above, except for two parameters; electrodeposition was effected using a potential of 3.0 V, and the copper sample was deposited for 60 seconds. The results are shown in Figure 4.8.

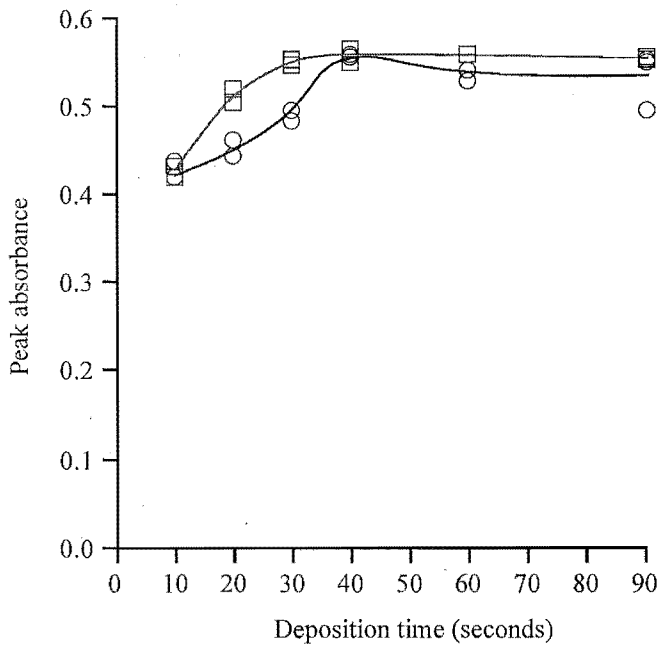

Figure 4.7 Copper absorbance as a function of deposition time and potential. Copper deposited onto palladium-modified furnace from 20 µL of 20 ppb solution in 1% HNO_3, using deposition potentials of 2.0 V (□) and 4.5 V (○). Copper absorbance measured at 324.7 nm.

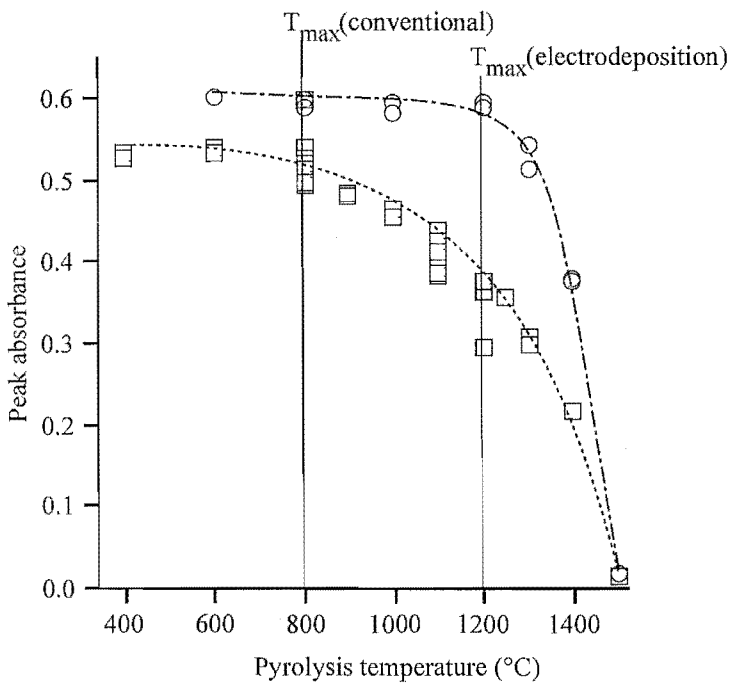

Figure 4.8 Pyrolysis curves for copper, thermally deposited on pyrolytic graphite (□), and electrodeposited on palladium-modified pyrolytic graphite (○). For thermal deposition, copper was conventionally deposited using 20 µL of 20 ppb solution prepared in 1% HNO_3. For electrodeposition, copper was electrodeposited onto a palladium-modified furnace for 60 seconds at 3.0 V, using the same copper solution as for the thermal deposition. The high-temperature deposition protocol was used. Copper absorbance was measured at 324.7 nm.

Absorbance-Time Profiles

The relative absorbance-time profiles for copper, conventionally deposited on pyrolytic graphite, and electrodeposited on palladium-modified pyrolytic graphite, are shown in Figure 4.9. The deposition conditions were the same as for the above pyrolysis-temperature experiment. For the conventional deposition measurement, the sample (in 1% HNO_3) was pyrolysed at 800 °C, and then atomised using a temperature ramp from 150 °C to 2300 °C at 2000 °C s^{-1}. For the electrodeposition measurement, the sample was pyrolysed at 600 °C, and then atomised using a temperature ramp from 400 °C to 2300 °C at 1900 °C s^{-1}. Assuming a linear temperature-ramp rate, the temperatures at the point of atomisation (time = 1.0 second) are 2150 °C and 2300 °C respectively, for thermally and electrodeposited copper.

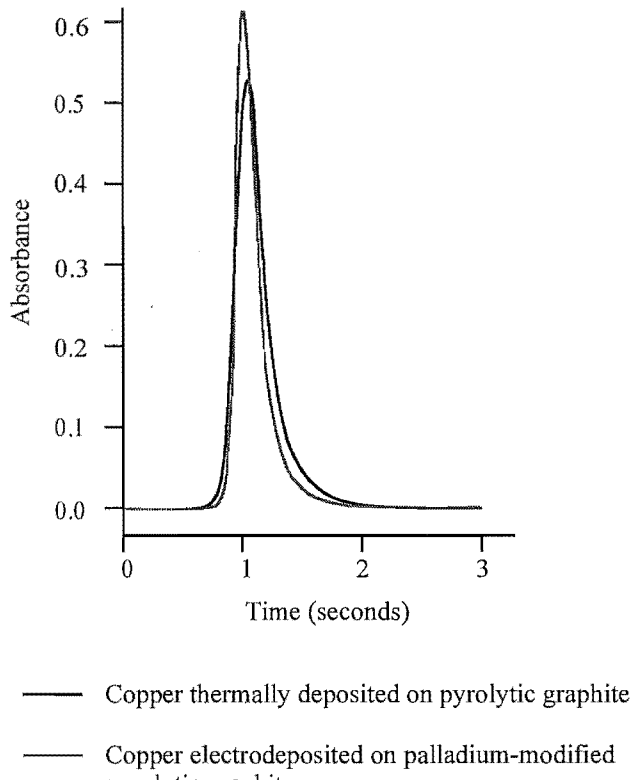

Figure 4.9 Absorbance-time profiles for atomisation of copper deposited by different methods. For thermal deposition, copper was conventionally deposited using 20 µL of 20 ppb solution prepared in 1% HNO_3. For electrodeposition, copper was electrodeposited onto a palladium-modified furnace for 60 seconds at 3.0 V, using the same copper solution as for the thermal deposition. The high-temperature deposition protocol was used. Copper absorbance was measured at 324.7 nm.

4.3.1.3 Discussion

The most important result in this section, is that copper can be readily determined by ED-ETAAS. The protocol developed for lead determination serves equally well for copper determination. Figure 4.7 shows that electrodeposition is complete after 60 seconds —the same time as used for lead determination. The absorbance-time profiles in Figure 4.9 show that the ED-ETAAS method offers greater sensitivity than conventional (thermal) ETAAS analysis. This is probably because the sharper absorbance-time profiles give rise to higher peak absorbances. It may be that the integrated absorbances are little different, however, no measurements were made in peak integration mode to answer this question.

The maximum pyrolysis temperatures for copper are the same as those that were determined for lead under the same conditions. One major difference between the pyrolysis curves for lead and copper is that the copper curves both have an x-intercept at 1500 °C, whereas the two lead curves meet the x-axis at very different temperatures. This difference may be because the pyrolysis curve for conventional copper determination was determined using a furnace that had previously been used with palladium modifier. It is possible that sufficient residual palladium remained on the furnace to effect a small degree of copper stabilisation. The comparable curve for lead was determined using a new furnace. Alternatively, surface imperfections in the aged pyrolytic graphite allow the copper to penetrate into the furnace surface. This phenomenon, which has been studied in-depth by Jackson *et al.*,[183] leads to some stabilisation of the copper deposit, and hence broadened absorbance-time profiles which are shifted to higher temperatures.

Irrespective of the age of the furnace, in the absence of chloride, copper has a relatively high thermal stability and is routinely determined without use of a specific modifier.[37] For routine analysis in non-chloride media, not only is the additional stability provided by palladium usually considered superfluous, but the modifier itself can introduce interferences. Welz *et al.*[184] reported a spectral interference from palladium when copper was determined at the 324.7 nm line while using deuterium background correction. This interference was not observed at the less sensitive 327.4 nm line, or in instruments equipped with Zeeman-effect background correction. This interference was not observed in our system, perhaps because of the small amount of palladium used for ED-ETAAS (ca 0.3 μg) compared with that used by Welz *et al.* (15 μg).

Unfortunately, copper is subject to chloride interference, and in high-chloride media, considerable loss of analyte is observed.[45] It is likely that these effects can be minimised by the matrix removal and palladium-effected stabilisation afforded by the ED-ETAAS protocol. This initial investigation showed that copper is readily determined by ED-ETAAS using similar parameters to those used for lead determination. The ED-ETAAS protocol developed here was used as a foundation for further studies involving copper determination from saline media, (as described in Chapter Five) and speciation studies of copper (Chapter Seven).

4.3.2 Bismuth

4.3.2.1 Effect of Deposition Medium

The efficiency of bismuth electrodeposition was evaluated using several different deposition media. Sample solutions were prepared containing 4 x 10^{-8} M bismuth in either: 1% HNO_3, 0.5 M NaCl, 1.5% HCl, 0.5% H_2SO_4, or 1.0% H_2SO_4. The electrodeposition protocol was similar to that used for lead determination. The furnace was firstly modified by depositing palladium from 30 μL of 10 ppm solution containing 0.1% HNO_3. The palladium deposit was dried at 110 °C prior to sample deposition. The bismuth was deposited from 20 μL of

solution for 60 seconds, re-deposited from 40 µL of 0.1% HNO_3 for 60 seconds, and then rinsed with 40 µL of water for 5.0 seconds. Electrodeposition was carried out using an applied potential of 2.0 V, and the high-temperature deposition protocol. Following deposition, the samples were pyrolysed at 1100 °C and then atomised at 2300 °C. The resulting absorbances, measured at the 306.8 nm bismuth resonance line, are shown in Table 4.4.

Bismuth deposition medium	Mean peak absorbance (n=4)	RSD
1% HNO_3	0.382	4.2%
0.5 M NaCl / 1.5% HNO_3	0.405	4.4%
1.5% HCl	0.376	3.4%
0.5% H_2SO_4	0.394	6.3%
1.0% H_2SO_4	0.397	7.9%

Table 4.4. Comparison of deposition media for bismuth determination by ED-ETAAS. Bismuth was deposited onto palladium-modified pyrolytic graphite from 20 µL of 4 x 10^{-8} M solution, for 60 seconds, at 2.0 V, using the high-temperature deposition protocol. Samples were pyrolysed at 1100 °C and atomised at 2300 °C. Absorbances were measured at 306.8 nm.

4.3.2.2 Thermal Stability of Bismuth Deposits

Pyrolysis Curves

The pyrolysis curves for Bi determination were compared using conventional ETAAS, in the absence of palladium, and using ED-ETAAS in the presence of palladium. For electrodeposition, the furnace was modified with palladium by depositing 30 µL of a 10 ppm solution containing 0.1% HNO_3, for 20 seconds. The palladium deposit was dried at 110 °C prior to analyte deposition. Bismuth was deposited for 20 seconds from 20 µL of 4 x 10^{-8} M solution containing 1% HNO_3. The deposit was then rinsed with 40 µL of water for 5.0 seconds. Electrodeposition was carried out using an applied potential of 2.0 V, at room temperature, with inert gas flowing over the electrolysis medium. For conventional deposition, 20 µL of the same bismuth solution was used. In both cases, the samples were dried, pyrolysed at varied temperatures, and atomised at 2300 °C. The results are shown in Figure 4.10.

Absorbance-Time Profiles

The absorbance-time profiles for bismuth atomisation are compared in Figure 4.11 for bismuth thermally deposited on pyrolytic graphite, and for bismuth electrodeposited on palladium-modified pyrolytic graphite. The profiles were measured under the same conditions used for the bismuth pyrolysis curves (Figure 4.10); the experimental conditions were the same as those already described. The curve for electrodeposited bismuth was measured using a pyrolysis temperature of 900 °C, while that for thermally deposited bismuth was measured using a pyrolysis temperature of 600 °C.

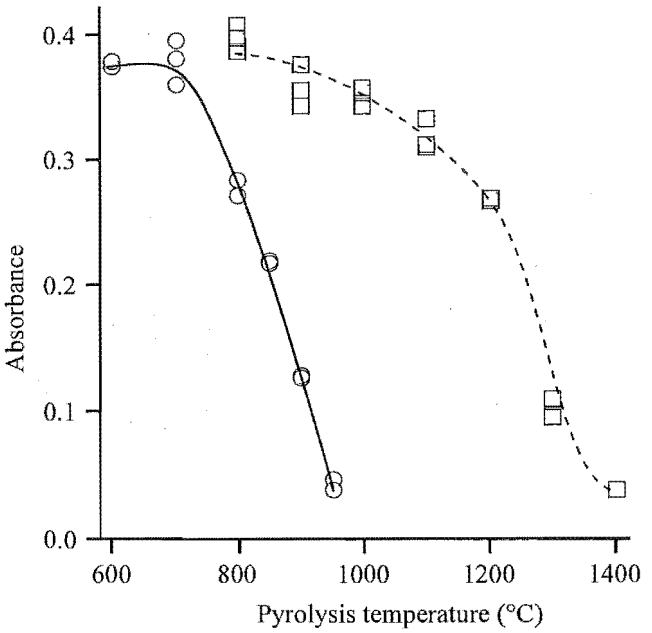

Figure 4.10. Pyrolysis curves for bismuth; thermally deposited on pyrolytic graphite (○) and electrodeposited on palladium-modified pyrolytic graphite (□). Bismuth was deposited from 20 µL of 4 x 10^{-8} M solution prepared in 1% HNO_3. Electrodeposition was effected at room temperature with inert gas on, using a deposition potential of 2.0 V. Samples were atomised at 2300 °C and the absorbance measured at 306.8 nm.

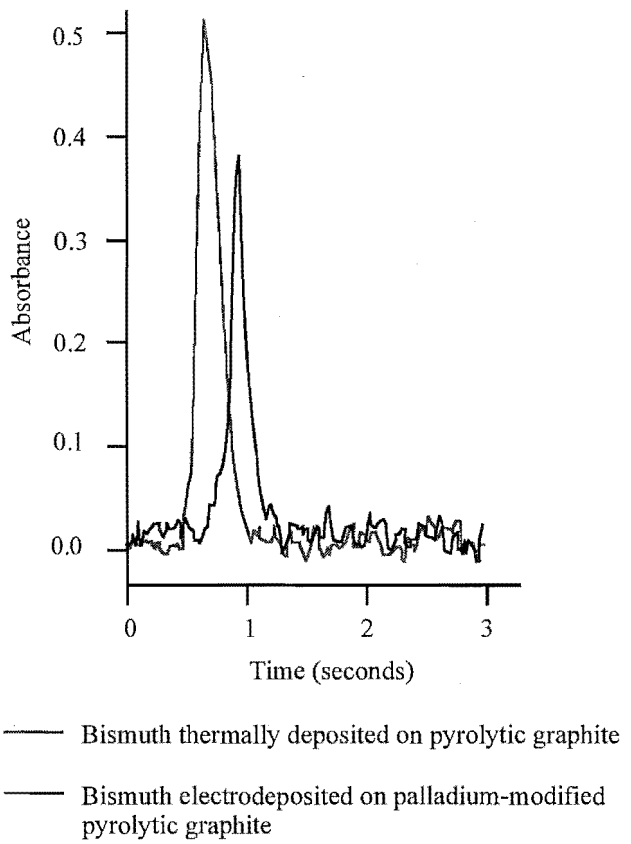

Figure 4.11. Absorbance-time profiles for bismuth atomisation. Bismuth was deposited from 20 µL of 4 x 10^{-8} M solution containing 1% HNO_3. Palladium, where used, was deposited from 30 µL of 10 ppm solution prepared in 0.1% HNO_3. The electrodeposited sample was pyrolysed at 900 °C, the thermally deposited sample at 600 °C. Electrodeposition was effected at room temperature with inert gas on, using a deposition potential of 2.0 V. Sample atomisation was at 2300 °C, and the absorbance measured at 306.8 nm.

4.3.2.3 Discussion

The comparison of electrolysis media for bismuth deposition (Table 4.4) shows that bismuth electrodeposits equally well from all of the media tried. The poor precision was attributed to baseline noise due to weak emission from the bismuth hollow cathode lamp. The pyrolysis curves shown in Figure 4.10 show that electrodeposited bismuth on palladium is significantly stabilised relative to thermally deposited bismuth on pyrolytic graphite. However, while the bulk of the bismuth is stabilised to temperatures above 1000 °C, some loss is observed at temperatures as low as 900 °C. Thus, while most of the bismuth is greatly stabilised by the palladium, the maximum loss-free pyrolysis temperature shifts only 200 °C; from 700 °C for thermally deposited bismuth on pyrolytic graphite, to *ca.* 900 °C for the electrodeposited bismuth on palladium. For further work involving electrodeposited bismuth on palladium (from acetate-containing media; Chapter Seven), a pyrolysis temperature of 1100 °C was used. The small loss of analyte was considered insignificant relative to the corresponding decrease in background absorbance due to residual acetate.

The absorbance-time profiles shown in Figure 4.11 reflect the palladium-induced stability increase that is exhibited in the pyrolysis curves. The appearance temperatures for the two palladium deposits are separated by about 300 °C, indicating better analyte stabilisation than is demonstrated by the pyrolysis curves.

The relative sensitivity for bismuth determination by conventional ETAAS and ED-ETAAS can be inferred from the peak absorbance measurements used to construct the pyrolysis curves shown in Figure 4.11. The sensitivity for bismuth determination, as derived from these curves, was similar for the two methods. The anomalous results shown in the absorbance-time profiles are because the only recorded peak profile for conventional ETAAS determination happened to be uncharacteristically large.

4.3.3 Cadmium

4.3.3.1 Effect of Deposition Medium

In order to optimise analytical sensitivity, cadmium deposition efficiency was evaluated using several different deposition media. The ED-ETAAS protocol used was as for lead determination; i.e. the furnace was modified by depositing 30 µL of 10 ppm palladium solution for 20 seconds. The modifier was dried at 110 °C, and then 20 µL of 2.4 ppb cadmium solution was electrolysed for 40 seconds. The sample deposition was followed by an optional 40 second acid re-deposition from 40 µL of 0.1% HNO_3. Electrodeposition was carried out using the high temperature deposition protocol, and a 2.0 V deposition potential. Samples were pyrolysed at 800 °C, and atomised at 2450 °C. Absorbances, shown in Table 4.5, were measured at the 228.8 nm cadmium line.

Sample medium	No acid re-deposition: mean peak absorbance (n=4)		30 second acid re-deposition (40 µL 0.1% HNO_3: mean peak absorbance (n=4)	
1% HNO_3	0.537	(RSD = 0.9%)	0.587	(RSD = 0.9%)
1.5% HNO_3	0.463	(RSD = 3.3%)	0.564	(RSD = 1.2%)
1% HCl	0.056	(RSD = 25%)	0.532	(RSD = 2.2%)
1.5% HCl	0.180	(RSD = 14%)	0.508	(RSD = 0.4%)
2.0% HCl	0.222	(RSD = 16%)	0.501	(RSD = 0.7%)
1% H_2SO_4	0.559	(RSD = 0.7%)	0.534	(RSD = 1.3%)
1.5% H_2SO_4	0.518	(RSD = 2.7%)	0.525	(RSD = 1.7%

Table 4.5 Effect of sample medium on cadmium determination by ED-ETAAS. Cadmium electrodeposited for 40 seconds onto palladium-modified pyrolytic graphite, from 20 µL of 2.4 ppb solution. Electrodeposition effected at 2.0 V, using the high-temperature deposition protocol. Samples pyrolysed at 800 °C and atomised at 2450 °C. Absorbances measured at 228.8 nm.

4.3.3.2 Effect of Deposition Time

In order to determine whether cadmium deposition was reaching completion, the absorbance for cadmium atomisation was studied as a function of deposition time. The furnace was modified by depositing 30 µL of 10 ppm palladium solution containing 0.1% HNO_3 for 20 seconds. The furnace was dried at 120 °C, and 20 µL of 2.4 ppb cadmium solution in 1% HNO_3 was electrolysed for varying lengths of time. Electrodeposition was carried out using the high temperature deposition protocol, and a 2.0 V deposition potential. Samples were pyrolysed at 800 °C and atomised at 2450 °C. The absorbances as shown in Figure 4.12, were measured at the 228.8 nm cadmium line.

4.3.3.3 Thermal Stability of Cadmium Deposits

Pyrolysis Curves

The pyrolysis curves for cadmium determination by conventional ETAAS and ED-ETAAS were compared. Cadmium was determined using 20 µL samples of 2.4 ppb cadmium solution prepared in 1.0% HNO_3. For ED-ETAAS determination, the same protocol was used as for the deposition-time experiment, except that the pyrolysis temperature was varied. The results are shown in Figure 4.13.

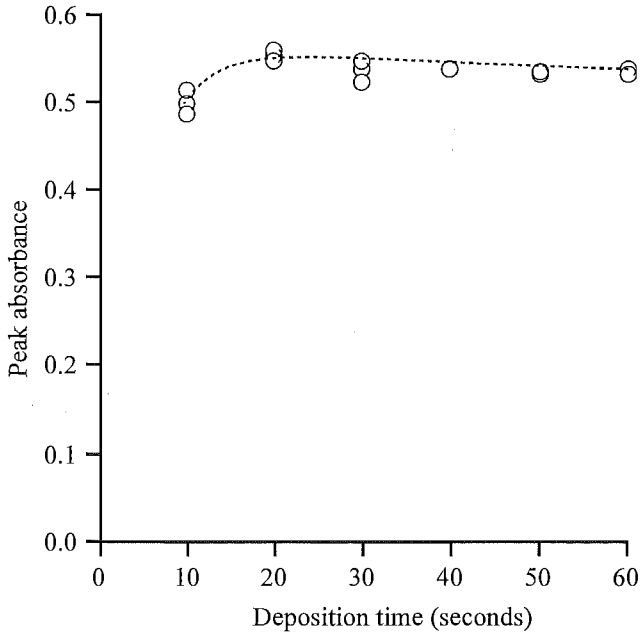

Figure 4.12 Effect of sample deposition time for cadmium determination by ED-ETAAS. Cadmium electrodeposited onto palladium-modified pyrolytic graphite, from 20 µL of 2.4 ppb solution containing 1% HNO_3. Electrodeposition effected at 2.0 V, using the high-temperature deposition protocol. Samples pyrolysed at 800 °C and atomised at 2450 °C. Absorbances measured at 228.8 nm.

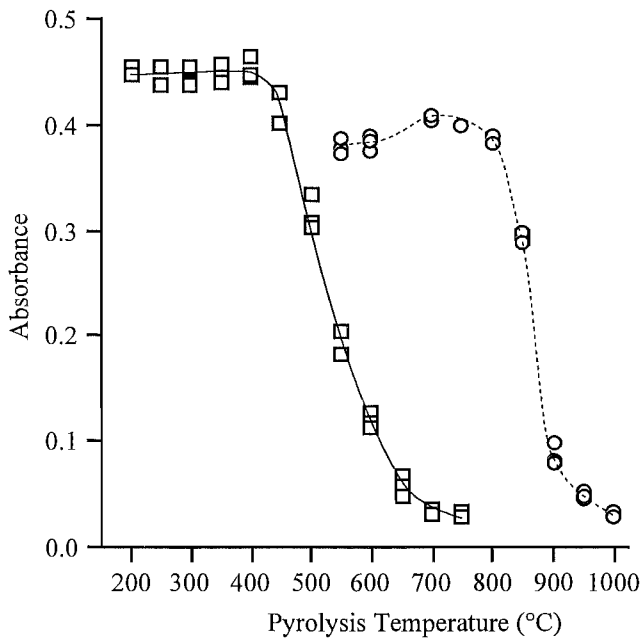

Figure 4.13. Comparison of pyrolysis curves for cadmium determined by conventional ETAAS (□) and by ED-ETAAS (○). For ED-ETAAS, cadmium was electrodeposited onto palladium-modified pyrolytic graphite, from 20 µL of 2.4 ppb solution containing 1% HNO_3. Electrodeposition was effected at 2.0 V, using the high-temperature deposition protocol. Samples were atomised at 2450 °C and the absorbances measured at 228.8 nm.

Absorbance-Time Profiles

Absorbance-time profiles for Cd determination by conventional ETAAS, and by ED-ETAAS were compared. Cadmium was determined from 4.0 ppb solution prepared in 1% HNO_3. For conventional ETAAS, a 20 µL sample was dried, pyrolysed at 300 °C, equilibrated at 200 °C, and then atomised at 2450 °C, using a temperature ramp rate of 1875 °C s^{-1}. For ED-ETAAS, the furnace was modified by depositing 30 µL of 10 ppm palladium solution containing 0.1% HNO_3, for 20 seconds. The deposit was dried at 120 °C prior to sample deposition. Cadmium was electrodeposited from 20 µL of solution for 60 seconds. Electrodeposition was carried out using the high temperature deposition protocol, and a 2.0 V deposition potential. Samples were pyrolysed at 900 °C, equilibrated at 400 °C, and atomised at 2450 °C using a temperature ramp rate of 1863 °C s^{-1}. The absorbances, measured at the 228.8 nm cadmium line are shown in Figure 4.14.

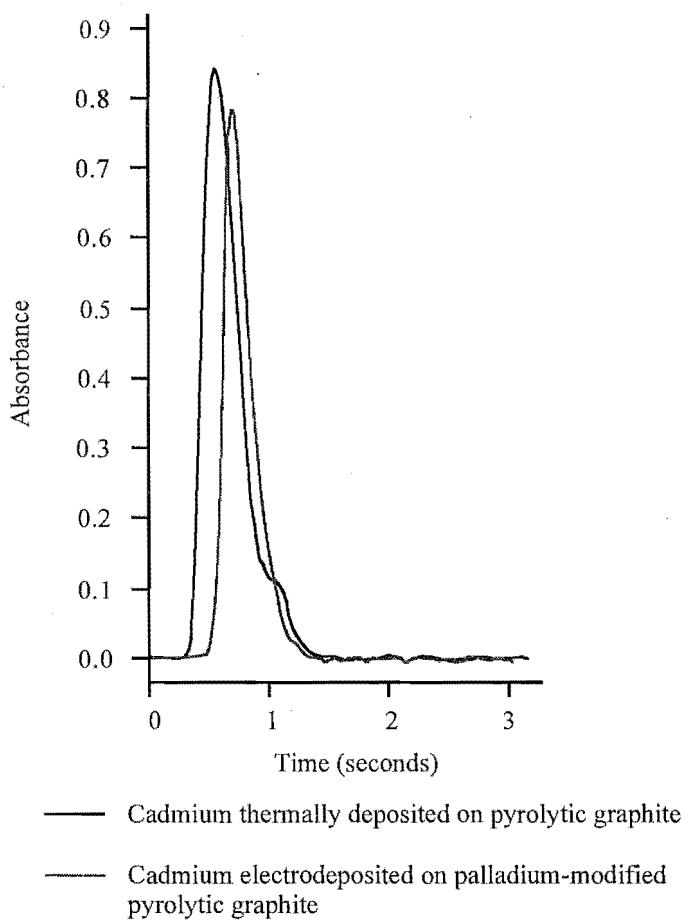

Figure 4.14. Absorbance-time profiles for cadmium atomisation. Cadmium deposited from 20 µL of 4.0 ppb solution containing 1.0% HNO_3. For ED-ETAAS determination, cadmium was deposited for 60 seconds onto a palladium-modified furnace surface using a potential of 2.0 V, and the high-temperature deposition protocol. Atomisation temperature ramp rates for ETAAS and ED-ETAAS were 1875 °C s^{-1} and 1863 °C s^{-1} respectively, with starting temperatures of 200 °C and 400 °C.

4.3.3.4 Discussion

Table 4.5 shows that when an acid (HNO_3) re-deposition step is included, cadmium is recovered with good efficiency from all of the media tested, with the best sensitivity obtained using the 1% HNO_3 deposition medium. For the samples deposited from HCl, the sensitivity was slightly lower, and decreased with increasing HCl concentration. This decreased sensitivity can be attributed to chloride interference during pyrolysis/atomisation.

Where the acid re-deposition step was omitted, as for lead deposition (Table 4.1), the sensitivity for cadmium deposition from HCl media was greatly reduced. The best sensitivity for deposition from HCl was obtained from the highest HCl concentration—the converse of what would be expected if the decreased sensitivity was due to 'chloride interference' during pyrolysis/atomisation. If the decreased sensitivity was due to less efficient deposition from low concentrations of HCl, then un-deposited cadmium would be removed from the furnace with the spent deposition medium. Therefore, we would not expect the sensitivities to be so similar when the same sample is re-deposited from nitric acid. The reason/s for these apparently contradictory results are not well understood.

Figure 4.12 shows that cadmium deposition from nitric acid reaches a maximum within twenty seconds. However, as can be seen from the absorbance profiles in Figure 4.14, sensitivity for determination by ED-ETAAS is lower than that obtained by conventional ETAAS; especially if peak areas are considered. The characteristic mass (by peak absorbance) calculated for cadmium determination by ED-ETAAS was 0.5 pg. The instrument manufacturer's data for the GF3000/908 system cites a characteristic mass of 0.25 pg.

The pyrolysis curves (Figure 4.13) show that, as for lead, the thermal stability of cadmium is greatly enhanced by electrodeposition onto the palladium-modified furnace. The maximum loss-free pyrolysis temperature increased from 400 °C, for conventional ETAAS, to 800 °C for ED-ETAAS. This stability increase is reflected in the absorbance-time profiles shown in Figure 4.14. The temperature difference between the two peaks is actually greater than it appears, because although similar temperature ramp rates were used to measure the profiles, the initial temperature for the thermal cadmium determination was 200 °C lower than that for the electrodeposited cadmium.

Overall, the ED-ETAAS protocols developed for lead determination also offer good sensitivity and enhanced thermal stability for cadmium determination. The protocol developed here was used as a basis for determination of cadmium from saline matrices as described in Chapter Five.

Chapter Five

Reducible Metals in Sodium Chloride Media

5.1 INTRODUCTION

This chapter presents studies aimed at determining reducible metals in saline media (such as marine or estuarine waters). The ED-ETAAS protocol developed in the previous chapter was adapted for this purpose, using 0.5 M sodium chloride solution as a model for natural saline waters.

There are three main experimental sections in this chapter. The first describes method development for lead determination in 0.5 M NaCl solution. The deposition parameters (time, potential, temperature etc.) are examined and optimised for the NaCl medium. The effects of residual NaCl on sensitivity are examined and methods for decreasing the amount of residue explored. The problems of 'non-labile' lead and sample carry-over, and methods used to counter them, are discussed.

The second experimental section is devoted to determination of copper in saline media. The effects of rinsing and acid re-deposition are examined. Pyrolysis and calibration curves are compared with those for determination from 1% HNO_3 medium. Results for copper determination in seawater using ED-ETAAS are presented.

The third experimental section is devoted to cadmium determination in saline media. The pyrolysis and calibration curves are compared with those for cadmium determination from 1% HNO_3 medium. Results of cadmium determination in seawater using ED-ETAAS are presented.

A final section discusses the advantages and disadvantages of ED-ETAAS as a method for determining reducible metals in saline waters.

5.2 LEAD DETERMINATION IN SODIUM CHLORIDE SOLUTION

5.2.1 Experimental and Results

Determination of lead in sodium chloride media was investigated over a period of several months, during which time the ED-ETAAS method was refined to give optimum analytical sensitivity. Variations in furnaces, analysis protocols, and sample preparation techniques over this period produced different absolute sensitivities from different experiments. Thus, the effects of experimental parameters should only be compared from within any single experiment.

5.2.1.1 Deposition Parameters

Initial attempts to measure lead in sodium chloride solution used the ED-ETAAS protocol as developed by Matousek and Powell,[97] in which lead was deposited from a 0.5 M NaCl/1 % HNO_3 matrix at room temperature, using a potential of *ca.* 5.0 V. In the present work, this method gave considerably lower sensitivity for lead in 0.5 M NaCl/1 % HNO_3 solution than for lead in 1% HNO_3 solution. In an effort to obtain the same sensitivity for the two media, various deposition parameters were investigated and optimised.

Deposition Time

The furnace was modified by electrolysing 30 µL of 10 ppm palladium solution, prepared in 0.1% HNO_3, for 20 seconds. The palladium deposit was then rinsed with 30 µL of water for 5.0 seconds and dried at 110 °C. Lead was deposited from 20 µL of 50 ppb solution, which was prepared in 0.1% HNO_3/0.5 M NaCl. The lead deposit was rinsed twice with 50 µL of water for 5.0 seconds. Deposition was effected at 4.5 V using the low-temperature deposition protocol. A series of measurements was made using different deposition times. The lead deposits were dried at 110 °C, pyrolysed at 400 °C, and atomised at 2300 °C. The absorbances, measured at 283.3 nm, are shown in Figure 5.1.

Deposition Potential

The furnace was modified by electrolysing 30 µL of 10 ppm palladium solution, prepared in 0.1% HNO_3, for 20 seconds. The deposit was rinsed with 40 µL of 1% HNO_3 for 5.0 seconds and then dried at 110 °C. Lead was deposited from 20 µL of 50 ppb solution, which was prepared in 1% HNO_3/0.5 M NaCl. The lead deposit was re-deposited from 40 µL of 1% HNO_3 for 60 seconds and then rinsed with 40 µL of water for 5.0 seconds. Deposition was effected at varying potentials using three different sets of electrolysis conditions. These were:

a) room temperature deposition, no inert gas flow
b) 45 °C deposition, no inert gas flow
c) 45 °C deposition, inert gas flow over sample during electrolysis.

The deposits were dried at 110 °C, pyrolysed at 800 °C, and atomised at 2300 °C. Lead absorbances, measured at 283.3 nm, are shown in Figure 5.2.

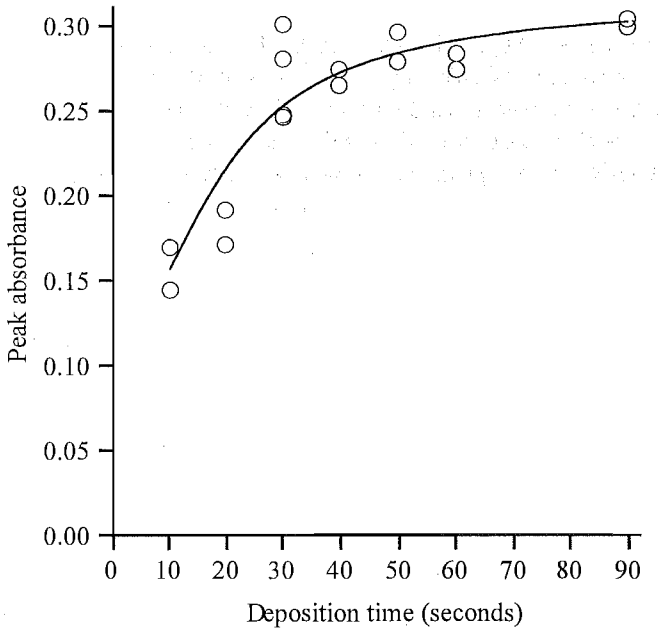

Figure 5.1 Effect of deposition time for lead determination in 0.1% HNO_3/0.5 M NaCl. Lead was deposited onto palladium-modified furnace from 20 µL of 50 ppb solution and rinsed twice with 50 µL of water for 5 seconds. Deposition was effected using a low temperature deposition protocol and a potential of 4.5 V. The lead deposits were dried at 110 °C, pyrolysed at 400 °C, and atomised at 2300 °C. Lead absorbance was measured at 283.3 nm.

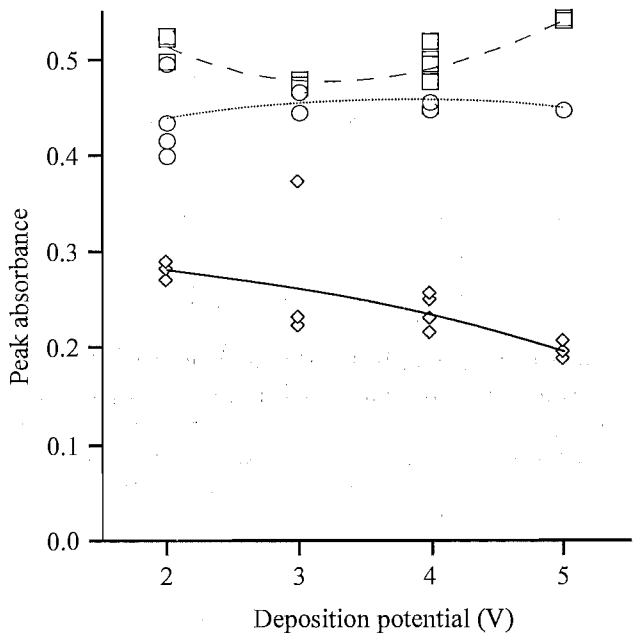

Figure 5.2 Effect of deposition potential for lead determination in 0.5 M NaCl/1% HNO_3 media. Lead was deposited onto palladium-modified furnace from 20 µL of 50 ppb solution. The lead deposits were re-deposited from 40 µL of 1% HNO_3 for 60 seconds and then rinsed with 40 µL of water for 5.0 seconds. The deposition conditions were: room temperature, no inert gas flow (◇); 45 °C, no inert gas flow (○); 45 °C, inert gas flow over sample during electrolysis (□). The lead deposits were dried at 110 °C, pyrolysed at 800 °C, and atomised at 2300 °C. Lead absorbance was measured at 283.3 nm.

A separate experiment was carried out to determine the amount of sample medium lost through evaporation during high-temperature deposition. A 20 µL sample was placed in the furnace as usual but, after 60 seconds of electrolysis, the remaining sample solution was removed with a micropipette and weighed. The mean mass for six samples after deposition at room temperature with no inert gas flow was 22.4 mg. For the six samples deposited at 45 °C with inert gas, the mean mass was 11.3 mg. Therefore, the sample volume is approximately halved by evaporation.

Gas Flow Rate

A series of measurements was made using the same conditions as for the preceding deposition-potential experiment but with varying gas flow rates. The gas flow was adjusted and metered using the controls on the GF2000 controller. The absorbances (at 283.3 nm), are shown in Figure 5.3.

Deposition Temperature

A series of measurements was made using the same conditions as for the deposition-potential experiment but with varying deposition temperatures. A series of measurements was made using deposition temperatures in the range 25-45 °C. The absorbances, measured at 283.3 nm, are shown in Figure 5.4.

Effect of Nitric Acid Concentration

The effect of the nitric acid concentration in the deposition medium was examined in order to optimise sensitivity. A series of 50 ppb lead solutions was prepared in 0.5 M sodium chloride solution with varying concentrations of nitric acid. Lead was deposited onto a palladium-modified furnace for 60 seconds from 20 µL aliquots of the standard solutions. The lead deposit was re-deposited from 35 µL of 0.1% HNO_3 for 60 seconds and rinsed with 40 µL of water for 5 seconds. High-temperature deposition conditions (45 °C) and a potential of 2.0 V were used throughout. Samples were pyrolysed at 1100 °C and atomised at 2300 °C. The lead absorbances, measured at 283.3 nm, are shown in Figure 5.5.

5.2.1.2 Residual Sodium Chloride—Effects and Control

Effect of Deposition Potential

The amount of lead 'lost' as a molecular chloride during pyrolysis and atomisation is related to the amount of sodium chloride remaining in the furnace after the electrodeposition and rinsing process. The relationship between the amount of residual sodium chloride and the absorbance for lead was explored by comparing the peak lead absorbance with the concomitant background absorbance. The effect of pyrolysis temperature was also examined.

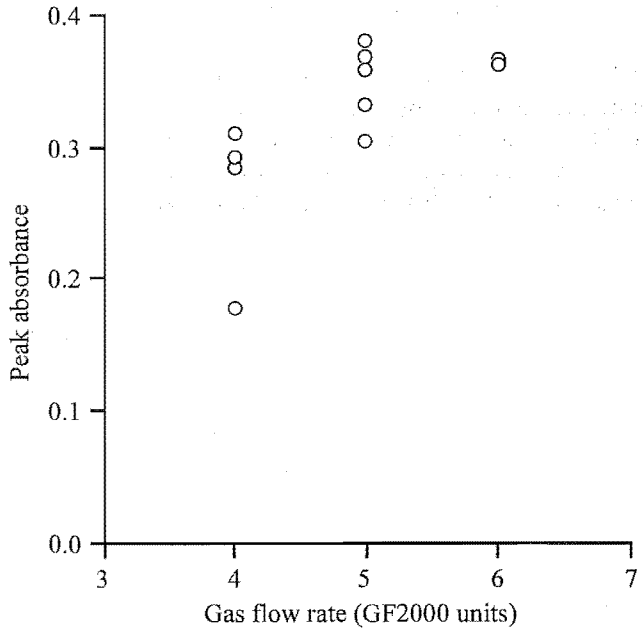

Figure 5.3 Effect of inert gas flow rate on lead deposition from 1% HNO_3/0.5 M NaCl. Lead was deposited onto palladium-modified furnace from 20 µL of 50 ppb solution. The lead deposits were re-deposited from 40 µL of 1% HNO_3 for 60 seconds and then rinsed with 40 µL of water for 5.0 seconds. Deposition was effected at 45 °C using a potential of 4.5 V. The lead deposits were dried at 110 °C, pyrolysed at 800 °C, and atomised at 2300 °C. Lead absorbance was measured at 283.3 nm.

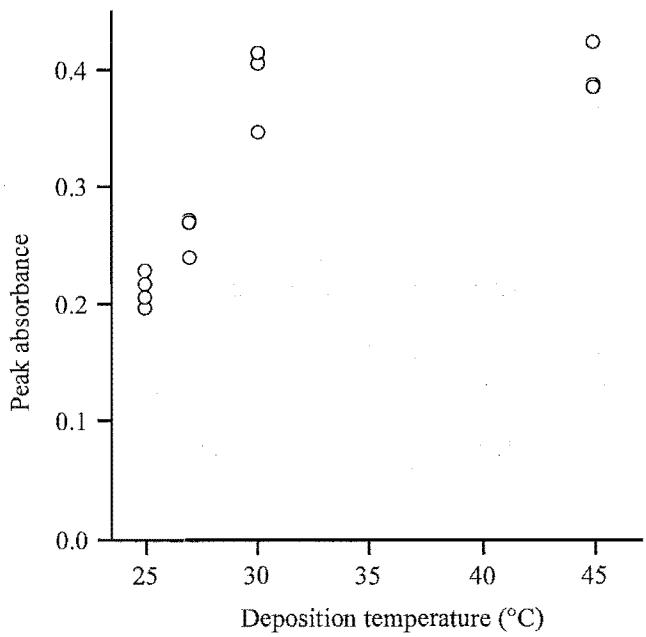

Figure 5.4 Effect of deposition temperature for lead determination in 1% HNO_3/0.5 M NaCl. Lead was deposited for 60 seconds onto palladium-modified furnace from 20 µL of 50 ppb solution. Lead deposits were re-deposited from 40 µL of 1% HNO_3 for 60 seconds and then rinsed with 40 µL of water for 5.0 seconds. Deposition was effected using a potential of 4.5 V with the inert gas flow switched to setting five. The lead deposits were dried at 110 °C, pyrolysed at 800 °C, and atomised at 2300 °C. Lead absorbance was measured at 283.3 nm.

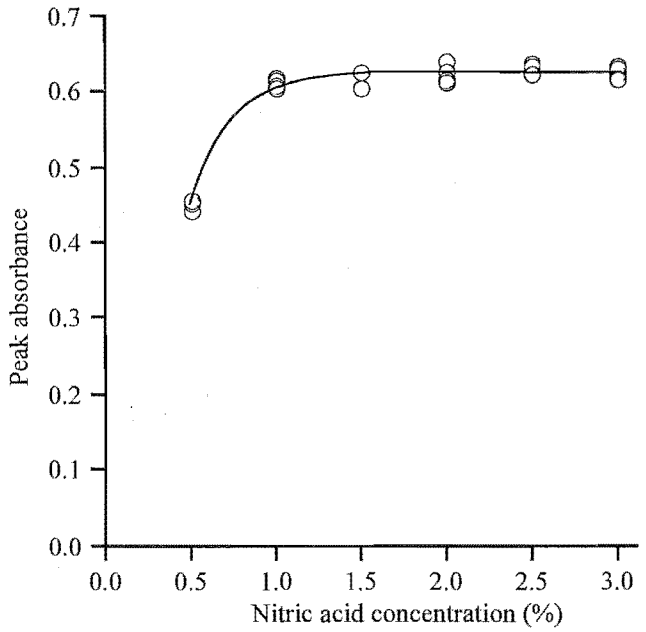

Figure 5.5 Effect of nitric acid concentration. 20 µL of 50 ppb lead sample was deposited onto a palladium-modified furnace for 60 seconds. The deposit was re-deposited from 35 µL of 0.1% HNO_3 for 60 seconds, then rinsed with 40 µL of water for 5 seconds. High temperature deposition conditions and a potential of 2.0 V were used throughout. Samples were pyrolysed at 1100 °C and atomised at 2300 °C. The lead absorbances were measured at 283.3 nm.

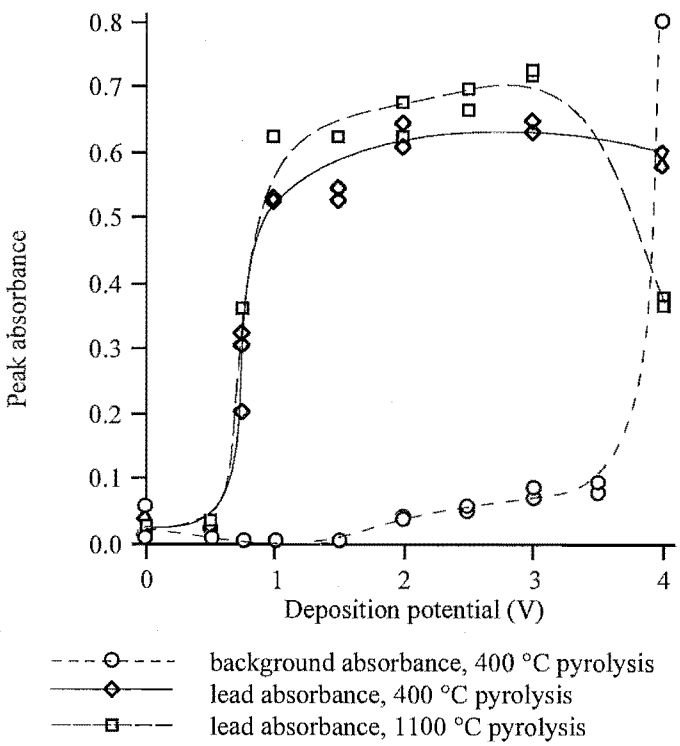

Figure 5.6 Effect of deposition potential on the background and lead absorbances for determination of lead in 0.5 M NaCl/1% HNO_3 media. Lead was deposited onto a palladium-modified furnace from 20 µL of 50 ppb solution for 60 seconds. The lead deposit was re-deposited from 40 µL of 0.1% HNO_3 for 30 seconds. All depositions were effected at room temperature with the inert gas flow on. The deposit was dried at 150 °C, pyrolysed, equilibrated at 400 °C, and atomised at 2300 °C. The lead and background absorbances were measured at 283.3 nm.

The furnace was modified by depositing palladium from 30 µL of 10 ppm solution, containing 0.1% HNO_3, for 20 seconds. Lead was deposited from 20 µL of 50 ppb Pb^{2+} solution in 0.5 M NaCl/1.5% HNO_3 for 60 seconds, using potentials in the range 0.0-4.0 V. The lead deposit was re-deposited from 40 µL of 0.1% HNO_3 for 60 seconds. All depositions were effected at room temperature with the inert gas flow on. The deposit was dried at 150 °C, pyrolysed at either 400 °C or 1100 °C, equilibrated at 400 °C, and atomised at 2300 °C. The lead and background absorbances were measured at 283.3 nm. The results are shown in Figure 5.6. The background absorbance for an 1100 °C pyrolysis temperature (not shown) showed a similar dependence on deposition potential to that for the 400 °C pyrolysis, but with values *ca.* 40% lower.

Thermal Stability of Sodium Chloride

The pyrolysis curves for sodium chloride volatilisation from two different surfaces were compared. The two surfaces were pyrolytic-coated graphite, and palladium-modified pyrolytic-coated graphite. Where used, the palladium modifier was deposited from 30 µL of a 10 ppm solution containing 0.1% HNO_3. After 20 seconds deposition, the palladium was dried at 110 °C. A 20 µL volume of sample solution containing 50 ppb lead, 0.5 M NaCl, and 1% HNO_3 was electrolysed at 3.0 V for 60 seconds. The furnace was then rinsed with 40 µL of water for 5.0 seconds, dried to 400 °C, and then fired to 2300 °C. For the un-modified furnace, the background absorbance was measured at 283.3 nm. Where the modifier was used, the sensitivity at this wavelength was insufficient, so the background absorbance was measured at 261.4 nm. For comparison of the results (Figure 5.7), the absorbances for sodium chloride on the un-modified surface have been scaled to compensate for different sensitivities at the two wavelengths. The scaling factor of 2.2 was derived from the molecular absorption spectrum for sodium chloride.[3] The scaling affects the apparent sensitivity but not the volatilisation temperature.

As an adjunct to the sodium chloride pyrolysis curves, the absorbance profiles for volatilisation of sodium chloride from un-modified and palladium-modified furnaces were compared. The deposition conditions and solutions used were the same as for the pyrolysis curve experiment except for the heating rate during the volatilisation step. To magnify any differences in the absorbance profiles, the heating rate was decreased to 238 °C s^{-1}. The pyrolysis temperature used was 500 °C. The background absorbances were measured at 283.3 nm and 261.4 nm for the un-modified and palladium-modified furnaces respectively. The results (as shown in Figure 5.8) are not scaled.

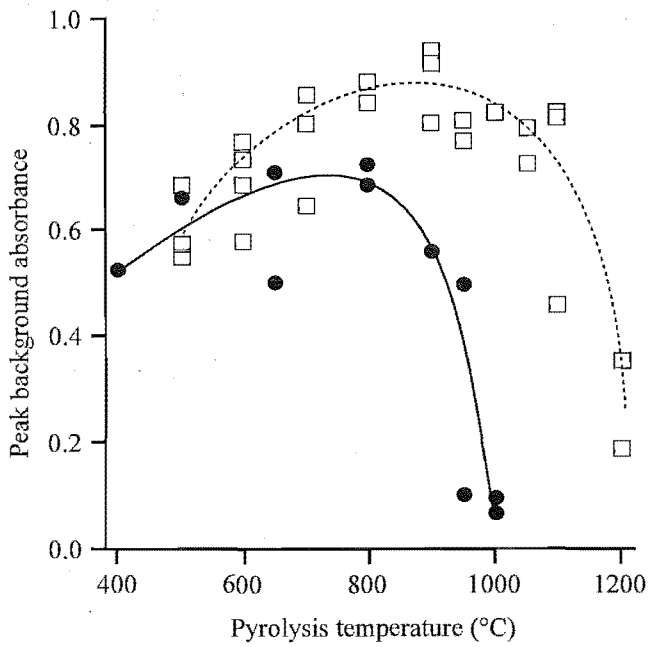

Figure 5.7 Pyrolysis curves for sodium chloride volatilisation from pyrolytic-coated graphite (□), and palladium-modified pyrolytic-coated graphite (●). A 20 µL volume of sample solution containing 50 ppb lead, 0.5 M NaCl, and 1% HNO_3 was electrolysed for 60 seconds. The furnace was then rinsed with 40 µL of water for 5.0 seconds, dried to 400 °C, pyrolysed and then fired to 2300 °C. The background absorbances for the un-modified, and palladium-modified furnaces were measured at 283.3 and 261.4 nm respectively. To aid comparison, the data collected at 283.3 nm have been scaled.

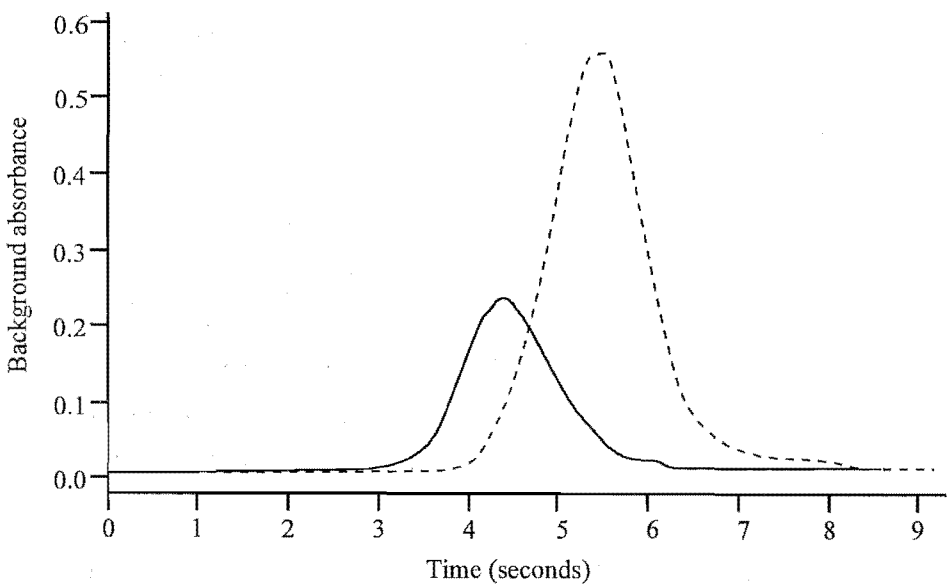

Figure 5.8 Absorbance profiles for sodium chloride volatilisation from pyrolytic-coated graphite (·····), and palladium-modified pyrolytic-coated graphite (——). A 20 µL sample containing 50 ppb lead, 0.5 M NaCl, and 1% HNO_3 was electrolysed in the relevant furnace for 60 seconds. The furnace was then rinsed with 40 µL of water for 5.0 seconds, dried, pyrolysed at 500 °C and then fired to 2300 °C. The background absorbances for the un-modified, and palladium-modified furnaces were measured at 261.4 and 283.3 nm respectively.

Effects of Residual Sodium Chloride

In order to examine the effect of residual sodium chloride on lead atomisation, the amount of sodium chloride remaining in the furnace after electrodeposition and rinsing was determined. The effect of adding this amount of sodium chloride to a lead sample that had been deposited from HNO_3 was then measured.

Lead was deposited onto a palladium-modified furnace from 20 µL volumes of 50 ppb lead solution for 60 seconds. Two different sample media were used: 1% HNO_3 and 1.5% HNO_3/ 0.5 M NaCl. The lead deposits were re-deposited from 40 µL of 0.1% HNO_3 for 60 seconds and rinsed with 40 µL of water for 5 seconds. High-temperature deposition conditions and a potential of 2.0 V were used throughout. Samples were pyrolysed at 1100 °C and atomised at 2300 °C. Lead and background absorbances were measured at 283.3 nm.

The mean background absorbance for the sample prepared in 0.5 M NaCl/1% HNO_3 was 0.014 (n=3). In order to gauge the amount of sodium chloride required to produce a background absorbance of this magnitude, the HNO_3-based sample was deposited in the same way. 20 µL of $3x10^{-4}$ M NaCl ($6x10^{-9}$ moles) was then added prior to the drying step. The mean background absorbance produced from this was 0.035 (n=2). This indicated that the amount of residual chloride under these deposition conditions was less than 6×10^{-9} moles. (i.e. less than 0.06% of the original sample matrix.)

To determine the effect that this amount of sodium chloride has on lead atomisation, the experiment was repeated measuring the lead absorbance rather than the background. The mean absorbance for lead deposited from 1% HNO_3 was 0.689 (n=5). For the same sample with 20 µL of $3x10^{-4}$ M NaCl added prior to drying, the mean absorbance was 0.694 (n=3). This indicates that the amount of sodium chloride remaining after deposition and rinsing ($< 6 \times 10^{-9}$ moles), has no adverse effects on the peak absorbance for lead determination.

The relative lead, and background (NaCl) absorbance-time profiles for the 50 ppb lead sample prepared in 0.5 M NaCl/1.5% HNO_3 are shown in Figure 5.9.

5.2.1.3 Sample Equilibration

During determination of lead in 0.5 M NaCl/1% HNO_3 solutions it was observed that measurements changed with time, and that freshly prepared sample solutions gave results different from aged samples. This phenomenon was further investigated, using both ED-ETAAS and ASV.

A 50 ppb lead solution was prepared in an ASV cell by adding in order: 5 mL of 1.0 M NaCl, 1.0 mL of 500 ppb Pb^{2+} (containing 0.125 M HNO_3), 4.0 mL of water, and 100 µL HNO_3 (conc.). A 1.0 mL aliquot of the solution was removed for lead determination by ED-ETAAS the remainder was analysed by ASV. For both methods, the sample was measured as soon as possible after the time of mixing, and then at 20 minute intervals over a period of 250 minutes.

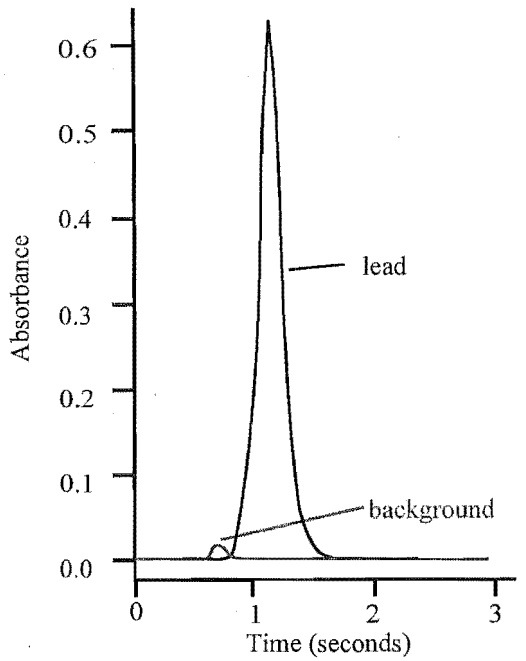

Figure 5.9 Absorbance-time profiles for the atomic and background signals during atomisation of a 50 ppb lead sample prepared in 0.5 M NaCl/1.5% HNO_3. A 20 µL sample was electrolysed in a palladium-modified furnace for 60 seconds. The deposit was then re-deposited from 40 µL of 0.1% HNO_3 for 60 seconds and rinsed with 40 µL of water for 5 seconds. High-temperature deposition conditions and a potential of 2.0 V were used throughout. The sample was pyrolysed at 1100 °C for lead measurements, and at 400 ° C for background measurements. Atomisation was carried at 2300 °C in both cases. Lead and background absorbances were measured at 283.3 nm.

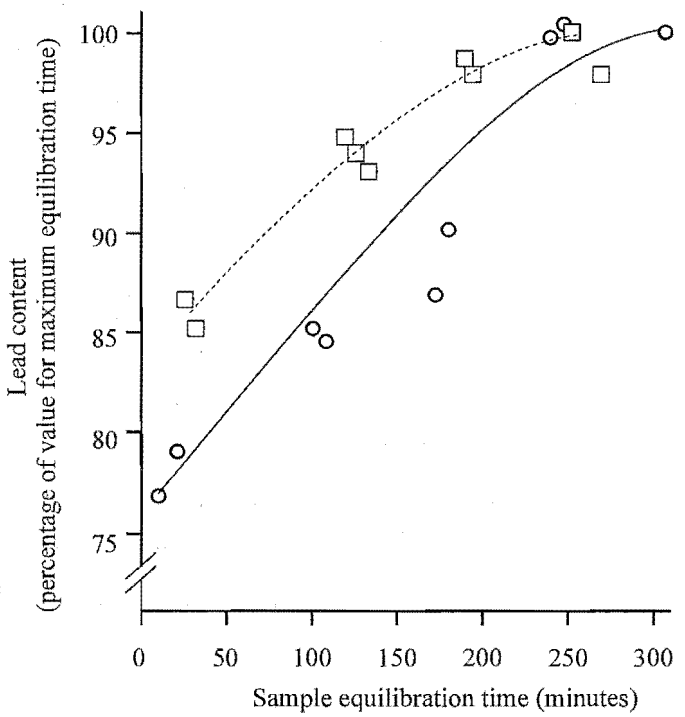

Figure 5.10 Effect of equilibration time on the amount of lead measured in 0.5 M NaCl/1% HNO_3 solution by ED-ETAAS □), and ASV (○). The 50 ppb lead solution was prepared by adding in order: 5 mL of 1.0 M NaCl, 1.0 mL of 500 ppb Pb^{2+} (containing 0.125 M HNO_3), 4.0 mL of water, and 100 µL (conc.) HNO_3.

For ED-ETAAS analysis, 20 µL of the lead sample was electrolysed in a palladium-modified furnace for 60 seconds at 2.0 V, re-deposited for 60 seconds from 40 µL of 0.1% HNO_3, and then rinsed for 5.0 seconds with 40 µL of water. High-temperature deposition conditions were used throughout. The sample was pyrolysed at 1100 °C and atomised at 2300 °C. The lead absorbance was measured at 283.3 nm.

For ASV analysis, the sample was first purged for 10 minutes with nitrogen. Lead was deposited onto a hanging mercury drop electrode for 120 seconds at -0.7 V and the peak current measured (at *ca.* -0.52 V) as the potential was ramped to -0.2 V. Square-wave stripping parameters were as outlined in the Chapter Two.

The results for both experiments are shown in Figure 5.10. The data, expressed as percentages, represent the raw absorbance/currents at time 't', relative to the absorbance/current measured at the maximum equilibration time (282 minutes for ED-ETAAS and 307 minutes for ASV).

In subsequent experiments the sample-equilibration problem was countered by preparing sample solutions in the order: lead, acid, water, sodium chloride. The sample solutions were also subjected to a brief heat treatment—accomplished by microwaving the samples. For determination of lead in freshly prepared samples, this microwave treatment immediately produced absorbance readings equivalent to those for samples aged at room temperature. To ascertain whether microwaved and non-microwaved samples would eventually equilibrate to give the same sensitivity, a series of differently prepared samples was allowed to equilibrate overnight prior to analysis. The absorbances for the samples were then compared. Four 1.0 mL samples contained 50 ppb lead were prepared. Two samples in 1% HNO_3 media and two in 0.5 M NaCl/1.5% HNO_3. The mixing order for sample components was: lead, acid, water, sodium chloride. One sample of each medium was microwaved on high power (700 W) for 10 seconds. All four samples were then covered and allowed to stand overnight before analysis.

The samples were analysed for lead using ED-ETAAS. The furnace was first modified by electrodepositing palladium for 20 seconds from 30 µL of a 10 ppm solution prepared in 0.1% HNO_3. It was then dried at 110 °C and 20 µL of the lead sample solution electrolysed for 60 seconds. The lead was re-deposited from 40 µL of 0.1% HNO_3. All depositions were carried out at 2.0 V under high-temperature deposition conditions. Samples were pyrolysed at 1100 °C and atomised at 2300 °C. The absorbance was measured at the 283.3 nm lead line. Results for analysis of the equilibrated lead samples are shown in Table 5.1.

Sample medium	Microwaved for 10 seconds (mean peak absorbance)	Not microwaved (mean peak absorbance)
1% HNO_3	0.611 (n = 8, RSD = 6.0%)	0.602 (n = 10, RSD = 1.2%)
1.5% HNO_3 / 0.5 M NaCl	0.607 (n = 5, RSD = 1.5%)	0.617 (n = 10, RSD = 0.9%)

Table 5.1 Effect of sample medium and preparation method for lead determination by ED-ETAAS. Lead was deposited onto a palladium-modified furnace from 20 µL of solution and re-deposited from 40 µL of 0.1% HNO_3. Deposition was effected at 2.0 V under high-temperature conditions. Lead samples equilibrated overnight prior to analysis. The lead deposits were pyrolysed at 1100 °C and atomised at 2300 °C. Lead absorbance was measured at 283.3 nm.

5.2.1.4 Analyte Carry-over

Problems were encountered with carry-over from one sample to the next. If a sample of low concentration was analysed following a sample of high concentration, the first reading for the low concentration sample would be higher than for subsequent measurements. If samples were analysed in the reverse order, the first reading for the high concentration sample would be lower than for subsequent readings. This phenomenon was observed for both conventional and electrodeposition-coupled ETAAS. The effect was particularly apparent for ED-ETAAS determination of alternating samples that contained the same lead concentration but were prepared in different media (HNO_3 vs 0.5 M NaCl/1% HNO_3). The first measurement for the 0.5 M NaCl/1% HNO_3 sample was invariably higher than subsequent readings, and the first reading for the HNO_3 samples was lower.

Sample carry-over was not observed when the platinum-iridium capillary was replaced with a conventional PTFE sample delivery tube (conventional thermal analysis). Therefore the effect was attributed to analytes adsorbing onto the inside of the platinum-iridium delivery tube. Prevention of this requires a delivery tube that analyte cannot adsorb to. While the conventional PTFE delivery tube achieves this aim, PTFE is unsuitable for ED-ETAAS analysis because it cannot double as an anode. Therefore, a new delivery probe was constructed which combined a PTFE delivery tube with a separate platinum anode. A schematic diagram of this probe is shown in Chapter Two; Figure 2.3.

The PTFE delivery probe/anode was tested by looking for carry-over when alternately analysing 50 ppb lead samples prepared in HNO_3, and 0.5 M NaCl/1.5% HNO_3. Lead was deposited under high-temperature deposition conditions onto a palladium-modified furnace from 20 µL of sample solution for 60 seconds. The deposit was rinsed with 40 µl of water for 5.0 seconds prior to drying, pyrolysis at 1100 °C and atomisation at 2300 °C. The lead absorbance was measured at 283.3 nm. The results from this experiment (Figure 5.11b) are contrasted with a set of measurements made using the Pt/Ir sample delivery tube (Figure 5.11a). The conditions for the experiment with the Pt/Ir delivery tube were the same as those used with the PTFE probe except that the rinse step was replaced with a 10 second re-deposition from 0.1% HNO_3.

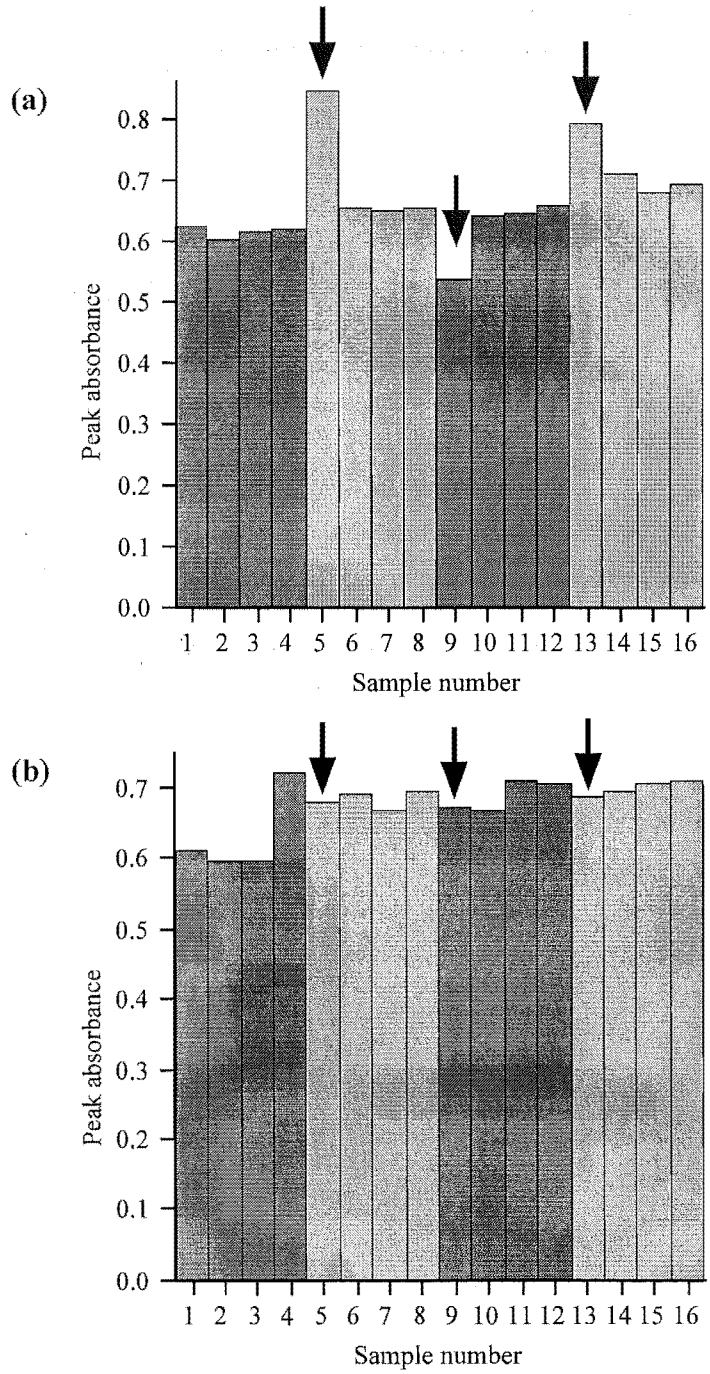

Figure 5.11 Analyte carry-over for the conventional Pt/Ir delivery probe (a) compared with that for the PTFE delivery probe (b). Lead was deposited for 60 seconds onto a palladium-modified furnace from 20 µL of 1% HNO_3 (□), and 0.5 M NaCl/1% HNO_3 (▨). Lead deposits were re-deposited from 40 µL of 0.1% HNO_3 (a); or rinsed with 40 µL of water (b); pyrolysed at 1100 °C and atomised at 2300 °C. Lead absorbance was measured at 283.3 nm.

5.2.2 Discussion

5.2.2.1 Deposition Parameters

Initial attempts to determine lead in saline media used the original ED-ETAAS protocol as developed by Matousek and Powell.[97,99] In the present work, the sensitivity of this method for saline media was markedly lower that for nitric acid media. ASV analysis of the spent ED-ETAAS electrolysis medium indicated that electrodeposition was only 70-90% efficient. Experiments to determine the effects of residual NaCl on ETAAS lead analysis were also carried out. Following these investigations, the poor sensitivity for saline media was attributed to a combination of non-quantitative lead deposition and interference by (large amounts of) residual chloride during pyrolysis/atomisation. Based on these assumptions, various parameters were investigated in an attempt to improve the deposition efficiency.

The effect of deposition time on sensitivity is shown in Figure 5.1. Extended deposition times had little effect on the sensitivity, so alternative means of improving deposition efficiency were sought. Based on the work of Sioda *et al*,[55] it was hypothesised that the equilibrium,

$$\text{deposit (Pb)} + \text{oxidant} \rightleftharpoons Pb^{2+} + \text{reductant} \qquad \text{(Reaction 5.1)}$$

was affected by an increased concentration of oxidant species in the deposition medium. Electrolysis of the sodium chloride solution at 4.5 V produces Cl_2. Simultaneous H^+ consumption at the cathode leads to NaOH formation; the solution becomes strongly basic. Under such conditions, species likely to be formed from chloride electrolysis include such oxidants as ClO_2^- and ClO_3^-. Efforts to improve deposition efficiency centred on lowering the concentrations of these oxidant species.

One important factor in the formation of oxidant species is the deposition potential. In basic solution, oxidation of chloride ion to the various oxychloride species or chlorine gas requires large positive potentials. This is illustrated by the reduction potentials (vs. NHE).

$$ClO_3^- + 3H_2O + 6e^- \rightleftharpoons Cl^- + 6OH^- \qquad E^\circ = 0.62\ V$$

$$ClO_2^- + 2H_2O + 4e^- \rightleftharpoons Cl^- + 4OH^- \qquad E^\circ = 0.76\ V$$

$$Cl_2(g) + 2e^- \rightleftharpoons 2Cl^- \qquad E^\circ = 1.36\ V$$

In contrast, E° for the reduction of the Pb^{2+} ion is comparatively small; -0.13 V. Therefore it was reasoned, that by choosing an appropriately low deposition potential (and therefore low anodic and cathodic currents), it would be possible to deposit lead while minimising formation of oxidising species.

The other approach considered was to lower the concentration of oxidants O_2 and Cl_2 in the deposition medium by decreasing their solubilities. Two methods were explored. The first was to raise the temperature of the electrolysis medium during sample deposition. The

second was to bathe the solution with inert gas during sample deposition. In practice, these objectives were met by carrying out sample deposition during the first step of the furnace temperature program. This made it possible to adjust the deposition temperature, and switch the inert gas flow on and off.

The effects of deposition potential, increased deposition temperature, and inert gas flow during sample deposition are shown in Figure 5.2. The lowest sensitivity was observed when using the original ED-ETAAS protocol; room temperature deposition at 5.0 V. Sensitivity was marginally improved by using a lower deposition potential, but was still only 50% of the maximum obtained. At the lower deposition potentials, the pH of the deposition medium remained acidic and production of chlorine gas and related oxidants was relatively low. In this situation, the deposition equilibrium is slightly more favourable.

Sensitivity was greatly enhanced when deposition was effected at elevated temperature. The reason for this could be a combination of several factors: enhanced deposition kinetics, decreased oxidant concentrations through reduced solubility of chlorine and oxygen, and improved sample stirring through convection. The further increase in sensitivity when the inert gas flow was switched on could be attributed to both enhanced sample stirring, and to a further decrease in oxidant concentration.

The effects of different gas flow rates were explored further, as shown in Figure 5.3. While elevated gas flow rates gave higher sensitivity, the gas tended to push the sample solution out of the furnace (through the sample introduction port) during electrolysis. With this in mind, a gas flow rate of 5.0 was chosen for further work. This was sufficient to give high sensitivity without pushing the sample solution out of the furnace.

The effect of deposition temperature is shown in Figure 5.4. An increase of 5 °C was sufficient to almost double the sensitivity; further increases had little added effect. This observation suggests that convection may play an important part in the improved sensitivity. Another effect of increased temperature is to evaporate the sample. For an evaporating solution that is saturated with oxidant gases, the evaporation increases the analyte concentration while the oxidant concentration remains relatively constant. This improves the deposition efficiency by driving the deposition-dissolution equilibrium, reaction 5.1, to the left. However, evaporation of the sample solution can lead to crystallisation of matrix components such as sodium chloride. This is undesirable because such deposits are more difficult to remove in the rinse step that precedes pyrolysis and atomisation. The deposition temperature chosen for further work was 45 °C as this gave good sensitivity without completely evaporating the sample.

The effect of nitric acid concentration on deposition efficiency is shown in Figure 5.5. The decrease in deposition efficiency at low acid concentrations is slightly more marked than was observed in non-saline media (Figure 4.1). For future work in saline media, a nitric acid concentration of 1.5% was used. This gave good sensitivity, and in some cases seemed to give superior deposition efficiency to the 1.0% medium.

5.2.2.2 Residual Sodium Chloride

The amount of sodium chloride remaining in the furnace after electrolysis depends on the deposition potential. It increases rapidly at deposition potentials above 3.5 V (this is illustrated in Figure 5.6). There are two possible reasons for this effect. The first is that the sodium chloride becomes intercalated in the pyrolytic graphite furnace coating. The second is that effervescence, caused by rapid hydrogen evolution, spatters sample solution onto the ends and top of the furnace. These areas are not reached by subsequent rinse steps so sodium chloride from the original sample solution is still present during pyrolysis/atomisation. This latter explanation seems more likely given that the background is readily lowered if the furnace is removed and rinsed with distilled water prior to atomisation. Further, the background absorbance becomes large at the same potential at which rapid gas evolution begins.

The other feature of interest in Figure 5.6 is the effect of pyrolysis temperature. When the sample is deposited at high potentials (>3.5 V), high temperature pyrolysis produces lower absorbances than low temperature pyrolysis. One possible explanation for this is that during high temperature pyrolysis, lead reacts with Cl_2 generated from NaCl decomposition. The resulting lead chloride is volatilised and 'lost' from the furnace. In contrast, 400 °C pyrolysis temperatures are insufficient to decompose the residual sodium chloride, so no lead is lost during pyrolysis. Upon atomisation the furnace temperature is sufficiently high to dissociate any lead chloride formed. Therefore the amount of lead measured using low-temperature pyrolysis is higher than for high-temperature pyrolysis. This effect can be expected where furnace temperature ramp rates are sufficiently high (approximating isothermal conditions) and only small amounts of residual sodium chloride are present.

Hence, when significant amounts of residual sodium chloride remain in the furnace after electrodeposition, a lower pyrolysis temperature is preferable. However, when deposition is effected at low potentials, the amount of residual sodium chloride is sufficiently small that the analytical signal is unaffected by the pyrolysis temperature (400 °C or 1100 °C).

The effect of pyrolysis temperature on the background absorbance is shown in Figure 5.7. The shift in the pyrolysis curves in the presence of the palladium modifier suggests that sodium chloride has a reduced stability on the palladium-modified furnace—the converse of what happens with the lead analyte. This is further illustrated in Figure 5.8, which shows that when no palladium is present, significantly more sodium chloride is retained on the furnace. In this situation, the sodium chloride requires a higher volatilisation temperature. One possible explanation is that in the absence of palladium, sodium chloride penetrates the pyrolytic graphite surface of the furnace, giving greater retention and slower volatilisation kinetics. This is prevented by the palladium modifier which 'seals' the furnace surface.[97,147] Another explanation is that the palladium occupies the 'active surface sites' at which sodium (chloride) is most strongly adsorbed.

The different effects of palladium on the lead analyte (stabilisation) and the residual sodium chloride ('de-stabilisation') serve to temporally separate sodium chloride volatilisation from lead atomisation. This temporal separation, as illustrated in Figure 5.9, further decreases any detrimental effects of residual sodium chloride on lead atomisation. It also helps to explain why a small amount of sodium chloride (6×10^{-7} moles), added to the furnace prior to atomisation, has no effect on lead absorbance.

5.2.2.3 Sample Equilibration

Unlike conventional ETAAS which measures total metal content, electrochemical techniques measure only labile metal species (see Chapter Seven). Thus, because of the incorporated electrodeposition step, ED-ETAAS does not measure insoluble metal species or non-labile complexes. Therefore, while not of great concern for ETAAS analysis, hydrolysis of analyte metals (or formation of other complexes that are not electrochemically labile) can have a drastic effect on ED-ETAAS measurements. Such hydrolysis is believed to be responsible for the sample equilibration phenomenon shown in Figure 5.10.

The origin of the 'sample hydrolysis effect' is unclear. Lead stock solutions were prepared in 0.125 M HNO_3, giving a solution pH of about 1.0. Equilibrium calculations indicated that no hydrolysis should occur at such low pH. The sample solutions were prepared at a final concentration of 1% HNO_3 to give an even lower pH, again preventing the formation of hydrolysed species at equilibrium. However, it was observed that the order of mixing and dilution during sample preparation affected the sensitivity of ED-ETAAS measurements. By inference, it is likely that (polymeric) hydrolysed lead species are formed during sample preparation. The hydrolysed lead species then slowly dissociate (or dissolve) as the system equilibrates. This effect was particularly apparent for a 10-fold dilution of 500 ppb lead solution into 0.5 M NaCl, followed by acidification with HNO_3. Time-dependent dissociation/dissolution of the non-labile species formed accounts for the equilibration curves shown in Figure 5.10. A similar increase in apparent analyte concentration is shown by the curve determined by ASV. The higher percentage of lead measured by the ED-ETAAS technique reflects the more forcing conditions used during ED-ETAAS electrodeposition i.e. elevated temperature, and depletion of 'free' (labile) metal from the electrolysis medium.*

Two methods were used to counter the problem of lead hydrolysis. Firstly, the order of mixing/dilution for sample preparation was changed so that the lead stock solution was acidified and diluted with water before addition of the sodium chloride stock solution. With this method, the initial (t=0) absorbances for lead solutions prepared in 0.5 M NaCl/1% HNO_3 were 92% of the limiting values. The lead was fully labilised by microwaving the sample

* The relative effects of quantitative versus non-quantitative depletion of the sample solution are discussed fully in Chapter Seven.

solutions at high power for 10 seconds (1.0 mL sample). Table 5.1 shows that after 24 hours equilibration, microwaved and non-microwaved solutions prepared in this fashion contain the same amount of labile lead.

Initial absorbance measurements for 50 ppb lead samples prepared in the order: lead, acid, water, NaCl, and then microwaved, were the same as those for lead solutions prepared in HNO_3. Thus, calibration for measurement of lead in saline media can be achieved using 'simple' acidified lead standards.

5.2.2.4 Analyte Carry-over

Analyte carry-over arising from analyte adsorption on the inside of the Pt/Ir delivery tube/anode was such a problem that in many cases, the first of a series of replicate measurements on a sample could not be used. The extent of this problem is illustrated in Figure 5.11(a).

The first two approaches used in trying to solve the carry-over problem were both attempts to modify the properties of the original Pt/Ir capillary tube. The first, was to silanise the Pt/Ir capillary using dichlorodimethylsilane solution. Whether the silanising was successful could not be determined, but the carry-over was not ameliorated. The second method tried, was lining the inside of the capillary with a polymer; poly(o-phenylenediamine). The capillary surface was prepared and the o-phenylenediamine electro-polymerised using the method of Malitesta *et al.*[185] In an attempt to coat the inside of the capillary, it was placed in a flow system, and o-phenylenediamine was pumped through it during electrolysis. Although the polymer was clearly visible on the end surfaces of the capillary, the carry-over problem was not overcome. It is possible that current densities in the centre of the capillary during the electro-polymerisation process were too low to fully coat the capillary with o-phenylenediamine.

The third, and most successful method used to combat the problem of analyte carryover was to replace the Pt/Ir capillary with a PTFE probe which incorporated a platinum anode (Figure 2.3). As illustrated in Figure 5.11(b), the carry-over effect was greatly decreased by using this probe for introducing samples into the furnace. However, there were two disadvantages of the PTFE probe. The first was its large size relative to the Pt/Ir probe. The increased size made it difficult to align the probe with the sample introduction hole in the furnace. The greater volume also meant that the volumes of sample and rinse solutions had to be decreased. These solutions tended to be pushed out of the furnace by the nitrogen gas flow during electrolysis.

The second major disadvantage of the probe was its flexible platinum/PTFE composite construction. This made the probe temperature-sensitive in the same way as a bi-metal strip. Small fluctuations in air temperature during the course of an analysis caused the probe to bend, hence spoiling its alignment with the furnace sample introduction hole. As a conse

quence of this, the instrument could not be left to run unattended. Because of these problems, the PTFE probe tip was not used for further work. Hence the problem of analyte carryover is unresolved as yet. The ideal answer would be a Pt/Ir capillary lined with PTFE. Both Pt/Ir capillary and PTFE tubing are commercially available in suitable sizes to construct such a probe. However, financial constraints prevented this happening during the course of this research.

5.3 COPPER DETERMINATION IN SEAWATER

In this section, the ED-ETAAS method developed for determination of lead in sodium chloride media was used to measure copper in seawater. The amount of copper measured in standard solutions, prepared by different methods, was compared in order to establish that ED-ETAAS is sensitive to sample speciation and to make some inference about the distribution of copper in the seawater sample.

5.3.1 Experimental and Results

Seawater samples were collected as described in Chapter Two. A series of solutions was prepared from the un-acidified 0.45 μm-filtered sample as shown in Table 5.2. These sub-samples were subjected to different levels of filtration (0.45 and 0.025 μm), pre-acidification, and UV photolysis 24 hours before analysis. All solutions were further acidified to 1.5% HNO_3 and microwaved on high power for 10 seconds (per each 1.0 mL sample) immediately prior to determination.

The furnace was modified by electrolysing 30 μL of 10 ppm palladium solution, prepared in 0.1% HNO_3, for 20 seconds. The furnace was then dried to 110 °C, and 20 μL of sample solution deposited for 60 seconds. The copper deposit was then rinsed with 40 μL of water for 5.0 seconds. High-temperature deposition conditions and a potential of 2.0 V were used throughout. Samples were pyrolysed at 900 °C and atomised at 2450 °C. The peak copper absorbance was measured at 324.8 nm.

The standard additions calibration curve for a pre-acidified, photolysed and 0.45 μm filtered sub-sample is shown in Figure 5.12. The calculated copper concentration for this sample was 1.6±0.4 ppb. The methods of preparation, peak absorbances, and approximate concentrations (calculated using the standard additions plot) for the other sub-samples are shown in Table 5.2. Concentration errors were calculated from the least squares analysis of the standard additions curve (as described in Section 2.7).

Sample preparation method:	Mean peak absorbance (blank corrected, n=4)	Calculated concentration
1) Filtered to 0.45 μm.	0.039±0.006	0.9±0.4 ppb
2) Filtered to 0.025 μm and pre-acidified to 0.02% HNO_3 (*ca.* pH 2.5).	0.046±0.008	1.1±0.4 ppb
3) Filtered to 0.45 μm and pre-acidified to 0.02% HNO_3 (*ca.* pH 2.5).	0.039±0.001	0.9±0.4 ppb
4) Filtered to 0.025 μm, pre-acidified to 0.02% HNO_3 (*ca.* pH 2.5), and photolysed for four hours.	0.064±0.002	1.5±0.4 ppb
5) Filtered to 0.45 μm, pre-acidified to 0.02% HNO_3 (*ca.* pH 2.5), and photolysed for four hours.	0.067±0.004	1.6±0.4 ppb

Table 5.2 The effect of different sample preparation techniques on the amount of copper measured by ED-ETAAS in Lyttelton seawater. Samples were pre-equilibrated for 24 hours after preparation and then further acidified to 1.5% HNO_3 prior to analysis. 20 μL of each sample was electrolysed for 60 seconds in a palladium-modified furnace at 2.0 V under high-temperature conditions. The deposit was rinsed with 40 μL of water, dried, pyrolysed at 900 °C, and atomised at 2450 °C. The copper absorbance was measured at 324.8 nm. Calibration was achieved using the slope of the standard addition plot in Figure 5.12.

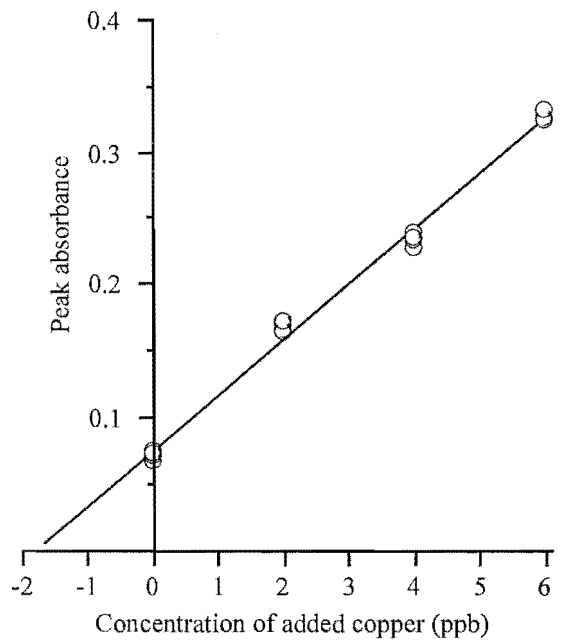

Figure 5.12 Standard additions calibration plot for the determination of total soluble copper in seawater. The Lyttelton seawater sample was filtered to 0.045 μm, pre-acidified to 0.02% HNO_3 (*ca.* pH 2.5), photolysed for four hours, and allowed to stand for 24 hours. Sub-samples (1.0 mL) were spiked with known amounts of copper and further acidified to 1.5% HNO_3 for ED-ETAAS analysis. 20 μL of the sample was electrolysed for 60 seconds in a palladium-modified furnace at 2.0 V under high-temperature conditions. The deposit was rinsed with 40 μL of water, dried, pyrolysed at 900 °C, and atomised at 2450 °C. The copper absorbance was measured at 324.8 nm.

5.3.2 Discussion

Determination of copper in sea water is complicated by the speciation of copper in marine environments. Copper is present in seawater both as mono- and di-valent ions which may be adsorbed onto colloids, complexed to a variety of organic and inorganic ligands, or distributed in micro-organisms.[186] It is therefore important to define which copper species are measured by a given method. Such a definition depends upon the analysis technique used, and the methods of sample collection and preparation. ETAAS measures the total copper content of a sample regardless of the chemical form. Unfortunately, the high sodium chloride content usually precludes direct ETAAS analysis of un-modified seawater samples. Anodic stripping voltammetry is more suited to seawater analysis because it less affected by the high salt concentration. However, unlike ETAAS, only electrochemically labile metals are measured by ASV. In order to determine total metal content, samples must be acidified/digested to dissolve colloids or particulates, and photolysed with UV radiation to decompose refractory organic ligands. In the same way, the electrodeposition step in ED-ETAAS makes the technique sensitive only to labile metals. Thus to measure total metal content by ED-ETAAS, samples require the same pre-treatment steps as for ASV analysis.

The seawater sample, analysed using standard additions calibration, (Figure 5.12) was prepared in much the same way as would be used for measuring total soluble copper by ASV; filtered to 0.45 μm, acidified, and photolysed prior to analysis. The different preparation methods for the samples shown in Table 5.2 would be expected to give different results depending on the original distribution of copper in seawater. For example, if a large proportion of copper was bound to colloidal particles, we would expect to measure less copper in the samples filtered to 0.025 μm than in those filtered to 0.45 μm. If instead, the available copper was bound to organic ligands, then we would anticipate measuring a greater copper concentration in the photolysed samples. If all of the copper was present in a free or weakly-bound form, then there should be no significant difference in the amount of copper measured for any of the different sample preparations.

As can be seen from Table 5.2, more copper was measured in the acidified and photolysed samples than in those that were merely acidified. The difference can be attributed to copper-organic complexes that are decomposed by photolysis. For the non-photolysed samples, there was no significant difference in the amount of copper measured regardless of the filtration level. This implies that very little copper is adsorbed on colloidal particles in the 0.025-0.45 μm range. The copper measured in these solutions is likely to be present either as Cu^{2+}, or as Cu^{I} or Cu^{II} complexed to OH^-, Cl^-, SO_4^{2-}, or HCO_3^-.[186] The remaining copper, strongly bound to organic ligands, is not sufficiently labile to be electrodeposited and is not measured in non-photolysed samples

This experiment shows that the ED-ETAAS method is sufficiently sensitive for copper determination in coastal seawater and that chloride interferences are not a problem. Further, unlike conventional ETAAS, the ED-ETAAS method is sensitive to copper speciation.

5.4 CADMIUM DETERMINATION IN SEAWATER

Cadmium is difficult to determine in seawater by ETAAS, because of the high volatility of cadmium and the large sodium chloride background absorbance at the cadmium wavelength. Cadmium determination in seawater usually requires a combination of a modifier and Zeeman-effect background correction,[187,188] or a preconcentration/matrix separation step.[48,189] Other workers have used electrodeposition to pre-concentrate cadmium and separate it from the sample matrix prior to ETAAS analysis.[27,90] In this section of work ED-ETAAS was used to directly measure the cadmium content of Lyttelton Harbour seawater. This was accomplished using a modification of the method developed for lead determination in sodium chloride media.

5.4.1 Experimental and Results

A sample of Lyttelton Harbour seawater was collected as described in Chapter Two. This was filtered to 0.45 μm. A sub-sample of the seawater was acidified to 0.02% HNO_3 and photolysed for five hours in a quartz tube. A series of 1.0 mL aliquots of both the photolysed and the non-photolysed water were spiked with known amounts of cadmium and then further acidified to 1.5% HNO_3 and microwaved on high power for 20 seconds immediately before analysis.

The furnace was modified by electrolysing 30 μL of 10 ppm palladium solution, prepared in 0.1% HNO_3, for 20 seconds. 20 μL of sample was then electrolysed for 60 seconds, re-deposited from 40 μL of 0.1% HNO_3 for 30 seconds, and rinsed with 40 μL of water for 5.0 seconds. All deposition was effected at 2.0 V, under high-temperature deposition conditions. The sample was dried, pyrolysed at 550 °C, and atomised at 2400 °C. The cadmium absorbance was measured at 228.8 nm.

For the non-photolysed sample, no cadmium was measured. The standard additions plot for the pre-acidified photolysed sample is shown in Figure 5.13. The cadmium concentration determined from this plot was 0.10±0.04 ppb.

5.4.2 Discussion

Cadmium was determined in seawater by ED-ETAAS with no matrix interference problems. The fact that 0.10 ppb cadmium was measured in the photolysed sample, but the non-photolysed sample was below the detection limit, suggests that the method is sensitive to cadmium speciation. Release of metals by photolysis/acidification is normally indicative of complexation by organic ligands. However, since organic-complexes are not thought to be important in marine cadmium chemistry,[186] it was inferred that the difference between the two samples was due to cadmium adsorbed on particles that had not been removed by filtration (ie. particles ≤ 0.45 μm). In this case, the photolysed samples were acidified five hours prior to analysis whereas the non-photolysed samples were acidified immediately prior to analysis. Thus, desorption of cadmium from particulates could have been due to acidification rather than photolysis.

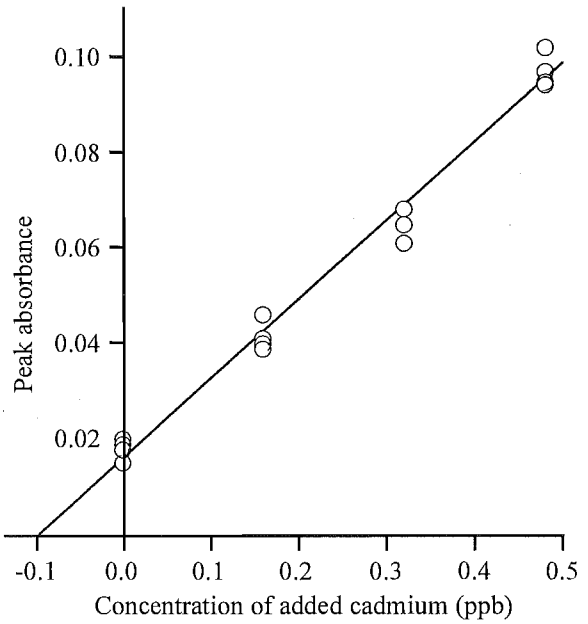

Figure 5.13 Standard additions plot for determination of total cadmium in Lyttelton Harbour water by ED-ETAAS. Seawater prepared by photolysing a 0.45 μm-filtered, acidified (0.02% HNO_3) sample for four hours, and then further acidifying to 1.5% HNO_3. 20 μL of the sample was electrolysed in a palladium-modified furnace for 60 seconds, re-deposited from 40 μL of 0.1% HNO_3 for 30 seconds, and rinsed with 40 μL of water for 5.0 seconds. All deposition was effected at 2.0 V, under high-temperature deposition conditions. The sample was dried, pyrolysed at 550 °C, and atomised at 2400 °C. The cadmium absorbance was measured at 228.8 nm.

While interferences posed no difficulties for the analysis, lack of sensitivity was a problem. While the detection limit was not formally calculated, an estimate calculated from the data for figure 5.13 gives a detection limit of 0.034 ppb. Thus it can be seen that the measured level of cadmium in the seawater is only three times the detection limit of the technique. The detection limit could be lowered in several ways. The sample size for determination could be increased from 20 μL to *ca.* 35 μL. Alternatively, a multiple injection technique could be used, in which several aliquots of sample are electrolysed before a single atomisation. This technique was used successfully by Chuang and Huang,[188] but may not markedly improve detection limits for ED-ETAAS because of the associated decrease in precision. An EDL light source could also be used to improve detection limits and sensitivity.[190]

This experiment showed that ED-ETAAS was a suitable method for determining total cadmium in coastal seawater, provided that samples were acidified and photolysed before analysis. Although sensitivity could be a problem for such low levels of cadmium, there is scope for further improvement in this area.

Chapter Six

Mercury Determination

This chapter examines the suitability of ED-ETAAS as a method for determining mercury in natural waters. The introduction discusses mercury in the environment and the methods used to measure it. The relative attributes and drawbacks of these methods are discussed. The second section describes the development of an experimental protocol for determination of mercury by ED-ETAAS. The ED-ETAAS method is compared with a cold-vapour protocol in which elemental mercury is accumulated on a palladium-modified furnace prior to ETAAS determination.

6.1 INTRODUCTION

Mercury is one of the most toxic elements, and its toxicity to humans has been well established.[186] Because of its unique ability to exist as both a liquid and a volatile species at ambient temperature, mercury is also one of the most ubiquitous of the heavy metals. The environmental chemistry of mercury is complex, with many mercury species being cycled continuously though the atmosphere, waters, sediments, and living organisms. These mercury species include elemental mercury, inorganic mercury (Hg^{I} and Hg^{II}), and a host of organomercury compounds.[191] Each part of the environment is dominated by a different mercury species, and each has a different level of toxicity to humans.[192] Very low levels of mercury in the environment are bio-concentrated though the food-chain and can reach toxic levels in the higher animals. The most famous example of such bio-accumulation was the Japanese tragedy of Minamata Bay, where seawater contamination resulted in poisoning of the fish-eating populace. Forty families were affected by mercury poisoning, and one third of the cases proved fatal.[191] Consequently there is a great deal of interest in determining trace and ultra-trace mercury levels. Both the total mercury concentration and the levels of the individual mercury species are of interest due to their different biological uptakes and toxicities.

A number of methods have been used for mercury determination. For relatively high concentrations of mercury (above 10 ppb), spectrophotometric methods such as that of Jiang *et al.*,[193] are suitable. Electrochemical methods are now becoming more popular and in some cases can provide superior detection limits. For example, Meyer *et al.* reported an ASV method that used a glassy carbon electrode and differential pulse detection.[194] The detection limit for this method was an extremely low 5×10^{-14} M (10 pg L^{-1}). However, the method only measures elemental and inorganic mercury.

The most common methods of mercury analysis are those based on the cold vapour technique, in which mercury compounds are reduced to elemental mercury vapour and quantified by atomic absorption spectrometry. Conventionally this is done by adding a reducing agent to a large volume (*ca.* 50 mL) of acidified sample, and passing the resultant mercury vapour into a quartz cell which is placed in the light path of the atomic absorption spectrometer. Nowadays, however, cold vapour analysis more commonly uses a continuous flow system to produce the mercury vapour. Such systems have a higher sample throughput and can include extra features such as online microwave sample digestion.[195-198] Continuous flow systems produce mercury vapour at a slower rate than the traditional batch method so some form of preconcentration is frequently employed in order to improve detection limits.

Various preconcentration methods have been used. Long known for its mercury amalgamating properties, gold has been a popular choice for use as a substrate for mercury preconcentration. For example, Bruhn *et al.* accumulated mercury vapour on gold-platinum gauze.[199] The mercury was released by heating and was passed into a quartz cell for determination. A detection limit of 0.033 mg kg^{-1} was established for determination of mercury in human hair. Debrah *et al.* used a similar method, but with ICP-MS detection, to obtain a detection limit of 200 pg L^{-1} for mercury in water samples.[200]

In-situ collection of mercury vapour within the graphite furnace is also becoming popular. Lee *et al.* used a gold-coated graphite disk which was placed inside the atomiser to accumulate mercury vapour.[167] Collection efficiency was reported to be 100% for the lifespan of the disk (*ca.* 1000 firings). The collection efficiency of different metals was compared by Kumar and Meeravali[168], who accumulated mercury vapour on Au, Pd/Au, and Pt/Rh meshes which were wrapped around pyrolytic-coated graphite platforms and placed within the atomiser. The highest sensitivity and lowest detection limit (and by inference, the most efficient accumulation), were obtained using the gold trap.

Other authors have collected mercury vapour directly on the inside of the graphite furnace, using a noble metal coating to adsorb the mercury. This method was used by Hladky *et al.* for determining mercury in concentrated mineral acids.[201] The furnace was coated with gold by thermal reduction of a Au^{III} solution. Mercury vapour was then accumulated on the gold-modified surface. The same approach has been used with several alternative furnace modifiers including palladium,[132] and iridium, zirconium, and tungsten.[202] A variation on the method was used by Yan *et al.*, who found that palladium^{II} chloride trapped mercury vapour more efficiently than palladium metal.[135] A detection limit of 628 pg L^{-1} for a 50 mL sample was reported (40 seconds vapour accumulation) for this very sensitive technique.

Although cold vapour methods offer high sensitivity, they require extra equipment and often have problems arising from high reagent blanks.[203] Conventional ETAAS determination offers greater simplicity, faster sample throughput, and less sample preparation.[169] The high volatility of mercury and some of its compounds makes the use of chemical modifiers

essential for direct ETAAS determination of mercury. Such modifiers fall into two main groups: the inorganic modifiers such as thioacetamide or ammonium sulfide which form relatively refractory mercury compounds, and the noble metals such as gold and palladium which form mercury amalgams/intermetallics. Of the two modifier types, the noble metals generally provide a greater degree of stabilisation.[203]

Bermejo-Barrera *et al.* used conventional ETAAS with a palladium modifier to determine mercury in seawater.[109] The best detection limit obtained, using a pre-reduced palladium modifier and a 20 µL sample, was 1.9 ppb. Ni and Chan compared the performance of gold, platinum, and palladium modifiers; the maximum pyrolysis temperatures for mercury determination using the three modifiers were 250 °C, 300 °C, and 500 °C respectively.[106] Using the palladium modifier, the detection limit for the technique was 0.2 ng of mercury for a 100 µL sample (2.0 ppb). Bulska *et al.* also compared the effects of various noble metals as modifiers for mercury determination.[169] Palladium modifier provided a maximum pyrolysis temperature of 400 °C, and a 20-fold sensitivity increase over the use of no modifier at all. Maximum sensitivity was obtained using a gold-rhodium modifier (1.05 times that for palladium) but the maximum pyrolysis temperature for this was only 150 °C. Sensitivity for a gold modifier was only one tenth of that obtained for the palladium modifier. The best detection limit for the technique (6 µg L^{-1}) was obtained using either a gold/rhodium modifier, or an electrodeposited palladium modifier.

In this chapter, different modifiers were compared for determination of mercury by ED-ETAAS. The relevant electrodeposition parameters were optimised, and the linear working range and characteristic mass for the technique determined. The ED-ETAAS method was then compared with a cold vapour method, in which mercury vapour was collected on either $PdCl_2$ or electrodeposited Pd, prior to ETAAS determination.

6.2 EXPERIMENTAL AND RESULTS

6.2.1 ED-ETAAS Determination

In order to obtain maximum sensitivity for mercury determination, the parameters involved in the electrodeposition process were studied and optimised. Following this, the relative stabilisation and sensitivity offered by different modifiers was evaluated.

For all ED-ETAAS measurements presented in this chapter, the following experimental conditions were used (unless otherwise stated): Palladium modifier was deposited for 20 seconds from 30 µL of 10 ppm solution prepared in 0.1% HNO_3. Palladium deposits were dried at *ca.* 100 °C prior to sample deposition. Sample volumes were 20 µL. All depositions were effected using a deposition potential of 2.0 V and high-temperature deposition conditions (45 °C, inert gas on). Peak absorbances for mercury atomisation were measured at the 253.7 nm mercury resonance line.

6.2.1.1 Deposition Parameters

Effect of Deposition Time

Mercury was deposited onto a palladium-modified furnace for 10-60 seconds from a 2.7×10^{-6} M (541 ppb) solution prepared in 1% HNO_3. The sample was pyrolysed at 300 °C and atomised at 2300 °C. The results are shown in Figure 6.1.

Effect of Deposition Potential

Mercury was deposited onto a palladium-modified furnace for 40 seconds from a 4×10^{-6} M solution prepared in 1% HCl, using potentials between 0.0 and 2.0 V. The sample was re-deposited from 40 µL of 0.1% HNO_3 for 60 seconds, pyrolysed at 250 °C and atomised at 2400 °C. The results are shown in Figure 6.2.

Effect of Deposition Medium

Mercury was deposited onto a palladium-modified furnace from 2.7×10^{-6} M solutions which were prepared in several different media. The resulting mercury deposits were pyrolysed at 300 °C and atomised at 2300 °C. The experiment was repeated with a 30 second re-deposition step (35 µL of 0.1% HNO_3) for some samples. The sample deposition media and results are shown in Table 6.1.

Sample deposition medium	Mean peak absorbance (no re-deposition, n = 3)		Mean peak absorbance (30 second acid re-deposition, n = 3)	
0.5% HNO_3	0.448	RSD = 1.7%	——	——
1.0% HNO_3	0.538	RSD = 3.4%	0.369	RSD = 6.1%
1.5% HNO_3	0.542	RSD = 1.8%	——	——
0.5% H_2SO_4	0.472	RSD = 1.6%	——	——
1.0% H_2SO_4	0.534	RSD = 4.6%	0.445	RSD = 3.2%
1.0% HCl	0.076	RSD = 11.5%	0.599	RSD = 1.9%
1.5% HCl	0.039	RSD = 16.6%	——	——
0.5% $HClO_4$	0.174	RSD = 5.6%	0.271	RSD = 1.3%
1.0% $HClO_4$	0.125	RSD = 14.5%	——	——

Table 6.1. The effect of deposition medium and re-deposition for ED-ETAAS determination of mercury from 2.7×10^{-7} M solution. Mercury was deposited onto a palladium-modified furnace (with or without a 30 second re-deposition from 35 µL of 0.1% HNO_3), pyrolysed at 300 °C, and atomised at 2300 °C.

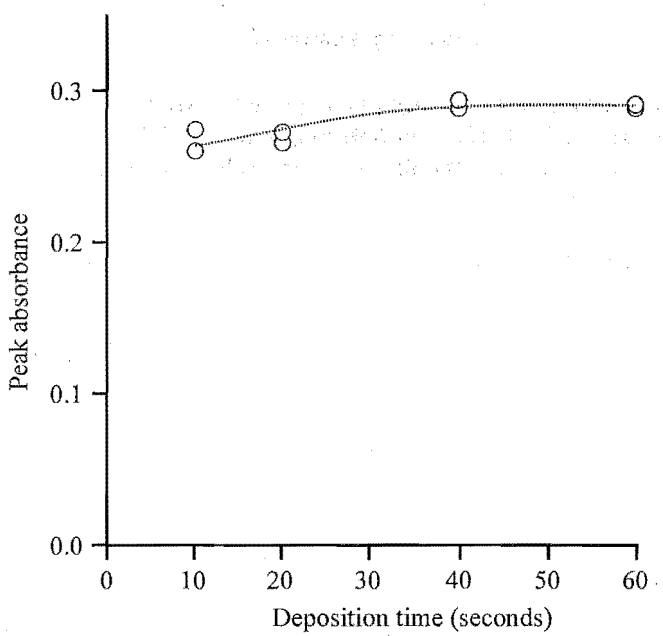

Figure 6.1 Effect of deposition time. Mercury was deposited onto a palladium-modified furnace for 10-60 seconds from a 2.7×10^{-6} M solution prepared in 1% HNO_3. The sample was pyrolysed at 300 °C and atomised at 2300 °C.

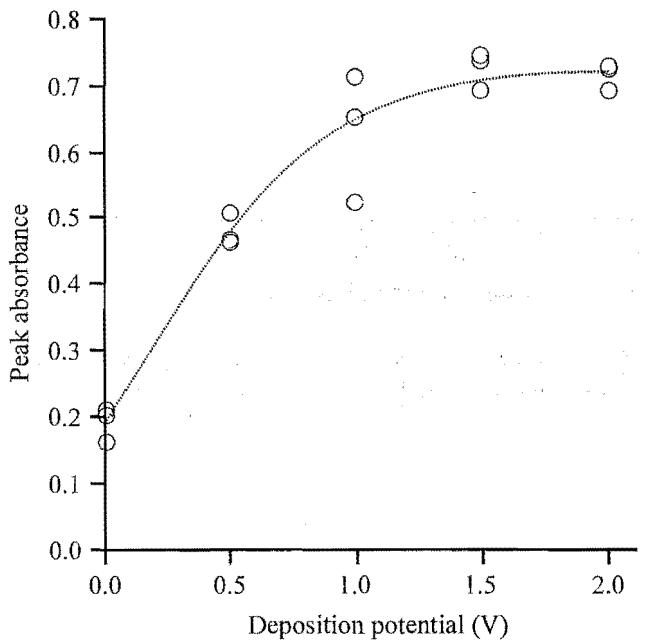

Figure 6.2 Effect of deposition potential. Mercury was deposited onto a palladium-modified furnace for 40 seconds at 0.0-2.0 V, from a 4×10^{-6} M solution prepared in 1% HCl. The sample was re-deposited from 40 µL of 0.1% HNO_3 for 60 seconds, pyrolysed at 250 °C and atomised at 2400 °C.

6.2.1.2 Method Characterisation

Thermal Stability for Mercury Deposits

The thermal stability for electrodeposited mercury was compared with that for thermally deposited mercury. Electrodeposition was effected using palladium and gold modifiers. Conventional deposition was effected using both an unmodified furnace, and with ammonium sulphide, and electrodeposited palladium modifiers. The pyrolysis curves for each experiment are shown in Figure 6.3. Because different sensitivities are obtained for each modifier, and because experiments were carried out using different mercury standards, the pyrolysis curves are presented as a percentage of the maximum mercury absorbance obtained for each experiment. (The absolute sensitivities are discussed in the subsequent section.)

The conditions used for each experiment were:

Conventionally-deposited mercury on unmodified pyrolytic graphite: 24 µL of 2.7×10^{-6} M mercury solution, prepared in 1% HNO_3, was injected into the furnace. The sample was dried at 110 °C, pyrolysed (150-350 °C), and atomised at 2300 °C.

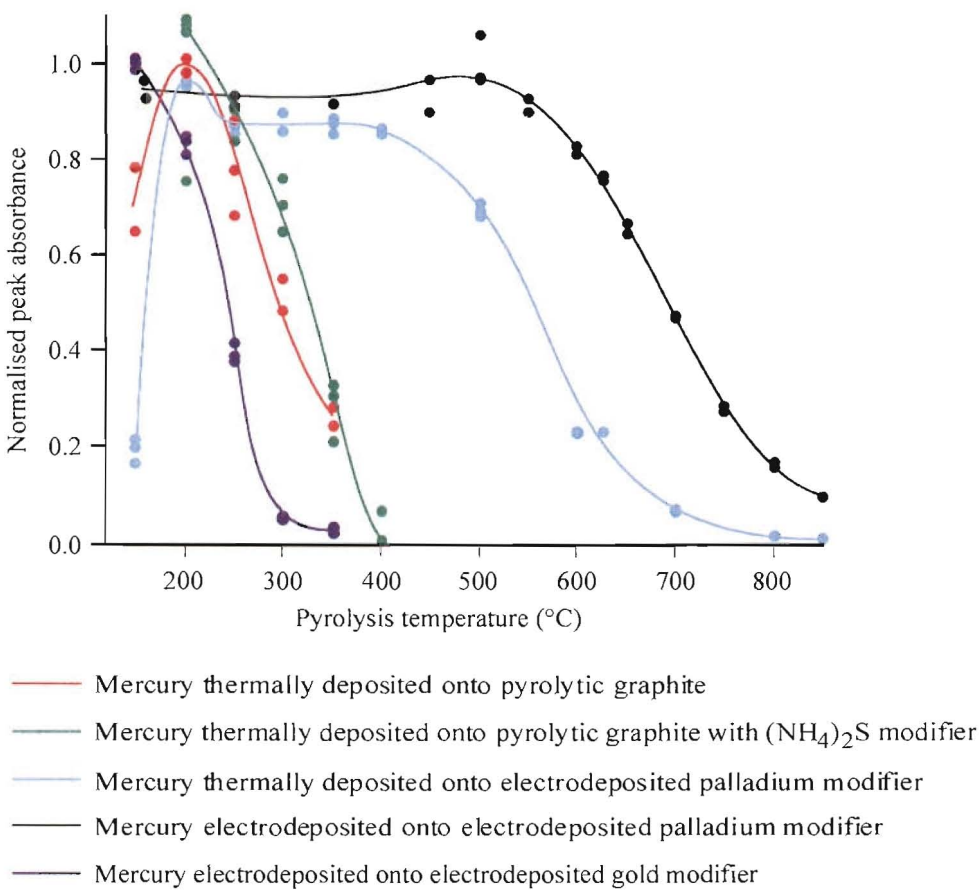

Figure 6.3 Mercury pyrolysis curves for different modifiers and deposition protocols. Peak mercury absorbances for each experiment have been normalised by setting the mean peak absorbance for the most sensitive pyrolysis temperature equal to 1.0.

Conventionally-deposited mercury with ammonium sulphide modifier: 11.3 µL of 5.3×10^{-6} M mercury solution, prepared in 1% HNO_3, and 10 µL of 2% $(NH_4)_2S$ solution were injected into the furnace. The sample was dried at 110 °C, pyrolysed (150-400 °C), and atomised at 2300 °C.

Conventionally-deposited mercury on electrodeposited palladium modifier: 20 µL of 4×10^{-6} M mercury solution, prepared in 1% HCl, was injected into a palladium-modified furnace. The sample was dried at 100 °C, pyrolysed (150-820 °C), and atomised at 2400 °C.

Electrodeposited mercury on electrodeposited palladium: 24 µL of 2.7×10^{-6} M mercury solution, prepared in 1% HNO_3, was electrolysed for 60 seconds in a palladium-modified furnace. The sample was dried at 135 °C, pyrolysed (160-850 °C), and atomised at 2300 °C.

Electrodeposited mercury on electrodeposited gold modifier: The furnace was modified by electrolysing 30 µL of 10 ppm gold solution, prepared in 0.075% HCl/0.025% HNO_3, for 20 seconds. Mercury was then electrodeposited for 60 seconds from 20 µL of 4×10^{-6} M solution (prepared in 0.1% HNO_3). The deposit was dried at 110 °C, pyrolysed (150-350 °C), and atomised at 2400 °C.

Comparison of Modifiers for Mercury Determination

The relative sensitivities for mercury determination using different modifiers and deposition protocols were inferred from the blank-corrected absorbances for standard mercury solutions as analysed using the different protocols. The protocols compared were: thermally deposited mercury with ammonium sulphide modifier, electrodeposited mercury on electrodeposited gold modifier, and electrodeposited mercury on electrodeposited palladium modifier.

For the thermal determination of mercury with ammonium sulphide modifier, 20 µL of 4×10^{-6} M mercury solution (prepared in 1% HCl) and 10 µL of ammonium sulphide solution were placed in the furnace, dried, pyrolysed at 150 °C, and atomised at 2400 °C. The experiment was performed using two different concentrations of ammonium sulphide solution—2% and 40% (w/v). The results for this experiment were compared with those for 20 µL of the same mercury solution electrolysed in a palladium-modified furnace for 40 seconds at 2.0 V. The deposit was re-deposited from 40 µL of 0.1% HNO_3, pyrolysed at 200 °C, and atomised at 2400 °C. The relative absorbances obtained for the two protocols are shown in Table 6.2.

In a second experiment, gold and palladium modifiers were electrodeposited onto the furnace from 35 µL of 10 ppm solutions as described in the section on thermal stability. Mercury was then electrodeposited using the same protocol as for the previous experiment. The relative absorbances obtained for the two protocols are shown in Table 6.2.

Method of analysis	Normalised mean peak absorbance (n=4)	RSD
ETAAS: 2% $(NH_4)_2S$ modifier	0.37	13.2%
ETAAS: 40% $(NH_4)_2S$ modifier	0.39	13.8%
ED-ETAAS: palladium modifier	1.00	3.9%
ED-ETAAS: gold modifier	0.91	1.2%

Table 6.2 Relative peak absorbance for determination of mercury (*ca.* 8×10^{-11} g) by conventional ETAAS (with ammonium sulphide modifier) and by ED-ETAAS (with electrodeposited palladium and gold modifiers). Mercury was determined from 20 µL of 4×10^{-6} M solution, prepared in 1% HCl.

Characteristic Mass

The characteristic mass for mercury determination by ED-ETAAS with palladium modifier was determined using replicate blank-corrected measurements of a 4×10^{-6} M mercury solution prepared in 1% HCl. The mercury was deposited from calibrated volumes (21.3 µL) onto electrodeposited palladium, for 40 seconds. The sample was then re-deposited for 30 seconds from 30 µL of 0.1% HNO_3. The blank-corrected mean peak absorbance for four replicate measurements was 0.828 (RSD=8.8%). This corresponds to a characteristic mass of 91 pg.

Linear Working Range

To establish the linear working range for mercury determination by ED-ETAAS, a calibration curve was prepared. Mercury was deposited onto a palladium-modified furnace from standard solutions, prepared in 1.5% HCl, in the range 0.0 - 7.2 µM. The mercury deposits were re-deposited from 0.1% HNO_3, dried, pyrolysed at 250 °C, and atomised at 2400 °C. The blank-corrected results are shown in Figure 6.4. The detection limit for the technique was not formally determined. However, an estimate based on five replicate measurements of the blank (for the calibration curve in Figure 6.4) indicates a detection limit of *ca.* 9×10^{-8} M (18 ppb).

6.2.2 Cold Vapour Determination

A cold-vapour mercury analysis protocol was developed, in which elemental mercury was accumulated on a palladium-modified furnace prior to ETAAS determination (CV-ETAAS). This method is an adaptation of previously reported palladium-based techniques.[132,135] The objects of the work were to compare CV-ETAAS with ED-ETAAS, and to compare the collection efficiency for the electrodeposited modifier with that for the palladium chloride modifier (as recommended by Yan and Ni[135]).

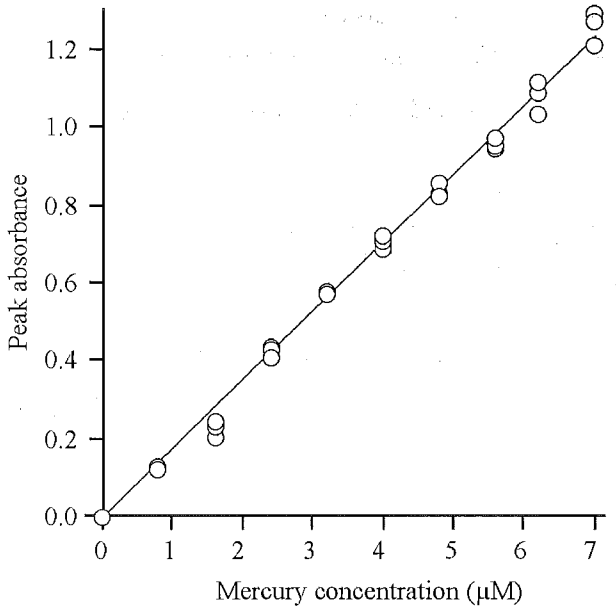

Figure 6.4 Calibration curve for mercury determination by ED-ETAAS. Mercury was deposited from 20 μL of 1.5% HCl solution onto a palladium modified furnace and redeposited from 40 μL of 0.1% HNO_3. A pyrolysis temperature of 250 °C and an atomisation temperature of 1400 °C were employed.

Mercury vapour was produced using the HG3000 hydride generator (a schematic diagram of this apparatus is shown in Figure 2.4). The reductant used was 0.3% (w/v) $NaBH_4$ prepared in 0.3% (w/v) NaOH solution. This was freshly prepared each day. A 14% (v/v) HCl solution was used to control the pH. The HG3000 used a flow-rate of 8.4 mL of sample per minute. Mercury vapour produced by the HG3000 was passed into a heated furnace (200 °C) which had been pre-modified with palladium. The vapour was collected for sixty seconds. To compensate for the time taken by the mercury vapour to pass through the length of the sample introduction tube, the HG3000 was started 60 seconds prior to the start of vapour collection.

A typical furnace temperature program for the cold vapour analysis is given in Table 2.4. The collection temperature was 200 °C, the atomisation temperature was 2400 °C.

6.2.2.1 Comparison of Modifiers for CV-ETAAS

Two different forms of palladium modifier were used for mercury vapour collection: electrodeposited metal, and dried (non-reduced) palladium chloride. The electrodeposited palladium surface was prepared by electrolysing 35 μL of 10 ppm palladium solution, prepared in 0.1% HNO_3, for 20 seconds. The palladium chloride modifier was prepared by drying 40 μL of 500 ppm palladium solution, prepared in 7% HCl, onto the surface of the furnace at 200 °C.

The electro-reduced palladium modifier was compared with the palladium chloride modifier using the absorbance obtained for 84 ng mercury prepared in 2% HNO_3. The mean peak absorbances for replicate measurements are shown in Table 6.3.

	Mean peak mercury absorbance using palladium chloride modifier (n = 5)		Mean peak mercury absorbance using electrodeposited palladium modifier (n = 5)	
Blank	0.108	RSD = 8.1%	0.135	RSD = 9.1%
Sample	0.269	RSD = 3.4%	0.386	RSD = 2.5%
Sample (blank-corrected)	0.161	RSD = 8.8%	0.251	RSD = 9.4%

Table 6.3 Relative sensitivity for mercury determination by CV-ETAAS, using electro-reduced palladium and palladium chloride modifiers. Mercury vapour was produced from an 84 ng sample which was prepared in 2% HNO_3. The vapour was collected on the modified furnace for 60 seconds at 200 °C.

6.2.2.2 Sensitivity

The sensitivity for mercury determination by CV-ETAAS on a palladium-modified furnace was calculated from the calibration curve shown in Figure 6.5. Mercury standards in the range 0.00 to 0.15 µM were analysed using a 60 second collection time (8.4 mL of sample per analysis). This sampling method corresponds to determination of 0.0 to 250 ng of mercury. The blank corrected data are plotted in Figure 6.5. The mean peak absorbance for the blank (n=5) was 0.136 with an RSD of 9.0%.

The characteristic mass for the CV-ETAAS method was calculated from the slope of the calibration curve (Figure 6.5). The slope (0.38 µg abs^{-1}) corresponds to a characteristic mass of 1.7 ng.

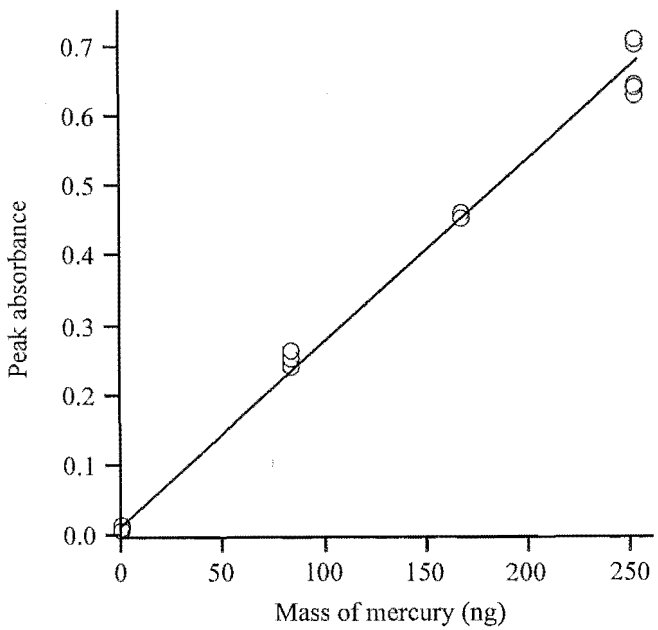

Figure 6.5 Calibration curve for CV-ETAAS determination of mercury using an electrodeposited palladium modifier. Mercury vapour was produced from standards in the range 0.00 to 0.15 µM, which were prepared in 2% HNO_3. The vapour was collected for a period of 60 seconds at a temperature of 200 °C.

The detection limit for the technique was not formally determined. However, an estimate based on five replicate measurements of the blank indicated a detection limit of *ca.* 14 ng. The practical limitation on the detection limit was the size of the reagent blank. A 60 second vapour accumulation produced a reagent blank of *ca.* 0.1 abs, which was attributed to impurities in the sodium borohydride reductant. Because the size of the blank was proportional to the accumulation time, extended accumulation times were not used. Accordingly, a detection limit based on a practical accumulation time was determined. For a sixty second accumulation time (8.4 mL of sample used), the 14 ng detection limit corresponds to a concentration detection limit of 8.4×10^{-9} M (1.7 ppb).

6.3 DISCUSSION

6.3.1 ED-ETAAS Determination

6.3.1.1 Deposition Parameters

Figure 6.1 shows the effect of deposition time on the peak absorbance for mercury determination. A deposition time of 40 seconds gave good precision and maximum sensitivity. Therefore this was used for all further work.

The effect of the deposition potential is shown in Figure 6.2. Increasing the potential in the range 0.0 to 1.5 V produced higher mercury absorbances, but further increasing the potential from 1.5 to 2.0 V did not bring about any additional improvement. Hence, the optimum deposition potential chosen for mercury determination was the same as that used for the previously determined metals: 2.0 V.

The effect of the deposition medium on the peak mercury absorbance is shown in Table 6.1. Deposition from HNO_3 and H_2SO_4 media both provided good sensitivity. The peak absorbances observed for these two acids were similar. For both, sensitivity was decreased when a 30 seconds re-deposition from 0.1% HNO_3 was included in the analysis protocol. The reason for this is unclear, but in hindsight, it may have been caused by an insufficient re-deposition time. The re-deposition time of 30 seconds was chosen based on the deposition time curve shown in Figure 6.1 and the re-deposition time curve for lead, shown in Figure 4.3. However, for both of these curves, the sample matrix/re-deposition medium was 1.0% HNO_3. If the deposition kinetics for 0.1% HNO_3 are slower, then the 30 second deposition time may have been insufficient to re-deposit mercury that, on withdrawal of the probe/anode, dissolved in residual sample medium. If this was the case, possible remedies include using a more concentrated (1.0%) re-deposition solution, and/or using a longer re-deposition time (60 seconds). At the time however, this matter was not further investigated.

Sensitivity for deposition from $HClO_4$ was poor; *ca.* 30% of that from the HNO_3 medium. Whether this was due to poor deposition efficiency or to loss of mercury during pyrolysis is not known. When a re-deposition step from 1% HNO_3 was included, the peak absorbance for

mercury deposited from $HClO_4$ increased, but not to the level observed for the other acids. This indicates that the low absorbances for $HClO_4$ media were a combination of poor deposition and pyrolysis losses.

The effect of HCl, as a deposition medium for mercury determination, was similar to that for cadmium determination (Table 4.5). Poor sensitivity was observed for samples deposited from HCl and analysed without a re-deposition step. However, when a re-deposition step (0.1% HNO_3) was included, sensitivity was markedly increased. A likely explanation for this is that residual HCl is diluted by, and largely removed from the furnace with the HNO_3 re-deposition medium; this removal of residual chloride preventing subsequent low temperature formation (and loss) of volatile mercury chlorides.

The 1% HCl deposition/0.1% HNO_3 re-deposition protocol gave higher peak mercury absorbances than were obtained for either HNO_3 or H_2SO_4 deposition media. Consequently, this protocol was used for all further work.

6.3.1.2 Method Characterisation

Figure 6.3 shows the relative thermal stabilities for mercury deposited using different deposition protocols and modifiers. The highest degree of stabilisation was achieved by electrodepositing the mercury onto electrodeposited palladium. The maximum pyrolysis temperature was 500 °C; an increase of 100 °C over the next most stable deposit—thermally deposited mercury on electrodeposited palladium. The apparent maximum pyrolysis temperature for thermally deposited mercury (200 °C) was unchanged by the addition of ammonium sulphide modifier. However, the sensitivity was greatly enhanced—the peak absorbance was *ca.* five times larger in the presence of the ammonium sulphide modifier.

The gold modifier decreased the thermal stability relative to that for thermally deposited mercury on unmodified pyrolytic graphite. However, the sensitivity was improved more than twofold. This is shown in Table 6.2, which compares the relative peak absorbances for electrodeposition onto gold and palladium modifiers, and for thermal deposition using ammonium sulphide modifier. The maximum sensitivity observed was for electrodeposited mercury on electrodeposited palladium. The decreased sensitivity for thermally deposited mercury with ammonium sulphide modifier could be explained either by low temperature volatilisation losses, or by differing atomisation kinetics. Further investigation would require examining the integrated absorbances under isothermal atomisation conditions.

The characteristic mass for mercury determination using the ED-ETAAS protocol with palladium modifier (91 pg) compares favourably with the theoretical value of 69 pg calculated by L'vov[204] and with experimental values obtained by other workers. Bulska *et al.*[205] and Shan and Wen[36] reported a characteristic masses of 110 pg for mercury determination using palladium modifiers. Welz *et al.*[108] reported a characteristic mass of 97 pg for mercury determination using a mixed palladium-magnesium nitrate modifier. Considerably lower values (33.1-

70.5 pg) were reported by Bermejo-Barrera *et al.*[109] who used various palladium-based modifiers for direct mercury determination, and by Lee *et al.*[167] (20 pg) who used a gold modifier to collect mercury vapour. However, such low values are the exception rather than the norm for mercury determination.

The linear working range for mercury determination by ED-ETAAS with palladium modifier is inferred from the calibration plot shown in Figure 6.4. This extends from 0.45 μM (the limit of determination) to 7.0 μM (0.09 ppm to 1.4 ppm). This working range could be extended by altering the sample volume within the range 10-35 μL. (The sample volume used in this work was 20 μL.)

6.3.2 CV-ETAAS Determination

The primary aims of this section of work were: to compare the collection efficiency for electrodeposited palladium modifier with that for the palladium chloride modifier recommended by Yan and Ni,[135] and to compare the detection limits for CV-ETAAS with those for ED-ETAAS. Table 6.3 shows that the sensitivity obtained using the electrodeposited palladium was greater than that obtained with palladium chloride. The apparent disagreement with the results of Yan and Ni is probably caused by both the different surface coverages/ morphologies, and different collection efficiencies for electro-reduced, and thermally-reduced palladium modifiers (see Section 3.1.4). Thus, while palladium chloride may be superior to thermally reduced palladium as a modifier for mercury vapour accumulation, it is surpassed by electro-reduced palladium.

The characteristic mass calculated for the method (1.7 ng) shows that the technique is far less sensitive than ED-ETAAS. This is probably due to inefficient production and transport of mercury vapour from the sample solution. The HG3000 (Figure 2.4) uses a flow-injection method with a short reaction time to produce mercury vapour. Because of this, the amount of mercury vapour produced is very dependent on reaction kinetics. If mercury in the sample solution has not been quantitatively reduced by the time the reaction mixture reaches the gas-liquid separator, unreacted mercury is "lost". Further, the HG3000 does not drive mercury vapour from solution with a purge gas. The argon flow serves only to transport gaseous mercury from the gas-liquid separator through the delivery tube. Mercury vapour is carried out of the reduction mixture and into the argon stream along with hydrogen. Hence, further losses occur as non-volatilised elemental mercury is pumped to waste along with the reaction mixture. It is also possible that "capture" of the mercury vapour on the palladium surface is not 100% efficient, but this is difficult to test in practice.

Inefficient production and collection of mercury vapour is not an insurmountable problem provided that the sample volume is sufficient to permit extended vapour production/ collection. Thus, although the sensitivity for CV-ETAAS, as defined by the characteristic mass, is only one twentieth of that for ED-ETAAS, the detection limit is a factor of ten lower. This

apparent contradiction is a consequence of the relative sample sizes for the two techniques: *ca.* 20 µL for ED-ETAAS versus *ca.* 8.4 mL (per minute) for CV-ETAAS.

The detection limit for the CV-ETAAS technique can theoretically be lowered further by extending the sample collection time. However, in practice this is prevented by the size of the reagent blank. For a 60 second collection time, the peak absorbance for the reagent blank was *ca.* 0.1. This was largely attributable to impurities in the sodium borohydride reductant. Changing to a more pure grade of borohydride, or to the more commonly used stannous chloride, would undoubtedly decrease the size of the reagent blank and afford lower detection limits. Unfortunately, neither of these reagents was available during the course of this work.

The linear working range for the CV-ETAAS technique (as used), was from the limit of determination (42 nM) to 0.15 µM. This could be extended through the use of more pure reagents and, if necessary, sample dilution.

During the course of this research, the opportunity did not arise to test either protocol (ED-ETAAS or CV-ETAAS) with organo-mercury compounds. It is known that methylmercury compounds are not reduced by sodium borohydride unless some form of sample pre-treatment is used.[206,196] However, both organic and inorganic mercury are reduced by stannous chloride. Therefore, the relative proportions of organic and inorganic mercury in a sample can be determined by difference using CV-ETAAS and a selective reduction process, achieved through the choice of reductant.[202] Total mercury is determined using stannous chloride reduction, whereas inorganic mercury is determined by borohydride reduction.

Determination of organomercury compounds by ED-ETAAS would require their direct reduction on the palladium modified furnace surface. Frick and Tallman found that a deposition potential of -1.0 V (vs. Ag/AgCl) did not effect efficient reduction of organomercury compounds on a pyrolytic graphite electrode.[64] Therefore, unless palladium catalyses the reduction, it is unlikely that organomercury compounds can be directly determined using ED-ETAAS. However, it should be possible to quantify organic and inorganic mercury by difference. Inorganic mercury can be determined directly by ED-ETAAS. Total mercury could be determined following a pre-treatment step which converts organic to inorganic mercury.

Chapter Seven

Metal Speciation

This chapter introduces the concept of metal speciation, and discusses some of the methods used to measure it. The experimental sections are devoted to metal speciation analysis by ED-ETAAS, using the electrodeposition step to differentiate between "free" and EDTA-bound metal. The metals investigated were bismuth, lead, copper and nickel. Studies were carried out using buffered solutions.

7.1 INTRODUCTION

Elements in a system such as a natural water can be present in many chemical forms or species. Examples of different species include various oxidation states of a transition metal and different complexes of a soluble ion. Speciation analysis of metals is concerned with differentiating between the individual species which make up the total element concentration. This differentiation is important because different species can exhibit varying levels of toxicity in an environmental system. Often, it is the simple aqua ion which shows greatest toxicity. The availability of this metal ion is a function of the stability and lability of the metal complexes. Strong complexation can decrease the availability of toxic metal ions, thus ameliorating their effects. For example, the toxicity of the Al^{3+} ion towards plants is markedly decreased in the presence of high concentrations of organic ligands.[207] Hence, metal speciation and its determination play an important part in understanding metal toxicities in natural systems. In particular, analysts are designing methods to differentiate between the very labile ("free"), and less labile or inert fractions of an element.

Such metal speciation studies can be readily carried out using ASV, which can differentiate between free, moderately labile, and, with sample pretreatment, inert metal species. ASV has the advantages of high sensitivity, ready analysis of high salt matrices such as seawater, and the simultaneous determination of up to four elements. However, it has a much lower sample throughput than conventional ETAAS, and for many sample matrices, relies on time-consuming standard addition calibration; a minimum sample volume of *ca.* 5.0 mL is usually required. ASV is limited to amalgam-forming metals that can be reduced at potentials positive of *ca.* -1.2 V (vs SCE) and reversibly oxidised at potentials negative of the mercury oxidation potential (*ca.* 0.45 V vs SCE). This eliminates the determination of such elements as:

i) Manganese and iron and aluminium, which have reduction potentials negative of -1.2 V.
ii) Cobalt, which has limited solubility in mercury.
iii) Nickel, manganese, chromium and cobalt, which are not oxidised reversibly from mercury.
iv) Platinum, palladium, silver and gold, which are oxidised at potentials positive of the mercury oxidation potential.

In contrast, ETAAS has high sample throughput, and is not restricted by the reduction potentials of analytes. However, conventional ETAAS is capable only of measuring the total metal concentration. Thus to date, ETAAS has received limited application in the field of speciation, except as a post-fractionation technique. Das and Chakraborty[208] reviewed the literature from 1980-1994, and found that in most of the published studies, individual species were separated in a prior treatment by ion exchange, solvent extraction, or chromatographic methods. Conventional ETAAS was then used to determine the total elemental concentration in the resulting fractionated solutions. Unfortunately, the two-step nature of these methods makes them relatively complex. This can contribute to decreased sample throughput, decreased precision, and increased likelihood of introducing contaminants to the sample.

Some attempts have also been made to measure speciation by ETAAS using *ex-situ* electrodeposition. (These studies are described in Section 1.5.2.) Analytes were deposited onto electrodes which were then transferred to an ETAAS instrument for quantitation. However, such techniques are relatively awkward and suffer from the same drawbacks as the hyphenated chromatographic-type methods— they are slow, and difficult to automate.

The electrodeposition step of the ED-ETAAS technique provides scope for differentiating between "free" and inert species. The operational simplicity of this automated technique is a vast improvement over the involved nature of many of the other hyphenated methods, and the *in situ* deposition does not provide the opportunity for sample contamination. Further, ED-ETAAS suffers few of the disadvantages of ASV. The available voltage window is not limited by mercury oxidation or water reduction, and analytes need not be capable of amalgam formation.

The work described in this chapter explores the possibility of effecting metal species fractionation using ED-ETAAS. The aim was to differentiate between free and EDTA-bound metal using the principle that the reduction potential of a metal is affected by complexation reactions.[209] The difference between the standard reduction potentials of the metal, and an inert metal ligand complex can be described by a relationship derived from the Nernst equation:[210]

$$\Delta E_{\frac{1}{2}} = E_{\frac{1}{2}(\text{complex})} - E_{\frac{1}{2}(\text{free metal})} = -k \log \alpha_{ML} \qquad \text{(Equation 7.1)}$$

where k = 2.3 RT/nF; R is the gas constant, T is the absolute temperature and F is the Faraday constant. For a one electron reduction at 25 °C, k = 59 mV, and for a two electron reduction, k is approximately 30 mV. The α coefficient for complexation of the metal by ligand 'L' is defined by:

$$\alpha_{ML} = K'_{ML}[L'] + 1 \qquad \text{(Equation 7.2)}$$

where [L′] is the concentration of L not complexed by the metal, and K′ is the conditional stability constant for the formation of ML.

Thus, it was predicted that shifts in the reduction potential due to complexation, would provide the key to fractionation of metal species by ED-ETAAS. The objective was to discriminate between complexed and non-complexed metal ions through the use of selective reduction potentials— a negative overpotential to reduce both complexed and non-complexed metal, and a less negative potential to reduce only the non-complexed metal. This approach was tested using the EDTA complexes of four metals; bismuth, lead copper, and nickel.

7.2 EXPERIMENTAL AND RESULTS

7.2.1 Bismuth

For ED-ETAAS experiments, the following conditions were used: Palladium was deposited using a 30 second electrolysis of 30 µL of 10 ppm solution prepared in 0.1% HNO_3. Bismuth samples were deposited from 20 µL of solution for 60 seconds. The bismuth deposit was rinsed with 40 µL of water for 5.0 seconds, dried, pyrolysed at 1100 °C, and atomised at 2300 °C. The absorbance was measured at the 306.8 nm resonance line. Electrodeposition was effected at room temperature (to minimise complex labilisation), but with the inert gas switched on (to effect convectional stirring). The deposition potentials used are given for each experiment.

The bismuth standards used in this section were 9.6×10^{-7} M (200 ppb) bismuth with varied concentrations of EDTA (0.0 to 1.9×10^{-6} M), prepared in 0.04 M NaCl/0.01% HNO_3. Because of the relatively low lability of the bismuth-EDTA complex,[211] the standards were heated to boiling in a water bath for 30 minutes, and allowed to equilibrate overnight prior to analysis. Speciation modelling using Solgaswater[102] suggested that under these conditions, bismuth would be quantitatively complexed by EDTA.

7.2.1.1 Effect of Deposition Potential

The effect of the deposition potential was examined for two of the bismuth solutions. One containing 9.6×10^{-7} M bismuth and no EDTA ('free bismuth'), and another containing the same concentration of bismuth and 1.92×10^{-6} M EDTA ('EDTA-complexed bismuth'). These two solutions were analysed by ED-ETAAS using a range of deposition potentials. The peak absorbances are plotted against the deposition potential in Figure 7.1.

7.2.1.2 Deposition Potential Calibration

ED-ETAAS experiments are performed using uncontrolled deposition potentials, thus the actual potentials on the cathode and anode during the electrolysis are not precisely known. The actual electrode potentials during electrolysis of a 9.6×10^{-7} M bismuth solution were determined in separate experiments, using the furnace simulation apparatus and protocol described in Section 2.3.2. The results are shown in Figure 7.2.

7.2.1.3 Speciation; Comparison of ED-ETAAS and ASV

It was established from Figure 7.1 that free Bi^{3+} is reduced at an applied potential of *ca.* 0.8 V while bismuth in the Bi-EDTA complex is not. Therefore a deposition potential of 0.8 V should allow discrimination between free and EDTA-bound bismuth. This hypothesis was tested by measuring free bismuth in a series of pre-equilibrated solutions that contained varying concentrations of EDTA (prepared as described in Section 7.2.1). The experiment was carried out at two temperatures, 25 °C and 45 °C, in order to determine any temperature dependence of the technique. The same solutions were also analysed by ASV, using parameters as given in Section 2.3.1. Bismuth was deposited at -0.45 V (vs. Ag/AgCl) for five minutes, and stripped to +0.10 V. The stripping current was measured at *ca.* -0.154 V vs. Ag/AgCl. The results of the ED-ETAAS and ASV experiments are compared in Figures 7.3a and 7.3b.

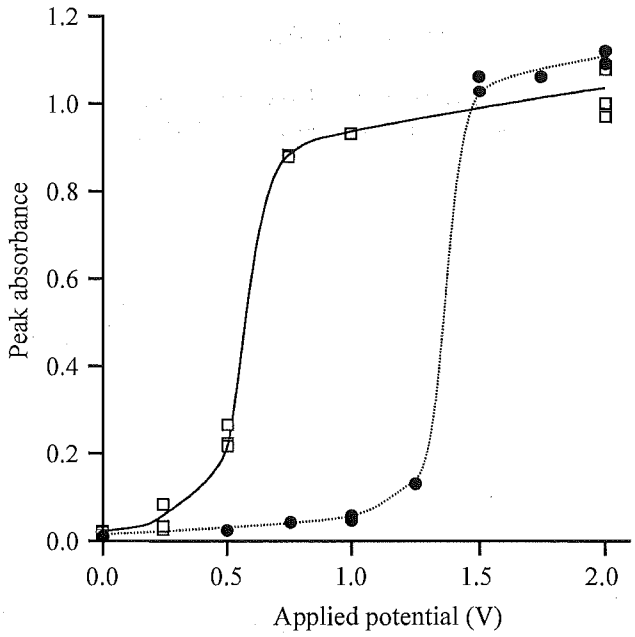

Figure 7.1 The effect of deposition potential on absorbance for 'free' bismuth (□) and EDTA-complexed bismuth (●) Bismuth was deposited onto a palladium modified furnace for 60 seconds from 20 µL samples, which contained 9.6×10^{-7} M bismuth in 0.04 M NaCl/0.01 M HNO_3, with and without 1.92×10^{-6} M EDTA. The deposition potential was varied from 0.0 to -2.0 V.

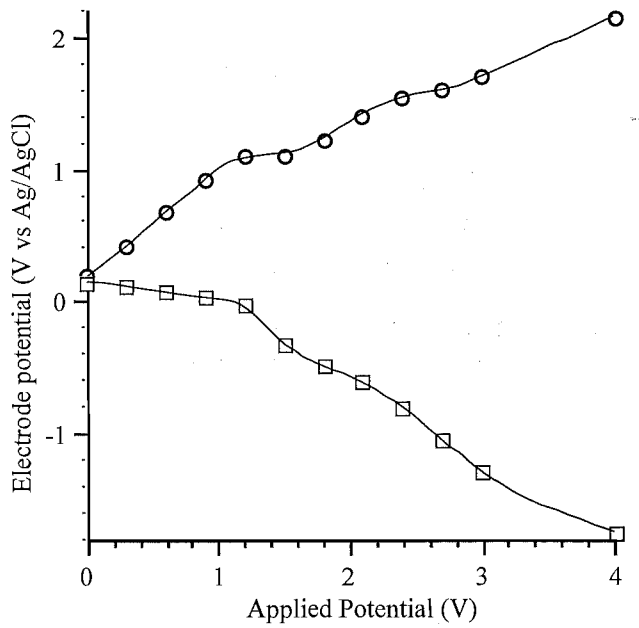

Figure 7.2 Electrode potential calibration for bismuth electrodeposition. Potentials measured between the Ag/AgCl reference electrode, and the cathode (□) and anode (○) during deposition of 9.6×10^{-7} M bismuth prepared in 0.04 M NaCl/0.01% HNO_3.

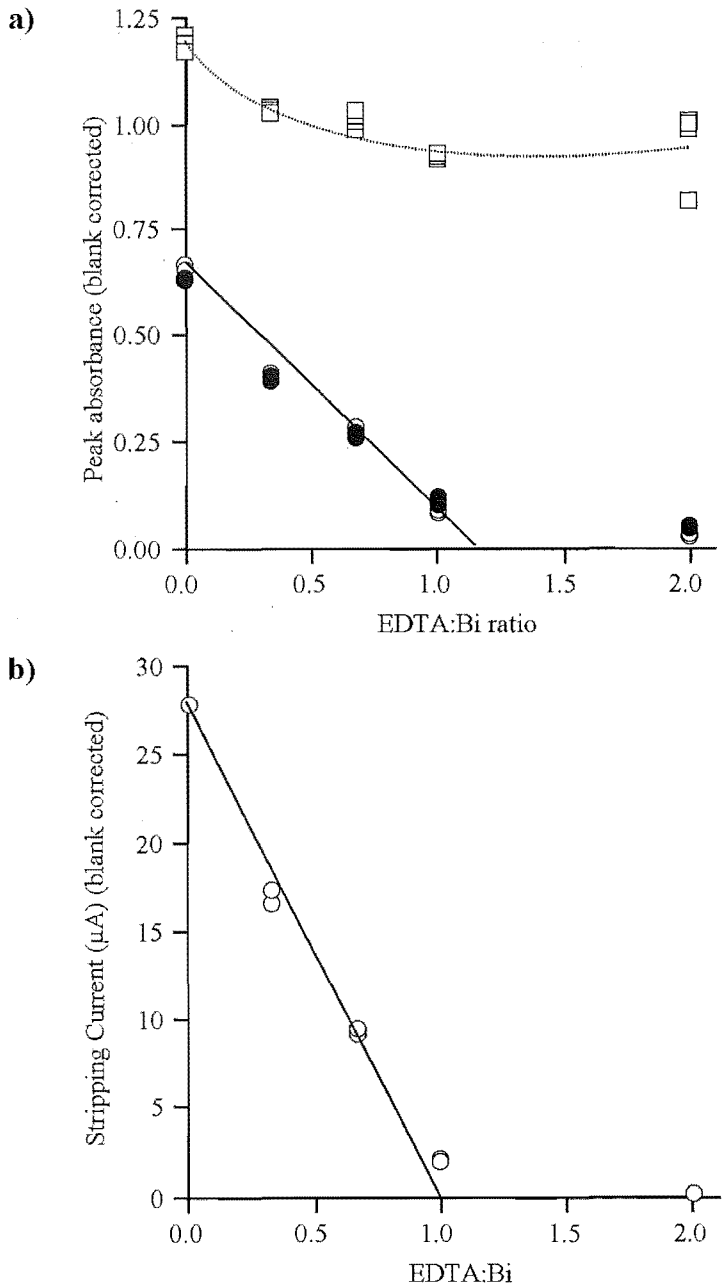

Figure 7.3 Effect of EDTA:bismuth ratio on ED-ETAAS peak absorbance **(a)**, and SW-ASV stripping current **(b)** for solutions containing 9.6×10^{-7} M bismuth prepared in 0.04 M NaCl/0.01% HNO_3. For ED-ETAAS experiments, sample solutions were deposited onto a palladium modified furnace at 25 °C/0.8 V (●), 25 °C/0.6 V (○), and 45 °C/0.6 V (□).

7.2.2 Lead

The deposition medium for lead speciation studies had to fulfil several criteria. It had to provide buffering at a pH that allowed stoichiometric binding of lead and EDTA (pH *ca.* 4.5), and the conjugate base of the buffer had to be non-complexing so that it did not compete with the EDTA. Further, the medium had to have sufficient ionic strength to provide conductivity for electrolysis to occur at a significant rate.

The simplest buffer system available at pH 4.5 was acetic acid/acetate. The speciation of the lead-EDTA system in acetate buffer was modelled using Solgaswater.[102] For a 3×10^{-7} M lead solution prepared in 0.1 M acetate, the model indicated that only 7% of the lead was present as the Pb^{2+}-aqua ion; the rest being present as acetate species. Accordingly, acetate concentrations were kept to the minimum level that provided sufficient buffering. Problems of low electrolyte conductivity at the lower acetate concentrations were countered by adding 0.01 M KNO_3 to increase the ionic strength.

7.2.2.1 Effect of Deposition Potential

The effect of the deposition potential was examined for 3×10^{-7} M lead solutions in the presence and absence of EDTA. Initial investigations failed to locate a potential at which the free lead could be selectively reduced in the presence of EDTA-bound lead. This problem was attributed to the EDTA-lead complex adsorbing onto the palladium modifier, thus giving rise to a lead absorbance irrespective of the deposition potential. To avoid this problem, subsequent experiments were carried out in the absence of palladium modifier.

Two lead solutions (2.25×10^{-6} M), one containing 3×10^{-6} M EDTA, were prepared in 0.001 M acetate/0.01 M potassium nitrate at pH 4.5. 20 µL sample aliquots were electrolysed in an unmodified furnace for 90 seconds using a range of deposition potentials (0.0 to 2.4 V). The deposits were then rinsed with 35 µL of water for 5.0 seconds. Electrodeposition was effected at room temperature, with the inert gas flow switched on. Samples were pyrolysed at 700 °C and atomised at 2350 °C. A plot of the deposition potential versus the lead absorbance is shown in Figure 7.4.

7.2.2.2 Deposition Potential Calibration

The cathode and anode potentials during electrolysis of a 2.4×10^{-8} M lead solution (prepared in 0.1 M acetate/0.1 M NaCl at pH 4.7*) were determined using the furnace simulation apparatus and protocol described in Section 2.3.2. The results are shown in Figure 7.5.

---

* This experiment was carried out prior to the modelling experiments which determined that lower concentrations of acetate were desirable for lead speciation experiments.

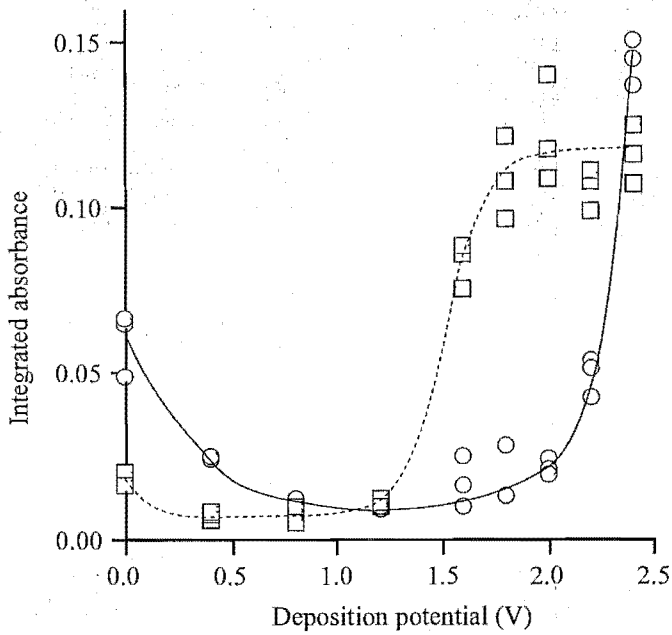

Figure 7.4 Effect of deposition potential on lead absorbance for a 90 second deposition from 20 µL of 2.25×10^{-6} M lead solution in the presence (○), and absence (□) of 3×10^{-6} M EDTA. Samples were prepared in 0.001 M acetate/0.01 M potassium nitrate at pH 4.5. Electrodeposition was effected at room temperature, with the inert gas flow switched on. Samples were pyrolysed at 700 °C and atomised at 2350 °C.

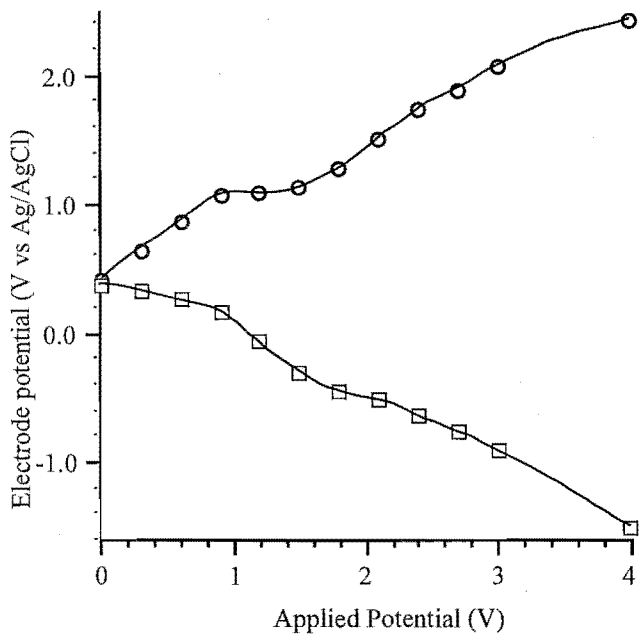

Figure 7.5 Calibration of electrode potentials for lead electrodeposition. Potentials were measured in a palladium-modified furnace, between the Ag/AgCl reference electrode, and the cathode (□) and anode (○). The solution used for the electrolysis was 2.4×10^{-8} M lead prepared in 0.1 M acetate/0.1 M NaCl at pH 4.7.

7.2.2.3 ED-ETAAS Speciation: Effect of Deposition Time

It was established from Figure 7.5 that free Pb^{2+} is reduced at an applied potential of *ca.* 1.9 V with minimal reduction of the Pb-EDTA complex. This deposition potential was used to measure free lead in the presence of varying amounts of EDTA. To establish whether species within the sample re-equilibrate significantly during electrolysis, the experiment was performed twice, using different deposition times.

A series of lead standards (6.0×10^{-7} M) containing varying amounts of EDTA (0.0 to 7.5×10^{-7} M) was prepared in 0.001 M acetate/0.01 M potassium nitrate at pH 4.5. 20 µL aliquots were electrolysed in an unmodified furnace at an applied potential of 1.9 V. Two different deposition times were used: 10 seconds and 60 seconds. The lead deposits were rinsed twice with 35 µL of water for 10 seconds, and then re-deposited from 35 µL of 0.01 M HNO_3 for 30 seconds. Samples were pyrolysed at 700 °C and atomised at 2350 °C. The lead absorbance was measured at 283.3 nm. The results are shown in Figure 7.6.

As a comparison, the effect of the EDTA:lead ratio was examined using ASV. A series of lead standards (3.0×10^{-7} M) containing varying amounts of EDTA (0.0 to 3.0×10^{-7} M) was prepared in 0.001 M acetate/0.01 M potassium nitrate at pH 4.5. Samples were analysed using the protocol described in Section 2.3.1. Lead was deposited at -0.60 V for five minutes, and stripped to -0.10 V. The stripping current was measured at *ca.* -0.41 V vs Ag/AgCl. The experiment was performed twice; once using a 'fast' stirring speed during sample deposition, and once using a quiescent deposition step. The resulting stripping currents for the two experiments differed by an order of magnitude because of the different stirring rates used. Hence, to permit ready comparison, the results shown in Figure 7.7 are displayed as percentages of the mean stripping current obtained for the solution that contained no EDTA.

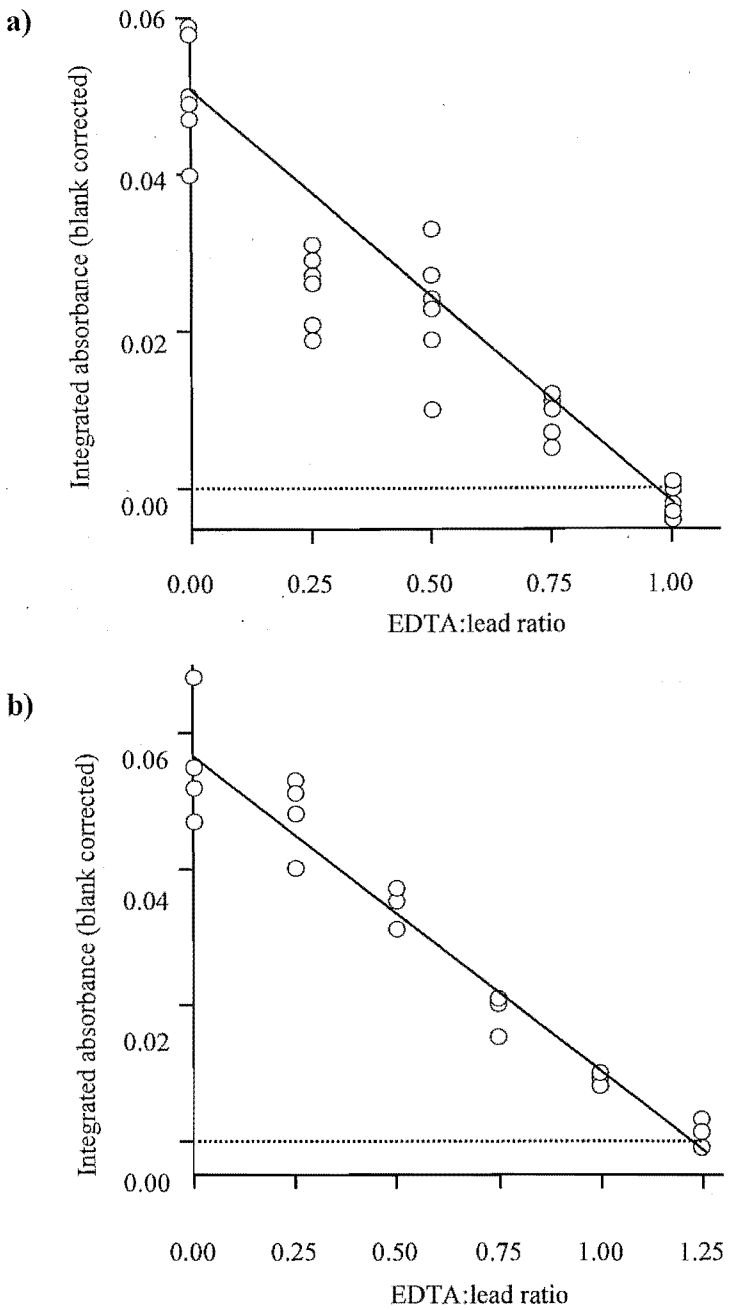

Figure 7.6 Effect of EDTA:lead ratio on ED-ETAAS absorbance, for 10 seconds deposition **(a)**, and 60 seconds deposition **(b)**, from 6.0×10^{-7} M lead standards prepared in 0.001 M acetate/0.01 M nitrate at pH 4.5 containing varying amounts of EDTA. 20 µL sample aliquots electrolysed at 1.9 V at room temperature, with the inert gas switched on. Deposits were rinsed twice with 35 µL of water for 10 seconds, and then re-deposited from 35 µL of 0.01 M HNO_3 for 30 seconds. Samples were pyrolysed at 700 °C and atomised at 2350 °C. Lead absorbance was measured at 283.3 nm.

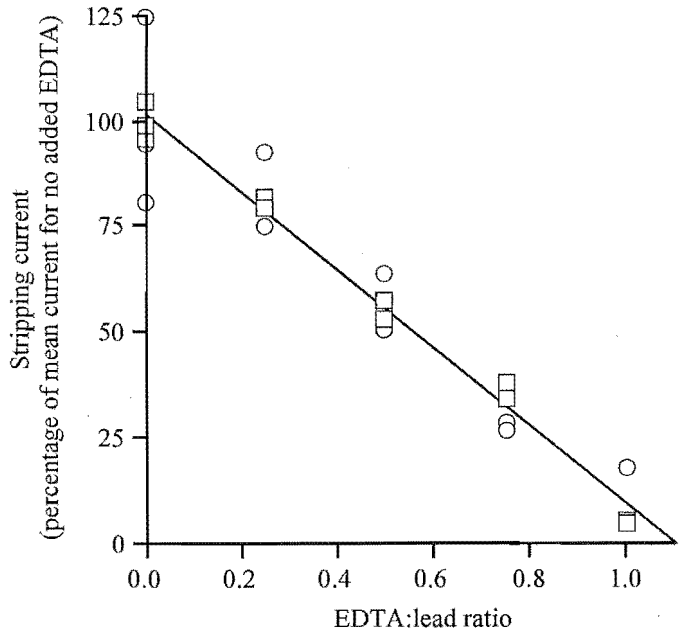

Figure 7.7 Effect of EDTA:lead ratio on ASV stripping current for stirred deposition (□) and quiescent deposition (○) from 3.0×10^{-7} M lead standards prepared in 0.001 M acetate/0.01 M nitrate at pH 4.5 containing varying amounts of EDTA. Samples were analysed using the protocol described in Section 2.3.1. Lead was deposited at 0.60 V for five minutes, and stripped to -0.10 V. The stripping current was measured at *ca.* -0.41 V vs Ag/AgCl.

7.2.3 Copper

7.2.3.1 Effect of Deposition Potential and Buffer Composition

The effect of the deposition potential was examined for 1.6×10^{-7} M copper solutions in the presence, and absence, of EDTA. Three different media were compared to determine which gave the best separation of the reduction potentials for free and EDTA-complexed copper. These media were: 0.05 M KNO_3, 0.015 M acetate buffer (pH 4.5), and 0.05 M hexamine buffer (pH 4.5). The EDTA concentrations used were: 3.6×10^{-7} M (nitrate and acetate media) and 2.5×10^{-5} M (hexamine media).

20 µL sample aliquots were electrolysed in a palladium-modified furnace using potentials ranging from 0.0 to 3.0 V. The deposits were then rinsed with 35 µL of water for 5.0 seconds. Electrodeposition was effected at room temperature, with the inert gas flow switched on. Samples were pyrolysed at 800 °C and atomised at 2500 °C. Plots of the deposition potential versus the copper absorbance are shown in Figure 7.8.

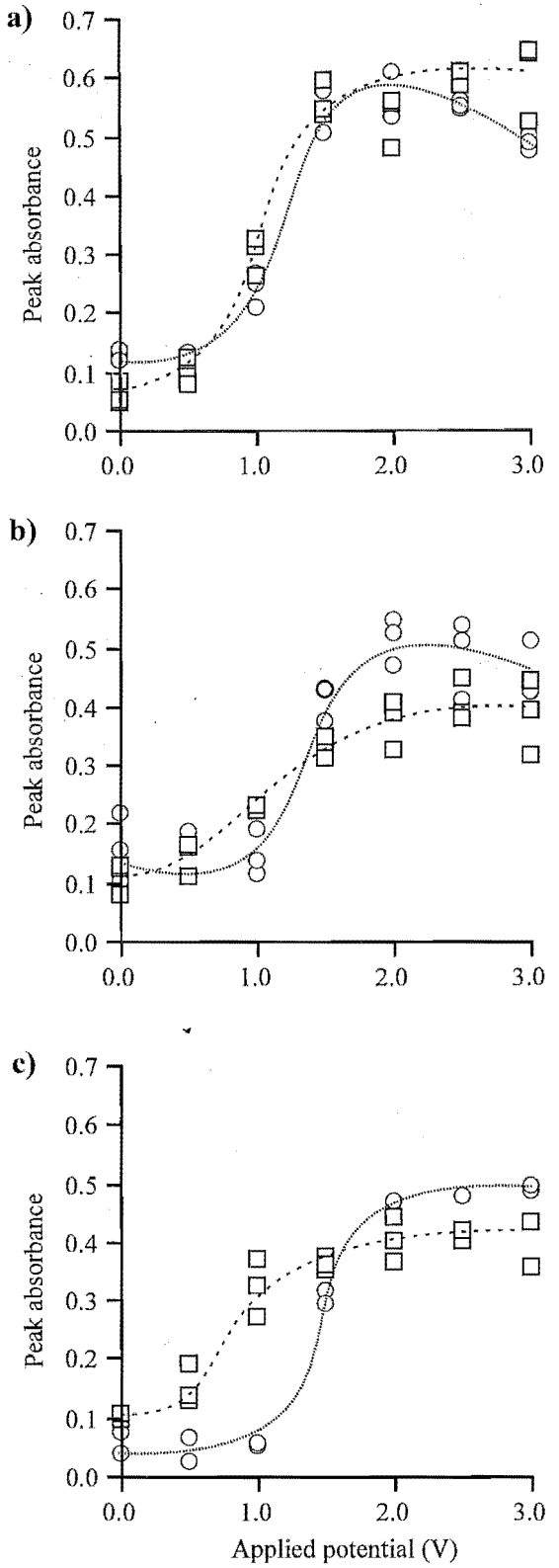

Figure 7.8 The effect of deposition potential on absorbance for 'free' copper (□) and EDTA-complexed copper (●) in (**a.**) 0.05 M KNO_3 solution, (**b.**) 0.015 M acetate buffer (pH 4.5), and (**c.**) 0.05 M hexamine buffer (pH 4.5). Copper was deposited onto a palladium-modified furnace for 60 seconds from 20 µL samples, which contained 1.6×10^{-7} M copper in the presence and absence of excess EDTA. Deposits were rinsed with 35 µL of water for 5.0 seconds, pyrolysed at 800 °C and atomised at 2500 °C.

7.2.3.2 Deposition Potential Calibration

The cathode and anode potentials during electrolysis of a 1.6×10^{-7} M copper solution, prepared in 0.15 M acetate/0.1 M NaCl at pH 4.5, were determined using the furnace simulation apparatus and protocol described in Section 2.3.2. The results are shown in Figure 7.9.

7.2.3.3 Speciation

The possibility of fractionating copper species by ED-ETAAS was further investigated. A series of 1.6×10^{-7} M copper solutions was prepared in 0.05 M hexamine buffer (pH 4.5) containing EDTA concentrations which ranged from 0.0 to 3.2×10^{-7} M. 20 µL samples were electrolysed for 60 seconds in a palladium modified furnace with a deposition potential of 1.0 V. Deposition was effected at room temperature with the inert gas flow switched on. The deposits were rinsed with 35 µL of water for 5.0 seconds, pyrolysed at 800 °C, and atomised at 2500 °C. The results are shown in Figure 7.10.

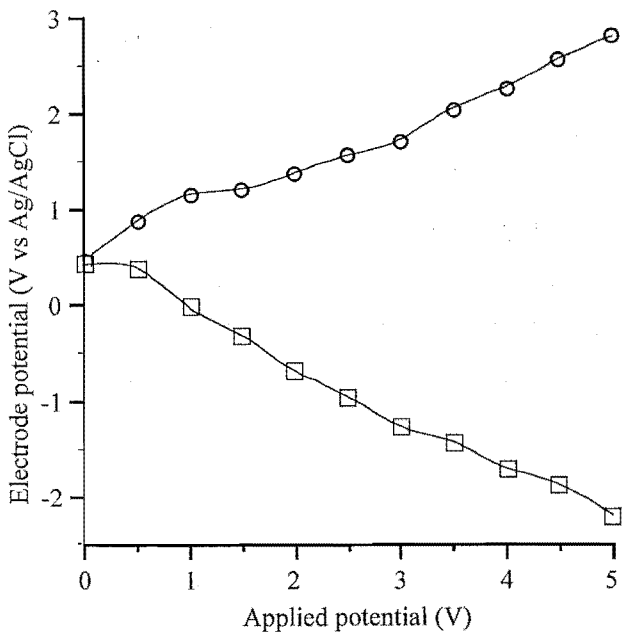

Figure 7.9 Calibration of electrode potentials for copper electrodeposition. Potentials were measured in a palladium-modified furnace, between the Ag/AgCl reference electrode, and the cathode (□) and anode (○). The solution used for the electrolysis was 1.6×10^{-7} M copper prepared in 0.15 M acetate/0.1 M NaCl at pH 4.5.

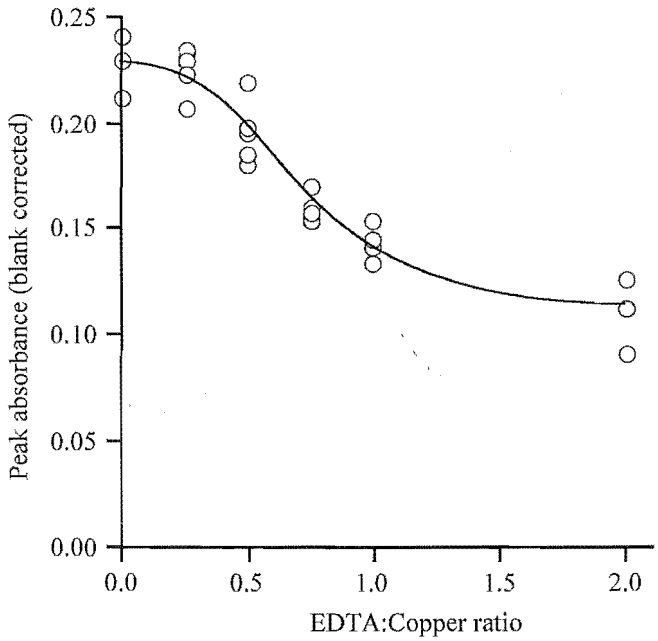

Figure 7.10 Effect of EDTA:copper ratio on ED-ETAAS absorbance for analysis of 6.0×10^{-7} M copper standards prepared in 0.05 M hexamine at pH 4.5, containing varying amounts of EDTA. 20 µL sample aliquots were electrolysed at 1.0 V for 60 seconds at room temperature, pyrolysed at 800 °C and atomised at 2500 °C. Copper absorbance was measured at 324.8 nm.

7.2.3.4 Fractionation of Cu^{2+} and Cu-Fulvate complexes

An attempt was made to apply the ED-ETAAS technique to speciation in copper(II)-fulvate solutions. The effect of deposition potential was examined for 1.6×10^{-7} M copper solutions prepared in 0.1 M acetate buffer (pH 5.5), in the presence and absence of fulvic acid (2.8 mg L^{-1}). 20 µL sample aliquots were electrolysed in a palladium-modified furnace using a range of deposition potentials (0.0-3.0 V). Deposition was effected at room temperature with the inert gas on. The deposits were rinsed once with 40 µL of water for 5.0 seconds, pyrolysed at 900 °C, and atomised at 2450 °C. The results are shown in Figure 7.11.

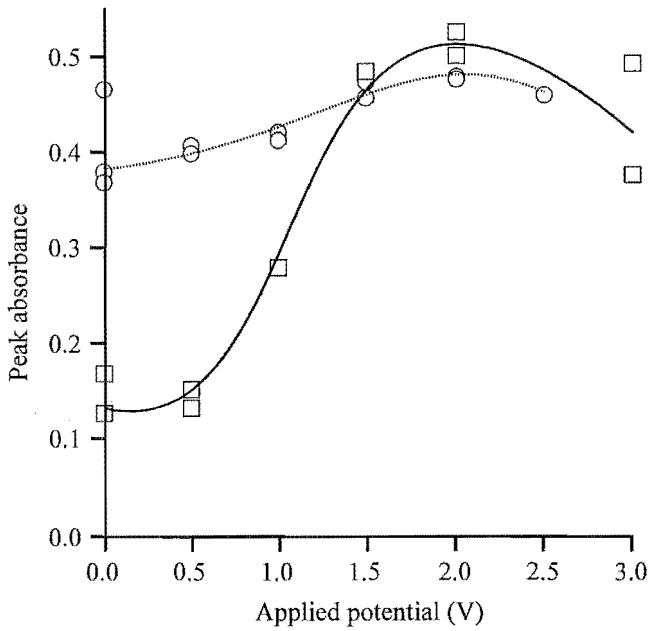

Figure 7.11 Effect of deposition potential on absorbance for 1.6×10^{-7} M copper solutions prepared in 0.1 M acetate buffer (pH 5.5), in the presence (○) and absence (□) of fulvic acid (2.8 mg L^{-1}). 20 µL sample aliquots were electrolysed in a palladium-modified furnace, at room temperature with the inert gas on. The deposits were rinsed once with 40 µL of water for 5.0 seconds, pyrolysed at 900 °C, and atomised at 2450 °C.

7.2.4 Nickel

7.2.4.1 Effect of Deposition Potential

The effect of the deposition potential was examined for 6.8×10^{-7} M nickel solutions in the presence and absence of excess EDTA (4×10^{-6} M) prepared in 0.14 M ammonia/ammonium chloride buffer (pH 7.3). 20 µL aliquots of the samples were electrolysed in a palladium-modified furnace for 60 seconds using deposition potentials ranging from 0.0 to 3.0 V. Deposition was effected at 45 °C with inert gas flow switched on. The deposits were pyrolysed at 900 °C and atomised at 2600 °C. The results are shown in Figure 7.12.

7.2.4.2 Deposition Potential Calibration

The cathode and anode potentials during electrolysis of a 6.8×10^{-7} M nickel solution, prepared in 0.14 M ammonia/ammonium chloride buffer (pH 7.3), were determined using the furnace simulation apparatus and protocol described in Section 2.3.2. The results are shown in Figure 7.13.

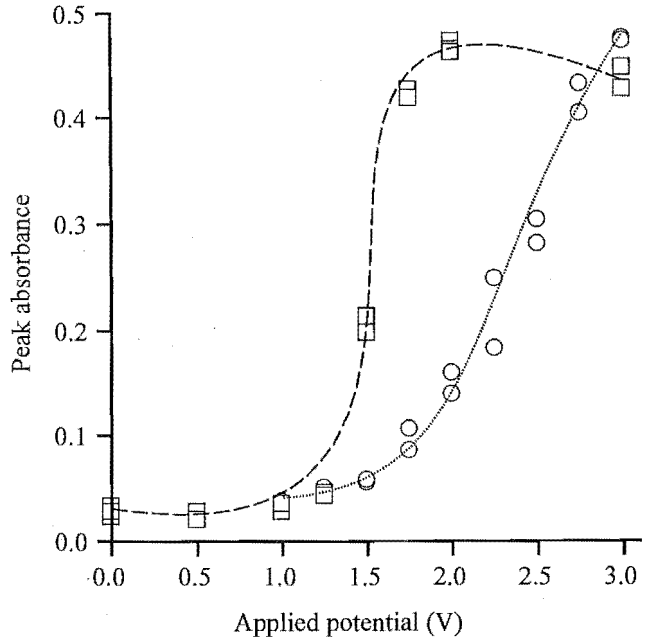

Figure 7.12 The effect of deposition potential on absorbance for 'free' nickel (□) and EDTA-complexed nickel (●). Nickel was deposited onto a palladium modified furnace for 60 seconds from 20 µL samples, which contained 6.8×10^{-7} M nickel in 0.14 M ammonia/ammonium chloride buffer (pH 7.3) with and without 4.0×10^{-6} M EDTA. The deposition potential was varied from 0.0 to -3.0 V. Deposition was effected at 45 °C with inert gas flow switched on. The deposits were pyrolysed at 900 °C and atomised at 2600 °C.

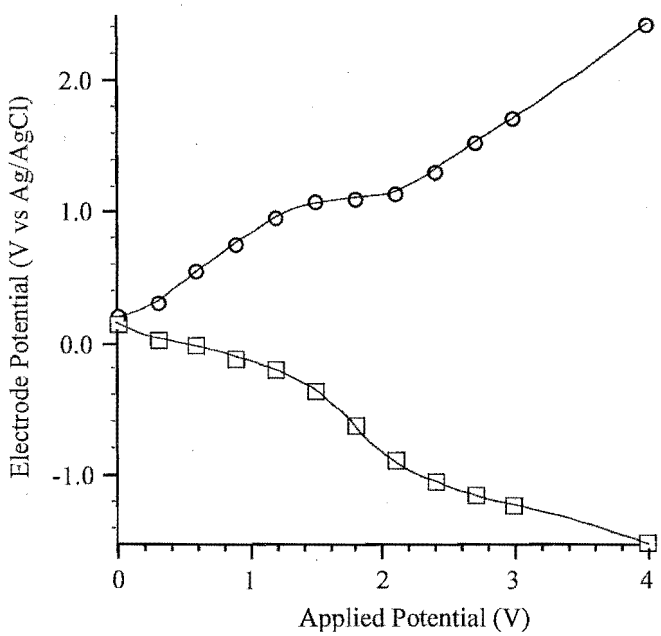

Figure 7.13 Calibration of electrode potentials for nickel electrodeposition. Potentials were measured in a palladium-modified furnace, between the Ag/AgCl reference electrode, and the cathode (□) and anode (○). The solution used for the electrolysis contained 6.8×10^{-7} M nickel, prepared in 0.14 M ammonia/ammonium chloride buffer (pH 7.3).

7.2.4.3 Speciation

Fractionation of nickel species by ED-ETAAS was further investigated by analysing a series of 6.8×10^{-7} M nickel solutions which contained various concentrations of EDTA ($0.0 - 3.4 \times 10^{-6}$ M), prepared in 0.14 M ammonia/ammonium chloride buffer (pH 7.3). 20 µL samples were electrolysed for 60 seconds in a palladium modified furnace with a deposition potential of 2.0 V. Deposition was effected at room temperature with the inert gas flow switched on. The deposits were rinsed with 35 µL of water for 5.0 seconds, pyrolysed at 800 °C, and atomised at 2500 °C. The results are shown in Figure 7.14.

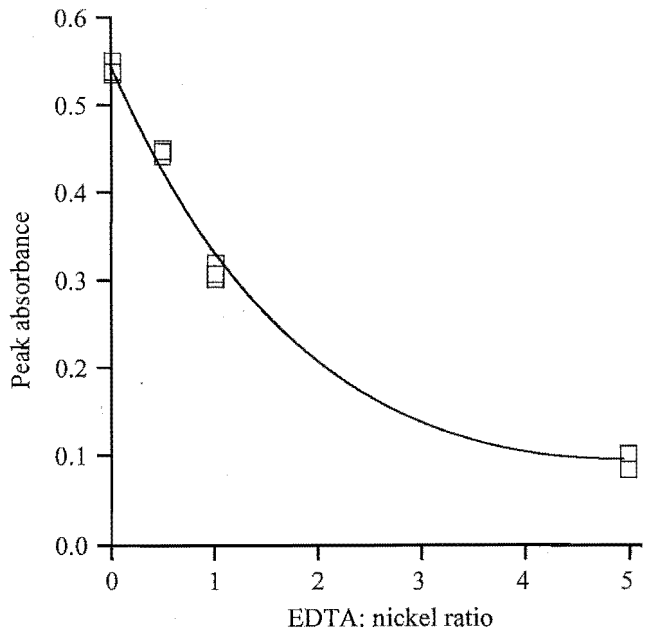

Figure 7.14 Effect of EDTA:nickel ratio on ED-ETAAS absorbance for analysis of 6.8×10^{-7} M nickel standards prepared in 0.14 M ammonia/ammonium chloride buffer (pH 7.3), containing varying amounts of EDTA. 20 µL sample aliquots were electrolysed at 2.0 V for 60 seconds at 45 °C with the inert gas switched on. Deposits were pyrolysed at 900 °C and atomised at 2600 °C.

7.3 DISCUSSION

7.3.1 Bismuth

Figure 7.1 shows the ED-ETAAS absorbance as a function of the (uncontrolled) deposition potential for Bi^{3+} and Bi-EDTA$^-$. The distinct curves for the reduction of the two species, which are analogous to polarographic waves, show that a more negative potential is required to reduce bismuth in Bi-EDTA$^-$. This follows the trend predicted by Equation 7.1, which indicates that $E_{1/2}$ for reduction of the complex will be shifted by an amount proportional to its stability constant. Bismuth forms a very stable complex with EDTA, with a stability constant log K = 25.68 (1.0 M $NaClO_4$, 25 °C).[103] Substitution of log K into Equation 7.1 yields a theoretical $\Delta E_{1/2}$ of -0.387 V. The experimental $\Delta E_{1/2}$ value was obtained after calibrating the uncontrolled-potential $E_{1/2}$ values for Bi^{3+} (0.55 V), and Bi-EDTA$^-$ (1.35 V), using the curves presented in Figure 7.2. This resulted in $E_{1/2}$ values of approximately 0.1 V and -0.1 V (vs Ag/AgCl) for Bi^{3+} and Bi-EDTA$^-$ respectively: hence, $\Delta E_{1/2}$ was *ca.* -0.2 V.

Several factors could contribute to the large discrepancy between the calculated and experimental values of $\Delta E_{1/2}$. Firstly, the deposition potential calibration (Figure 7.2) is of limited application. During electrodeposition processes such as those used in ED-ETAAS, the electrolysis current decreases as a function of time.[212] In the uncontrolled-potential electrolysis used in ED-ETAAS, the electrode potential also changes with time. This was also observed in the ED-ETAAS simulation experiments that were used for calibrating deposition potentials. The calibrated potentials shown in Figure 7.2 are the potentials measured within *ca.* 10 seconds of switching on the uncontrolled potential. The measured potentials then became more negative with time. Thus, the calibration curve shown in Figure 7.2 can only be used to approximate the initial electrode potentials during electrolysis. It is not possible to control the electrode potentials over the duration of the electrolysis unless a three-electrode system coupled to a potentiostat is used.

A second factor contributing to the difference between the calculated and experimental $\Delta E_{1/2}$ values relates to the method used to calculate the theoretical value. The function used for this purpose (Equation 7.1) is a purely thermodynamic expression which takes no account of kinetic factors such as the diffusion layer thickness at the electrode surface, or the ligand exchange rates (lability) of the metal-ligand complexes. Theoretical studies which take kinetic parameters into account have been made by Zirino and Kounaves,[212] and by Shuman and Cromer,[213] who described the theoretical current-potential relationships for reduction of metals and their complexes at the hanging mercury drop electrode (HMDE). Theory and experimental verification showed that $\Delta E_{1/2}$ is related to a number of factors including the electrolysis time, the diffusion coefficient for the metal-ligand complex, the diffusion layer thickness, the electrode area, and the rate constant (k_s) for the reduction of the metal ligand species (Reaction 7.1).[213]

$$ML + ne^- \overset{k_s}{\rightleftharpoons} M + L^{n-} \qquad \text{(Reaction 7.1)}$$

Recently, Branica and Lovric[214] used ASV to study the pseudopolarography of totally irreversible redox reactions. Specifically, this study considered the pseudopolarography of stable and inert complexes of metal ions with polydentate ligands such as NTA and EDTA. The authors pointed out that the pseudopolarographic $\Delta E_{1/2}$ for an irreversible redox reaction at a thin mercury film rotating disc electrode is given by a more complex function of log K:[214]

$$E_{1/2(ML)} - E_{1/2(M)} = \frac{RT}{nF} \ln\frac{K\lambda\delta}{Dt_{acc}} - \frac{RT}{\alpha nF} \ln\frac{k_s\delta}{D} \qquad \text{(Equation 7.3)}$$

where R, T, n, and F have their usual meanings, K is the stability constant for the complex ML, λ is the mercury film thickness, δ is the diffusion layer thickness, D is the diffusion coefficient for ML, t_{acc} is the accumulation time, α is the charge transfer coefficient, and k_s is the rate constant for Reaction 7.1.

In this work, the possible effect of bismuth hydrolysis on $\Delta E_{1/2}$ was also considered. A Solgaswater[102] model indicated that at pH 2.0, only *ca.* 10% of the bismuth is present as Bi^{3+}—the remainder being present as $BiOH^{2+}$ (80%) and $Bi(OH)_2^+$ (10%). However, the small log K value for the $BiOH^{2+}$ complex (-1.09 at I = 0.0, 25 °C[215]), means that $E_{1/2}$ for $BiOH^{2+}$ should not be significantly different from $E_{1/2}$ for Bi^{3+}. Thus, $\Delta E_{1/2}$ will not be affected by the presence of $BiOH^{2+}$.

For the purpose of this work, the experimental $\Delta E_{1/2}$ value for the bismuth-EDTA system (obtained by plots of deposition potential versus absorbance) was sufficient to determine potentials that could be used to selectively deposit non-complexed metal. Figure 7.1 shows that an uncontrolled potential of 0.8 V selectively deposited $Bi^{3+}/BiOH^{2+}/Bi(OH)_2^+$ without substantial deposition of Bi-EDTA$^-$. The small absorbances measured for Bi-EDTA$^-$ at deposition potentials below 1.2 V could be attributable either to adsorption of the Bi-EDTA$^-$ complex onto the palladium, or to residual Bi-EDTA$^-$ which was not removed by the post-deposition rinsing process. The Bi-EDTA$^-$ complex is considered to be inert[211] so these absorbances are unlikely to stem from partial reduction of a labile Bi^{3+} species.

Figure 7.3 shows the effect of increasing EDTA concentration for analysis of a 9.6×10^{-7} M Bi^{3+} solution by (a) ED-ETAAS and (b) ASV. The ASV results (7.3b) closely match those expected for a non-labile species. The results for ED-ETAAS (7.3a) at room temperature also closely follow this model, although they indicate either a partial reduction of the Bi complex (*ca.* 5-10%), or retention of complex on the furnace by adsorption.

Figure 7.3a shows that a significantly higher absorbance is observed when electrolysis is effected at an elevated temperature (45 °C). The enhanced sensitivity at Bi : EDTA = 1 : 0 indicates that room-temperature deposition is non-quantitative. Incomplete deposition at room temperature may be due to a lack of convective sample stirring during room-temperature electrolysis, but may also be related to dissociation kinetics. If the species $BiOH^{2+}$ is only partially labile, then we would expect the lability, and hence the deposition efficiency to increase with temperature.

In addition to enhanced deposition at 45 °C, Figure 7.3a shows that the amount of lead measured shows little dependence on the EDTA concentration. This may indicate lability of the Bi-EDTA$^-$ complex. Although such lability is not observed by ASV, two different factors may contribute to its observation in this case. The convection controlled (slow) stirring during deposition leads to a relatively thick diffusion layer for ED-ETAAS, increasing the residence time of the complex within the diffusion layer. The raised temperature increases the rate of the complex dissociation equilibrium, further increasing the apparent lability of the complex under these conditions.

One other consideration when comparing results from conventional electrochemical experiments (ASV, polarography etc.) with those from ED-ETAAS experiments relates to the exhaustive deposition protocol used for ED-ETAAS. For conventional electrochemical analysis, the concentrations of the metal and ligand in the bulk solution are assumed to be unaffected by processes at the electrode surface and remain constant. Hence equilibrium processes in the solution are unaffected by electrode processes. However, in the case of ED-ETAAS, the metal concentration in the bulk solution decreases thoughout the course of the electrolysis. Thus, in contrast to the ASV technique where lability is defined by the ability of a complex to dissociate within the diffusion layer (fractions of a second), in ED-ETAAS there is scope for re-equilibration of metal-ligand complexes over the duration of the electrolysis —an effective timescale of 60 seconds. Overall, this serves to constantly decrease the metal:ligand ratio in the sample over the duration of the deposition.

In the case of the Bi-EDTA complex, where log K is large, and stoichiometric binding is predicted, there should be no net difference due to exhaustive electrolysis between the amount of free metal measured by ASV and ED-ETAAS, provided that the complex does not dissociate within the diffusion layer. However, for a labile complex that does dissociate within the diffusion layer, the increasing ratio of ligand to metal throughout the electrolysis will increase the rate of formation of ML relative to the rate of dissociation, effectively decreasing the apparent lability of the complex. This effect will lead to "stretched" pseudopolarograms with low limiting slopes.

7.3.2 Lead

Figure 7.4 shows the effect of deposition potential on lead absorbance for deposition of lead in the presence and absence of excess EDTA. Maximum deposition of 'free lead' is attained at an applied potential of *ca.* 1.8 V whereas significant reduction of the Pb-EDTA complex only begins at applied potentials greater than *ca.* 2.1 V. This potential 'window' was sufficient to allow selective deposition of free lead. The experimental $\Delta E_{1/2}$ for the lead/lead-EDTA system was determined after calibrating the apparent $E_{1/2}$ values obtained from Figure 7.4 against the referenced potentials shown in Figure 7.5. This method gave an experimental $\Delta E_{1/2}$ of ca -0.3 V, compared to an $\Delta E_{1/2}$ value of -0.366 calculated from Equation 7.1 (using log K = 18.52; 0.1 M KNO_3, 25 °C).[103]

A distinctive feature of the lead-EDTA system, contrasting with the Bi-EDTA system, is that the lead-EDTA complex is strongly adsorbed to the palladium-modified furnace (results not shown). This was largely prevented by excluding the palladium deposition step from the analysis protocol. However, Figure 7.4 shows that some $Pb(EDTA)^{2-}$ still adsorbs to the pyrolytic graphite surface at low deposition potentials. Comparison with Figure 7.5 reveals that the adsorption occurs at applied potentials for which the actual electrode potential on the furnace ('cathode') surface is positive. This suggests adsorption of the negatively charged $(Pb\text{-}EDTA)^{2-}$ species onto the positively charged pyrolytic graphite.

Figure 7.7 shows the effect of EDTA concentration on lead stripping current for ASV analysis of solutions containing 3.0×10^{-7} M Pb^{2+}. The experiment was carried out using two different stirring protocols; a 'fast' stirred deposition (700 rpm), and a quiescent (unstirred) deposition. Different diffusion layer thicknesses for these two experiments should lead to different results for measurement of a pseudo-labile complex (if the timescale for dissociation is similar to that for the ASV experiment). However, the regression lines for the two data sets plotted in Figure 7.7 are virtually identical. This result, and the intercept at EDTA:Pb $\approx$ 1:1, confirms previous reports that for a deposition potential of -0.7 V, the lead-EDTA complex is inert on the ASV timescale.[216] Therefore, the lead-EDTA complex is expected to be inert for unstirred deposition during ED-ETAAS analysis.

Figure 7.6 shows the effect of EDTA concentration on absorbance for ED-ETAAS analysis of solutions containing 6.0×10^{-7} M Pb^{2+}. The x-intercept for a 10 second deposition period, occurs at a 1:1 ratio of lead to EDTA—consistent with a complex that is inert on the experimental timescale. However, for a 60 second deposition, the x-intercept occurs at a 1.25:1 EDTA:lead ratio. This change is consistent with pseudo-lability of the $Pb(EDTA)^{2-}$ complex under ED-ETAAS conditions, however, this explanation is not supported by the ASV results.

An interpretation of the conflicting results presented in Figures 7.6a and 7.6b, is that the $Pb(EDTA)^{2-}$ complex slowly penetrates the surface of the unprotected (no palladium modifier) pyrolytic-coated graphite furnace. (It has been shown that pyrolytic graphite is not impermeable.[147]) Such a sub-surface species would not be readily removed by post-deposition rinses. Thus, the longer the deposition time, the more penetration would occur, and the more complexed lead would be measured.

The variable precision observed in Figures 7.4 and 7.6 is largely attributable to the absence of palladium modifier. This requires the use of lower pyrolysis temperatures, which leads to less efficient removal of residual acetate prior to atomisation. The lack of precision is also due to incomplete deposition, and hence, poor overall sensitivity. For all metals studied (except nickel), quantitative deposition was only observed at low pH ($\leq$ *ca.* 1.0). Thus, for speciation studies in buffer solutions, only a fraction of the available analyte is deposited. Where deposition was effected at room temperature the fraction of deposited metal is lower still due to the lack of convectional stirring during electrolysis. Non-quantitative deposition was not considered to be a great problem, any more than it is in ASV analysis, provided that the fraction of analyte deposited is constant for a given set of conditions. The only drawback is the corresponding decrease in sensitivity.

7.3.3 Copper

There is a clear difference between the results for copper and those for the other cations studied. This may be attributed to the much greater lability of copper complexes. Figure 7.8 shows the effect of deposition potential on absorbance for copper deposition in the presence and absence of excess EDTA. A different effect is observed for each of the three media; a) 0.05 M KNO_3, b) 0.015 M acetate buffer (pH 4.5), and c) 0.05 M hexamine buffer (pH 4.5).

The deposition potential versus absorbance curves obtained in 0.05 M KNO_3 media (Figure 7.8a) are almost identical for copper and copper-EDTA. It is possible that both the complex lability and the chemistry of the electrolyte solution play a part in this. During electrolysis, the pH of the unbuffered deposition medium was observed to decrease rapidly. From an initial pH of *ca.* 3.0, the pH rapidly dropped below 2.0. Solgaswater calculations indicate that under the deposition conditions used, significant complexation of copper and EDTA does not occur below *ca.* pH 2.2. Thus, it is possible that both of the curves shown in Figure 7.8a represent reduction of free Cu^{2+}.

The plot for copper deposition in 0.015 M (pH 4.5) acetate media (Figure 7.8b) shows that again, there is no potential window that could be exploited to selectively deposit free copper. The curve for copper-EDTA is similar to that obtained in nitrate media, but with a slight shift in $E_{1/2}$. The increased pH is a likely cause for this change. The lower slope of the "free" copper curve is possibly related to the speciation of copper in the acetate medium. A Solgaswater model predicts that at pH 4.5, in 0.015 M acetate, only *ca.* 70% of the copper is free; the remainder is present as the copper-acetate complex. Thus, the curve shown in Figure 7.4b could be a composite of two processes; reduction of Cu^{2+}, and reduction of less labile $Cu(OAc)^{+}$. This effect has been observed for other ligands,[217] but was not observed for the copper-acetate system by Figura and McDuffie.[216]

The broad pseudopolarogram of the "free" copper curve may also indicate irreversible reduction processes. However, a broad pseudopolarogram was not observed for reduction of the Cu-EDTA complex, which is known to be reduced irreversibly on mercury.[218] The alternative explanation for the broad copper reduction curve is that $Cu(OAc)^{+}$ and/or Cu^{2+} are adsorbed onto the furnace (and thus measured) at potentials below those at which they are reduced.

The ED-ETAAS-pseudopolarograms for reduction of copper and copper-EDTA in hexamine buffer are shown in Figure 7.8c. In this case, a useful potential window exists in which free copper can be selectively reduced in the presence of $Cu(EDTA)^{2-}$. This indicates that the $Cu(EDTA)^{2-}$ complex is not labile on the timescale used in ED-ETAAS deposition. Previous studies indicate that the lability of $Cu(EDTA)^{2-}$ depends on the deposition medium. Tuschall and Brezonik[219] found that the complex was inert in an acetate buffer (on the ASV timescale).

Figura and McDuffie[216] observed the same inertness, but noted that the complex was partially labile in Tris buffer. The increased lability was attributed to the complexing ability of the Tris buffer.

The experimental $\Delta E_{1/2}$ for the copper/copper-EDTA system was determined after calibrating the apparent $E_{1/2}$ values obtained from Figure 7.8c against the referenced potentials shown in Figure 7.9. This method gave an experimental $\Delta E_{1/2}$ of ca -0.45 V, compared to an $\Delta E_{1/2}$ value of -0.416 calculated from Equation 7.1 (using log K = 18.7; 0.1 M KNO_3, 25 °C).[103]

Figure 7.8c shows that a deposition potential of 1.0 V gives maximum free copper deposition with minimum $Cu(EDTA)^{2-}$ deposition. The effect of increasing EDTA concentration on absorbance, for a $1.6x10^{-7}$ M copper solution deposited at 1.0 V, is shown in Figure 7.10. The lack of an x-intercept at a 1:1 ratio indicates either adsorption of $Cu(EDTA)^{2-}$ onto the furnace surface, or some complex lability. Although such lability would conflict with the ED-ETAAS-pseudopolarograms shown in Figure 7.8c, it can be seen that a very small change in the applied potential could effect $Cu(EDTA)^{2-}$ reduction. Given the uncontrolled nature of the deposition potential, this seems a likely explanation for the apparent contradiction. Thus, the copper-EDTA complex could be considered 'quasi-labile' on the ED-ETAAS timescale.

Figure 7.11 shows the effect of the deposition potential on absorbance for ED-ETAAS analysis of 1.6×10^{-7} M copper solutions in the presence and absence of fulvic acid. The two curves indicate that at potentials greater than 2.0 V, both the free and fulvate-bound copper are reduced. However, at lower voltages a large proportion of the fulvate-bound copper is also measured. It is unlikely that the copper-fulvate complex is reduced at lower potentials than copper, so it is likely that the high absorbances result from adsorption of the hydrophobic fulvate complex onto the surface of the furnace—either to the palladium modifier, or to the pyrolytic graphite. Therefore, application of the ED-ETAAS technique to fractionation of copper species requires media with very low organic content such as potable waters or seawater.[97]

7.3.4 Nickel

Figure 7.12 shows the effect of deposition potential on absorbance for nickel deposition in the presence and absence of excess EDTA. The curve for $Ni(EDTA)^{2-}$ has a much smaller limiting slope than was observed for the bismuth, lead, or copper -EDTA complexes. This points to irreversibility of the $Ni(EDTA)^{2-}$ reduction process. As a consequence, the experimental $\Delta E_{1/2}$, determined after calibrating the apparent $E_{1/2}$ values against the referenced potentials shown in Figure 7.13, is large—*ca.* -0.65 V, compared to $\Delta E_{1/2}$ of -0.385 V calculated from Equation 7.1 (log K = 18.52; 0.1 M KNO_3, 25 °C).[103] Although the experimental $\Delta E_{1/2}$ is larger than that for any of the other metals studied, there is no window in which free nickel can be selectively deposited in the presence of EDTA. The greatest differentiation between free and EDTA-complexed nickel occurs at deposition potentials in the range 1.8-2.0 V.

Figure 7.14 shows the effect of increasing EDTA concentration (on absorbance) for a 1.6×10^{-7} M nickel solution electrolysed at 2.0 V. Speciation models (Solgaswater[102]) of nickel and EDTA system predict stoichiometric complexation in ammonium buffer at pH 7.3 (Figure 7.15). From this model, it follows that the x-intercept for Figure 7.14 should occur at an EDTA:nickel ratio of 1:1. However, the experimental curve does not intercept the x-axis at all. The limiting peak absorbance of *ca.* 0.1 suggests that a significant fraction of the $Ni(EDTA)^{2-}$ complex is reduced at 2.0 V. This is consistent with the results shown in Figure 7.12. Both of these results suggest that the $Ni(EDTA)^{2-}$ complex is pseudo-labile under ED-ETAAS conditions.

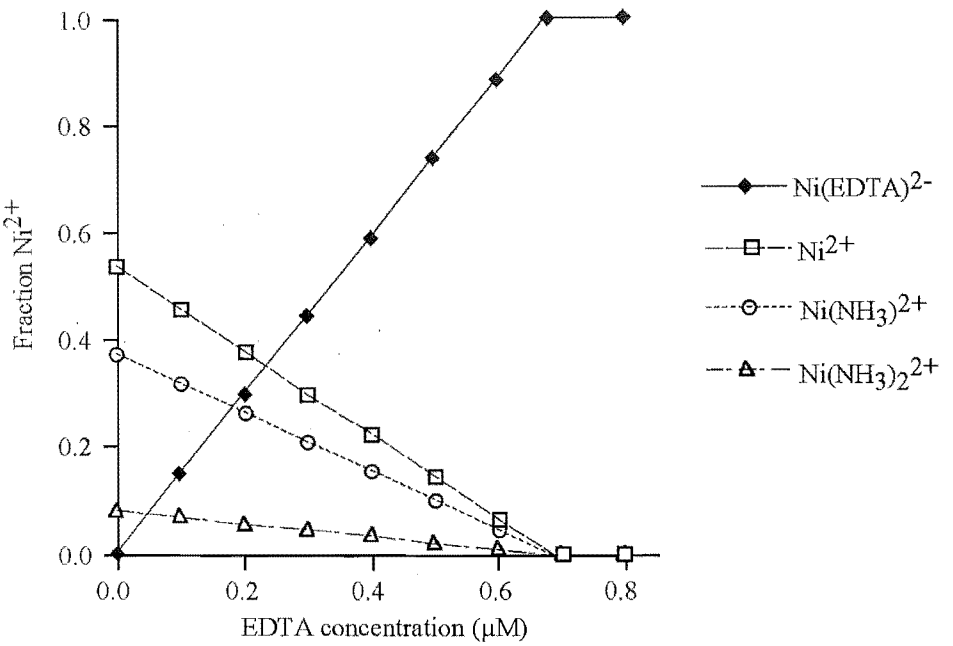

Figure 7.15 Speciation of nickel with increasing EDTA concentration, as calculated for a 6.8×10^{-7} M Ni^{2+} solution prepared in 1.14 M ammonium buffer at pH 7.3.

In general however, nickel is known to be one of the less labile divalent cations, with a specific rate constant for water exchange on Ni^{2+} of $k = 3 \times 10^4$ M^{-1} s^{-1}. Furthermore, the $Ni(EDTA)^{2-}$ complex forms slowly at low concentrations, as apply at the endpoint in volumetric analysis.[220] The apparent lability observed in ED-ETAAS analysis may be related to the increased deposition temperature used for nickel determination (45 °C). The speciation studies for bismuth, lead and copper (carried out subsequent to the nickel studies) were performed at room temperature. Thus it is possible that $Ni(EDTA)^{2-}$ lability would not be observed with room temperature deposition. However, the speciation of nickel was not re-investigated during the course of this work.

Chapter Eight

Arsenic Determination and Speciation

The first section of this chapter describes the occurrence of arsenic and its toxicity in the environment. Arsenic speciation and its toxicological significance are introduced, and various methods of arsenic determination and fractionation are discussed. The experimental section outlines the development of an ED-ETAAS method to determine inorganic As^{III} and total arsenic. Developmental work concentrated on determining arsenic from As^{III} standards. Subsequent work established protocols to differentiate between As^{III} and As^{V}. The method developed was used to determine As^{III} and total arsenic in natural waters. The results were validated by comparison with an established hydride-generation method. The relative attributes of the ED-ETAAS protocol are discussed.

8.1 INTRODUCTION

8.1.1 Arsenic Occurrence and Toxicity

Arsenic is the twentieth most abundant element in the earth's crust, and is a component of more than 245 minerals.[221] Consequently, arsenic is a common contaminant of metallic ores and subterranean-sourced waters. Arsenic enters the environment naturally through volcanic processes and weathering of rocks, but the process is greatly accelerated by anthropogenic activities such as mining, smelting of arsenic-containing ores, and burning of fossil fuels. Industrial arsenic use also contributes to arsenic distribution. Arsenic salts have been widely used as pesticides and herbicides, which are released into the environment. Fortunately, such applications are being phased out in most parts of the world.[222] Other industrial uses of arsenic include glass-making, electronics, ceramics, fireworks, textiles, tanning, cosmetics, metallurgy, and veterinary medicine.

Environmental arsenic is present in numerous forms which are distributed throughout the atmosphere, the water, the soil and sediments, and the biosphere. The most mobile species are those which are volatile or water-soluble. Volatile arsenic species include arsine (AsH_3) and organo-substituted arsines (AsR_3). Water soluble species largely comprise soluble inorganic arsenites and arsenates, along with a variety of organo-arsenic moieties, the most common of which are monomethylarsonic acid (MMA) and dimethlyarsenic acid (DMA).[223] Each of these species, shown overpage, has a different toxicity towards humans.

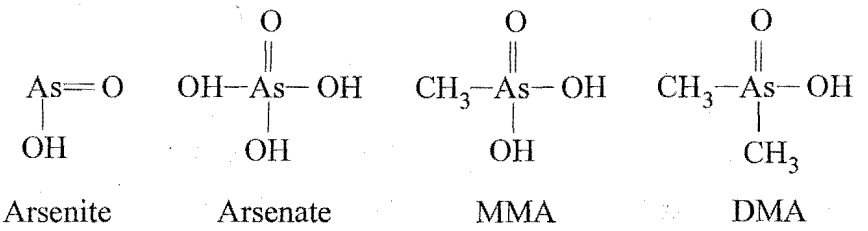

Inorganic As^{V} and As^{III} have different mechanisms of action in the body. Arsenate (As^{V}) behaves very much like phosphate, and can substitute for phosphate in normal cell reactions, thus interfering with cell function. Arsenite (As^{III}) binds readily to thiol groups in proteins and because of this, inactivates many enzymes.[192] In contrast to inorganic arsenite and arsenate, neither MMA no DMA bind strongly to biological molecules in humans. Hence, their relative acute toxicity is less than that of the inorganic forms. In general, inorganic As^{III} is considered to be ten times more toxic than As^{V}, which in turn is considerably more toxic than MMA, DMA or other minor arsenic species.[224]

In water, arsenic is largely found as inorganic arsenate with smaller quantities of arsenite. The ratio of arsenate to arsenic can vary. In aerated water, especially at high pH, arsenite tends to be oxidised to arsenate. At low pH, the reverse can occur, where arsenate is reduced to arsenite. The organoarsenic species such as MMA and DMA usually constitute only a small percentage of the total arsenic present.[224] It can be seen that while As^{III} is by far the most toxic species present in waters, it usually only constitutes a fraction of the total arsenic content. Correspondingly, total arsenic concentrations are not reliable measures of toxicity. For analysis of environmental samples, it is common practice to determine total inorganic arsenic, and ideally, arsenite concentrations. The minor organoarsenic species, which are of lower toxicity, are often not measured.

8.1.2 Arsenic Analysis

The methods that can be used to measure arsenic and its species in the environment are restricted by the low concentrations of interest—typically in the ppb-ppm region. The methods which are useful at these concentrations include neutron activation analysis (NAA),* mass spectrometry, electrochemical, and atomic absorption and emission. Of these, the most popular methods have been based on atomic absorption, particularly when coupled with hydride generation and trapping systems, although a number of voltammetric protocols have been reported. Mass spectrometry is becoming increasingly important, as developments in sample introduction, particularly electrospray and ICP, have provided ways of interfacing separation methods such as HPLC with mass spectrometric analysers.

---

* See Section 1.4 for a discussion of the relative attributes of neutron activation analysis.

8.1.2.1 Electrochemical Methods

Inorganic arsenic can be determined by several electrochemical methods. Arsenate is usually found to be inactive although its standard reduction potentials are not extreme, consequently, electrochemical methods generally measure only the more toxic arsenite species. Determination of arsenate by electrochemical methods usually requires a chemical pre-reduction step. Reduction potentials for selected inorganic arsenic species that occur in acidic media are given below. A complete list is given by Tomilov and Chomitov.[225]

$$H_2AsO_4^- + 3H^+ + 2e^- \rightarrow HAsO_2 + 2H_2O \qquad E^0 = +0.666\ V$$

$$HAsO_2 + 3H^+ + 3e^- \rightarrow As_{(s)} + 2H_2O \qquad E^0 = +0.248V$$

$$As_{(s)} + 3H^+ + 3e^- \rightarrow AsH_{3(g)} \qquad E^0 = -0.24V$$

Anodic stripping voltammetry using a gold electrode has been successfully used to measure arsenite with detection limits as low as 0.02 ppb.[226] Davis et al.[227] and Hamilton et al.[228] also used gold electrode ASV protocols, but included pre-analysis reduction steps in order to determine total arsenic. However, these methods can suffer from problems related to poor reproducibility of, and ready damage to, the gold electrode surface.[229]

Cathodic stripping voltammetry at the HMDE has been used to determine arsenite,[230] but interferences from copper (signal enhancement) necessitates removal of copper (by solvent extraction). An alternative approach has been to mask the copper interference by spiking samples with high concentrations of copper.[231] This is a particularly sensitive method, with detection limits in the sub-nanomolar region.[232,233] Total inorganic arsenic can also be determined by using a pre-reduction step.[232,234] The most apparent disadvantage of this method stems from the high concentrations of copper required (stock solutions ≥50 ppm), which are undesirable when the analysis area or instrumentation may also be used for trace copper determination.

Adsorptive stripping voltammetry has also been used for arsenic determination. Zima and van den Berg[229] used adsorption of an arsenite pyrrolidine dithiocarbamate complex onto the HMDE to determine arsenic in seawater. The detection limit of the technique was 0.2 ppb. However, the method was susceptible to interferences, particularly from copper, at levels lower than those frequently encountered in fresh waters.

8.1.2.2 Atomic Absorption

Direct determination of arsenic can be accomplished by ETAAS. However, the technique is insensitive to speciation and thus measures only total arsenic. The volatility of arsenic and its compounds is also a problem in ETAAS analysis. For an unmodified pyro-coated graphite furnace, the maximum pyrolysis temperature for As^{III} determination has been reported to be as low as 300 °C[190], while arsenobetaine is volatilised above 200 °C.[115] Despite the volatility of arsenic and its compounds, high-temperature pyrolysis is considered necessary to remove

or decrease atomisation interferences arising from phosphate,[170] aluminium, sodium, potassium, and sulphate[116] in samples. Consequently, chemical modifiers which reduce analyte volatility are essential for arsenic determination. Three of the most popular modifiers for this purpose are nickel, palladium, and tungsten which can raise the maximum As^{III} pyrolysis temperature to 1300 °C,[153] 1100-1400 °C,[235] and 1600 °C[115] respectively.

Even when chemical modifiers are used, different sensitivities are observed for various arsenic species. Slaveykova *et al.*[115] compared the relative sensitivities for six arsenic species while using five different tungsten and palladium-based modifiers. The modification that produced the most consistent characteristic masses for each species was a palladium nitrate modifier in a tungsten-treated furnace. This modification gave characteristic masses of 20 ± 1 pg for As^{III}, As^{V}, MMA, DMA, and arsenobetaine, with a characteristic mass of 29 pg for arsenocholine. The least favourable results were obtained when using an unmodified pyro-coated furnace, where characteristic masses ranged from 35 pg for As^{V}, to 72 pg for arsenocholine. The varying sensitivities reflect differences in the thermal stabilities, interactions with the modifiers, and atomisation mechanisms for each species.

In addition to thermal instability and interference problems, direct arsenic determination by ETAAS is further complicated by the relatively high detection limit of the technique. This is largely due to the analytical wavelength used for arsenic determination—193.7 nm. Hollow cathode lamps have a low output at this wavelength; a problem exacerbated by lens, mirror, and air absorption in the vacuum UV range. Further, many photomultipliers perform poorly below 200 nm.[3] These problems are largely overcome by using high intensity EDL sources which, through improved signal-to-noise ratios, provide detection limits an order of magnitude lower.[3]

8.1.2.3 Hydride-Generation Methods

Three of the problems encountered in ETAAS—low sensitivity, poor thermal stability, and lack of species fractionation capability—can be diminished or removed through the use of hydride generation techniques. Such protocols involve reducing the analyte to its corresponding hydride, which is then thermally decomposed prior to atomic absorption detection. The hydride is usually produced by reacting the sample with sodium borohydride under acidic conditions. The primary advantage of hydride generation is that it allows pre-concentration of the sample, which may be effected in two ways. The traditional approach to hydride generation uses a 'batch' method, in which the sample is reacted with sodium borohydride in a closed vessel. The evolved hydride is then directed towards the atomisation cell. This approach allows reduction of analyte from a large volume of sample (50-100 mL) at one time, producing a considerable increase in sensitivity over direct ETAAS determination. Alternatively, modern hydride generation systems frequently use a continuous flow reaction method. In both systems, the resulting arsine species can be collected and pre-concentrated in a cryogenic trap prior to atomisation.[236,237]

There are chemical problems associated with hydride generation. Foremost of these is the different sensitivity often observed for arsenate and arsenite. This is because As^{V} and As^{III} react with sodium borohydride at different rates. To circumvent this problem, an additional reductant (potassium iodide[238] or L-cysteine[239]) is frequently added to reduce As^{V} to As^{III} prior to the borohydride reaction. The borohydride reduction is also prone to interferences from other semi-metals,[240] and from various transition metals.[241] Some workers have attempted to counter these interferences by using electrochemical hydride generation.[241-243] However, because only As^{III} is electroactive, a chemical pre-reduction step is required to convert inorganic As^{V} to As^{III}.[244]

The thermal decomposition and detection of volatile arsenic-hydride species can be accomplished by several AAS methods. The output from the hydride generator can simply be directed into a flame, but sensitivity is limited because of strong absorption by the flame at the analytical wavelength. This problem is addressed by the use of a heated quartz cell, in which sensitivity is further enhanced by the increased residence-time of analyte atoms in the light-path. The quartz cell is a very popular method of atomising hydrides, particularly when the hydride is produced by the 'batch' method. However, for continuous flow generation which may require a post-production hydride concentration step, *in-situ* trapping within the graphite furnace is becoming increasingly popular.

In this technique, the hydride is accumulated on the inner surface of the graphite furnace and then atomised using a conventional ETAAS heating protocol. The efficiency of the accumulation step is greatly enhanced by coating the inside of the furnace with a noble metal modifier.[176] The use of a noble metal modifier also decreases the temperature required for analyte trapping. For example, a temperature of 780 K is required to trap AsH_3 on graphite, but this temperature is lowered to 470 K for trapping on palladium.[176] There is evidence that this is a consequence of catalytic hydride dissociation on the noble metal surface.[126,176]

In addition to acting as a trapping agent, the noble metal thermally stabilises the analyte. This leads to well defined atomisation-time profiles, and hence improved sensitivity. *In-situ* hydride pre-concentration is particularly useful for hydrides produced by continuous flow methods because it obviates the need for cryogenic trapping. The technique can be used to determine a number elements including lead,[160] cadmium,[130,245] bismuth,[129,] tin,[131,246] germanium[118] and selenium.[134] An extension of this technique, uses the in-furnace pre-concentration step followed by volatilisation as a means of sample introduction for ICP-MS analysis. This method can be used to simultaneously determine multiple elements.[166,247,248]

8.1.2.4 Fractionation of Arsenic Species

Methods which measure arsenic speciation fall into two broad categories. In the first, only inorganic arsenic species are of interest. Quantitation of the two main species, arsenite and arsenate, usually relies on a protocol that is specific for arsenite—which is determined in the first step of the analysis. A chemical reductant is then used to convert arsenate to arsenite. A repeat analysis gives the total inorganic arsenic content, following which the arsenate concentration can be calculated by difference. Methods of this type can use electrochemical detection, in which case selectivity is afforded by the electrochemically inert behaviour of the arsenate, or they may use hydride generation atomic absorption analysis, in which case selectivity is achieved by careful control of the conditions used to generate the hydride. Sodium borohydride reduces arsenite to arsine at pH values below 5.0. However, complete reduction of arsenate requires strongly acidic conditions ($pH \leq 0$) or the presence of a further reductant such as potassium iodide or L-cysteine.[249] Thus, by varying the pH and/or the reductant used, it is possible to determine arsenite only, or total inorganic arsenic.

In the second category of arsenic speciation methods, both organic and inorganic species are of interest. Methods used for such studies fall into two sub-groups. In the first, the arsenic species are separated by HPLC or ion chromatography and then determined by quartz furnace hydride generation AAS. A post-column photolysis step can be used to decompose species such as arsenocholine which do not ordinarily form volatile hydrides when reacted with sodium borohydride.[250] The sensitivity of such methods is limited by the amount of sample that can be loaded onto the chromatographic column. For example, for a 500 µL sample size, Zhang *et al.*[251] achieved detection limits ranging from 0.44 ppb for As^{V} to 0.92 ppb for MMA.

Lower detection limits can be achieved by the second approach to organo-arsenic fractionation, which relies on the differing volatilities of the various arsenic hydrides. In this protocol, arsenic species are reduced to their respective hydrides, which are then collected in a cryogenic trap. The trap is then heated slowly and the hydride species are sequentially volatilised and quantified by quartz furnace AAS. To differentiate As^{III} and As^{V} which produce the same hydride (AsH_3), pH-selective hydride generation is used; As^{III} is determined at pH *ca.* 5.0, and the total As^{III} and As^{V} is determined at pH *ca.* -0.5.[237,252] Equal sensitivity for various arsenic species can be achieved by careful pH control[253] and the use of a further reductant such as L-cysteine.[236] Sample volumes for this technique can be considerably larger than for the HPLC-based protocols. In conjunction with the pre-concentration step afforded by the cryogenic trap, extremely low detection limits can be attained. For example, Van Cleuvenbergen *et al.*[254] achieved detection limits in the range 0.002-0.0038 ppb for the determination of five organic and inorganic arsenic species in environmental water samples.

8.1.3 In This Chapter:

The remainder of this chapter is divided into four experimental sections and one discussion section. Section 8.2 describes development of an ED-ETAAS protocol for As^{III} determination. The various parameters affecting electrodeposition of As^{III} were examined. These included the deposition temperature and duration, as well as the deposition efficiencies for different media. The optimum pyrolysis temperature and the sensitivity of the method were then determined.

In Section 8.3 the ED-ETAAS protocol is extended to fractionation of arsenic species. The effects of the deposition medium and potential were examined and the method was then used to determine arsenite and arsenate concentrations in synthetic samples.

In section 8.4, arsenic fractionation protocols from the literature are experimentally evaluated as comparators for the ED-ETAAS method. The chosen method (hydride generation-ETAAS) was then used to validate ED-ETAAS results for environmental waters (Section 8.5). Each of the results sections is discussed in Section 8.6.

As for other chapters within this thesis, the experiments described in this section were performed over a period of months. Absolute sensitivity was variable over this period according to the age of the furnaces and the hollow cathode lamp used. Thus while trends can be observed across experiments, absolute absorbances should only be compared within a single experimental data set.

8.2 DETERMINATION OF ARSENITE BY ED-ETAAS

8.2.1 Experimental and Results

For all experiments in this section where palladium modifier was used, unless otherwise stated, the palladium was deposited by electrolysing 40 µL of 10 ppm palladium/0.1% HNO_3 for 20 seconds. The electrolysis was effected at the same potential as used for the corresponding arsenite deposition. For experiments where the arsenic deposition potential was varied, palladium was deposited at an applied potential of 2.0 V. All electrolyses were effected at 45 °C, with the inert gas flow switched on.

Unless otherwise stated, arsenite and arsenate solutions were prepared as described in Section 2.5.4. Arsenate stock was prepared by dissolving Na_2HAsO_4 in 1% HNO_3. Arsenite stock solution was prepared by dissolving As_2O_3 in 2.0 M potassium hydroxide solution and acidifying with 1.0% H_2SO_4. As work progressed, additional reagents were used to stabilise arsenite (hydrazine sulphate) and to remove traces of arsenate from arsenite stock solutions (L-cysteine).

8.2.1.1 Effect of Deposition Time and Acidity of the Deposition Medium

The effect of deposition time was examined by comparing the absorbances obtained for arsenite samples electrolysed for varying lengths of time. Three different concentrations of nitric acid were used for the deposition medium.

50 ppb arsenite samples were prepared in 0.05%, 0.55% and 1.05% nitric acid. 0.1 mM hydrazine sulphate was added as a stabiliser, to prevent oxidation of arsenite to arsenate. 30 µL sample aliquots were electrolysed in a palladium-modified furnace for varying durations (10-100 seconds). The deposits were then rinsed twice with 35 µL and then 40 µL of water, pyrolysed at 600 °C, and atomised at 2400 °C. Deposition was effected at 1.9 V. The results are shown in Figure 8.1.

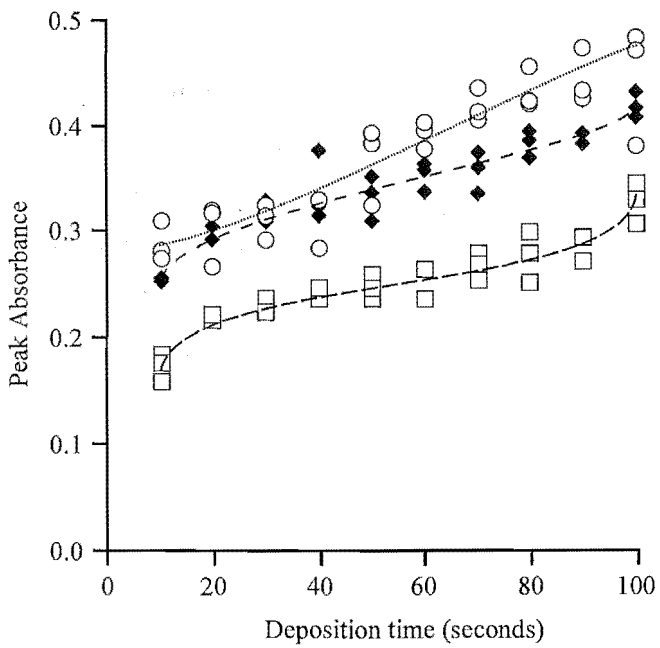

Figure 8.1 The effect of acidity and deposition time for ED-ETAAS analysis of 50 ppb arsenite samples. Samples were prepared in 0.05% HNO_3 (□) 0.55% HNO_3 (◆) and 1.05% HNO_3 (○) containing 0.1 mM hydrazine sulphate. 30 µL sample aliquots were electrolysed in a palladium-modified furnace, rinsed twice with 35 µL and then 40 µL of water, pyrolysed at 600 °C, and atomised at 2400 °C. Deposition was effected at 1.9 V.

8.2.1.2 Deposition Efficiency for ED-ETAAS

Effect of Hydrazine Sulphate

For field collection of arsenic-containing samples, it is common practice to add a preservative to prevent oxidation of arsenite to arsenate. With a view to future studies of arsenic speciation in natural waters, the effect of adding one such anti-oxidant to the deposition media was evaluated. The anti-oxidant chosen for this study was hydrazine sulphate.[233]

Samples containing 50 ppb arsenite were prepared in two different media: 1% HNO_3, and 1% HNO_3 / 0.1 mM hydrazine sulphate. 20 µL aliquots of these solutions were electrolysed for 60 seconds at 2.0 V, and redeposited for 10 seconds from 0.1% HNO_3. The deposits were pyrolysed at 600 °C and atomised at 2400 °C.

The mean peak absorbance for the sample prepared in 1% HNO_3 was 0.282 (n=6, RSD=9.2%). For the sample prepared in 1% HNO_3 / 0.1 mM hydrazine sulphate, the mean peak absorbance was 0.477 (n=6, RSD=6.1%). The mean integrated absorbances were respectively: 0.049 (RSD=16%) and 0.092 (RSD=5.1%). Consequently, samples for all subsequent experiments were prepared in hydrazine-containing media.

Percentage Deposition of Arsenite From 1% HNO_3/0.1 mM Hydrazine Sulphate Media

It was observed that lower sensitivity was observed for ED-ETAAS of arsenite solutions than for ETAAS analysis using electrodeposited palladium modifier. In an effort to explain the lower sensitivity observed for the electrodeposition method, the deposition efficiency for the electrolysis step was examined. 38 µL samples of 50 ppb arsenite, prepared in 1% HNO_3/-0.1 mM hydrazine sulphate, were electrolysed at 1.8 V in a palladium-modified furnace for 100 seconds. The spent deposition medium was then collected and analysed by conventional ETAAS with an electrodeposited palladium modifier.

The concentration of arsenic in the spent deposition medium was determined to be *ca.* 14.5 ppb. This result was then corrected for the sample-concentrating effects of sample evaporation during the electrolysis (raised temperature and inert gas flow). This correction was accomplished by weighing the collected deposition medium and comparing the average mass of samples electrolysed for 100 seconds with that for samples which were electrolysed for one second.* The average mass of the spent "100 second" medium was 20.9 mg (n=8, RSD=7.6%), whereas the average mass for the "1.0 second" medium was 38.7 mg (n=5, RSD=1.9%). Thus, taking this concentration factor of 1.85 into account the arsenic concentration in the unevaporated deposition medium was *ca.* 7.8 ppb. This corresponds to a deposition efficiency of 84%.

Effect of L-Cysteine

It was hypothesised that the less-than-quantitative deposition from 1% HNO_3/0.1 mM hydrazine sulphate medium was caused by the presence of electro-inactive arsenic species —presumably arsenate—in the arsenite standards. In order to test this theory and obtain arsenate-free standards, a reducing agent was added to the sample deposition medium. L-cysteine was chosen for this purpose because it is known to reduce As^V to As^{III},[255,256] and was considered unlikely to cause interferences during ETAAS analysis.

---

* This protocol was designed to account for spent sample medium that was not recovered by the autosampler probe. The same amount of sample medium remaining in the furnace after aspiration should be approximately the same for both 1.0 and 100 second depositions.

Two 50 ppb arsenate standards were prepared in 1% HNO_3/0.1 mM hydrazine sulphate, with one also containing 1% L-cysteine. These were analysed by ED-ETAAS, and by conventional ETAAS with an electrodeposited palladium modifier. Experimental conditions were as for the preceding experiment. Samples were prepared from fresh stock solutions. The results are shown in Table 8.1

Sample medium	Conventional ETAAS with palladium modifier	ED-ETAAS
1% HNO_3	0.515 RSD =6.7% *(0.122 RSD =6.3%)*	0.492 RSD =4.4% *(0.108 RSD =6.4%)*
1% HNO_3/ 1% L-cysteine	0.551 RSD =4.7% *(0.111 RSD =12%)*	0.619 RSD =4.3% *(0.133 RSD= 5.3%)*

Table 8.1 Relative peak and *(integrated)* absorbances for analysis of 20 µL of 50 ppb arsenate, prepared in 1% HNO_3 and 1% HNO_3,/1% L-cysteine. Samples were analysed by ED-ETAAS, and by ETAAS with an electrodeposited palladium modifier (n=4). Electrodeposition was effected at 1.8 V, for 60 seconds.

Percentage Deposition of Arsenite From 1% L-Cysteine Media

The efficiency of arsenite deposition from a 50 ppb solution, prepared in 1% HNO_3/1% L-cysteine/0.1 mM hydrazine sulphate, was determined in the same way as previously described for the 1% HNO_3/0.1 mM hydrazine sulphate medium. The concentration of arsenite in the spent deposition medium was below the detection limit of the analysis protocol used (i.e. ETAAS with electrodeposited palladium modifier). The detection limit for this particular experiment, estimated from blank measurements (n=3), was *ca.* 5 ppb. Therefore it follows that arsenite deposition from 1% HNO_3/1% L-cysteine is $\geq$ 90% efficient.

8.2.1.3 The Source of Electro-inactive Arsenic

Contamination of Stock Solutions

The possibility that stock arsenite solutions were contaminated with arsenate was investigated. This was achieved by analysing the stock arsenite solutions for arsenate. The method used for this purpose was the FIA method of Linares *et al.*[257] This method is based on the formation of arsenate-MoO_4^{2-} heteropoly acids under acidic conditions. Reduction of these species produces an intensely coloured Mo^V complex which is detected at 820 nm using a spectrophotometer.

Fresh stock solutions of arsenite and arsenate were prepared at a concentration of 100 ppm. These solutions were prepared in media of almost neutral pH because strong acidity interfered with the analysis. The stock arsenate solution was prepared in water and diluted to produce a series of standards ranging from 0.4 to 2.0 ppm. These standards were used to produce the calibration curve shown in Figure 8.2. Arsenite stock solution was prepared by dissolving solid As_2O_3 in 0.5 mL KOH, diluting with water, and neutralising with 31 µL of (conc) HNO_3. This stock was then diluted to produce a working standard of 2.0 ppm. FIA analysis

of this solution showed that the arsenate concentration was below the detection limit of the technique, which was estimated to be *ca.* 0.04 ppm arsenate. Thus, less than 2% of the arsenic in the arsenite standard was present as arsenate.

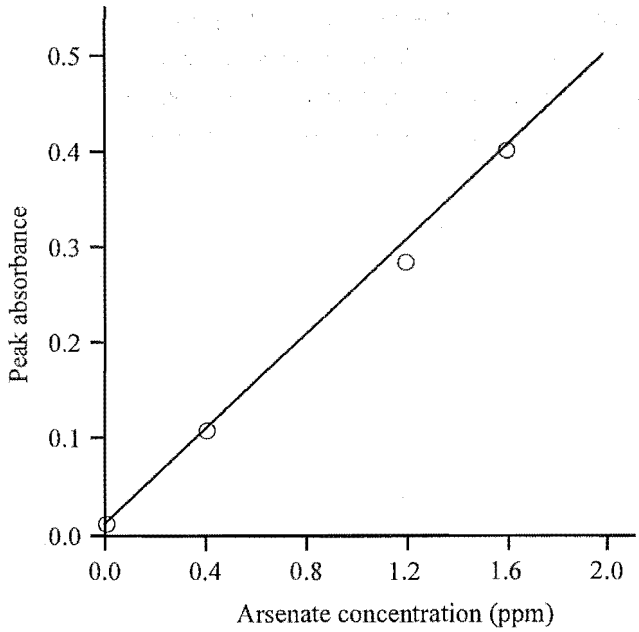

Figure 8.2 Calibration curve for the determination of arsenate by the FIA method of Linares *et al.*[257]

In-situ Arsenate Generation

The possibility that arsenate was being produced by *in-situ* oxidation of arsenite at the anode was investigated. This was done by analysing the spent sample deposition medium for total arsenic, and electro-inactive arsenic.

A working standard containing 100 ppb arsenite was prepared in 1% HNO_3/0.1 mM hydrazine sulphate, from a freshly prepared stock solution.* 20 µL aliquots of this standard were electrolysed for 100 seconds in a palladium-modified furnace at 1.8 V, 45 °C, with the inert gas on. After electrolysis, the spent solution was collected in a vial, and used to prepare two sub-samples—one diluted 50% with water, the other diluted 50% with 1% L-cysteine. These were then analysed by ED-ETAAS using the following protocol: 20 µL of sample was electrolysed at 1.8 V in a palladium-modified furnace for 100 seconds. The resulting deposit was rinsed with 30 µL of water for 40 seconds, and then rinsed with 35 µL of water for 40 seconds.

* The 1 ppm arsenite stock solution was prepared as described in Section 2.5.4, but with the addition of 0.5% L-cysteine. This was used to reduce any arsenate in the solution to arsenite. It was independently verified (results not shown) that the L-cysteine concentration in working solutions prepared by twenty-fold dilution of this stock (0.005%) was insufficient to reduce any residual arsenate present in the spent deposition medium.

The results showed no detectable arsenic in the sample that was prepared in water. However, for the sample that was prepared in 0.5% L-cysteine, a mean peak absorbance of 0.217 (n = 3, RSD = 5.8%) was recorded (a mean integrated absorbance of 0.041; RSD = 15.2%). (This was not calibrated against a standard solution at the time. However, absorbances of this magnitude usually correspond to arsenite concentrations of *ca.* 14-20 ppb.)

8.2.1.4 Analyte Stabilisation

Effect of Palladium

The thermally stabilising effects of the palladium modifier were evaluated by comparing absorbance-time profiles in the presence and absence of the modifier. Platform atomisation was used for this experiment because results, in the absence of palladium, were irreproducible when wall atomisation was used. When palladium was used, the platform was modified with palladium in same way as for furnace-wall modification, except that the modifier volume was decreased from 40 µL to 20 µL because of the platform's small sample cavity.

20 µL aliquots of 50 ppb arsenite, prepared in 1% HNO_3, were conventionally (thermally) deposited onto a pyrolytic-coated graphite platform, dried to 150 °C, pyrolysed at 600 °C, and atomised at 2400 °C.* The experiment was repeated using a palladium-modified platform. The results are shown in Figure 8.3. The double peak, observed for atomisation in the absence of palladium, became a single peak when pyrolysis temperatures above 600 °C were used; the low temperature component (left-hand shoulder) disappeared leaving only the higher-temperature component (right-hand shoulder). Absorbance-time profiles for electrodeposited arsenite on a palladium-modified platform (not shown), were the same as for the thermally deposited arsenite in the presence of palladium (Figure 8.3) except that the absolute sensitivity was diminished.

Pyrolysis Curves

Pyrolysis curves for arsenic deposited on palladium were examined in order to optimise the pyrolysis temperature used in the analysis protocol. The thermal stabilities of conventionally deposited, and electrodeposited arsenic were compared.

Arsenic was deposited thermally and by electrodeposition, onto a palladium modified furnace from 20 µL of 50 ppb arsenite prepared in 1.0% HNO_3. Electrodeposition was carried out for 60 seconds, at 3.0 V. The sample deposits were pyrolysed at temperatures ranging from 400 °C to 1550 °C, and atomised at 2400 °C. The results are shown in Figure 8.4.

---

* Actual temperatures on the surface of the platform would have been lower due to the cooling effect of the inert gas flow during pyrolysis and the poor thermal conductivity between the platform and furnace.

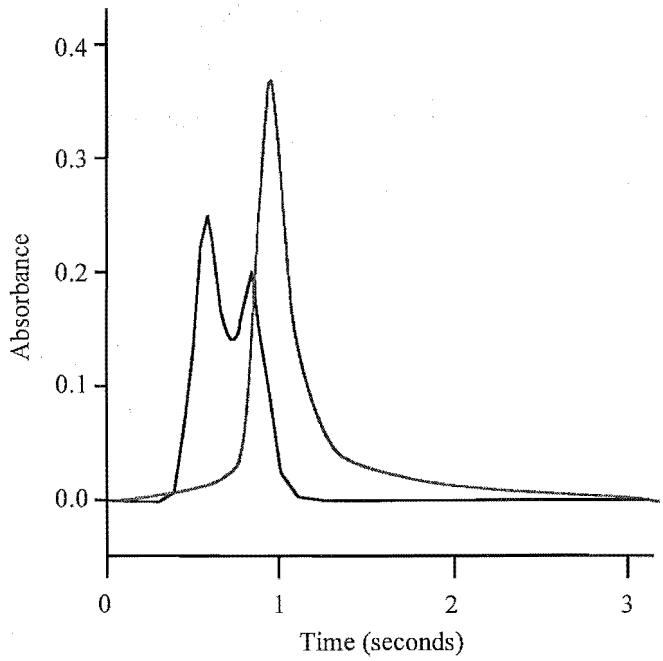

Figure 8.3. Absorbance-time profiles for arsenite atomisation in the presence (——) and absence (——) of electrodeposited palladium modifier. 20 μL aliquots of 50 ppb arsenite, prepared in 1% HNO_3, were conventionally (thermally) deposited onto a pyrolytic-coated graphite platform, dried to 150 °C, pyrolysed at 600 °C, and atomised at 2400 °C.

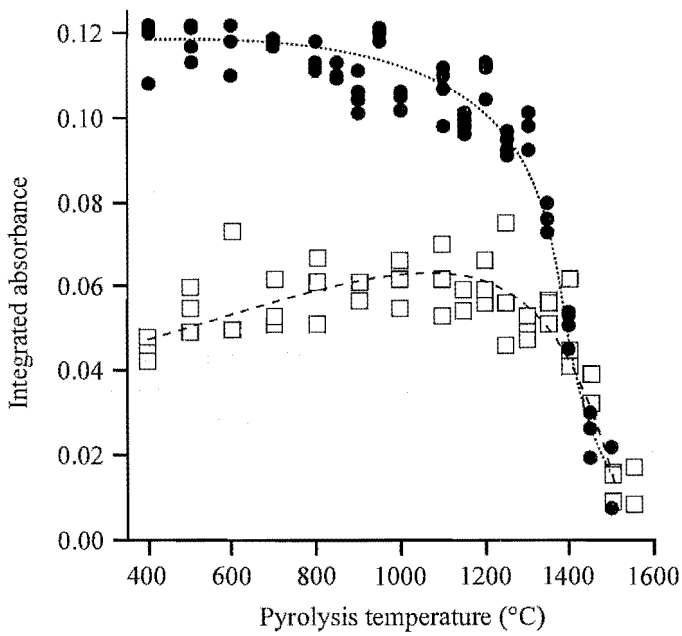

Figure 8.4 Effect of pyrolysis temperature on absorbance for arsenic electrodeposited (□) and conventionally deposited (●) onto a palladium-modified furnace. Samples were deposited from 20 μL of 50 ppb arsenite prepared in 1.0% HNO_3, and atomised at 2400 °C. Electrodeposition was effected for 60 seconds, at 3.0 V.

Absorbance-time Profiles

The absorbance-time profiles for arsenic determination by ETAAS and ED-ETAAS were compared. A 20 µL sample of 100 ppb arsenite, prepared in 1% HNO_3 / 1% L-cysteine was analysed by ETAAS with electrodeposited palladium modifier, and by ED-ETAAS. For ED-ETAAS, the sample was electrolysed in a palladium modified furnace for 100 seconds at 2.0 V. For both protocols, samples were pyrolysed at 500 °C, and atomised at 2400 °C using a 633 °C s^{-1} temperature ramping rate. The results are shown in Figure 8.5.

8.2.1.5 Sensitivity and Detection Limits

The detection limits for ED-ETAAS measurement of arsenite were determined. The effects of deposition medium (1% HNO_3 vs. 1% L-cysteine/1% HNO_3) and mode of absorbance measurement (peak vs integrated absorbance) were evaluated.

A fresh 100 ppm arsenate stock was prepared in 1% H_2SO_4/0.5% L-cysteine, and allowed to stand overnight. Duplicate 4 ppb samples were prepared by dilution of this stock; two in 1% HNO_3/0.1 mM hydrazine sulphate, and two in 1% L-cysteine/1% HNO_3/0.1 mM hydrazine sulphate. 39 µL aliquots (calibrated by mass) of these samples were electrolysed in a palladium-modified furnace for 60 seconds. The resulting deposit was rinsed once with 40 µL of water for 10 seconds, pyrolysed at 500 °C, and atomised at 2400 °C. Electrolysis conditions were: 2.0 V, 45 °C, with inert gas on. Eight replicate measurements were made for each duplicate sample. ie. 16 measurements for each sample medium. The results are shown in Table 8.2.

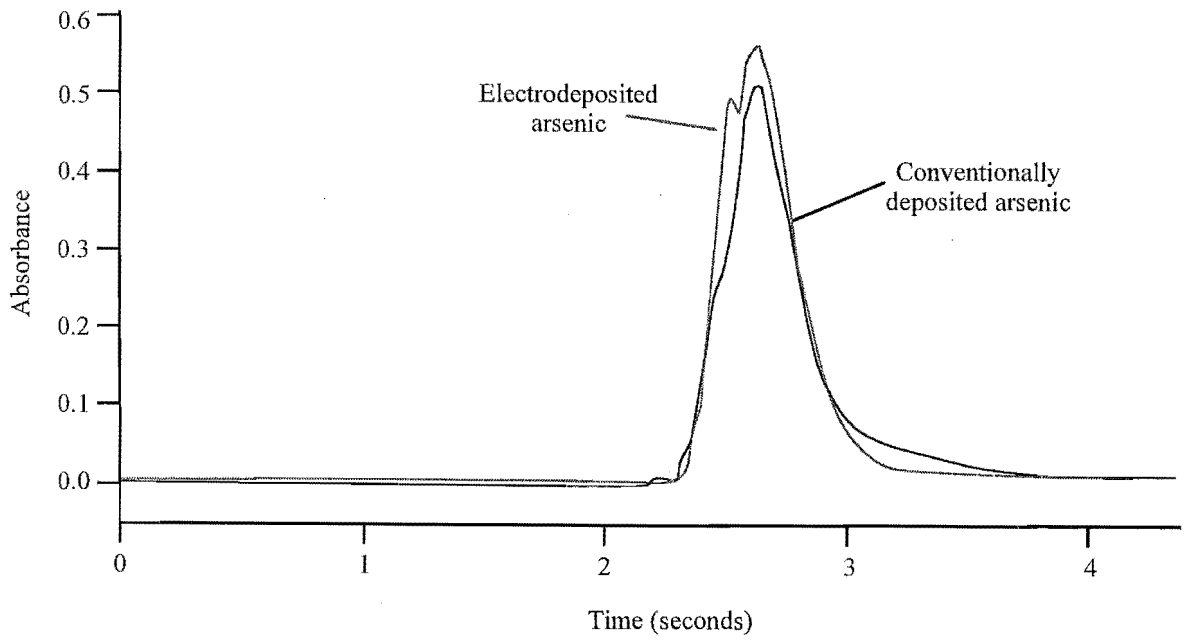

Figure 8.5 Absorbance-time profiles for determination of 2 ng arsenite by ED-ETAAS and by ETAAS with electrodeposited palladium modifier. Samples were prepared in 1% HNO_3 / 1% L-cysteine. For ED-ETAAS, the sample was electrolysed at 2.0 V for 100 seconds. For both protocols, samples were pyrolysed at 500 °C, and atomised at 2400 °C using a 633 °C s^{-1} temperature ramping rate.

	1% HNO_3 / 0.1 mM hydrazine sulphate		1% HNO_3 / 0.1 mM hydrazine sulphate / 1% L-cysteine	
Characteristic mass (n = 16)	7.5 pg	*(67 pg)*	6.6 pg	*(52 pg)*
Detection Limit (2σ, n = 16)	0.58 ppb	*(3.37 ppb)*	1.32 ppb	*(3.1 ppb)*

Table 8.2 Characteristic masses and detection limits for arsenite deposited from 39 µL aliquots of two different media, as determined using peak and *(integrated)* absorbances

8.2.1.6 Comparison of ETAAS and ED-ETAAS

To compare the relative sensitivities of arsenite determination by ETAAS and ED-ETAAS, calibration curves for arsenite determination were prepared for conventional ETAAS, and for ED-ETAAS. For both protocols, a pyrolytic-coated graphite furnace platform modified with electrodeposited palladium was used. Arsenate standards ranging from 10 to 140 ppb were prepared in appropriate media for each method: 1% HNO_3 for ETAAS, and 1% HNO_3/1% L-cysteine for ED-ETAAS. 27 µL samples were used for each measurement. For the ED-ETAAS protocol, sample deposition was effected at 2.5 V. For both protocols, samples were pyrolysed at 700 °C and atomised at 2400 °C. The results are shown in Figure 8.6.

The primary aim of this section was to establish an ED-ETAAS protocol that would allow separate determination of arsenite and arsenate in samples that contained both species. The strategy used to achieve this aim was based on the "electro-inactive" nature of arsenate. A brief investigation of monomethylarsonic acid determination was also conducted.

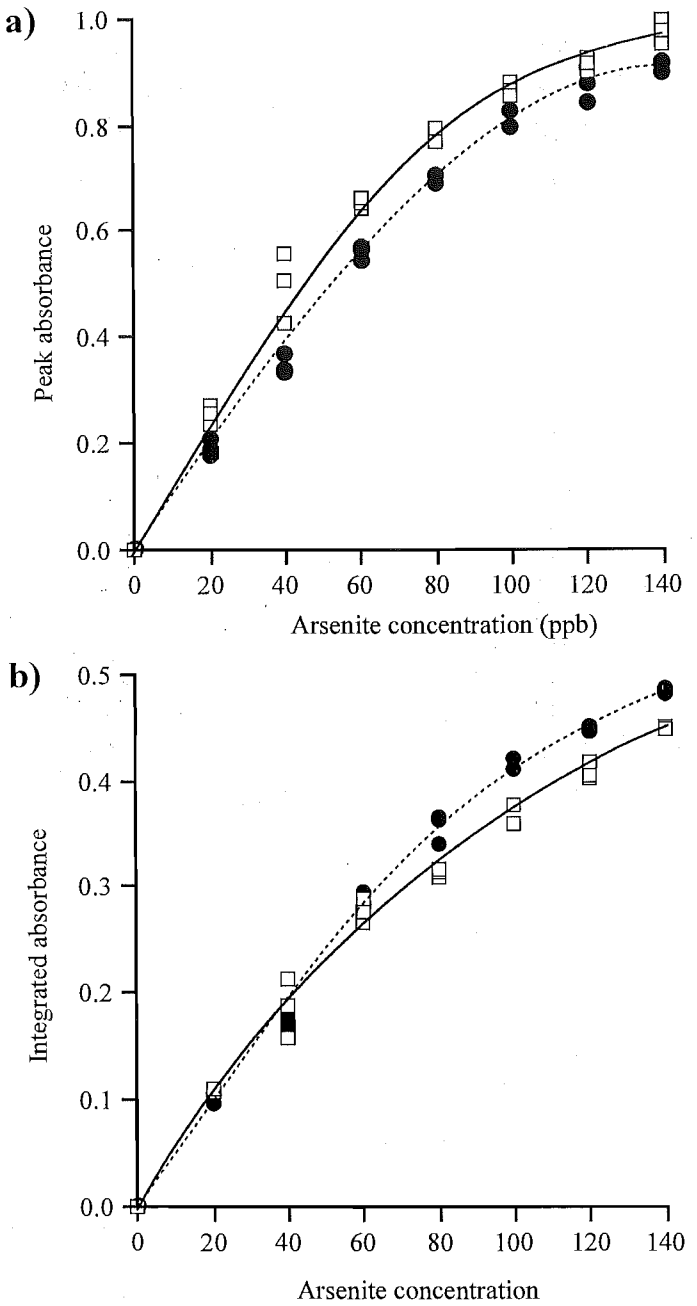

Figure 8.6 Calibration curves for arsenite determination using peak absorbance (a) and integrated absorbance (b) ETAAS with palladium modifier (□), and ED-ETAAS with palladium modifier (●). Samples for ETAAS were prepared in 1% HNO_3 whereas samples for ED-ETAAS were prepared in 1% HNO_3/1% L-cysteine. Arsenic was deposited onto a palladium-modified platform from 27 µL sample aliquots. For electrodeposition, samples were electrolysed for 60 seconds at 2.5 V. For both protocols, samples were pyrolysed at 700 °C and atomised at 2400 °C.

8.3 FRACTIONATION OF ARSENIC SPECIES BY ED-ETAAS

8.3.1 Determination of Arsenate

8.3.1.1 Effect of the Deposition Potential

20 µL aliquots of 50 ppb As^V and As^{III}, prepared in 1% HNO_3, were electrolysed in a palladium-modified furnace for 60 seconds. Electrolysis was effected at 45 °C, with inert gas on, using deposition potentials in the range 0.0-4.5 V. The deposits were pyrolysed at 600 °C, and atomised at 2400 °C. The results are shown in Figure 8.7.

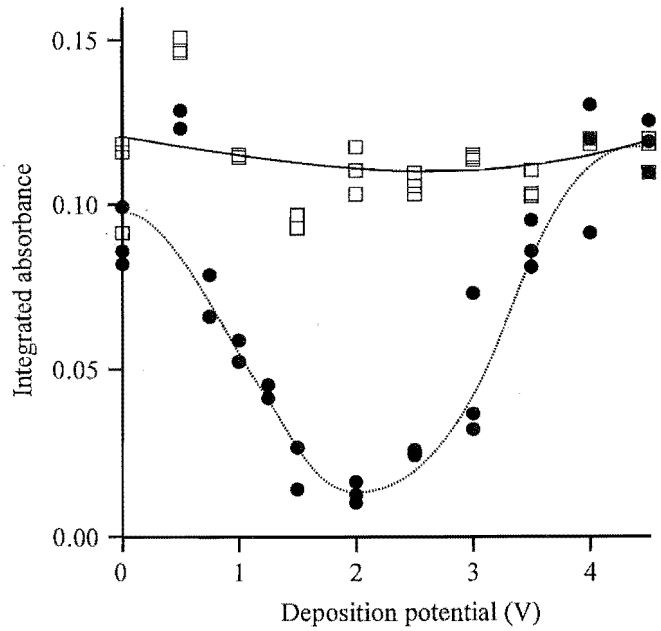

Figure 8.7 The effect of electrolysis potential on the deposition of 50 ppb arsenate (●) and arsenite (□) solutions prepared in 1% HNO_3. 20 µL samples were electrolysed in a palladium-modified furnace for 60 seconds. The deposits were pyrolysed at 600 °C, and atomised at 2400 °C.

8.3.1.2 Effect of L-Cysteine

The relative sensitivities for ED-ETAAS determination of arsenate and arsenite were compared, in the presence and absence of 1% L-cysteine.

Duplicate 50 ppb solutions of arsenite, and arsenate were prepared, both in 1% HNO_3, and in 1% HNO_3/1% L-cysteine media. 20 µL aliquots of these samples were electrolysed in a palladium-modified furnace at 2.0 V, 45 °C, with the inert gas on. The deposits were pyrolysed at 600 °C and atomised at 2400 °C. The results are shown in Table 8.3. For the L-cysteine-based medium, it was shown (using a *t*-test, with $P = 0.01$) that the absorbances for arsenite and arsenate were not significantly different.

	1% HNO_3 medium: peak and *(integrated)* absorbances (n = 6)	1% HNO_3/1% L-cysteine medium: peak and *(integrated)* absorbances (n = 6)
Arsenite	0.408, RSD = 7.03% *(0.076, RSD = 4.3%)*	0.588, RSD = 5.9% *(0.119, RSD = 8.8%)*
Arsenate	0.045, RSD = 17.3% *(0.014, RSD = 56%)*	0.602, RSD = 5.2% *(0.122, RSD = 5.45%)*

Table 8.3 Relative absorbances for ED-ETAAS determination of arsenate and arsenite in the presence and absence of L-cysteine using a deposition potential of 2.0 V.

8.3.2 Determination of MMA

The determination of MMA by ED-ETAAS was examined, and the sensitivity compared with that for arsenate and arsenite. The effect of the deposition potential was evaluated to determine whether MMA could be selectively determined in the presence of inorganic arsenic species.

8.3.2.1 Effect of Deposition Potential

Two 25 ppb solutions of MMA were prepared: one in 1% HNO_3 and one in 1% HNO_3 / 1% L-cysteine. 20 µL samples were electrolysed for 60 seconds at a range of potentials on a palladium-modified furnace platform. The deposits were pyrolysed at 700 °C and atomised at 2400 °C. The results are shown in Figure 8.8.

8.3.2.2 Relative Sensitivity for As^{III} and MMA

The relative absorbances for solutions containing As^{III} and MMA were compared. Samples containing 50 ppb arsenite/25 ppb MMA* were prepared in both 1% HNO_3 and 1% HNO_3/L-cysteine media. All samples were prepared in triplicate. 20 µL aliquots were then analysed by ED-ETAAS and by ETAAS with electrodeposited palladium modifier. Three replicate measurements were made for each sample ie. a total of nine measurements for each analyte/sample medium combination.

For ED-ETAAS analysis, samples were electrolysed for 60 seconds in a palladium-modified furnace at 1.9 V. The deposits were then rinsed with 36 µL of water for 5.0 seconds. For both ED-ETAAS and conventional protocols, samples were pyrolysed at 500 °C and atomised at 2400 °C. The results are shown in Table 8.4. Absorbances for MMA have been normalised to compensate for the lower concentration of the MMA standard. This assumes a linear calibration curve in the range 25-50 ppb.

---

* The different concentrations used here were due to an impure MMA sample, the stoichiometry of which, was not known until after this experiment was performed (see Section 2.5.4).

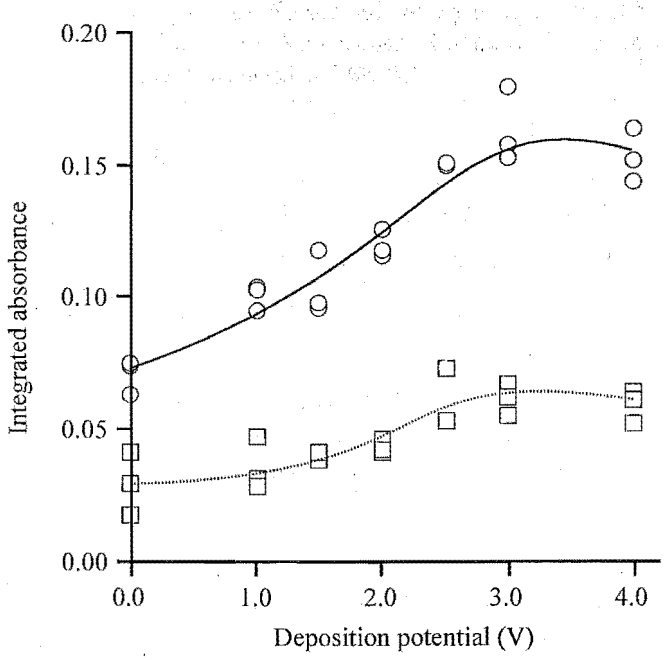

Figure 8.8 The effect of deposition potential on absorbance for ED-ETAAS analysis of 0.53 pg of MMA, prepared in 1% HNO_3 (□) and 1% HNO_3 / 1% L-cysteine (○). 20 µL samples were electrolysed for 60 seconds at a range of potentials on a palladium-modified furnace platform. The deposits were pyrolysed at 700 °C and atomised at 2400 °C.

	ED-ETAAS		ETAAS
	1% HNO_3 medium	1% L-cysteine/ 1% HNO_3 medium	1 % HNO_3 medium
As^{III}	0.312 RSD = 5.7%	0.367 RSD = 7.4%	0.419 RSD = 3.7%
	(0.077 RSD = 10.9%)	*(0.087 RSD = 7.1%)*	*(0.101 RSD = 3.3%)*
MMA	0.043 RSD = 14.0%	0.359 RSD = 11.1%	0.434 RSD = 4.2%
	(0.009 RSD = 198%)	*(0.086 RSD = 13%)*	*(0.101 RSD = 6.9%)*

Table 8.4 Comparison of mean peak and *(integrated)* absorbances for analysis of As^{III} and MMA. For ED-ETAAS analysis, samples were electrolysed for 60 seconds in a palladium-modified furnace at 1.9 V. The deposits were then rinsed with 35 µL of water for 5.0 seconds. For both ED-ETAAS and conventional protocols, samples were pyrolysed at 500 °C and atomised at 2400 °C.

8.3.3 Arsenic Fractionation in Synthetic Samples

The ED-ETAAS protocol was used to determine arsenite in a series of synthetic samples which contained 50 ppb arsenic, in varying As^{V}/As^{III} ratios. The results were compared with those for conventional ETAAS analysis (using electrodeposited palladium modifier) of the same solutions.

50 ppb solutions containing arsenite or arsenate each were prepared in 1% H_2SO_4 / 0.1 mM hydrazine sulphate media. Because the arsenite sample solution contained 0.25 mM L-cysteine (from dilution of the pre-reduced arsenite stock solution), the arsenate sample was also prepared containing 0.25 mM L-cysteine.

During analysis, the autosampler was used to prepare constant-volume samples (21.3 µL) that contained varying ratios of the two standard solutions. For ED-ETAAS, the samples were electrolysed at 1.8 V in a palladium-modified furnace for 100 seconds, rinsed with 30 µL of water for 40 seconds, then with 40 µL of water for 5.0 seconds. For both the ED-ETAAS and ETAAS protocols, samples were pyrolysed at 500 °C and atomised at 2400 °C. The results are shown in Figure 8.9.

8.4 EVALUATION OF ALTERNATIVE ARSENIC FRACTIONATION METHODS

In order to validate the ED-ETAAS arsenic determination protocol, it was necessary to either analyse standard reference materials, or to use an established method as a comparison. A standard reference material was unavailable within this department at the time of this research so a comparative analysis method was sought. Potentially suitable methods (according to the equipment available) were selected from the literature. On this basis, three protocols were chosen for further evaluation: two electrochemical methods, and one hydride-generation method.

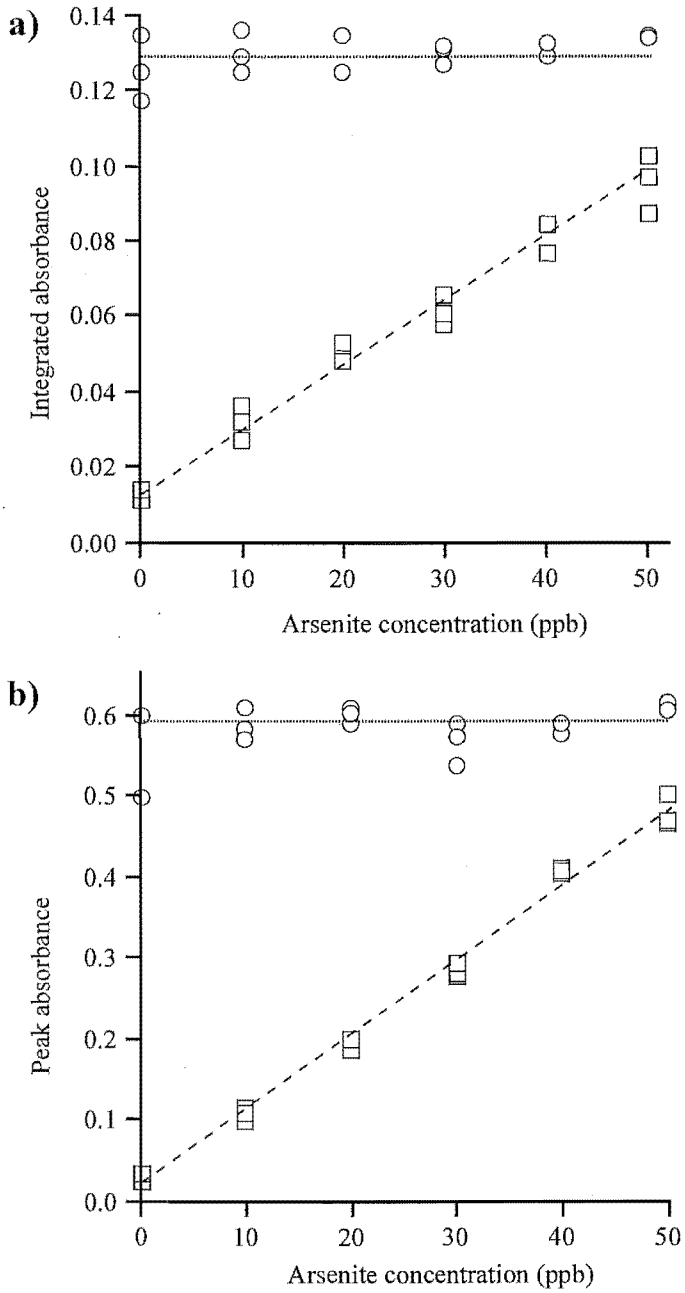

Figure 8.9 Analysis of 1.06 ng arsenic by ED-ETAAS (□) and ETAAS (○), using solutions containing various As^{III}/As^{V} ratios. Samples prepared in 1% H_2SO_4/0.1 mM hydrazine sulphate/0.25 mM L-cysteine media. For ED-ETAAS, samples were electrolysed in a palladium-modified furnace for 100 seconds, rinsed with 30 µL of water for 40 seconds, then with 40 µL of water for 5.0 seconds. For both the ED-ETAAS and ETAAS protocols, samples were pyrolysed at 500 °C and atomised at 2400 °C.

8.4.1 CSV in the Presence of Cu^{2+}

This cathodic stripping voltammetry method, originally developed by Sadana,[231] was used by Li and Smart[233] to determine sub-nanomolar concentrations of arsenite in natural waters. It involves reductive accumulation of arsenite on the HMDE, in the presence of 2.0 M HCl / 0.8 mM $CuCl_2$, as an intermetallic compound (Equations 8.1 and 8.2). This intermetallic is then reduced to produce an analytical current (Equation 8.3).

$$Cu^{2+} + 2e^- \rightarrow Cu(Hg) \qquad \text{(Equation 8.1)}$$

$$2As^{3+} + 3Cu(Hg) + 6e^- \rightarrow Cu_3As_2 + 3Hg \qquad \text{(Equation 8.2)}$$

$$Cu_3As_2 + 12H^+ + 12e^- + 3Hg \rightarrow 2AsH_3 + 3H_2 + 3Cu(Hg) \qquad \text{(Equation 8.3)}$$

For this work, the method of Li and Smart[233] was followed. A reagent solution that contained 2.0 M HCl / 50 ppm Cu^{2+} / 40 µM hydrazine sulphate was prepared. The solution was purged with nitrogen for five minutes, and then analysed to provide a measurement of the reagent blank. A range of arsenite concentrations, ranging from 0.0 to 115 ppb, was prepared by adding increments of a 1 ppm arsenite standard to the solution. Replicate analyses were made in between each addition.

Analysis involved depositing the arsenite at -0.55 V (vs. Ag/AgCl) for 60 seconds and then scanning the potential to -1.075 V (using square-wave). The arsenite reduction peaks were measured at -0.91 V vs. Ag/AgCl. The blank-corrected results are shown in Figure 8.10.

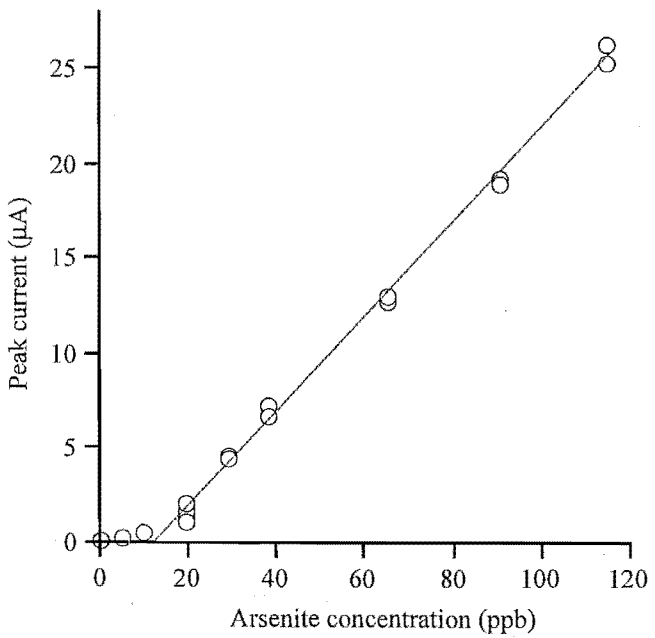

Figure 8.10 Calibration curve for determination of arsenite by CSV. Arsenite prepared in 2.0 M HCl/ 50 ppm Cu^{2+} / 40 µM Hydrazine sulphate. Arsenite was deposited at-0.55 V (vs. Ag/AgCl) for 60 seconds. The potential was then scanned to -1.075 V (using square-wave). Arsenite reduction peaks were measured at -0.91 V vs. Ag/AgCl.

8.4.2 CSV in the Presence of PDC

This protocol which measured arsenite was successfully used by Zima and van den Berg to determine total arsenic in seawater (a pre-reduction step was used to convert arsenate to arsenite).[229] Arsenic was accumulated on the HMDE as As(Hg) by accumulation at -0.3 V (vs. Ag/AgCl). The arsenic was re-oxidised by setting the potential to 0.0 V, forming an adsorbed arsenite-pyrrolidine dithiocarbamate (PDC) complex. The potential was then scanned to more negative potentials (*ca.* -0.8 V), reducing the PDC-arsenite complex to arsenite. The analytical current from this reduction, at *ca.* -0.2 V, was shown to be proportional to the arsenite concentration.

In this work, the method was tested by determining arsenite in a surface water from Johns Road, near a timber treatment plant (see Section 2.6.0.2). This water was known to contain *ca.* 20 ppb arsenite (determined by ED-ETAAS). A sample of Johns Road water was spiked with PDC and NaCl to produce a solution containing 1 μM PDC / 0.1 M NaCl. The solution was purged with nitrogen for five minutes. Arsenic was accumulated at -0.5 V for 300 seconds. The potential was then scanned from 0.05 to -0.70 V using the square wave stripping mode. The peak current was measured at *ca.* -0.04 V *vs.* Ag / AgCl. 100 μL standard additions of 1 ppm arsenite were used to quantify the arsenite content. The results are shown in Figure 8.11.

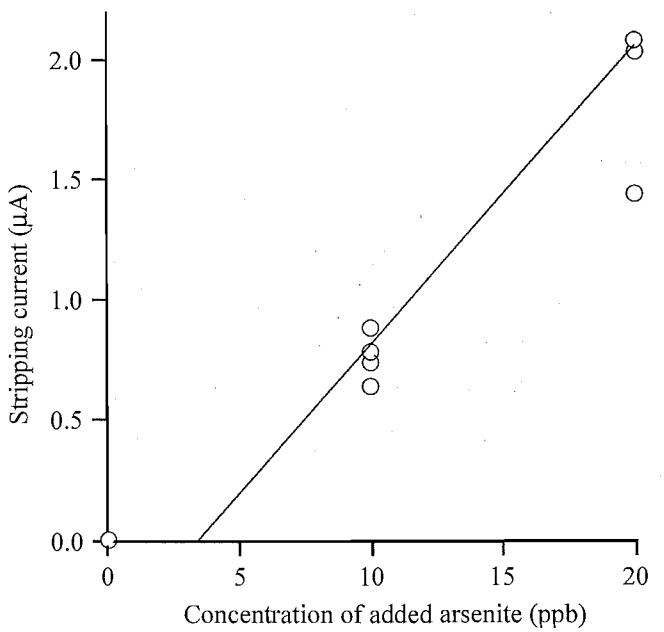

Figure 8.11 Standard additions plot for determination of arsenite in Johns Road water by CSV in the presence of 1 μM PDC / 0.1 M NaCl. The solution was purged with nitrogen for five minutes before depositing arsenic at -0.5 V for 300 seconds. The potential was then scanned from 0.05 to -0.70 V using the square wave stripping mode. The peak current was measured at *ca.* -0.04 V *vs.* Ag / AgCl.

A similar standard additions plot (i.e. with a positive x-intercept) was observed for analysis of Devil's Creek water. In an effort to explain the positive x-intercepts of these plots, possible interferences, as mentioned by Zima and van den Berg,[229] were examined. ETAAS analysis of the Johns Road water sample showed that it contained *ca.* 10 ppb copper. The effect of this copper concentration on the CSV analysis was investigated.

A solution containing 10 ppb arsenite was prepared in 1% HNO_3 / 0.1 M NaCl / 1 μM PDC. The solution was analysed by the CSV method, spiked with 10 ppb Cu^{2+}, and then analysed again. The resulting square-wave stripping voltammograms are compared in Figure 8.12.

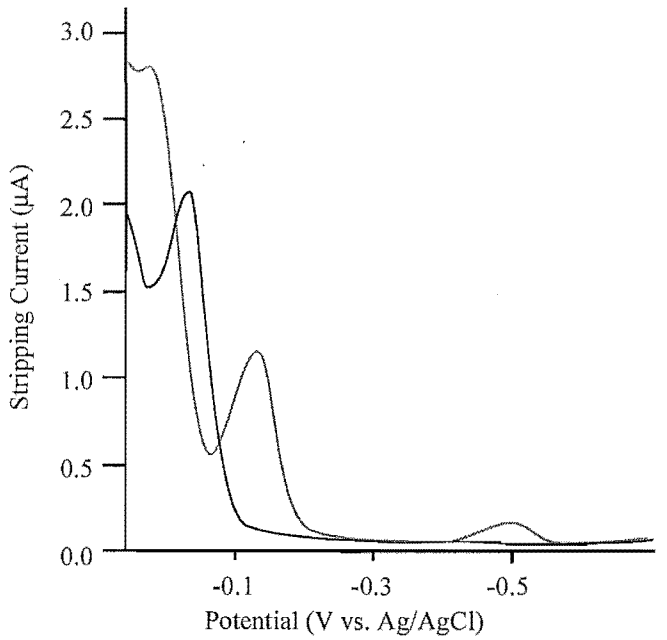

Figure 8.12 The effect of copper on arsenic determination by CSV in the presence of PDC. Square wave stripping voltammograms for arsenite in the presence(——) and absence(——) of 10 ppb Cu^{2+}. The sample solution was prepared in 1% HNO_3 / 0.1 M NaCl / 1 μM PDC.

8.4.3 Hydride-Generation ETAAS

The next arsenic fractionation method assessed was based on pH-dependent hydride generation. Reaction of arsenite with sodium borohydride produces arsine at pH values below 5.0, whereas arsenate only reacts at a significant rate below pH 2.0.[249] Based on this, a protocol was designed in which arsenite was reduced by sodium borohydride in acetate buffer (pH 5.0). The resulting arsine was accumulated on the inner surface of a furnace that had been modified with electrodeposited palladium, and measured by ETAAS. This technique is referred to as HG-ETAAS.

Arsine was produced using the GBC HG3000 hydride generator (see Section 2.2.2.6). The reductant used was 0.15% (w/v) sodium borohydride solution which contained 0.15% (w/v) potassium hydroxide. The pH regulator was *ca.* 0.5 M acetate buffer, pH 5.0. A 10 ppb arsenate standard and a series of arsenite standards ranging from 0.0 to 10 ppb were prepared in 1.0% HNO_3. Arsine gas produced by the HG3000 was passed into a heated furnace (400 °C) which had been pre-modified with palladium. The arsine was collected for 15 seconds. To compensate for the time taken by the arsine to pass through the length of the sample introduction tube, the HG3000 was started 45 seconds prior to the start of sample accumulation. The sample was then atomised at 2400 °C. Analysis of the standard solutions produced the calibration curve shown in Figure 8.13. The response measured for the 10 ppb arsenate solution was the same as for the blank.

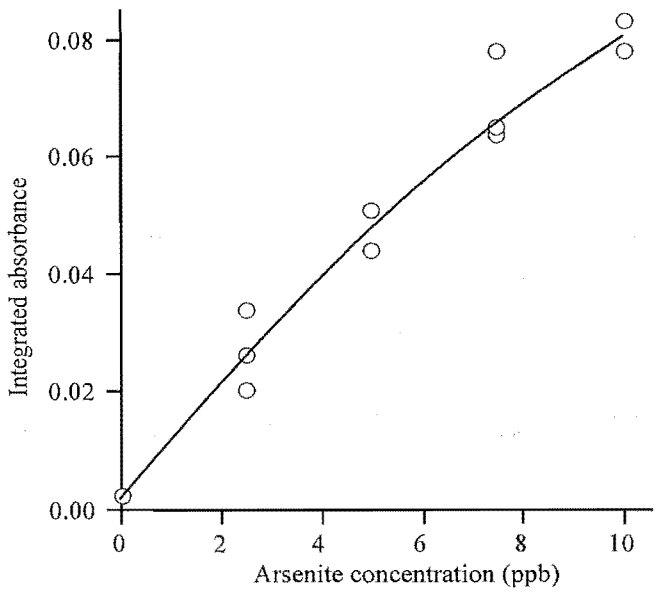

Figure 8.13 Calibration curve for determination of arsenite by pH-selective HG-ETAAS. Arsenite standards were prepared in 1% HNO_3 and reacted with sodium borohydride at pH 5.0. The resulting arsine was accumulated for 15 seconds on a palladium-modified furnace at 400 °C and atomised at 2400 °C.

8.5 FRACTIONATION OF ARSENIC SPECIES IN NATURAL WATERS

ED-ETAAS was used to determine arsenite and total arsenic in two natural waters. The waters used were from Devil's Creek, and Johns Road (see Section 2.6.0.2). Arsenite was determined following electrodeposition from 1% HNO_3. Total arsenic was determined following electrodeposition from 1% HNO_3 / 1% L-cysteine. For comparative analysis, arsenite was determined by HG-ETAAS with borohydride reduction at pH 5.0. Total arsenic was determined by ETAAS using an electrodeposited modifier.

ED-ETAAS and ETAAS: Samples of Devil's Creek, and Johns Road water were filtered to 0.025 μm, and prepared in two different media: 1% HNO_3 / 0.1 mM hydrazine sulphate, and 1% L-cysteine / 1% HNO_3 / 0.1 mM hydrazine sulphate. 20 μL sample aliquots were analysed by ED-ETAAS and by ETAAS. For ED-ETAAS, samples were electrolysed for 100 seconds at 1.8 V. The deposits were sequentially rinsed with 30 μL of water for 40 seconds, and 40 μL of water for 5 seconds. For both ED-ETAAS and ETAAS, samples were pyrolysed at 500 °C and atomised at 2400 °C. Separate calibration curves were measured for each protocol and sample medium.

HG-ETAAS: Samples of Devil's Creek, and Johns Road water were filtered to 0.025 μm. For the Devil's Creek water, which was not acidified, a 5 mL sample was diluted 10-fold to produce sufficient volume for the analysis. For the acidified Johns Road sample, a similar 10-fold dilution was performed, but with the addition of sufficient potassium hydroxide to raise the pH to *ca.* 3.0. This was so that sample acidity did not interfere with the buffering of the pH-selective hydride generation step. The two samples and calibration standards were analysed using the same protocol described in Section 8.4.3.

The results of the four different analyses are summarised in Table 8.5.

	Arsenite		Total Arsenic	
	HG-ETAAS	ED-ETAAS	ETAAS	ED-ETAAS
Devil's Creek Water	n/d *n/d*	n/d *n/d*	44.1±3.7 ppb *(51.9±3.0 ppb)*	44.7±2.9 ppb *(42.9±5.3 ppb)*
Johns Road Water	21±12 ppb *(23±12 ppb)*	23.1±4.0 ppb *(18.6±7.4 ppb)*	46.2±1.9 ppb *(52.9±6.2 ppb)*	46.8±3.9 ppb *(45.2±2.3 ppb)*

Table 8.5 Determination of arsenite and total arsenic in environmental waters. Results are shown for peak and *(integrated)* absorbances. (n/d = none detected.)

8.6 DISCUSSION

8.6.1 Arsenite Analysis

8.6.1.1 Deposition Efficiency

Figure 8.1 shows the effects of acidity and deposition time on the peak absorbance for arsenite determination by ED-ETAAS. It can be seen that lower acid concentrations produced smaller absorbances than for the 1.05 % HNO_3 medium. For all three media, almost fifty percent of the maximum absorbance was reached after only 10 seconds. However, unlike the metals investigated earlier, the arsenite deposition did not quickly reach a maximum. For all three media, the absorbance continued to increase up to the 100 second deposition time. In the case of the 1.05% HNO_3 medium, *ca.* 90% of the maximum deposition was effected within 60 seconds.

The amount of analyte deposition at the 60-second deposition time increased when the reducing agent hydrazine sulphate was added to the electrolysis medium (Section 8.2.1.2). The mean peak absorbance for a sample prepared in 1% HNO_3 increased from 0.280 to 0.477 in the presence of 0.1 mM hydrazine.

There are several possible explanations for this result. One is that the deposition kinetics are enhanced by the presence of a reducing agent i.e. the rate of chemical re-oxidation at the cathode is slowed relative to the rate of electrochemical reduction. Another is that there is a proportion of electro-inactive arsenate present in the arsenite standards, which is reduced by the hydrazine sulphate. However, a separate experiment (results not shown) indicated that arsenate is not reduced by low concentrations of hydrazine. A third possibility is that arsenate is produced *in-situ* during sample deposition—either by direct oxidation at the anode, or by oxygen which is produced at the anode. In either case, a reducing agent could decrease the rate of oxidation: either by decreasing the rate of arsenite oxidation kinetics at the anode, or by competitive reduction of oxygen in solution.

The deposition efficiency for arsenite in the presence of hydrazine sulphate was determined by analysis of the spent deposition medium to be *ca.* 80%. As a result, for analysis of samples prepared in 1% HNO_3 /1% hydrazine sulphate media, sensitivity observed for arsenic determination by ED-ETAAS was significantly lower than for ETAAS in the presence of electrodeposited palladium modifier.

In an attempt to gain a better understanding of the system and to improve the deposition efficiency, the reducing agent L-cysteine, which is known to reduce arsenate, was added to the deposition medium. Table 8.1 shows that the absorbances for ED-ETAAS arsenite determination were significantly enhanced for the L-cysteine containing media. This sensitivity enhancement was *ca.* 25%, for both peak and integrated absorbances. The effect of L-cysteine on the absorbances for conventional ETAAS was not statistically significant.

It was shown by analysis of the spent deposition medium, that arsenite deposition from a medium containing 1% L-cysteine/1% HNO_3/0.1 mM hydrazine sulphate was greater than 90% efficient. Unfortunately, we were unable to demonstrate quantitative deposition because of experimental limitations: the ETAAS method used to analyse the spent deposition medium was not sufficiently sensitive. However, comparison of the absorbances for ETAAS and ED-ETAAS shown in Table 8.1 suggests that deposition is quantitative.

Possible reasons for non-quantitative deposition in the absence of L-cysteine were investigated. We hypothesised that there was a fraction of electro-inactive arsenic, present or generated, in the arsenite standards. It was assumed that this electroactive arsenic was present as arsenate because arsenate is known to be electro-inactive, and to be reduced by L-cysteine. Two possible sources of arsenate in the arsenite standards were considered.

(i) Contamination of the solid As_2O_3, or formation of arsenate during preparation of the stock solution; either by atmospheric oxidation at high pH (during dissolution in KOH), or subsequent oxidation by the final nitric acid medium.* Either of these processes could produce an arsenite-depleted (arsenate-contaminated) stock arsenite solution.

(ii) *In-situ* arsenate generation during sample electrodeposition; ie. simultaneous reduction of arsenite to arsenic at the cathode, and oxidation of arsenite to arsenate at the anode. In this case, the spent deposition medium would be expected to contain a significant concentration of arsenate.

FIA analysis of the arsenite standards (Figure 8.2) showed that in freshly prepared standards, less than 2% of the total arsenic content was present as arsenate. This was not considered sufficient to produce the effects observed during ED-ETAAS analysis. However, in an effort to produce "pure" arsenite solutions, stock solutions were subsequently prepared containing 0.5% L-cysteine. This was used to reduce any arsenate in the solution to arsenite. It was independently verified (results not shown) that the L-cysteine concentration in working solutions prepared by twenty-fold dilution of this stock (0.005%) was insufficient to reduce arsenate. Thus the L-cysteine from dilution of stock solutions did not interfere with speciation studies.

The possibility that arsenate was being produced by *in-situ* oxidation of arsenite during electrodeposition was investigated. Following arsenic deposition from a solution containing 100 ppb arsenite/1% HNO_3/0.1 mM hydrazine sulphate, the spent electrodeposition medium was collected and re-analysed by ED-ETAAS. No electroactive arsenic was detected in the analysis, but when 0.5% L-cysteine was added to the sample, a mean peak absorbance of 0.217 was observed. This corresponds to an arsenite concentration of *ca.* 14-20 ppb (14-20% oxidation).

---

* To prevent this possibility, the sample medium for preparation of stock arsenite solutions was subsequently changed to 1% H_2SO_4

Thus, for arsenite samples containing negligible quantities of arsenate, a significant concentration of arsenate is measured following electro-deposition. Direct oxidation of arsenite at the anode and/or chemical oxidation by oxygen produced at the anode could be responsible for oxidation of the arsenite solution.

The consequence of this *in-situ* oxidation is that sensitivity for arsenite determination is decreased unless a reducing agent is added to counteract the oxidation process. In this situation, the concentration of arsenic determined corresponds to total arsenic rather than just arsenite (see Section 8.6.2).

8.6.1.2 Analyte Stabilisation

Figure 8.3 shows the effect of palladium on the absorbance-time profile for conventionally deposited arsenite. Not only is the profile shifted to a higher temperature in the presence of palladium, but the double peak observed in the absence of palladium is eliminated. The peak height increases in the presence of palladium, resulting in increased sensitivity for analysis by peak absorbance.

The effect of electrodeposition is shown in Figure 8.4, which compares pyrolysis curves for electrodeposited and conventionally deposited arsenite in the presence of palladium. The maximum pyrolysis temperatures are similar. However, for the conventionally deposited arsenite, the integrated absorbance decreases gradually with increasing pyrolysis temperature, up to *ca.* 1300 °C. In contrast, the integrated absorbance for electrodeposited arsenite increases up to a pyrolysis temperature of *ca.* 1200 °C and then decreases slightly before the maximum pyrolysis temperature of *ca.* 1350 °C. The maximum pyrolysis temperatures without substantial analyte losses were 1300 °C and 1350 °C for thermally deposited and electrodeposited arsenic respectively. The lower absolute absorbances for the electrodeposited arsenite stem from inefficient electrodeposition in the absence of L-cysteine.

Absorbance-time profiles for arsenite determination by ED-ETAAS and ETAAS with electrodeposited palladium modifier are compared in Figure 8.5. The appearance temperatures and peak absorbance temperatures are identical for the electrodeposited and thermally deposited samples. The profile for the electrodeposited sample has a higher peak absorbance than that for the thermally deposited sample, and also has more pronounced shoulder on the left-hand side. However, under normal analytical conditions, using an atomisation temperature ramp rate of *ca.* 2000 °C s^{-1}, there is no sign of this shoulder. It may be that it is a result of processes that occur only under the conditions used for this experiment; i.e at the slower atomisation temperature ramp rate of 630 °C s^{-1}.

Because of the electrochemical reduction step, electrodeposited arsenic is likely to be present in the metallic state, which is then stabilised by the palladium modifier. Two possible mechanisms could account for the formation of metallic arsenic. One is that during electrodeposition, arsenite is reduced directly to arsenic (Scheme 8.1). The other is that the electro-

reduction proceeds further, converting the arsenic deposit to arsine which is then adsorbed on the surface of the modifier. However, it has been shown that palladium-adsorbed arsine is oxidised to arsenic at temperatures as low as -80 °C.[258] Therefore, it is likely that any adsorbed arsine would be converted to arsenic before or during pyrolysis (Scheme 8.2). Thus, regardless of the reduction mechanism, electrodeposited arsenic is likely to be atomised/volatilised directly from a metallic arsenic-palladium species.

$$As^{III} \xrightarrow{e^-} As^0/Pd \qquad \text{(Scheme 8.1)}$$

$$As^{III} \xrightarrow{e^-} As^0/Pd \xrightarrow{e^-} AsH_3/Pd \xrightarrow{\Delta} As^0/Pd + H_2 \qquad \text{(Scheme 8.2)}$$

Styris *et al.* studied the atomisation of arsenic from palladium modified furnaces using mass spectrometry at atmospheric pressure.[146] The authors proposed that, for a pre-reduced palladium modifier, solid As_2O_3 interacts directly with the palladium forming a solid solution or intermetallic compound as shown in Scheme 8.3. This mixed palladium-arsenic compound may or may not contain oxygen ($m = 0, 1, 2, ...$). The proposed volatilisation mechanism for this species is shown in Scheme 8.4.

$$2x\text{Pd} + y\text{As}_2\text{O}_{3(S)} \rightarrow 2[\text{Pd}_x\text{As}_y\text{O}_m]_{(s)} + (3y\text{-}2m)\text{O}_{(g)} \qquad \text{(Scheme 8.3)}$$

$$[\text{Pd}_x\text{As}_y\text{O}_m] \xrightarrow{1590\ \text{K}} x\text{Pd}_{(l)} + y\text{As}_{(g)} + m\text{O}_{(g)} \qquad \text{(Scheme 8.4)}$$

Thus, it is possible that thermally deposited arsenic is volatilised from a mixed palladium-arsenic-oxygen compound, whereas electrodeposited arsenic is volatilised from a simpler palladium-arsenic intermetallic that does not contain oxygen.

8.6.1.3 Sensitivity and Detection Limits

The characteristic masses and detection limits for arsenite determination by ED-ETAAS are shown in Table 8.2. The characteristic masses for deposition from L-cysteine-containing media are lower, reflecting the better deposition efficiency and hence, higher sensitivity of the technique. The characteristic mass of 6.6 pg as determined by peak height, compares well with the instrument manufacturer's specifications (6 pg[190]), however, the characteristic mass calculated using the integrated absorbance (52 pg) is considerably higher than some literature values; e.g. 12.6 pg[116] and 14 pg.[153] Both of these characteristic masses were determined using platform-equipped furnaces and EDL light sources, which have been reported to double the sensitivity for arsenic determination.[3*] Furnace platforms were not routinely used during the course of this work, however, when they were used, the integrated absorbances were

---

* The increased sensitivity for the EDL over the HCL is due to the narrower width of the EDL emission lines. The theory relating to this phenomenon is beyond the scope of this thesis, however, a full discussion of the effects of emission line-widths on absorbance is given by Kirkbright and Sargent.[259]

markedly enhanced. An example of this is shown in Figure 8.6. A calculation of the characteristic mass based on the slope of the ED-ETAAS curve using integrated absorbance yields a value of M_0= *ca.* 30 pg. However, the characteristic mass determined by peak height is *ca.* 15 pg—higher than that for wall atomisation.

The detection limits for arsenite determination by ED-ETAAS are also shown in Table 8.2. These were lower for peak absorbance measurements than for integrated absorbances. This has been observed by other workers[46], and is attributed to the high level of baseline noise associated with the arsenic HCL. The higher detection limit for the L-cysteine-containing medium, using peak absorbance, may be related to background correction effects for sample atomisation in the presence of residual L-cysteine.

The relative sensitivities for arsenite determination by ED-ETAAS, and conventional ETAAS with a palladium modifier, are demonstrated by the calibration curves shown in Figure 8.6. While the sensitivities for both techniques are similar, the peak absorbances are larger for ETAAS, whereas the integrated absorbances are larger for ED-ETAAS. This reflects different absorbance-time profiles for conventionally and electrodeposited arsenic. The different atomisation profiles may suggest different atomisation mechanisms or different degrees of interaction between the arsenic and the palladium modifier.

8.6.2 Fractionation of Arsenic Species

8.6.2.1 Arsenate

Figure 8.7 shows the influence of the deposition potential on the electrodeposition of arsenate and arsenite. At applied potentials below 0.5 V, both species are measured, due to adsorption of the arsenate and arsenite anions onto the positively charged furnace surface (see plots of applied potential *vs.* electrode potential in Chapter 7). As the applied potential is increased to 2.0 V, the absorbance due to arsenite remains relatively constant, whereas the absorbance for arsenate decreases almost to zero. At this potential, arsenite is reducible and arsenate is electro-inactive. As the applied potential is increased above 3.0 V, significant quantities of arsenate are reduced. This result shows that arsenate is not truly electro-inactive, but can be reduced in the presence of palladium if a sufficiently negative potential is applied. A similar observation was made by Huiliang *et al.*[260] who reduced arsenate at a gold-coated platinum-fibre electrode using deposition potentials negative of -1.5 V (vs. Ag/AgCl). In this work, an applied potential of 3.0 V corresponds to a cathode potential of *ca.* -1.3 V. It is likely that the high arsenate absorbances shown in Figure 8.7, at deposition potentials above 3.0 V, are a result of direct arsenate reduction catalysed by the palladium furnace coating.

The lack of arsenate deposition at applied potential of *ca.* 2.0 V provides an opportunity for fractionating inorganic arsenic. Arsenite can be selectively determined using the 2.0 V deposition potential. Total inorganic arsenic, and thus by difference, arsenate, could be determined by a number of protocols. Figure 8.7 suggests that total inorganic arsenic could be

determined using a deposition potential of *ca.* 4.0 V. However, this avenue was not explored because experience with other metals showed that decreased precision and increased background absorbances were often associated with large deposition potentials. A second way of determining total arsenic is to use conventional ETAAS with electrodeposited palladium modifier. A third possibility is chemical pre-reduction of arsenate, allowing ED-ETAAS determination of total inorganic arsenic using a 2.0 V deposition potential. In the light of the enhanced sensitivity observed when the reducing agent L-cysteine was used during ED-ETAAS arsenite determination, this avenue was explored further.

Table 8.3 shows the results for ED-ETAAS analysis of arsenate and arsenite solutions in the presence and absence of L-cysteine. For the 1% HNO_3 deposition medium, the ratio of the arsenite to arsenate peak absorbance was 9.1:1. For the L-cysteine-containing deposition medium, there was no significant difference between the absorbances for arsenate and arsenite. As observed previously, the absorbance for arsenite was enhanced by a factor of *ca.* 50% in the presence of L-cysteine. The main cause for concern was the small but real absorbance for arsenate. It was established experimentally (results not shown) that the magnitude of this absorbance could be decreased by using a suitable rinsing protocol. This incorporated a series of rinses of increasing volume and was designed to remove "tide marks" of residues, caused by sample evaporation during electrodeposition. Thus for a sample volume of 20 µL, the first rinse was 30 µL, and the second and final rinse was 40 µL. Using this rinsing protocol, absorbances for arsenate 'deposited' from 1% HNO_3 media were below the level of baseline noise.

8.6.2.2 Monomethylarsonic acid (MMA)

The electro-reduction of organic derivatives of arsenic acid, such as MMA and DMA, requires a large hydrogen overvoltage. The following scheme has been proposed.[225]

$$\underset{\text{I}}{RAsH_2O_3} \xrightarrow{4e^-} \underset{\text{II}}{2RAsO} \xrightarrow{4e^-} \underset{\text{III}}{RAs{=}AsR} \xrightarrow{4e^-} \underset{\text{IV}}{2RAsH_2} \qquad \text{(Scheme 8.5)}$$

In weakly acidic solutions, reduction of alkyl arsenic acids (I) produces the alkyl hydrides (IV). By analogy with the behaviour of arsine, it is anticipated that the resulting hydrides adsorb to palladium, and undergo catalytic dissociation at low temperatures.[139]

The effect of deposition potential on absorbance for MMA is shown in Figure 8.8. For the 1% HNO_3 medium, there is limited deposition at potentials above 2.5 V. However, the absorbance, and hence the amount of deposition, more than doubles in the presence of L-cysteine. Le *et al.* proposed that L-cysteine reduces pentavalent organoarsenics to trivalent species.[253] By analogy with the situation for arsenite and arsenate, it is likely that the trivalent organoarsenic species are more electroactive than the pentavalent parent compounds.

Table 8.4 shows absorbances for arsenite and MMA, as determined by ED-ETAAS and ETAAS. For ED-ETAAS measurements using a 1% HNO_3 deposition medium, there was good selectivity for arsenite, but a small absorbance for MMA was observed. It may be possible to eliminate this using a rinse protocol such as that used to remove arsenate. However, for analysis of natural waters, MMA levels are generally far lower than those for arsenate[224] so a small MMA contribution to the arsenite measurement is unlikely to have a major effect on the analysis.

For ED-ETAAS measurements using a deposition medium containing L-cysteine, Table 8.4 shows that similar absorbances are obtained for MMA and arsenite. The differences between the mean absorbances are not statistically significant. This result is unexpected because Figure 8.8 suggests that MMA deposition in the presence of L-cysteine is incomplete after 60 seconds electrolysis at 2.0 V. A possible explanation for this is that L-cysteine reduction of MMA proceeds relatively slowly, and was incomplete when the measurements for the lower potentials (in Figure 8.8) were made.

ETAAS measurements of arsenate and MMA also produced mean absorbances that were not significantly different. These absorbances were significantly higher than those for ED-ETAAS determination. This situation contrasts with the results for a platform-equipped furnace shown in Figure 8.6, in which ED-ETAAS absorbances were similar to those for ETAAS. The difference may be related to the age of the L-cysteine solution. However, separate calibrations were performed whenever ED-ETAAS results were compared with those for ETAAS.

Thus, for fractionation of arsenic containing natural waters, ED-ETAAS analysis can be used to determine arsenite with only a very small contribution from any arsenate or MMA present. Total arsenic can be determined using ED-ETAAS with L-cysteine reduction, or by ETAAS with electrodeposited palladium modifier. Discrimination between MMA and arsenate was not achieved; however, this was considered less important than the primary aim of selective arsenite determination.

8.6.2.3 Arsenic Speciation in Synthetic Samples

The plots shown in Figure 8.9 demonstrate the ability of the ED-ETAAS method to discriminate between arsenite and arsenate. For solutions containing constant total arsenic concentrations but varying ratios of arsenite and arsenate, ED-ETAAS analysis produced a linear calibration curve in response to increasing arsenite concentration. Total arsenic analysis by ETAAS with an electrodeposited palladium modifier produced a line parallel to the x-axis, confirming that identical sensitivity is observed for ETAAS determination of arsenite and arsenate.

Absolute sensitivity for the solution containing 50 ppb arsenite was lower for ED-ETAAS than for ETAAS. This reflects incomplete electrodeposition in the absence of the L-cysteine reducing agent—it was necessary to omit this in order to selectively measure arsenite.

Comparison of integrated absorbance measurements (8.8a) with peak absorbance measurements (8.8b) for the ED-ETAAS analysis, shows that better sensitivity (relative to ETAAS) is obtained by using peak absorbances. Furthermore, peak absorbances provide better discrimination between arsenite and arsenate. The reason for this is not entirely clear, but may to be related to the way in which the ETAAS instrument integrates absorbance peaks that are hidden in a noisy baseline. Figure 8.14 shows the actual absorbance profiles for part of the ED-ETAAS experiment shown in Figure 8.9. It can be seen that for the 50 ppb arsenate solution, the peak height barely registers above the baseline noise. However, the instrument still calculates an integrated absorbance for the signal. However, it also seems possible that this integrated absorbance can be attributed to residual arsenate which is not rinsed from the furnace prior to atomisation, although no peak absorbance is registered—if it were merely an artefact of the ETAAS software, we would not expect the ED-ETAAS plot shown in Figure 8.9 to be so linear.

Thus, because of the better sensitivity and improved selectivity for arsenite, peak absorbances were chosen over integrated absorbances as the preferred measurement mode for arsenic determination.

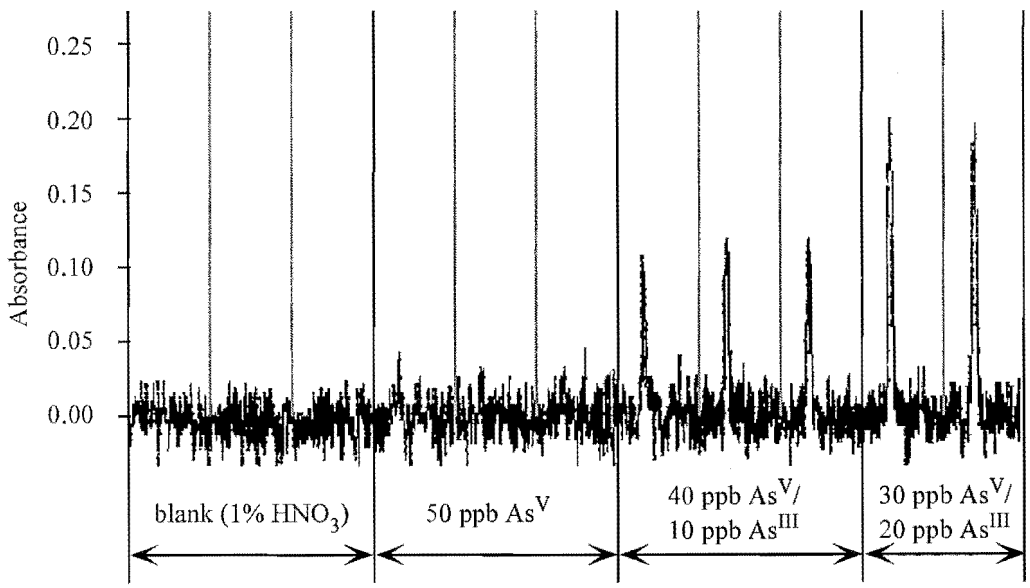

Figure 8.14 Absorbance-time profiles for ED-ETAAS analysis of the mixed arsenite/arsenate solutions described in Section 8.3.4.

8.6.2.4 Alternative Arsenic Fractionation Methods

Three candidate methods were evaluated with a view to finding a suitable method to compare with the ED-ETAAS arsenic fractionation protocol. The first of these candidates was the method of Li and Smart[233]: CSV in the presence of Cu^{2+}. A calibration curve for arsenite obtained using this method is shown in Figure 8.10. It can be seen that the curve is relatively linear, except at the region of lowest arsenite concentration. This curvature makes calibration difficult, and has been cited by other authors as a reason for not using this method.[229]

Two other problems were encountered with this method. Firstly, the stripping current for an arsenite-containing sample decreased over time, and with each replicate measurement. Li and Smart[233] attributed this to oxidation of arsenite by Hg^{2+} ion, which is formed by dissolution of the HMDE in the 2 M HCl sample medium. The effect was countered by adding 40 μM hydrazine sulphate to the deposition medium. However, in the present work, this did not prevent the analytical peak decreasing over time. The second problem with this method relates to the high concentration of copper required for the analysis. Spiking samples with copper to obtain a final concentration of 0.8 mM, requires the use of stock solutions in excess of 8.0 mM (500 ppm). Such high concentrations pose risks of contamination in an area where trace copper measurements are likely to be made.

In view of the non-linear calibration curve, unstable stripping currents, and high concentrations of copper required, CSV in the presence of Cu^{2+} was not considered a suitable method for arsenite determination.

The second method investigated was that of Zima and van den Berg[229]: CSV in the presence of pyrrolidine dithiocarbamate (PDC). This protocol was applied to the determination of arsenite in two natural waters; one from Devil's Creek, and one from Johns Road. The standard additions calibration plots for these analyses shared a common anomaly: the calibration line had a positive, rather than the usual negative, x-intercept. An example of this, the standard additions plot for analysis of Johns road water, is shown in Figure 8.11. In an effort to explain these unusual results, possible analytical interferents were investigated. Zima and van den Berg mentioned copper as an interferent, but for their seawater analysis, the copper levels were too low to pose a problem. With this in mind, the Johns road sample was analysed for copper using conventional ETAAS (results not shown). The analysis showed that the water contained *ca.* 10 ppb copper—considerably higher than the 3 ppb that Zima and Van den Berg determined as a maximum permissible level.

The effect of Cu^{2+} on the CSV analysis is shown in Figure 8.12. It can be seen that on addition of Cu^{2+} to the arsenite sample, the analytical peak at *ca.* -0.04 V is masked by the background current, and a new peak appears at *ca.* -0.14 V (*vs.* Ag/AgCl). Zima and van den Berg attributed this second peak to formation of a copper-PDC complex. In this work, efforts to remove the interfering copper from samples using solvent extraction (dithizone in CCl_4)

proved fruitless, as sufficient CCl_4 remained in the sample after extraction to interfere with the CSV analysis. At this point, we decided that determination of arsenic by CSV in the presence of PDC was not a suitable method for our purposes. Correspondingly, we turned our attention to the next candidate method: pH-selective hydride generation (HG)-ETAAS.

Figure 8.13 shows a calibration curve for determination of arsenite by pH-selective HG-ETAAS. The poor precision is likely to be caused by the large manual component in the analytical protocol; the tube which transports the arsine to the furnace is positioned by hand, and the arsine accumulation time is measured using a stopwatch. The variable position of the sample introduction tube may affect the efficiency of arsine trapping on the palladium modifier. The imprecise control of the accumulation time would also affect the amount of arsine trapped. A further contribution to the poor precision could be due to an inefficient gas-liquid separator in the HG3000 hydride generator. Vigorous effervescence from the borohydride reduction produces an aerosol which transfers sodium acetate from the reaction mixture to the furnace. On atomisation, this produces a background absorbance which increases with arsine accumulation time. This was countered by using a relatively low sodium borohydride concentration (compared with that used in Section 6.2.2 for mercury analysis).

The sensitivity of the method for arsenite determination was considered suitable for our purposes. Coupled with the observation that no absorbance was obtained for arsenate, the HG-ETAAS protocol was selected as a suitable method to compare with ED-ETAAS for arsenite determination.

8.6.2.5 Fractionation of Arsenic Species in Natural Waters

Four different methods were used to measure arsenic in two natural waters. ED-ETAAS and HG-ETAAS, were used to determine arsenite; total arsenic was determined using conventional ETAAS with an electrodeposited modifier, and ED-ETAAS with L-cysteine pre-reduction. The two waters were taken from environments likely to be contaminated by arsenic: the Devil's Creek catchment contains disused mine workings which tunnel though arsenic-containing rock; the Johns Road surface water was taken from an area adjacent to a timber treatment plant.

The results of the analyses are shown in Table 8.5. For the Devil's Creek water, no significant arsenite concentration was measured. This is not surprising given that the sample had been stored for a long period with no preservative. It is likely that any arsenite present at the time of sampling would have oxidised to arsenate during storage. The analyses for total arsenic all indicate a concentration of *ca.* 43-44 ppb except for one. The total arsenic determined by ETAAS using the integrated absorbance mode was 51.9 ppb. However, given that the other measurements all agree within experimental error, this result is considered to be an artefact of the poor calibration curve that was obtained for the experiment.

For the Johns Road water, both the HG-ETAAS and ED-ETAAS analyses determined an arsenite concentration of *ca.* 21 ppb. The large errors for the HG-ETAAS analysis are a consequence of poor precision for both calibration and the sample measurements. However, the close agreement with the ED-ETAAS result (within experimental error) suggests that the method is accurate, and that both methods measure the same arsenic fraction.

The analyses for total arsenic in Johns Road water determined a concentration of *ca.* 46 ppb. As for the Devil's Creek water, the arsenic concentration as determined by ETAAS using the integrated absorbance is relatively high. However, both of these anomalous measurements are based on the same calibration curve and thus are not considered to be significant.

Thus, ED-ETAAS has been shown to be a suitable method for determining both arsenite and total arsenic. For total arsenic, the precision and detection limits are similar to those for ETAAS. For arsenate, the precision is considerably better than for the HG-ETAAS protocol adopted in this work. Furthermore, the total automation of the ED-ETAAS technique decreases the likelihood of operator error and frees the analyst to perform other tasks. The detection limits of the HG-ETAAS method were not determined, but were not expected to be any better than for ED-ETAAS because of the poor precision of the technique as used in this work (see Figure 8.13). However, it is likely that the detection limits could be greatly improved if a more efficient gas-liquid separator and longer accumulation times were used.

Another attribute of the ED-ETAAS technique for arsenic determination is the electrodeposited palladium modifier. This was used not only for the ED-ETAAS protocols, but also for the ETAAS and HG-ETAAS measurements. The electrodeposition protocol provided a convenient and reproducible method of modifying the furnace.

Chapter Nine

Conclusions

The primary aims of this work were to gain an improved understanding of the ED-ETAAS protocol of Matousek and Powell[97,99] and to expand the method's application. The first of these aims was achieved by studying and optimising the individual components of the ED-ETAAS analysis. These included the stabilising action of the modifier, the parameters relating to successful electrodeposition of the analyte, and the effects of different sample media.

9.1 FUNDAMENTAL STUDIES

The effect of the electrodeposited modifier was examined in Chapter Three. The optimum electrodeposition protocol for palladium was a 20 second deposition from 0.1% HNO_3 using a 2.0 V electrolysis potential. Neither rinsing nor drying of the modifier was found to be necessary for effective analyte stabilisation. The electrodeposited palladium was shown to be slightly more stable to volatilisation than conventionally deposited palladium. The palladium modifier was not reusable and had to be redeposited for each analyte determination. The alternative modifiers, rhodium and iridium, were reusable; however, the sensitivity was greatly decreased for the second and subsequent analyses following modifier deposition. Furthermore, neither of these modifiers provided the same thermal stabilisation of analyte as did palladium.

The deposition of analyte metals was studied in Chapter Four. It was established that lead could be deposited from 1% HNO_3 media with greater than 90% efficiency within 60 seconds. Deposition efficiency from hydrochloric acid media was poor, demonstrating that sensitivity for the ED-ETAAS method is sample matrix dependent. Re-deposition and rinsing protocols were developed which were designed to remove sample matrix components while quantitatively retaining electrodeposited lead on the furnace surface. It was shown that for atomisation of lead from unmodified pyrolytic graphite, electrodeposited lead was more thermally stable than conventionally deposited lead. The stability of the electrodeposited lead was further enhanced by the electrodeposited palladium modifier which increased the maximum loss-free pyrolysis temperature from 800 °C, for lead electrodeposited on pyrolytic graphite, to 1200 °C for lead electrodeposited on palladium-modified graphite. Detection limits and sensitivity for the technique were comparable to those for conventional ETAAS.

Application of the method to determination of other metals from simple acid media showed that the protocol developed for lead could be used for the determination of bismuth, cadmium and copper with little or no modification. In contrast to the situation for lead, the acid used as an electrolysis medium for cadmium and bismuth had little effect on the deposition efficiency. For each metal, the palladium modifier was shown to provide varying degrees of thermal stabilisation, but was beneficial in all the analyses that were tested.

Although the ED-ETAAS protocol provides similar sensitivity to conventional ETAAS, the time taken for the various electrolysis and rinsing steps greatly decreases analytical throughput. A single sample measurement by ETAAS generally takes *ca.* 60-90 seconds. For ED-ETAAS, this time increases to between four and six minutes depending on the number of rinse steps required. Thus, because of the superior speed, conventional ETAAS remains the method of choice for analysis of samples in non-problematic media. The strength of ED-ETAAS lies in its ability to directly analyse media which contain large concentrations of salts, particularly sodium chloride, which can interfere in the ETAAS analysis.

9.2 DETERMINATION OF METALS FROM SALINE MEDIA

Chapter Five describes application of the ED-ETAAS method to metal determination in sodium chloride media. The deposition potential, temperature and gas-flow rate were optimised to maximise analyte deposition and minimise retention of sodium chloride on the furnace. It was demonstrated that the palladium modifier decreased both the amount and the thermal stability of sodium chloride that was retained on the furnace after electrolysis. Thus, the sodium chloride background for analysis of a 20 µL sample containing ca. 0.6 mg of sodium chloride was decreased to a negligible level. The protocol was refined to the point where equal sensitivity was observed for determination of 50 ppb lead in either 1% HNO_3 or 0.5 M sodium chloride/1% HNO_3 media.

A major problem encountered during analysis of sodium-chloride media was adsorption of analytes inside the Pt/Ir anode/sample injection capillary. As a result of this, the first replicate measurement for each sample was generally discounted, thus requiring four measurements per sample to obtain three useful ones. The adsorption problem was overcome using a different probe which incorporated a separate PTFE sample delivery tube and a platinum anode. However, the size and flexibility of this probe introduced new problems of sample overflow from the furnace and decreased maximum sample size. These problems could be addressed in future by a probe design similar to the present Pt/Ir capillary but incorporating an internal "sleeve" of PTFE to prevent analyte adsorption. Pt/Ir capillaries and PTFE tubing are both commercially available in sizes suitable for fabricating such a probe.

An advantage of ED-ETAAS over conventional ETAAS was demonstrated by successfully determining copper and cadmium levels in seawater. The high salt concentrations of a seawater sample matrix prevent direct determination by conventional ETAAS but represent an ideal sample medium for ED-ETAAS. However, this analysis also highlighted a principal disadvantage of ED-ETAAS for this application. The seawater used for the analyses was taken from a busy seaport at high tide and thus represents a relatively polluted sample. Even so, the levels of copper and cadmium measured were barely above the detection limits of the ED-ETAAS technique. For less polluted samples, taken from coastal waters or the open ocean, analyte pre-concentration by solvent extraction or ion-exchange would be required. These techniques inherently separate the analyte from the sample matrix, removing the need for ED-ETAAS: conventional ETAAS can perform the same analysis in less than half the time. Thus the use of ED-ETAAS for seawater analysis is restricted to relatively polluted waters such as those found in estuaries and harbours.

Other high-salt media which present problems for conventional ETAAS include biological fluids and some industrial wastes. These may offer more suitable applications for the ED-ETAAS method. For example, Najafi[173] demonstrated that ED-ETAAS could be successfully used to determine lead, cadmium, chromium, nickel and manganese in urine. However, while the high salt and urea concentrations in urine do not present a problem for ED-ETAAS, little is known at this stage about the effects of high protein concentrations.

Biological fluids such as blood and cell extracts can contain large amounts of protein. Several problems arising from this can be foreseen. Analytes which are complexed to proteins are likely to be electro-inactive, especially if they are bound in the centre of the protein structure. It is also possible that protein adsorption on the furnace surface (electrode fouling) could prevent quantitative analyte deposition, or change the deposition efficiency for samples that contain different proteins/concentrations. In addition, metal-containing proteins that adsorb to the furnace would cause otherwise inert metal complexes to be measured as labile. If protein does adsorb onto the furnace, this could also cause build-up of carbon from pyrolysed protein as a post-atomisation residue. Thus it is likely that for successful analysis of such samples, several other steps would have to be included in the ETAAS protocol. These could include acid and/or UV decomposition of proteins, filtration/centrifugation of samples, and oxygen ashing of samples within the furnace. Consequently, a great deal of further research is required before ED-ETAAS could be promoted as a suitable technique for analysis of protein-containing samples.

9.3 FURTHER APPLICATIONS

Having achieved the first of the main aims of this work, to improve our understanding of the mechanisms involved in the ED-ETAAS protocol, we undertook to expand the method's application. This work proceeded in two directions. Firstly, to determine elements that were difficult to determine by ETAAS and secondly, to explore the possibility of species fractionation by ED-ETAAS.

9.3.1 Determination of Mercury

The first expanded application of the ED-ETAAS technique was the determination of mercury, as described in Chapter Six. The sensitivity and detection limits for mercury determination by ED-ETAAS are comparable to those for conventional ETAAS using palladium modifier. However, the thermal stability for electrodeposited mercury on palladium was greater than that for conventionally deposited mercury on palladium; the maximum pyrolysis temperatures for the two techniques were 550 °C and 450 °C respectively. Furthermore, although it was not verified, it is likely that mercury could be determined in the presence of sodium chloride using ED-ETAAS; a problematic sample medium for conventional ETAAS.

Application of the ED-ETAAS method for mercury determination could be restricted by the relatively high detection limit (*ca.* 1.7 ppb). The detection limit for CV-ETAAS is a factor of ten lower, and could be further improved if reagents of higher purity were used. However, the lack of automation for the CV-ETAAS technique, combined with the relatively large consumption of sample and high purity (expensive) reagents makes ED-ETAAS the method of choice when detection limits are not an issue.

9.3.2 Metal Speciation

The next application of ED-ETAAS to be explored was the fractionation of complexed metal species. It was demonstrated that for inert EDTA-metal complexes, ED-ETAAS could be used to differentiate between free and complexed metal. However, for complexes that are labile or pseudo-labile on the experimental timescale, the ability of the technique to differentiate species was poor. It is likely that for metals and ligands with smaller equilibrium constants, log K, the ability to discriminate between species would be further restricted. For such complexes, the amount of free metal measured by ETAAS would be higher than that measured by ASV. This is because of the exhaustive deposition used in the ED-ETAAS technique; unlike the deposition step for ASV, the concentration of metal in the bulk solution decreases significantly as the deposition proceeds. This allows re-equilibration of metal ligand complexes, thus affecting the measured speciation within the sample.

Furthermore, it was shown that a common naturally occurring ligand, fulvic acid, adsorbed strongly to the furnace. As a consequence of this, both free and fulvate-bound metal was 'deposited' on the furnace surface; free metal by electrodeposition and fulvate-bound metal by adsorption. This prevented discrimination between the two species by ED-ETAAS.

Thus, it is possible in principle to distinguish between free and ligand-bound metal by ED-ETAAS. However, because of the likely disturbance of species equilibria within the sample and adsorption of some complexed species on the furnace surface, the method is unlikely to have any practical application in natural systems.

9.3.3 Determination and Speciation of Arsenic

The penultimate chapter of this work is devoted to the measurement of arsenic and its speciation by ED-ETAAS. This method was shown to be simple and reliable for determining both the total arsenic concentration and the concentration of the most toxic arsenic species, arsenite—an analysis which cannot be accomplished by conventional ETAAS. The comparative method, hydride generation-ETAAS, was relatively imprecise—limited perhaps by the manual nature of the technique. However, the pre-concentration step afforded by the hydride accumulation provides scope for considerable improvements in the detection limit. Thus where absolute detection limits are of primary importance, HG-ETAAS is the method of choice. However, where detection limits are not an issue, the automated ED-ETAAS method is simpler, and consumes smaller quantities of reagents and samples. For both techniques, detection limits and precision were adversely affected by baseline noise, which was attributed to the low intensity of the arsenic hollow cathode lamp. The use of a high intensity electrodeless discharge lamp would greatly improve both the precision and detection limits.

It has been shown in this work that it is possible to differentiate between As^{III} and other arsenic species. Preliminary studies by Najafi[173] suggest that it may be possible to differentiate between Cr^{III} and Cr^{VI}. Thus, although ED-ETAAS is not an ideal method for differentiating between free and complexed metal ions, it shows promise for determining various oxidation states of analyte species. This is an area for future research.

For any of the four techniques used in this work, ETAAS, ED-ETAAS, CV-ETAAS, and HG-ETAAS, the use of the palladium modifier was greatly beneficial, and in most cases essential. It has previously been shown that electrodeposited palladium provided more efficient stabilisation of selenium than did thermally deposited palladium.[159] In this work, it was demonstrated that electrodeposited palladium modifier is more stable to volatilisation than thermally reduced palladium, and that it provides better sensitivity than palladium chloride modifier for mercury determination by CV-ETAAS. Thus, not only is electrodeposition a simple and convenient way of palladium furnace modification, but the electrodeposition can enhance the performance of the modifier. Furthermore, the quantities of palladium required when electrodeposition is used are only *ca.* 0.5% of those used for conventional thermal deposition. This not only decreases consumption of a relatively expensive reagent, but also decreases the size of analyte blanks associated with modifier impurities. Therefore, the electrodeposited modifier is considered superior to thermally deposited modifier, regardless of whether the analyte is deposited by vapour/hydride accumulation, electrodeposition, or conventional means.

References

1. Walsh A.; The application of atomic absorption spectra to chemical analysis. Spectrochimica Acta, 1955, 7, 108-117.

2. Alkemade C.Th.J. and Milatz J.M.W.; Double-beam method of spectral selection with flames. *Journal of the Optical Society of America,* 1955, **45,** 583-584.

3. Welz B.; *Atomic Absorption Spectrometry.* Verlag Chemie, Weinheim, Germany, 1985.

4. Parsons M.L.; in *Analytical Instrumentation Handbook,* Marcel Dekker Inc., New York, 1990.

5. Slavin W.; Atomic absorption spectroscopy. The present and future. *Analytical Chemistry,* 1982, **54,** 685A-694A.

6. Gliksman J.E., Gibson J.E. and Kandetski P.E.; High precision determination of calcium in phosphate rock by atomic absorption spectrometry. *Atomic Spectroscopy,* 1980, **1,** 66-67.

7. L'vov B.V.; The analytical use of atomic absorption spectra. *Spectrochimica Acta,* 1961, **17,** 761-770.

8. L'vov B.V.; The potentialities of the graphite crucible method in atomic absorption spectroscopy. *Spectrochimica Acta Part B-Atomic Spectroscopy,* 1969, **24,** 53.

9. Massmann H.; Study of atomic absorption and atomic fluorescence in a graphite cuvette. *Spectrochimica Acta Part B-Atomic Spectroscopy,* 1968, **23B,** 215-226.

10. Slavin W.; The present and future of graphite furnace atomic absorption spectroscopy. *Trends in Analytical Chemistry,* 1987, **86,** 194-201.

11. Falk H. and Glissman A.; Spatially and temporally resolved temperature profiles in graphite furnaces. *Zeitschrift für Analytical Chemie,* 1986, **323,** 748-753.

12. Stephens R.; Reduction of magnet size in direct Zeeman atomic absorption spectrometry. *Journal of Analytical Atomic Spectrometry,* 1994, **9,** 675-678.

13. Cabon J.Y. and le Bihan A.; Direct determination of zinc in sea-water using electrothermal atomic absorption spectrometry with Zeeman-effect background correction - effects of chemical and spectral interferences. *Journal of Analytical Atomic Spectrometry,* 1994, **9,** 477-481.

14. Matousek J.P.; Interferences in electrothermal atomic absorption spectrometry, their elimination and control. *Progress in Analytical Atomic Spectroscopy,* 1981, **4,** 247-310.

15. Frech W., Lundberg E. and Cedergren A.; Investigations of some methods used to reduce interference effects in graphite furnace atomic absorption spectrometry. *Progress in Analytical Atomic Spectroscopy,* 1985, **8,** 237-370.

16. Doner G. and Akman S.; Mechanisms of magnesium chloride interferences on zinc in electrothermal atomic absorption spectrometry using a dual cavity platform. *Spectrochimica Acta Part B - Atomic Spectroscopy,* 1996, **51,** 181-187.

17. Cabon J.Y. and le Bihan A.; Interference of salts on the determination of lead by electrothermal atomic absorption spectrometry. Ion chromatographic study. *Spectrochimica Acta Part B - Atomic Spectroscopy,* 1996, **51,** 619-631.

18. Akman S. and Doner G.; Nickel chloride interferences on zinc and cobalt in graphite-furnace atomic-absorption spectrometry using a dual cavity platform. *Spectrochimica Acta Part B-Atomic Spectroscopy,* 1995, **50,** 975-984.

19. Hageman L.R., Nichols J.A., Viswanadham P. and Woodriff R.; Comparative interference study for atomic absorption lead determinations using a constant temperature *vs.* a pulsed-type atomiser. *Analytical Chemistry,* 1979, **51,** 1406-1412.

20. Manning D.C., Slavin W.S. and Myers S.; Sampling at constant temperature in graphite furnace atomic absorption spectrometry. *Analytical Chemistry,* 1979, **51,** 2375-2378.

21. Woodriff R. and Ramelow G.; Atomic absorption spectroscopy with a high-temperature furnace. *Spectrochimica Acta Part B-Atomic Spectroscopy,* 1968, **23,** 665-671.

22. Chakrabarti C.L., Wan C.C., Hamed H.A. and Bertels P.C.; Matrix interferences in graphite furnace atomic absorption spectrometry by capacitive discharge heating. *Analytical Chemistry,* 1981, **53,** 444-450.

23. L'vov B.V., Pelieva L.A. and Sharnopolskii A.I.; Decrease in the effect of the gases during the atomic absorption analysis of solutions in tube furnaces by evaporation of sample from a graphite substrate. *Zhournal Prikladnoi Spektroskopii,* 1977, **27,** 395-399.

24. Tsalev D.L., Slaveykova V.I. and Mandjukov P.B.; Chemical modification in graphite furnace atomic absorption spectrometry. *Spectrochimica Acta Part B-Atomic Spectroscopy,* 1990, **13,** 225-274.

25. Volynsky A.B.; Use of organic matrix modifiers in electrothermal atomic absorption spectrometry. *Journal of Analytical Chemistry,* 1995, **50,** 2-29.

26. Beisel N.F., Daamen F.I., Fuchspohl G.R. and Yudelevich I.G.; Application of matrix modifiers in the determination of trace impurities in complex objects by electrothermal atomic absorption spectrometry (review). *Journal of Analytical Chemistry of the USSR.,* 1993, **48,** 877-896.

27. Guevremont R.; Organic matrix modifiers for direct graphite furnace atomic absorption determination of cadmium in seawater. *Analytical Chemistry,* 1980, **52,** 1574-1578.

28. Guevremont R.; Organic matrix modifiers for direct determination of zinc in seawater by graphite furnace atomic absorption spectrometry. *Analytical Chemistry,* 1981, **53,** 911-914.

29. Nater E.A., Burau B.G. and Akeson M.; Fluoride matrix modifiers for the determination of aluminium by graphite furnace atomic absorption spectroscopy. *Analytica Chimica Acta,* 1989, **225,** 233-239.

30. Ericson S.P., McHalsky M.L. and Jaselskis B.; Fluoride salts as matrix modifiers for molybdenum determinations. *Atomic Spectroscopy,* 1987, **8,** 101-104.

31. Weast R.C.; *CRC Handbook of Chemistry and Physics (62nd Edition).* CRC Press Ltd, Boca Raton, Florida, USA, 1982.

32. Welz B., Schlemmer G., Ortner H. and Wegscheider W.; Scanning electron microscopy studies of surfaces from electrothermal atomic absorption spectrometry. *Progress in Analytical Spectroscopy,* 1989, **12,** 111-245.

33. Carnrick G., Schlemmer G. and Slavin W.; Matrix modifiers: their role and history for furnace AAS. *American Laboratory,* 1991, February, 120-131.

34. Ni Z-M and Shan X-Q; The reduction and elimination of matrix interferences in graphite furnace atomic absorption spectrometry. *Spectrochimica Acta Part B-Atomic Spectroscopy,* 1987, **42,** 937-949.

35. Tsalev D.L.; Chemical modification in electrothermal atomization atomic absorption spectrometry. *Atomic Spectroscopy,* 1991, **12,** 169-198.

36. Shan X-Q and Wen B.; Is palladium or palladium-ascorbic acid or palladium-magnesium nitrate a more universal chemical modifier for electrothermal atomic absorption spectrometry? *Journal of Analytical Atomic Spectrometry,* 1995, **10,** 791-745.

37. Welz B., Schlemmer G. and Mudakavi J.R.; Palladium nitrate-magnesium nitrate modifier for electrothermal atomic absorption spectrometry. Part 5: Performance for the determination of 21 elements. *Journal of Analytical Atomic Spectrometry,* 1992, **7,** 1257-1271.

38. Lancaster H.L., Marshall G.D., Gonzalo E.R., Ruzicka J. and Christian G.D.; Trace metal atomic absorption spectrometric analysis utilizing sorbent extraction on polymeric-based supports and renewable reagents. *Analyst,* 1994, **119,** 1459-1465.

39. Skoog D.A.; *Principles of Instrumental Analysis (third edition).* Saunders College Publishing, New York, 1985.

40. Vanderjagt H. and Stuyfzand P.J.; Methods for trace element analysis in surface water, atomic spectrometry in particular. *Fresenius' Journal of Analytical Chemistry,* 1996, **354,** 32-40.

41. Bersier P.M., Howell J. and Bruntlett C.; Advanced electroanalytical techniques versus atomic absorption spectrometry, inductively coupled plasma atomic emission spectrometry and inductively coupled plasma mass spectrometry in environmental analysis. *Analyst,* 1994, **119,** 219-232.

42. Copeland T.R. and Skogerboe R.K.; Anodic stripping voltammetry. *Analytical Chemistry,* 1974, **46,** 1257-1268A.

43. Batley G.E.; Electroanalytical techniques for the determination of heavy metals in seawater. *Marine Chemistry,* 1983, **12,** 107-117.

44. Tercier M.L. and Buffle J.; In-situ voltammetric measurements in natural waters: future prospects and challenges. *Electroanalysis,* 1993, **5,** 187-200.

45. Cabon J.Y. and le Bihan A.; The determination of Cr, Cu and Mn in seawater with transversely heated graphite furnace atomic absorption spectrometry. *Spectrochimica Acta Part B - Atomic Spectroscopy,* 1995, **50,** 1703-1716.

46. Cimadevilla E.A.C., Wrobel K. and Sanz-Medel A.; Capabilities and limitations of different techniques in electrothermal atomic absorption spectrometry for direct monitoring of arsenic, cadmium and lead contamination of sea-water. *Journal of Analytical Atomic Spectrometry,* 1995, **10,** 149-154.

47. Liu Z.S. and Huang S.D.; Determination of lead in sea-water with a graphite furnace atomic absorption spectrometer and an improved automatic on-line pre-concentration system. *Spectrochimica Acta Part B - Atomic Spectroscopy,* 1995, **50,** 197-203.

48. Abollino O., Aceto M., Sacchero G., Sarzanini C. and Mentasti E.; Determination of copper, cadmium, iron, manganese, nickel and zinc in Antarctic sea water. Comparison of electrochemical and spectroscopic procedures. *Analytica Chimica Acta,* 1995, **305,** 200-206.

49. Tsalev D.L., Slaveykova V.I. and Georgieva R.B.; Electrothermal atomic absorption spectrometric determination of volatile elements in biological materials in the presence of a mixed palladium-tungsten chemical modifier. *Analytical Letters,* 1996, **29,** 73-88.

50. Sioda R.E., Batley G.E., Lund W., Wang J. and Leach S.; Electrolytic preconcentration in instrumental analysis. *Talanta,* 1986, **33,** 421-428.

51. Reiger P.H.; *Electrochemistry (second edition).* Chapman and Hall, New York, 1995.

52. Anderson J.L. and Sioda R.E.; Electrodeposition as a preconcentration step in analysis of multicomponent solutions of metallic ions. *Talanta,* 1983, **30,** 627-629.

53. Sioda R.E.; A kinetic model of metal ion electrodeposition from solutions of ppm and ppb concentrations. *Analytical Letters,* 1983, **16,** 739-746.

54. Sioda R.E.; Preconcentration and preseparation by electrodeposition of traces of metals. *Talanta,* 1985, **32,** 1083-1087.

55. Sioda R.E.; Concentration limits of electrolytic preconcentration in instrumental analysis. *Analytical Chemistry,* 1988, **60,** 1177-1179.

56. Rogers L.B. and Stehney A.F.; The electrodeposition behaviour of a simple ion. *Journal of the Electrochemical Society,* 1949, **95,** 25-32.

57. Ciszewski A., Fish J.W. and Malinski T.; Deposition of trace metals on solid electrodes: experimental verification of limits of electrochemical preconcentration. *Analytical Chemistry,* 1989, **61,** 856-860.

58. Sioda R.E.; A simple model for electrolytic preconcentration performed with flow-through porous electrodes. *Analytica Chimica Acta,* 1990, **228,** 323-326.

59. Volland G., Tschoepel P. and Toelg G.; Electrodeposition in the hydrodynamic system of ng amounts of iron, cobalt, zinc and bismuth in the graphite tube. *Analytica Chimica Acta,* 1977, **90,** 15-23.

60. Hoppstock K., Garten R.P.H., Tschöpel P. and Tölg G; Purification of reagents and separation of element traces by electrodeposition onto a graphite tube cathode. *Fresenius' Journal of Analytical Chemistry,* 1992, **343,** 778-781.

61. Matousek J.P. and Powell H.K.J.; Analyte preconcentration and separation from small volumes by electrodeposition for electrothermal atomic absorption spectroscopy. *Talanta,* 1993, **40,** 1829-1831.

62. Pretty J.R., Duckworth D.C. and Van Berkel G.J.; Anodic stripping voltammetry coupled on-line with inductively coupled plasma mass spectrometry: optimization of a thin layer flow cell system for analyte signal enhancement. *Analytical Chemistry,* 1997, **69,** 3544-3551.

63. Beinrohr E., Rapta Miroslav R., Maw-Lin L., Tschöpel P. and Tölg G.; On-line electrochemical preconcentration of manganese for graphite furnace atomic absorption spectrometry using a flow-through electrochemical cell. *Mikrochimica Acta,* 1993, **110,** 1-12.

64. Frick D.A. and Tallman D.E.; Flow cell for the determination of mercury in water by electrodeposition followed by atomic absorption spectrometry. *Analytical Chemistry,* 1982, **54,** 1217-1219.

65. Yoshida Z. and Kihara S.; Electrodeposition of mercury on glassy carbon electrodes from very dilute mercury(II) solutions. *Journal of Electroanalytical Chemistry; Interfacial Chemistry,* 1979, **95,** 159-168.

66. Komarek J., Stavinoha P., Gomiscek S. and Sommer L.; Determination of copper by electrothermal AAS after electrodeposition on a graphite disk electrode. *Talanta,* 1996, **43,** 1321-1326.

67. Shiowatana J. and Matousek J.P.; Electrodeposition on pyrolytic graphite platforms for electrothermal atomic absorption spectroscopic determination of labile lead in saline water. *Talanta,* 1991, **38,** 375-383.

68. Matusiewicz H., Fish J. and Malinski T.; Electrochemical preconcentration of metals using mercury film electrodes followed by electrothermal vaporisation into an inductively coupled plasma and determination by atomic emission spectrometry. *Analytical Chemistry,* 1987, **59,** 2264-2269.

69. Seeger S., Haas H. and Mayer A.; A procedure for clean deposition of Pd-100 on surfaces. *Hyperfine Interactions,* 1994, **84,** 211-215.

70. Bard A.J., Faulkner L.R.; *Electrochemical Methods; Fundamentals and Applications.* John Wiley & Sons Ltd, New York, 1980.

71. Chen Z.F., Li J. and Wang E.K.; *In-situ* scanning tunnelling microscopic study of nickel electrodeposition on HOPG. *Journal of Electroanalytical Chemistry,* 1994, **373,** 83-87.

72. Michailova E., Peykova M., Stoychev D. and Milchev A.; On the role of surface active agents in the nucleation step of metal electrodeposition on a foreign substrate. *Journal of Electroanalytical Chemistry,* 1994, **366,** 195-202.

73. Stulíková A.; The deposition and stripping of mercury on a glassy carbon rotating disk electrode. *Journal of Electroanalytical Chemistry.,* 1973, **48,** 33-45.

74. Kuhn A. and Argoul F.; Revisited experimental analysis of morphological changes in thin-layer electrodeposition. *Journal of Electroanalytical Chemistry,* 1994, **371,** 93-100.

75. Staikov G., Juttner K., Lorenz W.J. and Budevski E.; Metal deposition in the nanometer range. *Electrochimica Acta,* 1994, **39,** 1019-1029.

76. Winand R.; Electrodeposition of metals and alloys—new results and perspectives. *Electrochimica Acta,* 1994, **39,** 1091-1105.

77. Martins M.E., Salvarezza R.C. and Arvia A.J.; A comparative study of the early stages of mercury, cadmium, lead, silver and copper electrodeposition on columnar and smooth platinum electrodes. *Electrochimica Acta,* 1996, **41,** 2441-2449.

78. Srinivasan R. and Gopalan P.; Order and disorder in electrochemical deposits of copper on graphite. *Surface Science,* 1995, **338,** 31-40.

79. Michaelis R., Zei M.S., Shai R.S. and Kolb D.M.; The effect of halides on the structure of copper underpotential-deposited onto Pt(111): a low energy electron diffraction and x-ray photoelectron spectroscopy study. *Journal of Electroanalytical Chemistry,* 1992, **339,** 299-310.

80. Lund W. and Larson B.V.; Application of electrodeposition techniques to flameless atomic absorption spectrometry. I. Determination of cadmium with a tungsten filament. *Analytica Chimica Acta,* 1974, **70,** 299-310.

81. Lund W. and Larson B.V.; Application of electrodeposition techniques to flameless atomic absorption spectrometry. II. Determination of cadmium in seawater. *Analytica Chimica Acta,* 1974, **72,** 57-62.

82. Lund W. and Larson B.V.; Application of electrodeposition techniques to flameless atomic absorption spectrometry. III. The determination of cadmium in urine. *Analytica Chimica Acta,* 1976, **81,** 319-324.

83. Czobik E.J. and Matousek J.P.; The application of electrodeposition on a tungsten wire to furnace atomic absorption spectrometry. *Spectrochimica Acta Part B-Atomic Spectroscopy,* 1980, **35,** 741-751.

84. Zhang G., Li J., Fu D., Hao D. and Xiang P.; Atomic absorption determination of traces of cadmium in urine after electrodeposition onto a tungsten wire. *Talanta,* 1993, **40,** 409-413.

85. Hoshino Y., Utsunomiya T. and Fukui K.; Graphite furnace atomic absorption spectrometry using selective adsorption of metal ions onto tungsten wire in aqueous solutions. *Chemistry Letters,* 1976, 947-950.

86. Thomassen Y., Larsen B.V., Langmyhr F.J. and Lund. W.; The application of electrodeposition techniques to flameless atomic absorption spectrometry Part IV. Separation and preconcentration on graphite. *Analytica Chimica Acta,* 1976, **83,** 103-110.

87. Veber M., Gomiscek S. and Stresko V.; Electrothermal atomic absorption spectrometry of elements after electrochemical deposition on graphite electrodes. *Analytical Chemistry,* 1987, **193,** 157-167.

88. Batley G.E. and Matousek J.P.; Determination of heavy metals in seawater by atomic absorption spectrometry after electrodeposition on pyrolytic graphite coated tubes. *Analytical Chemistry,* 1977, **49,** 2031-2034.

89. Batley G.E.; *In-situ* electrodeposition for the determination of lead and cadmium in sea water. *Analytica Chimica Acta,* 1981, **124,** 121-129.

90. Vrana A. and Komarek J.; Determination of cadmium and copper with ETAAS after electrochemical deposition on a graphite electrode. *Fresenius' Journal of Analytical Chemistry,* 1996, **355,** 321-323.

91. Vidal J.C., Monreal F. and Castillo J.R.; Determination of cadmium by electrothermal atomisation atomic absorption spectrometry after electrodeposition on a L'vov platform. *Analyst,* 1990, **115,** 539-543.

92. Vidal J.C., Sanz J.M. and Castillo J.R.; Speciation of Cr(VI)/Cr(III) by electrothermal atomisation AAS after electrodeposition on a L'vov platform. *Fresenius Journal of Analytical Chemistry,* 1992, **344,** 234-241.

93. Batley G.E. and Matousek J.P.; Determination of chromium speciation in natural waters by electrodeposition on graphite tubes for electrothermal atomisation. *Analytical Chemistry,* 1980, **52,** 1570-1574.

94. Fairless C. and Bard A.J.; Electrodeposition techniques for carbon rod flameless atomic absorption analysis. *Analytical Letters,* 1972, **5,** 433-438.

95. Torsi G., Desimoni E., Palmisano F. and Sabbatini L.; Determination of lead in sea water by electrothermal atomic absorption spectrometry after electolytic accumulation on a glassy carbon furnace. *Analytica Chimica Acta,* 1981, **124,** 143-154.

96. Matousek J.P., Grey R.; *Proceedings of 27th Colloquium Spectroscopy International.* Paper No. B-6.4, 1991.

97. Matousek J.P. and Powell H.K.J.; Coupled *in-situ* electrodeposition-ETAAS: A new concept in quantitative matrix-free analysis. *Spectrochimica Acta Part B-Atomic Spectroscopy,* 1995, **50,** 857-872.

98. Matousek J.P., Powell H.K.J., Davenport C.; *Proceedings of 28th Colloquium Spectroscopy International.* Paper No. TL 1.1; Matrix elimination in electrothermal AAS: a new approach, 1993.

99. Matousek J.P. and Powell H.K.J.; Analyte stabilization by electrodeposited palladium modifier for electrothermal atomic absorption spectrometry: characterization by scanning electron microscopy and anodic stripping voltammetry. *Talanta,* 1997, **44,** 1183-1193.

100. Zief M., Mitchell J.W.; *Contamination Control in Trace Element Analysis.* John Wiley & Sons, New York, 1976.

101. Smith M.; *Annual Environmental Audit: Metal-free Cleanroom.* Total Air Care, 1997.

102. Eriksson G.; An algorithm for the computation of aqueous multicomponent, multiphase equilibria. *Analytica Chimica Acta,* 1979, **112,** 375-383.

103. Pettit L.D., Powell H.K.J.; *SC-Database, Stability Constants Database.* (1992-1997) IUPAC/Academic Software,

104. *CA-Cricket Graph III.* (1.5.1) Computer Associates International Inc, New York.

105. Miller J.C., Miller J.N.; *Statistics for Analytical Chemistry.* Ellis Horwood Limited, Southampton, 1984.

106. Shan X-Q and Ni Z-M; Matrix modification for the determination of mercury using electrothermal atomic absorption spectrometry. *Acta Chimica Sinica,* 1979, **37,** 261-266.

107. Bulska E. and Jedral W.; Application of palladium- and rhodium-plating of the graphite furnace in electrothermal atomic absorption spectrometry. *Journal of Analytical Atomic Spectrometry,* 1995, **10,** 49-53.

108. Welz B., Schlemmer G. and Mudakavi J.R.; Palladium nitrate-magnesium nitrate modifier for electrothermal atomic absorption spectrometry. Part 3: Determinaton of mercury in environmental standard reference materials. *Journal of Analytical Atomic Spectrometry,* 1992, **7,** 499-503.

109. Bermejo-Barrera P., Moreda-Pineiro J., Moreda-Pineiro A. and Bermejo-Barrera A.; Comparative study of magnesium nitrate, palladium nitrate and reduced palladium for the direct determination of mercury in sea water by electrothermal atomization atomic absorption spectrometry. *Mikrochimica Acta,* 1996, **124,** 111-122.

110. Ma Y.Z., Li Z.K., Wang X.H., Wang J.Z. and Li Y.Q.; Determination of cadmium by electrothermal atomic absorption spectrometry using palladium and tartaric acid as a mixed chemical modifier and a tungsten-foil platform with the possibility of standardless analysis. *Journal of Analytical Atomic Spectrometry,* 1994, **9,** 679-683.

111. Araujo P.W., Gomez C.V., Marcano E. and Benzo Z.; Application of a fractional factorial design for the determination of cadmium by ETA-AAS in different atomization systems. *Fresenius' Journal of Analytical Chemistry,* 1995, **351,** 204-208.

112. Bermejo-Barrera P., Barciel-Alonso C. and Bermejo-Barrera A.; Determination of cadmium in slurries of marine sediment samples by electrothermal atomic absorption spectrometry using palladium and phosphate as chemical modifiers. *Mikrochimica Acta,* 1996, **124,** 251-261.

113. Yin X., Schlemmer G. and Welz B.; Cadmium determination in biological materials using graphite furnace atomic absorption spectrometry with palladium nitrate-ammonium nitrate modifier. *Analytical Chemistry,* 1987, **59,** 1462-1466.

114. Tahvonen R. and Kumpulainen J.; Determination of lead at low concentrations in food samples by electrothermal atomic absorption spectrometry. *Journal of Analytical Atomic Spectrometry,* 1994, **9,** 1427-1432.

115. Slaveykova V.I., Rastegar F. and Leroy M.J.F.; Behaviour of various arsenic species in electrothermal atomic absorption spectrometry. *Journal of Analytical Atomic Spectrometry,* 1996, **11,** 997-1002.

116. Bermejo-Barrera P., Moreda-Pineiro J., Moreda-Pineiro A. and Bermejo-Barrera A.; Comparison of different chemical modifiers for the direct determination of arsenic in sea water by electrothermal atomic absorption spectrometry. *Fresenius' Journal of Analytical Chemistry,* 1996, **355,** 174-179.

117. Xuan W.; Effects of Pd and Mg nitrate on the atomization of Ge in graphite furnace atomic absorption spectrometry. *Spectrochimica Acta Part B-Atomic Spectroscopy,* 1992, **47,** 545-551.

118. Ni Z.M. and Zhang D.Q.; Influence of sample deposition and coating with Zr and Pd on the atomization kinetics of germanium in graphite furnace atomic absorption spectrometry. *Spectrochimica Acta Part B - Atomic Spectroscopy,* 1995, **50,** 1779-1786.

119. Liu Y.M., Gong B.L., Li Z.H., Xu Y.L. and Lin T.Z.; Direct determination of selenium in a wild fruit juice by electrothermal atomic absorption spectrometry. *Talanta,* 1996, **43,** 985-989.

120. Gammelgaard B. and Jons O.; Comparison of palladium chemical modifiers for the determination of selenium in plasma by Zeeman-effect background corrected electrothermal atomic absorption spectrometry. *Journal of Analytical Atomic Spectrometry,* 1997, **12,** 465-470.

121. Volynsky A.B. and Krivan V.; Comparison of various forms of palladium used as chemical modifiers for the determination of selenium by electrothermal atomic absorption spectrometry. *Journal of Analytical Atomic Spectrometry,* 1996, **11,** 159-164.

122. Thomaidis N.S., Piperaki E.A. and Efstathiou C.E.; Comparison of chemical modifiers for the determination of gold in biological fluids by electrothermal atomic absorption spectrometry. *Journal of Analytical Atomic Spectrometry,* 1995, **10,** 221-226.

123. Zheng Y.S. and Su X.G.; Analysis without calibration curve for determination of indium in sediment and geochemical samples. *Mikrochimica Acta,* 1994, **112,** 237-243.

124. Iwamoto E., Shimazu H., Yokota K. and Kumamaru T.; Atomization of tin in saline water media in graphite furnace atomic absorption spectrometry with a tungsten-coated tube using palladium as a chemical modifier. *Analytica Chimica Acta,* 1993, **274,** 231-235.

125. Zhuang Z.X., Yang Y.B., Wang X.R., Deng Z.W. and Huang B.L.; Preliminary study on the use of palladium as a chemical modifier for the determination of silicon by electrothermal atomic absorption spectrometry. *Journal of Analytical Atomic Spectrometry,* 1993, **8,** 1109-1111.

126. Sturgeon R.E., Willie S.N., Sproule G.I., Robinson P.T. and Berman S.S.; Sequestration of volatile element hydrides by platinum group elements for graphite furnace atomic absorption. *Spectrochimica Acta Part B-Atomic Spectroscopy,* 1989, **44,** 667-682.

127. An Y., Willie S.N. and Sturgeon R.E.; Flow injection-hydride generation determination of arsenic with *in-situ* concentration in a graphite furnace. *Spectrochimica Acta Part B-Atomic Spectroscopy,* 1992, **47,** 1403-1410.

128. Ding W.W. and Sturgeon R.E.; Evaluation of electrochemical hydride generation for the determination of arsenic and selenium in sea water by graphite furnace atomic absorption with *in-situ* concentration. *Spectrochimica Acta Part B-Atomic Spectroscopy,* 1996, **51,** 1325-1334.

129. Haug H.O. and Liao Y.P.; Investigation of the automated determination of As, Sb and Bi by flow injection hydride generation using *in-situ* trapping on stable coatings in graphite furnace atomic absorption spectrometry. *Fresenius' Journal of Analytical Chemistry,* 1996, **356,** 435-444.

130. Infante H.G., Sanchez M.L.F. and Sanz-Medel A.; Ultratrace determination of cadmium by atomic absorption spectrometry using hydride generation with *in-situ* preconcentration in a palladium-coated graphite atomiser. *Journal of Analytical Atomic Spectrometry,* 1996, **11,** 571-575.

131. Tao G.H. and Fang Z.L.; Electrothermal atomic absorption spectrometric determination of ultra-trace amounts of tin by *in-situ* preconcentration in a graphite tube using flow injection hydride generation with on-line ion-exchange separation. *Talanta,* 1995, **42,** 375-383.

132. Doidge P.S., Sturman B.T. and Rettberg T.M.; Hydride generation atomic absorption spectrometry with *in-situ* preconcentration in a graphite furnace in the presence of palladium. *Journal of Analytical Atomic Spectrometry,* 1989, **4,** 251-255.

133. Docekal B., Dedina J. and Krivan V.; Radiotracer investigation of hydride trapping efficiency within a graphite furnace. *Spectrochimica Acta Part B-Atomic Spectroscopy,* 1997, **52,** 787-794.

134. Li Z., Zhe-Ming N. and Xiao-Quan S.; *In-situ* concentration of metallic hydrides in a graphite furnace coated with palladium. *Spectrochimical Acta Part B-Atomic Spectrometry,* 1989, **44,** 339-346.

135. Yan X-P, Ni Z-M and Guo Q-L; *In-situ* concentration of mercury vapour in a palladium-coated graphite tube: determination of mercury by atomic absorption spectrometry. *Analytica Chimica Acta,* 1993, **272,** 105-114.

136. Qiao H. and Jackson K.W.; Mechanism of modification by palladium in graphite furnace atomic absorption spectrometry. *Spectrochimica Acta Part B-Atomic Spectroscopy,* 1991, **46,** 1841-1859.

137. Voth-Beach L.M. and Shrader D.E.; Investigations of a reduced palladium chemical modifier for graphite furnace atomic absorption spectrometry. *Journal of Analytical Atomic Spectrometry,* 1987, **2,** 45-50.

138. Rettberg T.M. and Beach L.M.; Peak profile characteristics in the presence of palladium for graphite furnace atomic absorption spectroscopy. *Journal of Analytical Atomic Spectrometry,* 1989, **4,** 427-432.

139. Volynsky A.B.; Catalytic processes in graphite furnaces for electrothermal atomic absorption spectrometry. *Spectrochimica Acta Part B - Atomic Spectroscopy,* 1996, **51,** 1573-1589.

140. Jackson J.G., Novichikhin A., Fonseca R.W. and Holcombe J.A.; Mass spectral studies of thermal decomposition of metal nitrates: An introduction to the discussion of two mechanisms. *Spectrochimica Acta Part B - Atomic Spectroscopy,* 1995, **50,** 1423-1426.

141. L'vov B.V. and Novichikhin A.V.; Mechanism of thermal decomposition of anhydrous metal nitrates. *Spectrochimica Acta Part B - Atomic Spectroscopy,* 1995, **50,** 1427-1448.

142. Jackson J.G., Fonseca R.W. and Holcombe J.A.; Mass spectral studies of thermal decomposition of metal nitrates. *Spectrochimica Acta Part B - Atomic Spectroscopy,* 1995, **50,** 1449-1457.

143. McAllister T.; Equilibrium and mass spectrometry of nitrate decomposition in electrothermal atomic absorption spectrometry. *Journal of Analytical Atomic Spectrometry,* 1994, **9,** 427-430.

144. Sturgeon R.E., Chakrabarti C.L. and Langford C.H.; Studies on the mechanism of atom formation in graphite furnace atomic absorption spectrometry. *Spectrochimica Acta Part B-Atomic Spectroscopy,* 1976, **48,** 1792-1807.

145. Styris D.L., Prell L.J., Redfield D.A., Holcombe J.A., Bass D.A. and Majidi V.; Mechanisms of selenium vaporization with palladium modifiers using electrothermal atomization and mass spectrometric detection. *Analytical Chemistry,* 1991, **63,** 508-517.

146. Styris D.L., Prell L.J. and Redfield D.A.; Mechanisms of palladium-induced stabilization of arsenic in electrothermal atomisation atomic absorption spectroscopy. *Analytical Chemistry,* 1991, **63,** 503-507.

147. Majidi V. and Robertson J.D.; Investigation of high temperature reactions on solid substrates with Rutherford backscattering spectroscopy: Interaction of palladium with selenium on heated graphite surfaces. *Spectrochimica Acta Part B-Atomic Spectroscopy,* 1991, **46,** 1723-1733.

148. Wendl W. and Müller-Vogt G.; Chemical reactions of lead in graphite furnace atomic absorption spectrometry. *Journal of Analytical Atomic Spectrometry,* 1988, **3,** 63-66.

149. Yasuda K., Hirano Y., Kamino T. and Hirokawa K.; Relationship between the formation of intermetallic compounds by matrix modifiers and atomization in graphite furnace atomic absorption spectrometry, and an observation of the vaporization of intermetallic compounds by means of electron microscopy. *Analytical Sciences,* 1994, **10,** 623-631.

150. Volynsky A.B., Krivan V. and Tikhomirov S.V.; A radiotracer study on effectiveness of platinum metals as chemical modifiers in electrothermal atomic absorption spectrometry: behavior of selenium in a graphite furnace. *Spectrochimica Acta Part B - Atomic Spectroscopy,* 1996, **51,** 1253-1261.

151. Frech W., Li K., Berglund M. and Baxter D.C.; Effects of modifier mass and temperature gradients on analyte sensitivity in electrothermal atomic absorption spectrometry. *Journal of Analytical Atomic Spectrometry,* 1992, **7,** 141-145.

152. Klinkenberg H., Beeren T. and Van Borm W.; The use of an enriched isotope as an on-line internal standard in inductively coupled plasma mass spectrometry: a reference method for a proposed determination of tellurium in industrial waste water by means of graphite furnace atomic absorption spectrometry. *Spectrochimica Acta Part B-Atomic Spectroscopy,* 1993, **48,** 649-661.

153. Schlemmer G. and Welz B.; Palladium and magnesium nitrates, a more universal modifier for graphite furnace atomic absorption spectrometry. *Spectrochimica Acta Part B-Atomic Spectroscopy,* 1986, **41,** 1157-1165.

154. Pszonicki L. and Essed A.M.; Palladium and magnesium nitrate as modifiers for the determination of lead by graphite furnace atomic absorption spectrometry. *Chemia Analityczna,* 1993, **38,** 771-778.

155. Bermejo-Barrera P., Barciel-Alonso C., Aboal-Somoza M. and Bermejo-Barrera A.; Slurry sampling for the determination of lead in marine sediments by electrothermal atomic absorption spectrometry using palladium-magnesium nitrate as a chemical modifier. *Journal of Analytical Atomic Spectrometry,* 1994, **9,** 469-475.

156. Volynsky A.B. and Krivan V.; Colloidal palladium - a promising chemical modifier for electrothermal atomic absorption spectrometry. *Spectrochimica Acta Part B-Atomic Spectroscopy,* 1997, **52,** 1293-1304.

157. He B. and Ni Z-M; Minimization of sulfate interference on lead atomization with palladium-strontium nitrate as chemical modifier in electrothermal atomic absorption spectrometry. *Journal of Analytical Atomic Spectrometry,* 1996, **11,** 165-168.

158. Qiao H., Mahmood T.M. and Jackson K.W.; Mechanism of the action of palladium in reducing chloride interference in electrothermal atomic absorbtion spectrometry. *Spectrochimica Acta Part B-Atomic Spectroscopy,* 1993, **48,** 1495-1503.

159. Smith V.C.; Selenium Analysis By Electrothermal Atomic Absorption Spectrometry Using Electrodeposited Metal Modifiers. M.Sc. Thesis, University of Canterbury, New Zealand, 1995.

160. Tsalev D.L., D'Ulivo A., Lampugani L., Di Marco M. and Zamboni R.; Thermally stabilized iridium on an integrated, carbide-coated platform as a permanent modifier for hydride-forming elements in electrothermal atomic absorption spectrometry. Part 1. Optimization studies. *Journal of Analytical Atomic Spectrometry,* 1995, **10,** 1003-1009.

161. Rademeyer C., Radziuk B., Romanova N., Petter Skaugset N., Skogstad A. and Thomassen Y.; Permanent iridium modifier for electrothermal atomic absorption spectrometry. *Journal of Analytical Atomic Spectrometry,* 1995, **10,** 739-745.

162. Pozebon D., Dressler V.L. and Curtius A.J.; Determination of arsenic, selenium and lead by electrothermal vaporization inductively-coupled plasma mass spectrometry using iridium-coated graphite tubes. *Journal of Analytical Atomic Spectrometry,* 1998, **13,** 7-11.

163. Tsalev D.L., Dulivo A., Lampugnani L., Dimarco M. and Zamboni R.; Thermally stabilized iridium on an integrated, carbide-coated platform as a permanent modifier for hydride-forming elements in electrothermal atomic absorption spectrometry. Part 2. Hydride generation and collection, and behaviour of some organoelement species. *Journal of Analytical Atomic Spectrometry,* 1996, **11,** 979-988.

164. Tsalev D.L., Dulivo A., Lampugnani L., Dimarco M. and Zamboni R.; Thermally stabilized iridium on an integrated, carbide-coated platform as a permanent modifier for hydride-forming elements in electrothermal atomic absorption spectrometry. Part 3. Effect of L-cysteine. *Journal of Analytical Atomic Spectrometry,* 1996, **11,** 989-995.

165. Shuttler I.L., Feuerstein M. and Schlemmer G.; Long-term stability of a mixed palladium-iridium trapping reagent for *in-situ* hydride trapping within a graphite electrothermal atomizer. *Journal of Analytical Atomic Spectrometry,* 1992, **7,** 1299-1301.

166. Uggerud. H.T. and Lund W.; Use of palladium and iridium as modifiers in the determination of arsenic and antimony by electrothermal vaporization inductively coupled plasma mass spectrometry, following *in-situ* trapping of the hydrides. *Journal of Analytical Atomic Spectrometry.,* 1997, **12,** 1169-1174.

167. Lee S.H. and Jung K-H; Determination of mercury in environmental samples by cold vapour generation and atomic-absorption spectrometry with a gold-coated graphite furnace. *Talanta,* 1989, **36,** 999-1003.

168. Kumar S.J. and Meeravali N.N.; *In-situ* trapping of mercury vapors on Au, Pd-Au alloy or Pt-Rh alloy in the graphite furnace for the determination of Hg in environmental samples after microwave digestion. *Atomic Spectroscopy,* 1997, **18,** 166-168.

169. Bulska E., Kandler W. and Hulanicki A.; Noble metals as permanent modifiers for the determination of mercury by electrothermal atomic absorption spectrometry. *Spectrochimica Acta Part B-Atomic Spectroscopy,* 1996, **51,** 1263-1270.

170. Ni Z.M., Rao Z. and Li M.; Minimization of phosphate interference in the direct determination of arsenic in urine by electrothermal atomic absorption spectrometry. *Analytica Chimica Acta,* 1996, **334,** 177-182.

171. Thomaidis N.S., Piperaki E.A. and Siskos P.A.; Comparison of three digestion methods for the determination of the *aqua regia* soluble content of lead, cadmium and chromium in sewage sludges by ETAAS. *Mikrochimica Acta,* 1995, **119,** 233-241.

172. Tsalev D.L. and Slaveykova V.I.; Comparative study of ruthenium, rhodium and palladium as chemical modifiers in graphite furnace atomic absorption spectrometry. *Spectroscopy Letters,* 1992, **25,** 221-238.

173. Najafi N.M.; Electrodeposition Techniques For Interference Control In Electrothermal Atomic Absorption Spectrometry. Ph.D Thesis, University of New South Wales, Australia, 1997.

174. Dabeka R.W.; Refractory behaviour of lead in a graphite furnace when palladium is used as a modifier. *Analytical Chemistry,* 1992, **64,** 2419-2424.

175. Fonseca R.W., Pfefferkorn L.L. and Holcombe J.A.; Comparisons of selected methods for the determination of kinetic parameters from electrothermal atomic absorption data. *Spectrochimica Acta Part B - Atomic Spectroscopy,* 1994, **49,** 1595-1608.

176. Matusiewicz. H and Sturgeon R.E.; Atomic spectrometric detection of hydride forming elements following *in-situ* trapping within a graphite furnace. *Spectrochimica Acta Part B-Atomic Spectroscopy,* 1996, **51,** 377-397.

177. Matousek J.P. and Powell H.K.J.; *Unpublished results.*

178. Salmon S.G., David R.H. and Holcombe J.A.; Time shifts and double peaks for lead caused by chemisorbed oxygen in electrothermally heated graphite atomisers. *Analytical Chemistry,* 1981, **53,** 323-330.

179. Chen G.R. and Jackson K.W.; Low-temperature migration of lead, thallium, and selenium onto a palladium modifier during the analysis of solutions and slurries by electrothermal atomic absorption spectrometry. *Spectrochimica Acta Part B - Atomic Spectroscopy,* 1996, **51,** 1505-1515.

180. Bruhn C.G., Neira J.Y., Valenzuela G.D. and Nobrega J.A.; Chemical modifiers in a tungsten coil electrothermal atomizer - part 1 - Determination of lead in hair and blood. *Journal of Analytical Atomic Spectrometry,* 1988, **13,** 29-35.

181. Krug F.J., Silva M.M., Oliveira P.V. and Nobrega J.A.; Determination of lead in blood by tungsten coil electrothermal atomic absorption spectrometry. *Spectrochimica Acta Part B - Atomic Spectroscopy,* 1995, **50,** 1469-1474.

182. L'vov B.; Electrothermal Atomization - The way toward absolute methods of atomic absorption analysis. *Spectrochimica Acta Part B-Atomic Spectroscopy,* 1978, **33,** 153-193.

183. Jackson J.G., Fonseca R.W. and Holcombe J.A.; Migration of Ag, Cd and Cu into highly oriented pyrolytic graphite and pyrolytic-coated graphite. *Spectrochimica Acta Part B - Atomic Spectroscopy,* 1995, **50,** 1837-1846.

184. Welz B., Schlemmer G. and Mudakavi J.; Palladium nitrate-magnesium nitrate modifier for graphite furnace atomic spectrometry. Part 2. Determination of arsenic, cadmium, copper, manganese, lead, antimony, selenium, and thallium in water. *Journal of Analytical Atomic Spectrometry,* 1988, **3,** 695-701.

185. Malitesta C., Palmisano F., Torsi L. and Giorgio Zambonin P.; Glucose fast-response amperometric sensor based on glucose oxidase immobilised in an electropolymerised poly(o-phenylenediamine) film. *Analytical Chemistry,* 1990, **62,** 2735-2740.

186. Saliq M.; *Toxic Metal Chemistry In Marine Environments.* Marcel Dekker Inc., New York, 1992.

187. Sen-Gupta J.G. and Bouvier J.L.; Direct determination of traces of Ag, Cd, Pb, Bi, Cr, Mn, Co, Ni, Li, Be, Cu and Sb in environmental waters and geological materials by simultaneous multi-element graphite furnace atomic absorption spectrometry with Zeeman-effect background correction. *Talanta,* 1995, **42,** 269-281.

188. Chuang H. and Huang S-D; Direct determination of cadmium in seawater with a graphite furnace atomic absorption spectrometer. *Spectrochimica Acta Part B-Atomic Spectrometry,* 1994, **49,** 283-288.

189. Nakamura T., Oka H., Ishii M. and Sato J.; Direct atomization atomic absorption spectrometric determination of Be, Cr, Fe, Co, Ni, Cu, Cd, and Pb in water with zirconium hydroxide coprecipitation. *Analyst,* 1994, **119,** 1397-1401.

190. Chapple G., Athanasopoulos N.; *System 2000/3000 Graphite Furnace Methods Manual.* GBC Scientific Equipment Pty. Ltd., Victoria, Australia, 1991.

191. Mitra S.; *Mercury in the Ecosystem: Its Dispersion and Pollution Today.* Trans Tech Publications, Switzerland, 1986.

192. Fergusson J.E.; *The Heavy Elements: Chemistry, Environmental Impact and Health Effects.* Peramon Press, Great Britian, 1990.

193. Jiang W.Q., Zhu Y.R., Jin G. and Wu G.H.; Spectrophotometric determination of trace amounts of mercury(II) in waste water with p-azobenzenediazoaminoazobenzene sulfonic acid. *Analytical Letters,* 1996, **29,** 2221-2226.

194. Meyer S., Scholz F. and Trittler R.; Determination of inorganic ionic mercury down to $5x10^{-14}$ mol l^{-1} by differential pulse anodic stripping voltammetry. *Fresenius' Journal of Analytical Chemistry,* 1996, **356,** 247-252.

195. Tsalev D., Sperling M. and Welz B.; On-line microwave sample pre-treatment for hydride generation and cold vapour atomic absorption spectrometry. Part 1. The manifold. *Analyst,* 1992, **117,** 1729-1733.

196. Tsalev D.L., Sperling M. and Welz B.; On-line microwave sample pre-treatment for hydride generation and cold vapour atomic absorption spectrometry. Part 2. Chemistry and applications. *Analyst,* 1992, **117,** 1735-1741.

197. Saraswati R., Vetter T.W. and Watters R.L.; Determination of arsenic and mercury in an estuarine sediment standard reference material using flow injection and atomic absorption spectrometry. *Mikrochimica Acta,* 1995, **118,** 163-175.

198. Welz B., Tsalev D.L. and Sperling M.; On-line microwave sample pretreatment for the determination of mercury in water and urine by flow-injection cold vapour atomic absorption spectrometry. *Analytica Chimica Acta,* 1992, **261,** 91-103.

199. Bruhn C.G., Rodíguez A.A., Barrios C., Jaramillo V.H., Becerra J., González U., Gras N.T., Reyes O. and Seremi S.; Determination of total mercury in scalp hair of humans by gold amalgamation cold vapour atomic absorption spectrometry. *Journal of Analytical Atomic Spectrometry,* 1994, **9,** 535-541.

200. Debrah E. and Denoyer E.R.; Flow injection determination of mercury with preconcentration by amalgamation on a gold-platinum gauze by inductively coupled plasma mass spectrometry. *Journal of Analytical Atomic Spectrometry,* 1996, **11,** 127-132.

201. Hladky Z., Rísová J. and Fisera M.; Determination of mercury in concentrated mineral acids by electrothermal atomic absorption spectrometry using gold amalgamation. *Journal of Analytical Atomic Spectrometry,* 1990, **5,** 691-692.

202. Bermejo-Barrera P., Moreda-Pineiro J., Moreda-Pineiro A. and Bermejo-Barrera A.; Use of flow injection cold vapour generation and preconcentration on coated graphite tubes for the determination of mercury in polluted seawaters by electrothermal atomic absorption spectrometry. *Journal of Analytical Atomic Spectrometry,* 1997, **12,** 317-321.

203. Karadjova I., Mandjulov P., Tsakovsky S., Simeonov V., Stratis J.A. and Zachariadis G.A.; Determination of mercury by electrothermal atomic absorption spectrometry using different chemical modifiers or a slurry technique. *Journal of Analytical Atomic Spectrometry,* 1995, **10,** 1065-1068.

204. L'vov B.; Recent advances in absolute analysis by graphite furnace atomic absorption spectrometry. *Spectrochimica Acta Part B-Atomic Spectroscopy,* 1990, **45,** 633-655.

205. Thomaidis N.S., Piperaki E.A., Polydorou C.K. and Efstathiou C.E.; Determination of chromium by electrothermal atomic absorption spectrometry with various chemical modifiers. *Journal of Analytical Atomic Spectrometry,* 1996, **11,** 31-36.

206. Stoeppler M., Burow M., May K., Padberg S. and Kloster G.; Speciation studies for arsenic and mercury-applications and prospects. *Mikrochimica Acta,* 1992, **109,** 107-109.

207. Sposito G.; *The Environmental Chemistry of Aluminum.* CRC. Lewis Publishers, Boca Raton, Florida, 1996.

208. Das A.K. and Chakraborty R.; Electrothermal atomic absorption spectrometry in the study of metal ion speciation [review]. *Fresenius' Journal of Analytical Chemistry,* 1997, **357,** 1-17.

209. Heyrovsky J.; *Principles of Polarography.* Academic Press, New York, 1966.

210. Van Der Berg C.M.G.; Effect of the deposition potential on the voltammetric determination of complexing ligand concentrations in sea-water. *Analyst,* 1992, **117,** 589-593.

211. Florence T.M.; Determination of iron by anodic stripping voltammetry. *Electroanalytical Chemistry and Interfacial Electrochemistry,* 1970, **26,** 293-298.

212. Zirino A. and Kounaves S.P.; Anodic stripping peak currents: Electrolysis potential relationships for reversible systems. *Analytical Chemistry,* 1977, **49,** 56-59.

213. Shuman M.S. and Cromer J.L.; Pseudopolarograms: Applied potential-anodic stripping peak current relationships. *Analytical Chemistry,* 1979, **51,** 1546-1550.

214. Branica G. and Lovic M.; Pseudopolarography of totally irreversible redox reactions. *Electrochimica Acta,* 1997, **42,** 1247-1251.

215. Baes C.F., Mesmer R.E.; *The Hydrolysis of Cations.* Krieger, Malabar, Florida, 1976.

216. Figura P. and McDuffle B.; Use of Chelex resin for determination of labile trace metal fractions in aqueous ligand media and comparison of the method with anodic stripping voltammetry. *Analytical Chemistry,* 1979, **51,** 120-125.

217. Lewis B.L., Lunther G.W., Lane H. and Church T.M.; Determination of metal-organic complexation in natural waters by SWASV with pseudopolarograms. *Electroanalysis,* 1995, **7,** 166-177.

218. Shuman M.S.; Exchange of comments of evaluation of the copper anodic stripping voltammetry complexometric titration for complexing capacities and conditional stability constants. *Analytical Chemistry,* 1982, **54,** 998-1000.

219. Tuschall J.R. and Brezonik P.L.; Evaluation of the copper anodic stripping voltammetry complexation titration for complexing capacities and conditional stability constants. *Analytical Chemistry,* 1981, **53,** 1986-1989.

220. Schwarzenbach G., Flaschka H.; *Complexometric Titrations.* Methuen and Co. Ltd, London, 1969.

221. Morton W.E., Dunnette D.A.; *Health Effects of Environmental Arsenic.* John Wiley and Sons Inc., New York, 1994.

222. Leonard A.; *Arsenic (from: Metals and their Compounds in the Environment).* VCH, Weinheim, 1991.

223. Cullen W.R. and Reimer K.J.; Arsenic speciation in the environment. *Chemical Reviews,* 1989, **89,** 713-764.

224. Pontius F.W., Brown K.G. and Chen C-J; Health implications of arsenic in drinking water. *Journal of the American Water and Wastes Association,* 1994, September, 52-63.

225. Tomilov A.P., Chomutov N.E.; in *Encylopaedia of the Electrochemistry of the Elements,* **Vol. 2,** edited by: Bard A.J., Marcell Dekker Inc., New York, 1974.

226. Forsberg G., O'Laughlin J.W. and Megargle R.G.; Determination of arsenic by anodic stripping voltammetry and differential pulse voltammetry. *Analytical Chemistry,* 1975, **47,** 1586-1592.

227. Davis P.H., Gerald R.D., Griffin R.M., Matson W.R. and Zink E.W.; Determination of total arsenic at the nanogram level by high-speed anodic stripping voltammetry. *Analytical Chemistry,* 1978, **50,** 137-143.

228. Hamilton T.W. and Ellis J.; Determination of arsenic and antimony in electrolytic copper by anodic stripping voltammetry at a gold film electrode. *Analytica Chimica Acta,* 1980, **119,** 225-233.

229. Zima J. and van den Berg C.M.G.; Determination of arsenic in sea water by cathodic stripping voltammetry in the presence of pyrrolidine dithiocarbamate. *Analytica Chimica Acta,* 1994, **289,** 291-298.

230. Holak W.; Determination of arsenic by cathodic stripping voltammetry with a hanging mercury drop electrode. *Analytical Chemistry,* 1980, **52,** 2189-2192.

231. Sadana R.S.; Determination of arsenic in the presence of copper by differential pulse cathodic stripping voltammetry at a hanging mercury drop electrode. *Analytical Chemistry,* 1983, **55,** 304-307.

232. Eguiarte I., Alonso R.M. and Jimenez R.M.; Determination of total arsenic in soils by differential-pulse cathodic stripping voltammetry. *Analyst,* 1996, **121,** 1835-1838.

233. Li H. and Smart R.B.; Determination of sub-nanomolar concentrations of arsenic(III) in natural waters by square wave cathodic stripping voltammetry. *Analytica Chimica Acta,* 1996, **325,** 25-32.

234. Henze G., Wagner W. and Sander S.; Speciation of arsenic(V) and arsenic(III) by cathodic stripping voltammetry in fresh water samples. *Fresenius' Journal of Analytical Chemistry,* 1997, **358,** 741-744.

235. Bermejo-Barrera P., Moreda-Pineiro J., Moreda Pineiro A. and Bermejo-Barrera A.; Direct determination of arsenic in sea water by electrothermal atomization atomic absorption spectrometry using D_2 and Zeeman background correction. *Mikrochimica Acta,* 1998, **128,** 215-221.

236. Howard A.G. and Salou C.; Cysteine enhancement of the cryogenic trap hydride AAS determination of dissolved arsenic species. *Analytica Chimica Acta,* 1996, **333,** 89-96.

237. Van Elteren J.T., Das H.A., De Ligny C.L. and Agterdenbos D.; Arsenic speciation in aqueous samples using a selective As(III)/As(V) preconcentration in combination with an automatable cryotrapping hydride generation procedure for monomethylarsonic acid and dimethylarsenic acid. *Journal of Radioanalytical and Nuclear Chemistry; Articles,* 1994, **179,** 211-219.

238. Nielsen S. and Hansen E.H.; Determination of As(III) and As(V) by flow injection-hydride generation-atomic absorption spectrometry via on-line reduction of As(V) by KI. *Analytica Chimica Acta,* 1997, **343,** 5-17.

239. Chen H., Bridnle I. and Le Xiao-chun; Prereduction of arsenic(V) to arsenic(III), enhancement of the signal, and reduction of interferences by L-cysteine in the determination of arsenic by hydride generation. *Analytical Chemistry,* 1992, **64,** 667-672.

240. Walcerz M., Bulska E. and Hulanicki A.; Study of some interfering processes in arsenic, antimony and selenium determination by hydride generation atomic absorption spectrometry. *Fresenius' Journal of Analytical Chemistry,* 1993, **346,** 622-626.

241. Ding W.W. and Sturgeon R.E.; Interference of copper and nickel on electrochemical hydride generation. *Journal of Analytical Atomic Spectrometry,* 1996, **11,** 421-425.

242. Salzberg H.W. and Goldschmidt B.; Arsine evolution and water reduction at an arsenic cathode. *Journal of the Electrochemical Society,* 1960, **107,** 348-353.

243. Valdes J.L., Cadet G. and Mitchell J.W.; On-demand electrochemical generation of arsine. *Journal of the Electrochemical Society,* 1991, **138,** 1654-1658.

244. Schaumloffel D. and Neidhart B.; A FIA-system for As(III)/As(V)-determination with electrochemical hydride generation and AAS-detection. *Fresenius' Journal of Analytical Chemistry,* 1996, **354,** 866-869.

245. Infante H.G., Sanchez M.L.F. and Sanzmedel A.; Vesicular hydride generation—*in-situ* preconcentration - electrothermal atomic absorption spectrometry determination of sub-parts-per-billion levels of cadmium. *Journal of Analytical Atomic Spectrometry,* 1997, **12,** 1333-1336.

246. Haug H.O. and Liao Y.P.; Automated determination of tin by hydride generation using *in-situ* trapping on stable coatings in graphite furnace atomic absorption spectrometry. *Spectrochimica Acta Part B - Atomic Spectroscopy,* 1995, **50,** 1311-1324.

247. Sturgeon R.E.; Electrothermal vaporization inductively coupled plasma mass spectrometric detection of As, Sb, Se, Bi and Sn following preconcentration by *in-situ* collection of their hydrides. *Spectrochimica Acta Part B-Atomic Spectroscopy,* 1994, **49,** 1335-1345.

248. Marawi I., Wang J. and Caruso J.A.; Graphite furnace hydride preconcentration and subsequent detection by inductively coupled plasma mass spectrometry. *Analytica Chimica Acta,* 1994, **291,** 127-136.

249. Howard A.G.; (Boro)hydride techniques in trace element speciation - invited lecture. *Journal of Analytical Atomic Spectrometry,* 1997, **12,** 267-272.

250. López-Gonzálvez M.A., Gómez M.M., Cámara C. and Palacios M.A.; On-line microwave oxidation for the determination of organoarsenic compounds by high-performace liquid chromatography-hydride generation atomic absorption spectrometry. *Journal of Analytical Atomic Spectrometry,* 1994, **9,** 291-295.

251. Zhang X.R., Cornelis R., Dekimpe J. and Mees L.; Speciation of toxicologically important arsenic species in human serum by liquid chromatography hydride generation atomic absorption spectrometry. *Journal of Analytical Atomic Spectrometry,* 1996, **11,** 1075-1079.

252. Shaikh A. and Tallman D.E.; Species-specific analysis for nanogram quantitites of arsenic in natural waters by arsine generation followed by graphite furnace atomic absorption spectrometry. *Analytica Chimica Acta,* 1978, **98,** 251-259.

253. Le X-C, Cullen W.R. and Reimer K.J.; Effect of cysteine on the speciation of arsenic by using hydride generation atomic absorption spectrometry. *Analytica Chimica Acta,* 1994, **285,** 277-285.

254. Van Cleuvenbergen R.J.A., Van Mol W.E. and Adams F.C.; Arsenic speciation in water by hydride cold trapping-quartz furnace atomic absorption spectrometry: an evaluation. *Journal of Analytical Atomic Spectrometry,* 1988, **3,** 169-176.

255. Welz B., He Y. and Sperling M.; Flow injection on-line acid digestion and pre-reduction of arsenic for hydride generation atomic absorption spectrometry. A feasibility study. *Talanta,* 1993, **40,** 1917-1926.

256. Yin X., Hoffmann E. and Lüdke C.; Differential determination of arsenic(III) and total arsenic with L-cysteine as pre-reductant using a flow injection non-dispersive atomic absorption device. *Fresenius' Journal of Analytical Chemistry,* 1996, **355,** 324-326.

257. Linares P., De Castro M.D. and Valcárcel M.; Flow injection analysis of binary and ternary mixtures of arsenite, arsenate, and phosphate. *Analytical Chemistry,* 1986, **58,** 120-124.

258. Al-Daher I.M. and Saleh J.M.; Interaction of arsine with evaporated metal films. *Journal of Physical Chemistry,* 1972, **76,** 2851-2857.

259. Kirkbright G.F., Sargent M.; *Atomic Absorption and Fluorescence Spectrometry.* Academic Press, London, 1974.

260. Huiliang H., Jagner D. and Renman L.; Flow potentiometric and constant-current stripping analysis for arsenic(V) without prior chemical reduction to arsenic(III). *Analytica Chimica Acta,* 1988, **207,** 37-46.